NUCLEAR SAFETY

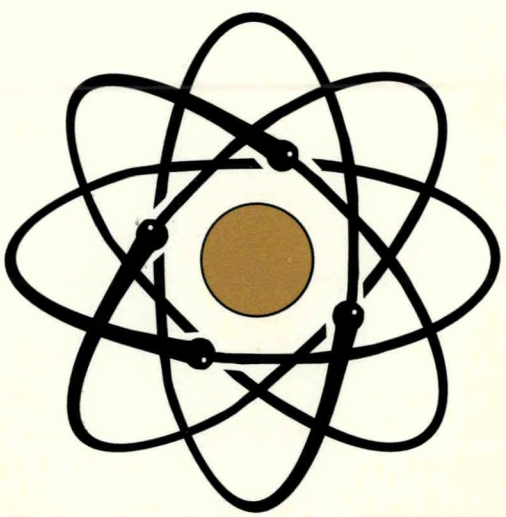

TECHNICAL PROGRESS JOURNAL

VOL. 37 – NO.4 OCTOBER – DECEMBER 1996

The Operational Performance Technology Section

The Operational Performance Technology (OPT) Section at Oak Ridge National Laboratory (ORNL) conducts analyses, assessments, and evaluations of facility operations for commercial nuclear power plants in support of the Nuclear Regulatory Commission (NRC) operations. OPT activities involve many aspects of facility performance and safety.

OPT was formed in 1991 by combining ORNL's Nuclear Operations Analysis Center with its Performance Assurance Project Office. This organization combined ORNL's operational performance technology activities for the NRC, DOE, and other sponsors aligning resources and expertise in such areas as:

- event assessments
- performance indicators
- data systems development
- trends and patterns analyses
- technical standards
- safety notices

OPT has developed and designed a number of major data bases which it operates and maintains for NRC and DOE. The Sequence Coding and Search System (SCSS) data base collects diverse and complex information on events reported through NRC's Licensee Event Report (LER) System.

OPT has been integrally involved in the development and analysis of performance indicators (PIs) for both the NRC and DOE. OPT is responsible for compiling and analyzing PI data for DOE facilities for submission to the Secretary of Energy.

OPT pioneered the use of probabilistic risk assessment (PRA) techniques to quantify the significance of nuclear reactor events considered to be precursors to potential severe core damage accidents. These precursor events form a unique data base of significant events, instances of multiple losses of redundancy, and infrequent core damage initiators. Identification of these events is important in recognizing significant weaknesses in design and operations, for trends analysis concerning industry performance and the impact of regulatory actions, and for PRA-related information.

OPT has the lead responsibility in support of DOE for the implementation and conduct of DOE's Technical Standards Program to facilitate the consistent application and development of standards across the DOE complex.

OPT is responsible for the preparation and publication of this award-winning journal, *Nuclear Safety,* now in its 37th year of publication sponsored by NRC. Direct all inquiries to Operational Performance Technology Section, Oak Ridge National Laboratory, P.O. Box 2009, Oak Ridge, TN 37831-8065. Telephone (423) 574-0394 Fax: (423) 574-0382.

A quarterly Technical Progress Journal
prepared for the U.S. Nuclear Regulatory
Commission by the Operational Performance
Technology Section at Oak Ridge National
Laboratory

Published by the
Office of Scientific and Technical Information
U.S. Department of Energy

NUCLEAR SAFETY

Vol. 37, No. 4 **October–December 1996**

TPJ-NS-37-No. 4
DE97000792

NUSAAZ 37(4), 1996
ISSN: 0029-5604

Nuclear Safety is a journal that covers significant issues in the field of nuclear safety.

Its primary scope is safety in the design, construction, operation, and decommissioning of nuclear power reactors worldwide and the research and analysis activities that promote this goal, but it also encompasses the safety aspects of the entire nuclear fuel cycle, including fuel fabrication, spent-fuel processing and handling, and nuclear waste disposal, the handling of fissionable materials and radioisotopes, and the environmental effects of all these activities.

Qualified authors are invited to submit articles; manuscripts undergo peer review for accuracy, pertinence, and completeness. Revisions or additions may be proposed on the basis of the results of the review process. Articles should aim at 20 to 30 double-spaced typed pages (including figures, tables, and references). Send inquiries or 3 copies of manuscripts (with the draftsman's original line drawings plus 2 copies and with black-and-white glossy prints of photographs plus 2 copies) to Dr. M. D. Muhlheim, Oak Ridge National Laboratory, P. O. Box 2009, Oak Ridge, TN 37831-8065.

The material carried in *Nuclear Safety* is prepared at the Oak Ridge National Laboratory's Operational Performance Technology Section, which is responsible for the contents. *Nuclear Safety* is funded by the U.S. Nuclear Regulatory Commission's Office of Nuclear Regulatory Research. Editing, composition, makeup, and printing functions are performed by the DOE Office of Scientific and Technical Information (OSTI). Sale and distribution are by the U.S. Government Printing Office; see the order form in the back of the publication for information on subscriptions, postage, and remittance.

EDITORIAL

High-Burnup Fuel Behavior Under Reactivity-Initiated Accident (RIA) Conditions

In the design and licensing of light-water reactors (LWRs), it is postulated that a small set of low-probability accidents called design-basis accidents (DBAs) will occur, and it is required that the reactor be able to accommodate or mitigate their consequences without affecting the public health and safety. The most severe in this set of DBAs in terms of challenging both the reactor and its associated systems is the large-break loss-of-coolant accident (LOCA). The characteristics of this accident serve to set the requirements for a number of the reactor's safety systems (e.g., the emergency core cooling system), including the design of the containment.

In addition to the LOCA, the other important class of accidents included in the set of DBAs has been the reactivity-initiated accidents (RIAs). In these postulated accidents, energy is deposited in the fuel and causes nearly adiabatic heating that may damage or even destroy the fuel if the power burst is sufficiently rapid and energetic. Consideration of RIAs has led to fast-acting reactor control systems as well as reactor core designs with negative power and void coefficients being inherent characteristics. The particular RIAs analyzed, respectively, for pressurized-water reactors (PWRs) and boiling-water reactors (BWRs) have been a control-rod ejection and a control-rod drop accident.

In the United States, as well as in most countries with LWRs, two types of threshold energies are important during an RIA: one is the cladding failure threshold used to calculate the number of failed fuel rods for the assessment of environmental consequences (i.e., radiological releases) and the other is the threshold for the release of mechanical energy as the result of potential molten fuel–coolant interactions and the loss of coolable geometry. For example, in the United States, the regulatory criterion for the cladding failure threshold for BWRs is the critical heat flux value related to departure from nucleate boiling, whereas for BWRs a similar value is used for high-power accidents, but for low-power- and zero-power-initiated accidents, an enthalpy value of 170 cal/g in the fuel is used. The regulatory criterion for mechanical energy release and coolability has been a limit of 280 cal/g for both PWRs and BWRs (a similar limit of 230 cal/g is used in Japan and 200 cal/g is used in France). These enthalpy values are based on results from fuel tests conducted mostly in the 1970s, most of them in U.S. experimental reactors (SPERT and PBF), and some later testing in Japan in the NSRR experimental reactor. All of these early tests used primarily fresh fuel (i.e., unirradiated), although a few had burnups up to the modest level of about 32 000 MWd/t. Even though questions were raised in the past about the accuracy of these values based on realistic plant calculations, it was thought that there was sufficient margin between the failure thresholds and the energies deposited, and there seemed no need to pursue this issue further in light of these perceived conservatisms.

The recent world-wide trend to substantially increase the fuel burnup to much higher levels (around 60 000 MWd/t with a corresponding increase in the fuel-cycle length to about four years) has led a number of countries to undertake new studies, both experimental and analytical, to evaluate the effects of the higher burnups on fuel behavior, especially fuel failure under RIA conditions. Interest peaked after two recent tests were performed (one in

(Continues on inside back cover.)

Introduction

[Editors note] The *Nuclear Safety* journal normally follows the standard practice for the use of the international system of units given by the American Society for Testing and Materials in ASTM E 380-93. An exception has been made in this issue only to report enthalpy and energy deposition in cal/g fuel rather than in J/kg because the regulatory requirements and guidance documents report values in cal/g. For example, in the United States, Standard Review Plan (NUREG-0800) Section 15.4.9, "Spectrum of Rod Drop Accidents (BWR)," states that the specific criteria necessary to meet the relevant requirements of GDC 28 [General Design Criteria given in 10 CFR 50, Appendix A] are, among others, that reactivity excursions should not result in radially averaged fuel rod enthalpy greater than 280 cal/g at any axial location in any fuel rod. One other unit must be mentioned. Fuel burnups may be reported in either GWd/tU or MWd/kgU. Because a metric tonne is 1000 kg, the use of MWd/kgU is transparent.

To aid readers in following the data reported by the various countries, where the fuel came from, where the tests were performed, etc., three tables have been provided listing the facilities, the nomenclature used to identify tests, and a list of acronyms.

Facilities used in performing the RIA tests

Abbreviation	Name
CABRI	name of the test reactor (France)
GIDRA	name of the test reactor (Russia)
IGR	Impulse Graphite Reactor (Russia)
JMTR	Japan Materials Testing Reactor (Japan)
NSRR	Nuclear Safety Research Reactor (Japan)
PBF	Power Burst Facility (U.S.)
SPERT	Special Power Excursion Reactor Test (U.S.)

Nomenclature to identify fuel specimens used in RIA tests

Test Series	Description
CDC	preirradiated (at the ETR in the U.S.) BWR-type fuel rods tested at the SPERT
GK	high-burnup fuel (42 MWd/kgU) from Genkai 1 (a commercial PWR in Japan) tested at the NSRR
HBO	high-burnup fuel from Ohi 1 (a commercial PWR in Japan) tested at the NSRR
H#T	high-burnup fuel from Novo Voronezh (a VVER in Russia) tested at the IGR
JM	medium-burnup fuel irradiated in an unpressurized helium environment of the JMTR and tested at the NSRR (JM test fuel was base-irradiated in the JMTR, and then was pulse-irradiated in the NSRR)
MH	high-burnup fuel (39 MWd/kgU) from Mihama 2 (a commercial PWR in Japan) tested at the NSRR
OI	high-burnup fuel (39 MWd/kgU) from Ohi 2 (a commercial PWR in Japan) tested at the NSRR
REP-Na	high-burnup fuel from a commercial PWR in France tested in a sodium loop at the CABRI
RIA 1-#	PWR fuel rods from the Saxton PWR prototype reactor tested at the PBF
RIA-ST-#	fresh PWR-type fuel rods tested at the PBF
TS	medium-burnup fuel from Tsuruga 1 (a commercial BWR in Japan) tested at the NSRR

List of Acronyms

Acronym	Description
ACPR	Annular Core Pulse Reactor (U.S.)
AO MZ	AO Mashinostroitelny Zavod (Electrostal)
bfc	bottom of fuel column
BWR	boiling-water reactor
CDC	capsule driver core (at SPERT)
CEA	Commissariat à l'Energie Atomique (France)
CZP	cold-zero power
DBA	design-basis accident
DBT	ductile-brittle transition
DNB	departure from nucleate boiling
EdF	Electricité de France
EOL	end of life
EPMA	electron probe microanalysis
EPRI	Electric Power Research Institute (U.S.)
ESCORE	EPRI steady-state core reload evaluator code
ETR	Engineering Test Reactor (U.S.)
FBR	fast breeder reactor
FGR	fission gas release
FRAP-T6	fuel rod analysis program, transient version 6 (U.S.)
FREY-01	Fuel Rod Evaluation System, Vol.1
GE	General Electric (U.S.)
HZP	hot-zero power
IAE	Institute of Atomic Energy of the National Nuclear Center of Kazakstan Republic (Russia)
IPSN	Institute for Protection and Nuclear Safety (France)
IVO	Imatran Voima Osakeyhtio (Finland)
JAERI	Japan Atomic Energy Research Institute (Japan)
LHGR	linear heat generation rate
LMR	liquid-metal reactor
LOCA	loss-of-coolant accident
LWR	light water reactor
METEOR	code for describing the fuel rods irradiation history (France)
MHI	Mitsubishi Heavy Industries, Ltd. (Japan)
MOX	mixed-oxide fuel
NFI	Nuclear Fuel Industries, Ltd. (Japan)
NRC	Nuclear Regulatory Commission (U.S.)
PATRICIA	name of the out-of-pile facility for thermal–hydraulic tests (France)
P/C gap	radial distance between the cladding inner surface and the fuel pellet
PCMI	pellet–cladding mechanical interaction
PIE	postirradiation examination
PROMETRA	program for measuring the mechanical properties of the cladding (France)
PTE	posttest examination
PWR	pressurized-water reactor
REP	pressurized-water reactor (reacteur à eau pressurisie)
RIA	reactivity-initiated accident
RIAR	Research Institute of Atomic Reactors (Russia)
RRC KI	Russian Research Centre "Kurchatov Institute" (Russia)
SCANAIR	code for describing the fuel behavior under an RIA transient, France
SED	strain energy density
SEM	scanning electron microscopy
SIA	Scientific Industrial Association
SILENE	name of an impulse reactor (France)
SIMS	secondary ion mass spectrometry
STP	standard temperature and pressure
TEM	transmission electron microscopy
TOSURA-REP	code for describing the irradiation of the fuel rods (France)
TRANSURANUS	European Institute for Trans-uranium Element Fuel Rod Performance code
TUBRNP	TRANSURANUS Burnup Model
TRIGA	Training Reactor and Isotopes Production, General Atomics (U.S.)
UE	uniform elongation
UTS	ultimate tensile strength
YS	yield stress

Special Issue on Reactivity-Initiated Accidents

Edited by D. B. Trauger

A Regulatory Assessment of Test Data for Reactivity-Initiated Accidents

By Ralph O. Meyer,[a] Richard K. McCardell,[b] Hee M. Chung,[c] David J. Diamond,[d] and Harold H. Scott[a]

Abstract: *An assessment is made of recent test data from France, Japan, and Russia and of earlier test data from the United States in relation to the safety analysis performed for reactivity-initiated accidents in power reactors in the United States. Considerations include mode of cladding failure, oxidation, hydriding, and pulse-width effects. From the data trend and from these considerations, we conclude that the cladding failure threshold for fuel rods with moderate-to-high burnup is roughly 100-cal/g fuel peak fuel-rod enthalpy for boiling-water reactors and pressurized-water reactors. Realistic plant calculations suggest that cladding failure would not occur for rod-ejection or rod-drop accidents and therefore that pellet fragmentation and enhanced fission-product release from fuel pellets should not have to be considered in the safety analysis for these reactivity accidents. The data base, however, is sparse and contains much uncertainty.*

Only a small number of design-basis accidents are postulated for licensing of light-water reactors (LWRs) in the United States, and one class of these events includes reactivity-initiated accidents. In pressurized-water reactors (PWRs), it is assumed that in the most severe of such accidents a control-rod housing in the pressure-vessel head breaks and the control-rod assembly is ejected from the core as a result of a pressure differential. The worst such potential accident would occur from zero-power conditions, and the minimum coolant temperature for such an accident would be 271 °C (520 °F) as set by Technical Specifications. Because initial heatup is accomplished with waste heat from the operating coolant pumps, coolant would flow through the core at this time. This is the so-called hot zero-power rod-ejection accident.

In boiling-water reactors (BWRs), the most severe postulated reactivity accident would also occur at zero power, and it is assumed that a control blade being withdrawn becomes detached from the drive, sticks, and then later drops rapidly out of the core. Because BWRs can heat up with nuclear heat, this accident could occur with the coolant at room temperature; however, coolant flow from at least one pump is required by Technical Specifications. This is the so-called cold zero-power rod-drop accident.

In the United States, two types of regulatory criteria have been used in safety analyses to address these reactivity-initiated accidents (U.S. Nuclear Regulatory Commission Standard Review Plan, Section 4.2, "Fuel System Design," NUREG-0800, Rev. 2, July 1981.) One is a limit of 280 cal/g fuel on peak fuel-rod enthalpy, and this limit was intended to (1) ensure coolability of the core after such an accident and (2) preclude the energetic dispersal of fuel particles into the coolant. (This and other

[a]U.S. Nuclear Regulatory Commission.
[b]Idaho National Engineering and Environmental Laboratory.
[c]Argonne National Laboratory.
[d]Brookhaven National Laboratory.

enthalpy values quoted here will always be taken as radial averages and given in calories per gram of UO_2 fuel.)

The other regulatory criterion consists of several threshold values that are used to indicate cladding failure—that is, the occurrence of a breach in the cladding that would allow fission products to escape. This criterion is used in calculating radiological releases for comparison with other limits. For PWRs, a critical heat flux value related to departure from nucleate boiling (DNB) is used. For BWRs, a similar value is used for high-power accidents, but for low-power and zero-power accidents, a peak fuel-rod enthalpy of 170 cal/g fuel is used.

In late 1993, a test was run in the CABRI test reactor in France. This test produced cladding failure at a peak fuel-rod enthalpy of about 30 cal/g fuel (15 cal/g fuel enthalpy rise). Fragmented fuel particles were dispersed from the fuel rod in this test, and enhanced fission-product release was observed. A short time later, in 1994, a similar test in the Nuclear Safety Research Reactor (NSRR) in Japan produced cladding failure at a peak fuel-rod enthalpy of about 60 cal/g fuel. These values were so far below the 170-cal/g fuel failure criterion that the U.S. Nuclear Regulatory Commission (NRC) initiated an investigation into this situation and issued an Information Notice to licensees.[1] The NRC regulatory staff then performed a review of the safety significance of this situation and concluded that there was no significant impact on public health and safety because of the low probability of the event and the high likelihood that core coolability would be maintained, although there might be some increase in the fuel damage fraction.

Notwithstanding this conclusion, there is still the question of the adequacy of NRC's regulatory criteria for this type of accident, and there are unanswered questions about the behavior of fragmented fuel particles and fission products released during such an event. Consequently the NRC research program has continued an investigation into the behavior of high-burnup fuel rods under conditions of reactivity-initiated accidents; this report is a summary of the work to date.

PLANT CALCULATIONS

One of the first considerations in assessing fuel damage during reactivity-initiated accidents is to understand the nature of the power transient that would involve high-burnup fuel. Licensing calculations for rod-drop and rod-ejection accidents are often done with conservative one-dimensional (1-D) or point kinetics models that do not resolve the local nature of the power pulse. Therefore a more detailed analysis was desired than could be found in a typical licensing safety analysis report.

Calculations for a rod-drop accident were performed with three-dimensional (3-D) neutron kinetics to assess what happens during a power transient in a BWR.[2] This analysis used the RAMONA-4B code[3] and two core models. A rigorous core model with a maximum bundle burnup of 30 MWd/kgU was used as well as a pseudo-high-burnup core model with burnups up to 60 MWd/kgU. The maximum fuel-bundle enthalpy was calculated to be about 45 cal/g fuel for the medium-burnup case and approximately 70 cal/g fuel for the pseudo-high-burnup case (low inlet subcooling was assumed in both cases). These values could be increased by about 15%, to 50 and 80 cal/g fuel, respectively, to represent peak fuel-rod enthalpy. In these calculations, the higher enthalpy value for the high-burnup case resulted from the increased control-rod worth of that particular core design. Power pulse widths (at half the maximum power) were in the range of 30 to 75 ms for both cases with narrower pulse widths accompanying higher power pulses.

Others have recently made similar calculations. Westinghouse used a full-core, 3-D model for a case described as "extremely limiting" and found a peak fuel-rod enthalpy of about 95 cal/g fuel for fuel rods with fuel burnups around 40 MWd/kgU.[4] This is about a factor of 2 lower than values they obtained with their standard licensing model. General Electric (GE), using a 3-D kinetics model, reported a peak fuel-rod enthalpy of <20 cal/g fuel for a fuel burnup of about 40 MWd/kgU; this is substantially lower than peak fuel-rod enthalpies calculated with their licensing model.[5] GE reported a pulse width of 75 ms. Electric Power Research Institute (EPRI), also using 3-D models, looked at a PWR case and a BWR case.[6] In both cases they found maximum fuel-bundle enthalpies around 40 cal/g fuel, which could be increased to about 45 cal/g fuel to represent peak fuel-rod enthalpy.

As analysts remove conservative assumptions and move toward better estimates for fuel-rod enthalpy, there is a corresponding need to improve the understanding of the uncertainty in these calculations. This was done by first examining the sensitivity of the maximum fuel-bundle enthalpy to fundamental parameters whose modeling introduces significant uncertainty that may increase with fuel burnup.[2] These parameters in-

clude the control-rod worth, Doppler reactivity coefficient, and delayed neutron precursor fraction.

The results of these sensitivity studies were then used in a simple model to determine the random uncertainty in fuel-bundle enthalpy. Figure 1 shows the results of a parametric study with ranges for the uncertainty (1 standard deviation) in dropped rod worth and Doppler coefficient and with the uncertainty in delayed neutron precursor fraction assumed to be 5%. A best-estimate point can be obtained with the use of engineering judgments of 10% for control-rod-worth uncertainty and 15% for the Doppler coefficient uncertainty. The related enthalpy uncertainty is 37% (as shown in Fig. 1), and it can be interpreted as the standard deviation on the random error.

In addition to the random component, systematic errors may be present when estimating the fuel-rod enthalpy distribution within a bundle. RAMONA-4B and most other kinetics codes calculate the fuel-bundle enthalpy, and estimates must be made of a bundle peaking factor to determine the fuel-rod enthalpy. In this study, an approximate bundle power reconstruction was used to estimate the local power peaking. It was determined that the peaking factor would be higher, by as much as 25%, than the 1.1 to 1.15 factor usually assumed for a rod-drop analysis. Adding this bias to the 2-sigma random error ($2 \times 37\%$) suggests that the actual fuel-rod enthalpy could be as much as 100% larger than the best-estimate calculation. Although this value will depend on the methodology used, other methods are expected to have similar errors.

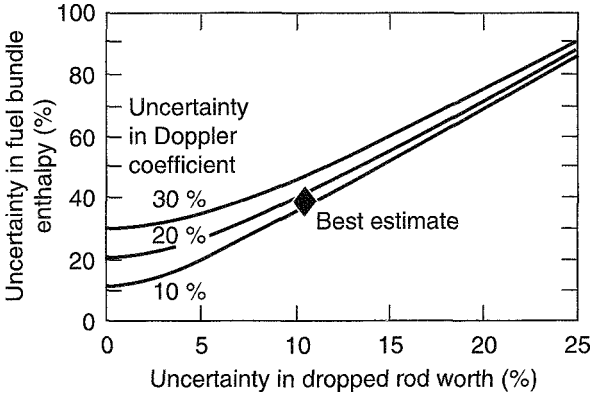

Fig. 1 Uncertainties in calculated fuel-bundle enthalpy as a function of random uncertainties in dropped rod worth and Doppler coefficient.

If the variability in this and other analyses is considered, our results are consistent with the others. All show that the expected peak fuel-rod enthalpy would be far below the 280-cal/g fuel limit and well below the 170-cal/g fuel cladding failure threshold, which is in question. On the basis of these plant calculations, it is assumed that peak fuel-rod enthalpy would not exceed 100 cal/g fuel should a PWR rod-ejection or a BWR rod-drop accident occur and that the power pulse width would not be less than 30 ms.

FUNDAMENTAL CONSIDERATIONS

When interpreting integral test data that appear to show a trend, it is helpful to know if there are underlying phenomena that could cause the trend. This is the situation for the French and Japanese test results that seem to show a reduction in the ability of the cladding to resist failure at high fuel burnup.

It is well known that Zircaloy cladding loses ductility and becomes more brittle at high fuel burnup.[7] There are three main effects. One results from the absorption into the Zircaloy of hydrogen that is released from the oxidation (corrosion) reaction. As the hydrogen concentration increases, hydrogen precipitates as hydrides in the metal and thus increases the metal's hardness and reduces its ductility. The second effect comes from oxygen itself, which is added to Zircaloy as an alloying element to increase strength. At even moderate fuel burnup levels, the concentration of oxygen can double and thus increase hardness and reduce ductility.[8] The third effect is lattice damage from fast neutrons, which further increases hardness and reduces ductility.

The French and Japanese test results also exhibited enhanced fission gas release, fragmentation of the oxide fuel pellets, and dispersal of some of those fragments into the coolant. High fuel burnup also affects the microstructure of the fuel pellets in a way that would lead to enhanced gas release and fragmentation.[9] The continued accumulation of fission gases in the oxide matrix causes the microstructure to change, particularly near the pellet periphery where the fuel burnup is greatest. The original oxide grain size is reduced, and high-pressure bubbles of fission gas attach themselves to the grain boundaries. Any sudden temperature increase, such as would occur during a reactivity accident, would cause gas expansion that could separate the fuel at the grain boundaries and fragment the material.

Thus there are fundamental phenomena that appear to explain the apparent reduction in cladding failure threshold, the observed dispersal of fuel fragments, and the enhancement of fission gas release.

MODE OF CLADDING FAILURE

Before discussing the test reactor data in detail, it is useful to look at the types of failures that have been observed. In particular, the following series of photographs will show some failures that resulted from a mechanical stress applied to the cladding by the expanding pellet—the so-called pellet–cladding mechanical interaction (PCMI)—and some failures that occurred because the cladding became too hot. The change in failure mode is undoubtedly related to the change in ductility of the cladding as it reaches higher fuel burnups and becomes heavily oxidized (and hydrided).

Figure 2 shows the fracture tip of specimen REP-Na1 (64 MWd/kgU) from the CABRI test program.[10–12] The fracture surface is nearly perpendicular to the cladding wall, and the failure occurred by crack initiation and growth. This is a brittle fracture with the cladding exhibiting no appreciable strain; the failure occurred by a PCMI at low temperature and a very low value of fuel-rod enthalpy.

Figure 3 shows the fracture tip of specimen HBO-1 (50 MWd/kgU) from the NSRR test program.[13–15] The outer part of the cladding failed in a brittle manner, but the inner part of the cladding exhibits the characteristic 45° angle of a ductile shear. This was also a PCMI failure that occurred at low temperature, but the cladding exhibited measurable strain.

Figure 4 shows the fracture tip of specimen 804-1 (6 MWd/kgU) from the Power Burst Facility (PBF) test program.[16] This cladding was even more ductile than HBO-1, and the failure was by pure ductile shearing throughout the wall thickness. Nevertheless, ductility was still limited sufficiently that the cladding did not accommodate the expansion of the pellet; the cladding failed by PCMI at a relatively low temperature. This fuel rod went on to experience high temperatures after the failure, as evidenced by the accumulation of oxide on the fracture surface, just as it appears on the outer surface and some of the inner surface.

Figure 5 shows the fracture tip of specimen 801-3 (zero burnup), also from the PBF test program.[17] This cladding did not fail by a PCMI at low temperature; rather, it reached a very high temperature, which

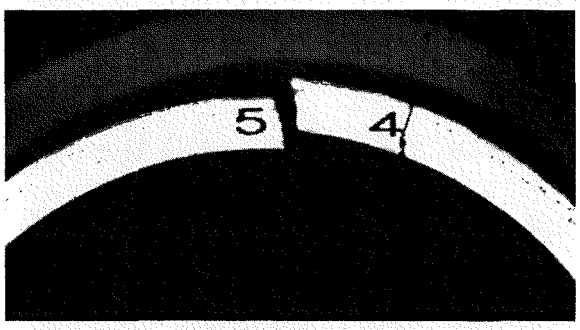

Fig. 2 Crack tip from test REP-Na1 (Table 1) showing brittle character of a PCMI fracture.

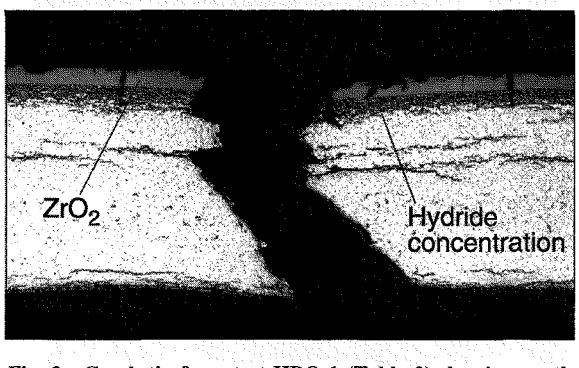

Fig. 3 Crack tip from test HBO-1 (Table 2) showing partly brittle and partly ductile character of a PCMI fracture.

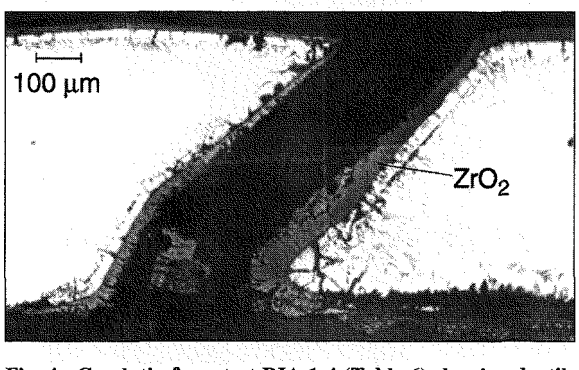

Fig. 4 Crack tip from test RIA 1-4 (Table 6) showing ductile character of a PCMI fracture and postfailure oxidation.

resulted in severe oxidation along with some wall thinning and thickening. The cladding failed during quenching, as can be inferred from the absence of further oxidation on the fracture surface.

Figure 6 shows the failure section of specimen H7T (47 MWd/kgU) from the Impulse Graphite Reactor (IGR) test program.[18–20] Like the previous case (Fig. 5), this niobium-alloy cladding had sufficient ductility to

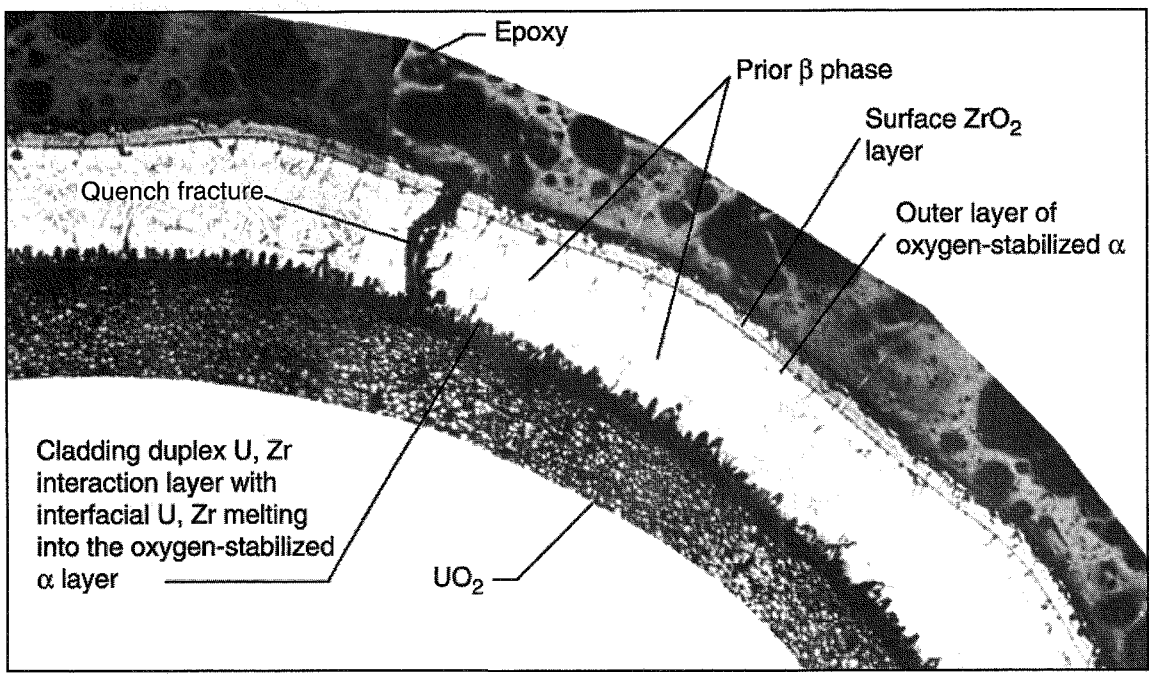

Fig. 5 Crack tip from test RIA 1-1 (Table 6) showing evidence of a high-temperature excursion and fracture on cooling.

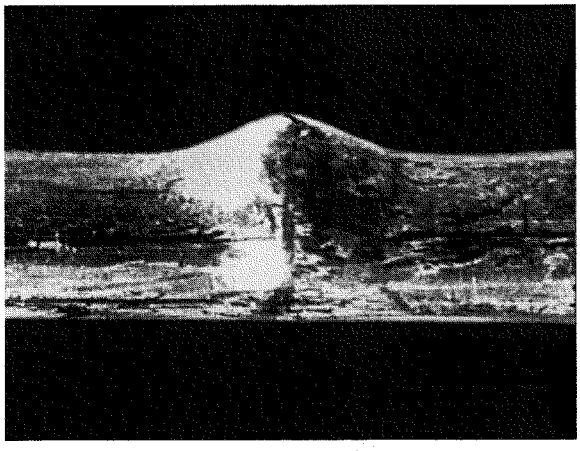

Fig. 6 Ballooned region of ruptured fuel rod from test H7T (Table 5).

survive the PCMI and accommodate higher fuel enthalpies. Unlike the previous case, this specimen had a large pressure differential across the cladding during the test so that it ballooned and failed by rupturing at an intermediate cladding temperature. It did not experience temperatures high enough to cause the extreme oxidation seen in Fig. 5.

Thus we see a transition from PCMI-type failures to high-temperature failures that is apparently related to available cladding ductility. Within the PCMI-type failures, there is a progression from more brittle to less brittle behavior.

TEST REACTOR DATA

Early test results on reactivity accidents from the Special Power Excursion Reactor Test (SPERT) and PBF test reactors in the United States were summarized by MacDonald et al.[21] More recent work from the NSRR test reactor in Japan has been reported by Fujishiro et al.[22] and Nakamura et al.[23] The maximum burnup of fuel rods tested in those earlier programs was about 42 MWd/kgU.

CABRI Test Reactor

The first test result with high-burnup fuel that exhibited cladding failure at a low fuel-rod enthalpy came from the CABRI test reactor, which is operated by the Nuclear Safety and Protection Institute in France. The reactor consists of a driver core in a water pool and a test loop with liquid sodium for the coolant.

The test loop was designed for research on fast reactors but has been used recently for this LWR project. Thus heat transfer was not representative of LWRs, and testing temperatures had to be kept high to keep the sodium liquid.

Table 1 lists the important characteristics of the high-burnup fuel tests performed in the CABRI sodium loop.[10–12] Test REP-Na1 is the test with the low failure enthalpy. Most of these tests have been performed with standard fuel rods from a commercial PWR in France. Pulse width, which is of special concern and is discussed in the following text, is determined largely by Doppler feedback characteristics of the core in the test reactor and is relatively fixed. For the CABRI reactor, the natural pulse width is around 9.5 ms. Because this is substantially narrower than a typical LWR prompt-critical pulse, the researchers at CABRI developed a technique to artificially broaden the pulse. One of the tests in Table 1 (REP-Na4) was performed with a broadened pulse.

NSRR Test Reactor

Shortly after the low-energy failure occurred in the CABRI program, a low-energy failure was observed in the NSRR test reactor. This reactor is operated by the Japan Atomic Energy Research Institute. NSRR is a TRIGA-type annular core pulse reactor in a water pool. Although a water loop has been used for some testing in NSRR, it is not used with highly radioactive irradiated fuel specimens. Tests with these specimens are conducted in an instrumented capsule at ambient conditions. The natural pulse width of NSRR is about 5 ms.

Table 2 lists the important characteristics of high-burnup fuel tests with PWR fuel that have been performed in the NSRR test reactor.[13–15] Test HBO-1 is the test with the low fuel-rod-failure enthalpy, and that result was later repeated in test HBO-5. These tests were performed with standard fuel rods from commercial PWRs in Japan.

Table 3 lists characteristics of some medium-burnup fuel tests in NSRR with PWR-type fuel rods. These test rods were not typical of irradiated commercial fuel rods inasmuch as they were irradiated in the Japan Materials Testing Reactor in an unpressurized helium environment. Thus they experienced no cladding creepdown and no cladding oxidation. Nevertheless, the cladding did accumulate neutron fluence, and this did affect the failure mode.

Table 4 lists characteristics of medium-burnup fuel tests in NSRR with standard fuel rods from a commercial BWR in Japan. Cladding in BWRs typically experiences low levels of uniform oxidation along with highly localized lens-shaped white oxides called nodules.[24] The nodules create underlying corrosion pits that can weaken the cladding, but failures were not seen in this test series with moderate burnup specimens.

IGR Test Reactor

During the 1980s and early 1990s, a large series of reactivity-initiated accident tests was carried out in the IGR test reactor by the Russian Research Center, the Kurchatov Institute. The IGR reactor is a uranium–graphite pulse reactor with a central experimental

Table 1 Characteristics of PWR Fuel Specimens Tested in Flowing Sodium at an Initial Temperature of 280 °C in the CABRI Test Reactor[a]

Test No.	Test date	Maximum burnup, MWd/kgU	Oxide thickness, μm	Energy deposit, cal/g fuel	Pulse width, ms	Peak fuel enthalpy, cal/g fuel	Clad strain, %	Clad fail, yes/no	Comments
REP-Na1	11/10/93	63.8	80	110	9.5	115	N/A	Yes	Enthalpy at failure 30 cal/g fuel;[b] oxide spalling, brittle failures; significant fuel loss
REP-Na2	6/10/94	33.0	4	211	9.5	209	3.5	No	
REP-Na3	10/6/94	52.8	40	120	9.5	125	2.1	No	
REP-Na4	7/28/95	62.3	80	97	64.0	96	0.4	No	No oxide spalling
REP-Na5	5/5/95	64.3	20	105	9.5	115	1.1	No	

[a]Cladding surface oxide thickness before RIA test; cladding type is Zircaloy-4 with 1.5% tin and stress relief annealed except for REP–Na3 with 1.3% tin; N/A is not available.

[b]The 15-cal/g fuel enthalpy increase at peak power locations corresponds to 30-cal/g fuel pellet averaged enthalpy (i.e., very early when the cladding was only slightly above 280 °C).

Table 2 Characteristics of PWR Fuel Specimens Tested in Stagnant Water at an Initial Temperature of 20 °C in the NSRR Test Reactor[a]

Test No.	Test date	Maximum burnup, MWd/kgU	Oxide thickness, μm	Energy deposit, cal/g fuel	Pulse width, ms	Peak fuel enthalpy, cal/g fuel	Clad strain, %	Clad fail, yes/no	Comments
MH-1	11/28/89	38.9	4	63	6.8	47	0.02	No	
MH-2	3/8/90	38.9	4	72	5.5	54	0.05	No	
MH-3	10/31/90	38.9	4	87	4.5	67	1.56	No	
GK-1	3/12/91	42.1	9–10	121	4.6	93	2.23	No	Large swelling
GK-2	3/17/92	42.1	9–10	117	4.6	90	1.05	No	Swelling
OI-1	11/10/92	39.2	15	136	4.4	106	1.49	No	
OI-2	1/27/93	39.2	15	139	4.4	108	4.77	No	
HBO-1	2/16/94	50.4	43	93	4.4	73	2.0–2.5	Yes	Enthalpy at failure 60 cal/g fuel; long axial cracks, large fuel loss
HBO-2	3/25/94	50.4	35	51	6.9	37	0.41	No	
HBO-3	10/19/94	50.4	23	95	4.4	74	1.51	No	
HBO-4	1/24/95	50.4	19	67	5.3	50	0.17	No	
HBO-5	1/31/96	44.0		103	4.4	79		Yes	Enthalpy at failure ~70 cal/g fuel[b,c]
HBO-6	2/6/96	49.0		103	4.4	79	1.11	No	*b, c*

[a]Cladding surface oxide thickness before RIA test; cladding type is Zircaloy-4; cold fill pressure 0.1 MPa all tests except MH-1, MH-2, MH-3, GK-1, and HBO-2.

[b]Burnup from preliminary evaluation.

[c]Oxide thickness measurements for HBO-5 and HBO-6 have not been completed and are shown in Fig. 7 with large error bars.

Table 3 Characteristics of Special PWR-Type Specimens Tested in Stagnant Water at an Initial Temperature of 20 °C in the NSRR Test Reactor[a]

Test No.	Test date	Maximum burnup, MWd/kgU	Oxide thickness, μm	Energy deposit, cal/g fuel	Pulse width, ms	Peak fuel enthalpy, cal/g fuel	Clad strain, %	Clad fail, yes/no	Comments
JM-1	7/20/89	22	0	130	9	92	0	No	
JM-2	1/11/90	27	0	120	9	84	0	No	
JM-3	9/6/90	20	0	184	7.7	132	0	No	Small swelling
JM-4	11/6/90	21	0	235	5.5	177	<7.5	Yes	12 small cracks; grain boundary separation; large swelling
JM-5	3/5/91	26	0	223	5.6	167	<3.5	Yes	20 small cracks correlate with local hydrides; large swelling

[a]Cladding surface oxide thickness before RIA test; JM test rods were irradiated in a helium environment, so no cladding oxidation occurred; cladding type is Zircaloy-4.

channel. Tests were performed with specimens in capsules under ambient conditions. As a rule, an experimental capsule contained two fuel rods: one high-burnup fuel rod and one fresh fuel rod. For safety reasons, instrument penetrations were not used when irradiated specimens were being tested, so the tests with high-burnup fuel were not instrumented. The natural pulse width for this reactor is about 700 ms, which is much broader than the pulses mentioned previously.

Table 4 Characteristics of BWR Fuel Specimens Tested in Stagnant Water at an Initial Temperature of 20 °C in the NSRR Test Reactor[a]

Test No.	Test date	Maximum burnup, MWd/kgU	Oxide thickness, μm	Energy deposit, cal/g fuel	Pulse width, ms	Peak fuel enthalpy, cal/g fuel	Clad strain, %	Clad fail, yes/no
TS-1	10/24/89	26	6	70	5.8	55	0.0	No
TS-2	2/7/90	26	6	82	5.2	66	0.4	No
TS-3	9/12/90	26	6	109	4.6	88	0.5	No
TS-4	1/17/91	26	6	110	4.3	89	0.4	No
TS-5	1/21/93	26	6	117	4.6	98	0.0	No

[a]Cladding surface oxide thickness before RIA test, 6 μm or less for all 5 tests, with nodules from 35 to 63 μm; cladding type is Zircaloy-2.

Table 5 Characteristics of VVER Fuel Specimens Tested in Stagnant Water at an Initial Temperature of 20 °C in the IGR Test Reactor[a]

Test No.	Test date	Maximum burnup, MWd/kgU	Oxide thickness, μm	Energy deposit, cal/g fuel	Pulse width, ms	Peak fuel enthalpy, cal/g fuel	Clad strain, %	Clad fail, yes/no	Comments
H1T	1990–92	51	5	253	800	160	~2.5	No	
H2T	1990–92	50	5	333	760	220	Large	Yes	Local balloon
H3T	1990–92	50	5	400	820	265	Large	Yes	Local balloon
H4T	1990–92	50	5	196	760	115	~0.2	No	
H5T	1990–92	50	5	251	840	171	Large	Yes	Local balloon
H6T	1990–92	50	5	141	800	80	~0	No	
H7T	1990–92	47	5	244	630	170	Large	Yes	Local balloon
H8T	1990–92	48	5	109	850	56	~0	No	

[a]Cladding surface oxide thickness before RIA test; cladding type is zirconium–1% niobium; cold fill pressure 1.7 MPa.

Table 5 lists the characteristics of the high-burnup fuel tests in the IGR reactor.[18–20] These tests were performed with standard fuel rods from a commercial VVER reactor in Russia. The main difference between the VVER fuel rods and PWR fuel rods is that the VVER rods have a different cladding alloy and a centerline hole in the fuel pellets.

PBF Test Reactor

During the period 1978 to 1980, reactivity accident tests were performed in the PBF test reactor for the NRC. The reactor consists of a driver core in a water pool and a pressurized-water test loop that could provide a wide range of test conditions. The PBF has a natural pulse width of about 20 ms and produces nearly prototypical conditions.

Table 6 lists the characteristics of the fuel tests in the PBF reactor.[16,17,25,26] Tests ST-1 to ST-3 were single-rod tests with fresh PWR-type fuel rods. The remainder of the tests were performed with PWR fuel rods from the Saxton PWR prototype reactor. Tests RIA 1-1 and 1-2 each contained four fuel rods, but they were in individual flow shrouds so that they behaved as single-rod tests. Test RIA 1-4 was a true multirod test with a 3 × 3 array of nine fuel rods. Test energies were relatively high in the PBF test series because that program was designed to examine fuel behavior near the 280-cal/g fuel peak fuel-rod enthalpy licensing limit.

SPERT Test Reactor

Earlier tests with irradiated fuel rods were performed in the SPERT test reactor for the U.S. Atomic Energy Commission. There were several SPERT facilities with different cores, and the core used for the tests of interest was the Capsule Driver Core (CDC); hence these tests are often referred to as CDC tests. Single rods were tested in an instrumented water-filled

Table 6 Characteristics of PWR-Type Specimens Tested in Flowing Water at an Initial Temperature of 265 °C in the PBF Test Reactor[a]

Test No.	Test date	Maximum burnup, MWd/kgU	Oxide thickness, μm	Energy deposit, cal/g fuel	Pulse width, ms	Peak fuel enthalpy, cal/g fuel	Clad strain, %	Clad fail, yes/no	Comments
RIA-ST-1 Burst 1	8/78	0	0	250	22	185	NM	No	
RIA-ST-2 Burst 2	8/78	0	0	330	17	250		Yes	
RIA-ST-2	8/78	0	0	345	17	260		Yes	
RIA-ST-3	8/78	0	0	300	20	225	NM	No	Cladding oxidation collapse and waisting
RIA 1-1 (four test rods)	10/7/78								
801-1		4.6	5	365	13	285		Yes	Irradiated rods fragmented and blocked flow channels during transient; unirradiated rods did so after transient
801-2		4.7	5	365	13	285		Yes	
801-3		0	0	365	13	285		Yes	
801-5		0	0	365	13	285		Yes	
RIA 1-2 (four test rods[b])	11/22/78								
802-1		5.2	5	240	16	185	2–3	No	
802-2		5.1	5	240	16	185	5–6	No	
802-3		4.4	5	240	16	185	2–3	Yes	Enthalpy at failure <140 cal/g fuel; 22 axial splits as the result of PCMI
802-4		4.5	5	240	16	185	5–6	No	
RIA 1-4 (nine test rods[c])	4/80								
804-1		6.1	5	295	11	277		Yes	Enthalpy at failure <<255 cal/g fuel; all corner rods failed early in transient by PCMI
804-3		5.5	5	295	11	277		Yes	
804-7		5.9	5	295	11	277		Yes	
804-9		5.7	5	295	11	277		Yes	
804-10		4.4	5	270	11	255		Yes	Enthalpy at failure <<255 cal/g fuel; all side rods failed early in transient by PCMI
804-4		5.0	5	270	11	255		Yes	
804-6		5.1	5	270	11	255		Yes	
804-8		4.7	5	270	11	255		Yes	
804-5		5.5	5	245	11	234		Yes	Clad melted as the result of contact with rods 804-8 and 804-9

[a]Cladding surface oxide thickness before RIA test; cladding type is Zircaloy-4; NM is not measured.

[b]In the RIA 1-2 test, rods 802-2 and 802-4 were opened and prepressurized to 2.4 MPa, rod 802-1 was opened and prepressurized to 0.105 MPa, and rod 802-3 was unopened.

[c]All nine RIA test rods were unopened.

capsule at ambient conditions. SPERT with the CDC had a natural pulse width of about 20 ms.

Table 7 lists the characteristics of the irradiated fuel tests in the SPERT reactor.[21,27] The test rods were BWR-type fuel rods manufactured to specifications being used by GE at that time except that many of the rods had a smaller outside diameter to achieve higher energy depositions. All the rods listed in Table 7 are of the smaller size except CDC-703 and -709. These smaller rods also had a correspondingly reduced cladding thickness and gas gap. Preirradiation to accumulate the burnup was done in the Engineering Test Reactor (ETR) at typically high power levels.

Table 7 Characteristics of BWR-Type Specimens Tested in Stagnant Water at an Initial Temperature of 20 °C in the SPERT Test Reactor[a]

Test No.	Test date	Maximum burnup, MWd/kgU	Oxide thickness, μm	Energy deposit, cal/g fuel	Pulse width, ms	Peak fuel enthalpy, cal/g fuel	Clad fail, yes/no	Comments
CDC-571	1969	4.6	~0	161	31	134	No	
CDC-568	1969	3.5	~0	199	24	165	Yes	Enthalpy at failure 147 cal/g fuel
CDC-567	1969	3.1	~0	264	18	219	Yes	Enthalpy at failure 214 cal/g fuel
CDC-569	1969	4.1	~0	348	14	289	Yes	Enthalpy at failure 282 cal/g fuel
CDC-703	1969	1.1	~0	192	15	159	No	12% diametral swelling
CDC-709	1969	1.0	~0	238	13	198	Yes	Enthalpy at failure 190 cal/g fuel; rod failed 280 ms after peak power
CDC-685	1970	13.1	~0	186	23	154	No	
CDC-684	1970	12.9	~0	200	20	166	No	Slight swelling
CDC-756	1970	32.7	65	176	17	146	Yes	Enthalpy at failure <143 cal/g fuel; one tiny PCMI crack
CDC-859	1970	31.8	65	190	16	158	Yes	Enthalpy at failure 85 cal/g fuel; very little fuel loss; three large PCMI cracks

[a]Cladding surface oxide thickness before RIA test, values for CDC-756 and -859 were estimated from the increase in rod diameter and are larger than expected from FRAPCON calculations; cladding type is Zircaloy-2.

INTERPRETATION OF DATA

Departure from Nucleate Boiling

Two groups of tests produced cladding failures by high-temperature processes. The high temperatures resulted from poor heat transfer to the coolant after DNB. These tests were the PBF tests with fresh PWR fuel, which exhibited a failure threshold around 225-cal/g fuel peak fuel-rod enthalpy, and the IGR tests with VVER fuel, which exhibited a failure threshold around 150-cal/g fuel peak fuel-rod enthalpy.

The IGR rods failed at a lower fuel-rod enthalpy and a correspondingly lower cladding temperature than the PBF fuel rods because (1) the IGR test capsule was unpressurized and (2) there was a large pressure differential across the cladding to cause ballooning with subsequent rupture (around 900 °C). The PBF test rods did not balloon and therefore did not rupture, and the cladding temperature continued to increase (above 1200 °C), which produced heavily oxidized cladding that fractured upon quenching. There was also no coolant flow in the IGR tests, which will be seen to lead to earlier DNB.

Some of the tests in NSRR, SPERT, and PBF were instrumented with cladding thermocouples so that the onset of DNB could be measured. One such study of cooling conditions during reactivity transients was conducted with shrouded single rods in the NSRR.[28] Results were found to depend on initial coolant temperature, shroud diameter, and coolant velocity, with the greatest sensitivity to coolant velocity. The DNB threshold was found at a peak fuel-rod enthalpy of approximately 60 cal/g fuel for no-flow conditions and 115 cal/g fuel for coolant flow of 1.8 m/s. Corresponding cladding failure thresholds were significantly higher at 175 cal/g fuel and 205 cal/g fuel, respectively.

We attempted to determine the onset of DNB from cladding temperature measurements from fuel-bundle tests in SPERT and PBF. To get this information, DNB was assumed to occur when the cladding temperature exceeded the saturation temperature by 50 °C. The time at which this temperature was reached was determined from thermocouple data, and then the fuel-rod enthalpy at that time was calculated from the power pulse.

There was quite a variation in results, ranging from a low of 70 cal/g fuel to well over 200 cal/g fuel. Nevertheless, the lowest values for fuel-rod enthalpy corresponded to cases in which there was no coolant flow, whereas the cases with coolant flow were generally higher. These results are consistent with the results from the NSRR discussed earlier.

Cladding Ductility

Except for the IGR tests with niobium-alloy cladding and the near-zero-burnup tests with Zircaloy-clad fuel, all the rest of the cladding failures in the data base resulted from PCMI. It seems clear that cladding failure by PCMI occurs when the cladding does not have sufficient ductility to accommodate the expansion of the fuel pellet during the transient and does not reach the higher temperatures following DNB before failure.

We have calculated the fuel-pellet expansion with FRAP-T for a pulse with a width of 30 ms and a peak fuel-rod enthalpy of 100 cal/g fuel. Although the code does not contain models for all of the important high-burnup effects, it at least describes fuel thermal expansion and gives an order-of-magnitude indication of fuel-pellet expansion; this magnitude is about 1.5%. Whereas pellet surface displacement might be more than this because of gas expansion and a portion of the displacement may be compensated by the fuel-to-cladding gap, displacements of this order must be accommodated by cladding strain. Zircaloy cladding appears to have sufficient ductility for these strains only when it is fresh, whereas Zr–1%Nb cladding used on the VVER fuel appears to have sufficient ductility even at high fuel burnups.

Oxidation and Burnup

The traditional way of plotting data from these tests uses burnup as the abscissa, but burnup is not the best choice for that variable. From fundamental considerations, it is expected that cladding ductility, and hence the propensity for failure, will depend on both burnup (related to fluence) and oxidation (related to hydride absorption). From the test data, however, oxidation seems to be the more important variable. Figure 7 illustrates this point. In three pairs of tests, specimens taken from higher elevations failed, whereas specimens taken from lower elevations of the same fuel rods did not fail under similar

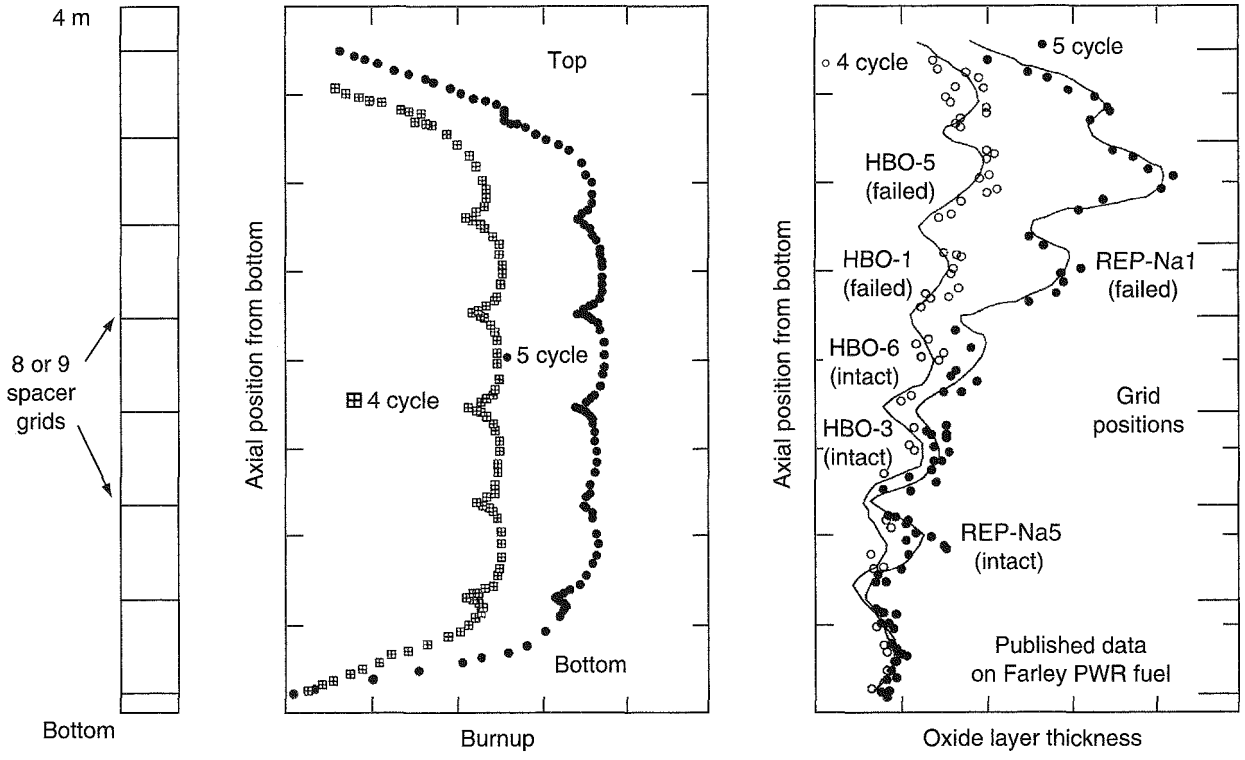

Fig. 7 Typical axial profiles of burnup and oxidation (Farley plant data) in relation to axial position in the core, with schematic indication of locations of test specimens from other reactors. HBO-X and REP-X represent test numbers.

test conditions. The major difference between the failed and non-failed specimens was the much higher amount of cladding oxidation at the higher elevations (related to higher core exit temperatures). Because of the relatively flat power profile along the rods, the burnups of the specimens in each pair were about the same.

Therefore the test data have been plotted as a function of cladding oxidation in Fig. 8; this figure will be used to help interpret the results available to date. The ordinate in Fig. 8 has been plotted as a function of fuel-rod enthalpy increase during the test, rather than total enthalpy, because enthalpy increase is more directly related to the PCMI failure mode.

Hydriding and Spalling Oxide

As cladding oxidation takes place, about 15% of the hydrogen released from the reaction of metal and water is absorbed in the Zircaloy cladding. The hydrogen uptake is much lower (~5%) in zirconium–niobium alloys. When the concentration of hydrogen reaches about 120 ppm in Zircaloy, the hydrogen is no longer soluble and zirconium hydride precipitates out in rod-like strings in the metal. These precipitates act as hardening sites along with oxygen, tin, and other alloying constituents. Consequently, the hardness of the cladding increases while the ductility decreases.

Because heat flows through the cladding during normal operation of the fuel, a small temperature gradient is maintained across the cladding thickness (ΔT about 40 °C), which is sufficient to cause migration of hydrogen toward the outer surface of the cladding as a result of hydrogen's tendency to move to cooler regions. This concentration of hydrides near the cladding outer diameter can be seen clearly in Fig. 3.

Of course, the uniform oxide layer on the outer surface of the cladding also supports a temperature gradient, acting as an insulator. Under certain conditions, heavy oxide layers begin to flake off, or spall, and thus leave local areas of the cladding in more intimate contact with the coolant. Those areas then run at cooler temperatures than average for the cladding surface, and hydrides migrate preferentially to those locations. Figure 9 shows one such local hydride concentration,

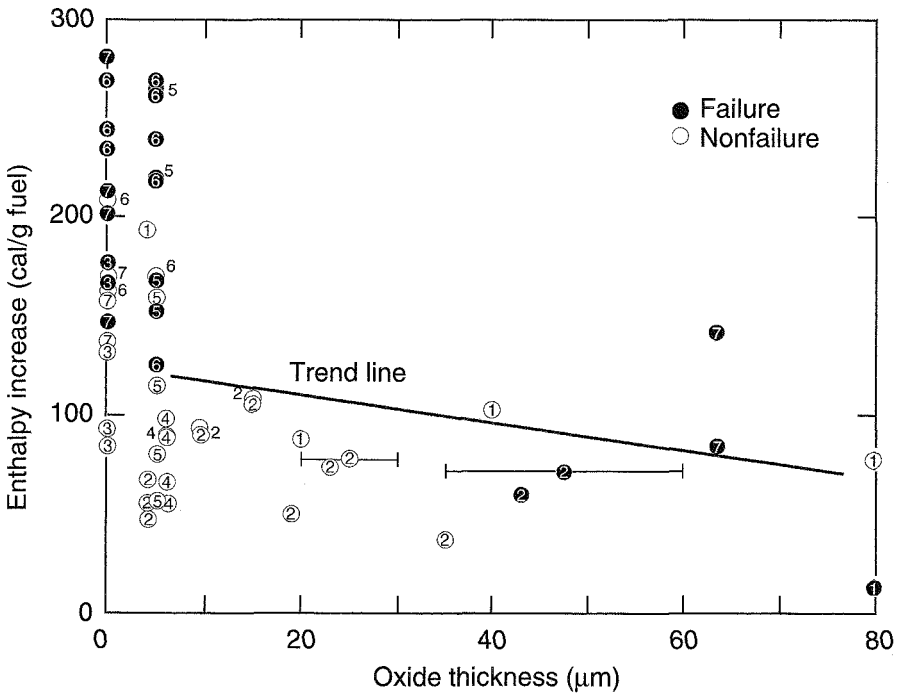

Fig. 8 Fuel-rod enthalpy increase for test data shown in the tables. Numbers in the circles refer to the appropriate table number for the data point. For example, a "1" in a circle refers to Table 1. The trend line is drawn to facilitate a discussion in the text and is not intended as a failure threshold.

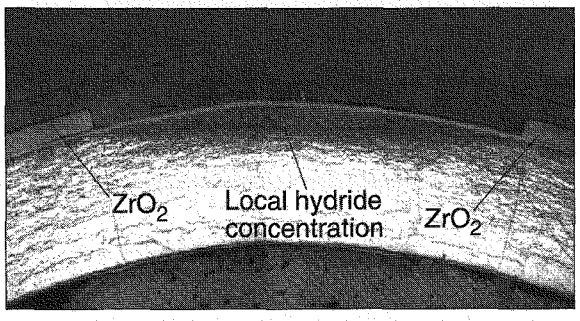

Fig. 9 High hydride concentration beneath an area where oxide spallation has occurred on a sibling of the rod used in test REP-Na1.

or blister, in a 5-cycle fuel rod beneath an area where the oxide has spalled off during normal operation.

Thus, when oxide spalling occurs, the underlying hydride concentration can be many times that of the average concentration. Similar localized regions of hydrogen concentration can also occur if large gaps exist between pellets in a fuel rod.[29]

Most of the hydrogen atoms in high-burnup Zircaloy cladding are contained in circumferentially oriented hydride stringers. Such hydrides are not particularly harmful to the mechanical properties of the cladding because the PCMI stresses are parallel to the circumferential orientation of the hydrides. As the oxide layer increases and the cladding is exposed to various mechanical loads, however, the concentration of radially oriented hydride stringers increases. Such radial hydrides are quite deleterious to the mechanical properties of the cladding, and radial hydrides are often found in association with spalled oxide that is close to stoichiometry and characteristically whitish in color.

High local concentrations of radial hydrides associated with spalling oxide are probably the reason that REP-Na1 failed with an unusually low fuel-rod enthalpy rise of 15 cal/g fuel. Further, the microstructure of REP-Na1 is not typical of most current reactor fuel. Consequently REP-Na1 has been treated as a separate case and was not used to determine the trend line in Fig. 8. This single test specimen, however, along with an understanding of the underlying phenomena, suggests that fuel rods with spalling oxide or pellet gaps may have little resistance to PCMI failure during a reactivity accident.

Pulse Widths

Table 8 summarizes the pulse widths that produced the test data being discussed along with the approximate range of pulse widths that would be expected in an LWR during a rod-drop or rod-ejection accident. With the exception of an artificially expanded pulse in CABRI, none of the test reactor pulses approximates the LWR pulses. The IGR reactor produced pulses that are ten times too broad, whereas all the rest of the test reactors produced pulses that are too narrow. The broadened pulses in CABRI may be very important for future testing, but little of the current data base has been generated with those more appropriate pulses.

Table 8 Pulse Widths for LWRs and Test Reactors

Reactor	Pulse widths, ms
NSRR	4.3 to 9.0
CABRI	9.5[a]
PBF	11 to 22
SPERT	13 to 31
LWRs	30 to 75
IGR	630 to 850

[a]Broadened to 64 ms for one test.

Because all the fuel rods tested in the broad-pulse IGR came from a Russian VVER, they had Zr–1%Nb cladding rather than Zircaloy cladding. This niobium alloy is more resistant to oxidation than Zircaloy, so in Fig. 8 these data are seen on the left side of the figure notwithstanding the fact that the burnup was quite high (45 to 50 MWd/kgU). Thus the trend line in Fig. 8 has been influenced more by tests in SPERT, CABRI, and NSRR, all of which had narrow pulses.

Three effects of narrow pulses have been considered: stress, temperature, and strain rate. Each is discussed in the following paragraphs.

A narrow pulse, which produced a certain fuel-rod enthalpy, was thought perhaps to give rise to a higher peak hoop stress in the cladding from PCMI than a broad pulse that produced the same enthalpy. This would be important because peak stress is likely to be the failure initiator regardless of the failure mechanism.

To test this hypothesis, calculations were done with the FRAP-T6 computer code to compare a 4.5-ms pulse (like that in NSRR) with a 30-ms pulse that might correspond to an LWR. Although FRAP-T6 in its present form has limitations as mentioned previously, comparative results from parametric calculations should be meaningful. The fuel-rod enthalpy for these calculations was chosen at a relatively low value

of 67 cal/g fuel to avoid reaching the cladding yield stress, which would then complicate the interpretation of results. Calculations have also been done at 100 cal/g fuel with the result that the peak stress was always the yield stress for narrow and broad pulses alike.

Figure 10 shows the results of these calculations. Although the hoop stress for the 30-ms pulse rises a little after the initial peak, the initial peak is somewhat lower than that for the 4.5-ms pulse. From sensitivity calculations it was found that the peak fuel-rod enthalpy for the 30-ms pulse would have to be increased about 10 cal/g fuel to raise its initial peak stress to the same level reached with the 4.5-ms pulse. Thus the NSRR tests would appear to be about 10 cal/g fuel too conservative because of the effect of enhanced stress from narrow pulses.

It was also thought that a narrow pulse might produce its peak hoop stress at a time when the cladding was cooler than would be the case for a broad pulse. With the use of the same calculations, this is seen to occur. Figure 10 shows that the 4.5-ms pulse produced a cladding temperature of about 30 °C at the time of peak hoop stress, whereas the 30-ms pulse produced a cladding temperature of about 150 °C at the time of its peak hoop stress. This difference of over 100 °C may be significant because the materials properties that control cladding failure—regardless of failure mechanism—are expected to be temperature dependent, as will be discussed further.

For reference, Fig. 11 shows the 30-ms pulse compared with a 700-ms pulse, like that of the IGR test reactor, for pulse magnitudes that produce 67-cal/g fuel peak fuel-rod enthalpy. Whereas the peak stress in the 700-ms pulse is somewhat higher (about the same as for the 4.5-ms pulse), the cladding temperature (about 210 °C) at the time the peak stress is applied is even higher than that of the 30-ms pulse because of substantial heat transfer.

The third pulse width effect that might affect the interpretation of test results is strain rate. Strain-rate hardening is known to occur in many metals, but the magnitude of such an effect is not known for Zircaloy in the range of strain rates around 1 s^{-1} (i.e., strains on the order of 1% occurring in a period of about 10 ms). Thus there is no way of knowing, at this time, if this effect is significant.

Temperature

Cladding temperature at the time of failure initiation should affect the threshold for PCMI failures. For brittle failures, such as in CABRI specimen REP-Na1 (Fig. 2), an increase in temperature would increase the fracture toughness of the material. This temperature sensitivity could be quite large if fuel-rod cladding experiences a ductile-to-brittle transition in this temperature range as has been observed for Zircaloy-2 pressure tubes.[30] For partly ductile PCMI failures, such as in NSRR specimen HBO-1 (Fig. 3), an increase in temperature would increase fracture toughness of the brittle hydride-rich layer beneath the oxide as well as increase ductility in the remaining metallic layer,

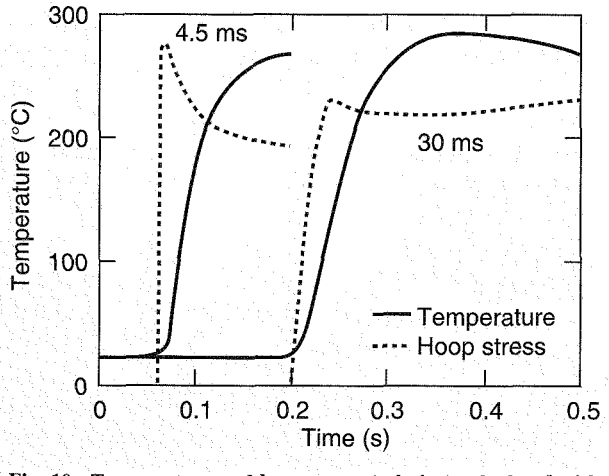

Fig. 10 Temperature and hoop stress (relative) calculated with the FRAP-T6 code for a 4.5-ms pulse (similar to NSRR) and a 30-ms pulse (similar to LWRs).

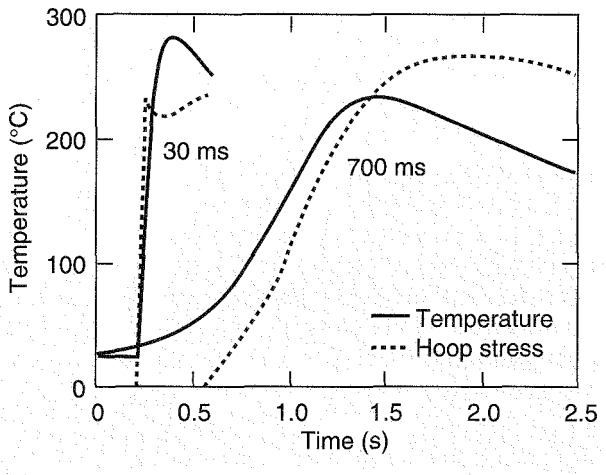

Fig. 11 Temperature and hoop stress (relative) calculated with the FRAP-T6 code for a 30-ms pulse (similar to LWRs) and a 700-ms pulse (similar to IGR).

hence accommodating more of the fuel pellet expansion. Thus an increase in temperature would always appear to be beneficial. Whereas this effect is expected to be significant, basic materials properties have not been measured under the appropriate conditions, so the effect cannot be quantified at this time.

Nevertheless, temperature effects should enter into the interpretation of the test data in two ways. First, the narrow test pulses that resulted in PCMI cladding failures probably caused those failures to occur at somewhat lower fuel-rod enthalpies than would occur in an LWR; those data points might thus appear lower than they should in Fig. 8. Second, the testing temperatures were not the same in all tests, and some large differences existed; data points for tests at hot conditions would be higher than they should be in Fig. 8 to apply to cold zero-power accidents and vice versa.

The NSRR and SPERT tests were conducted at room temperature. This would be appropriate for simulating cold zero-power accidents, but the narrow pulse widths would diminish the cladding temperature rise by about 120 °C for NSRR and about half that amount for SPERT. Thus those points should be a little low in Fig. 8 to apply to cold LWR accidents.

The IGR tests were also conducted at room temperature, but their wide pulses would enhance the temperature rise by about 60 °C. Hence those data points should be a little high to apply to cold accidents, but they might be a little low to apply to hot accidents because of the room temperature test conditions.

The PBF and CABRI tests were conducted at hot conditions (265 °C and 280 °C, respectively). These temperatures would be appropriate for simulating hot zero-power accidents, but the narrow pulse widths would diminish their cladding temperature rise. Thus these data points in Fig. 8 might be a little low for applying to hot accidents, but they might be too high for applying to cold accidents because of the test temperatures.

These temperature deviations must be taken into account qualitatively when trying to determine a trend in the data because temperature effects cannot be quantified on the basis of present knowledge.

Data Trend

A trend line has been drawn in Fig. 8 to roughly represent the failure threshold for PCMI cladding failures. Several comments can be made about this line.

First, the line slopes downward with increasing cladding oxidation. This is expected from fundamental considerations discussed previously. Next, the trend is not expected to go continuously down to the low failure level of REP-Na1 (at 80 μm of oxide thickness in Fig. 8) from the CABRI test program. The trend of failure threshold should fall precipitously once the hydride morphology changes, as happened in REP-Na1 in connection with oxide spalling.

The data points for REP-Na2 and REP-Na4 (nonfailures) at 40 and 80 μm of oxide thickness are slightly above the trend line because those tests were conducted at a high temperature and would be expected to have a higher failure threshold than rods tested at room temperature. The data points for HBO-1 and HBO-5 (at about 45 μm of oxide thickness in Fig. 8) are expected to fall the farthest below the trend line because they had the narrowest pulse widths in combination with the coldest test temperatures.

Failure Modeling

In concluding this discussion of the data, some comments about failure modeling can be made. In principle, brittle failures such as those occurring in the CABRI test, REP-Na1, could be modeled with linear-elastic fracture mechanics. Fracture toughness for high-burnup Zircaloy cladding has not been measured, however, so this approach would have limited success at this time.

The combination of brittle and ductile behavior, such as seen in the NSRR test, HBO-1, is being studied by Koss et al. using methods that have been employed in sheet-metal manufacturing.[31] These methods have not yet been demonstrated for zirconium-alloy tubing, and the analysis also depends on material properties that have not been measured.

Failure by ductile shearing, such as seen in the PBF test, RIA 1-4, should be amenable to straightforward analysis of uniform deformation. Again, simple stress–strain relations for high-burnup cladding under appropriate temperature, strain-rate, and loading conditions are not available.

Ballooning and rupture in the IGR tests are very similar to cladding behavior during loss-of-coolant accidents, which have been studied extensively in the past. Asmolov and Yegorova[20] used the NRC's FRAP-T6 code, which contains such models, to analyze these failures. Whereas the models are present, materials properties for high-burnup Zr–1%Nb cladding under ballooning conditions are not available.

Similarly, the high-temperature PBF failures could be modeled with oxidation rate laws and embrittlement

criteria as used for loss-of-coolant accidents. The appropriate correlations and materials properties are not available at this time.

Even DNB predictions, which are often used in regulation as a conservative indication of fuel failure, would be difficult. Heat-transfer correlations on which critical heat flux is determined are based on steady-state data and are not likely to apply well to rapid transients.

Attempts to model cladding failure for high-burnup fuel during rod-drop or rod-ejection accidents would be difficult and would probably not offer a good approach for regulatory assessment. This difficulty would be compounded by the fact that the failure mode would have to be known and mechanical properties would have to be measured for corresponding loading paths in irradiated cladding specimens. Therefore models like the strain–energy–density approach, which employ stress–strain data for various loading paths (axial tension, ring tension, and burst) and do not address different modes of failure, do not seem appropriate.[32]

CONCLUSIONS

Although the data base for reactivity transients with high-burnup fuel is small and the tests do not cover all the conditions of postulated accidents in LWRs, a number of important conclusions can be reached.

For reactivity transients, cladding failure caused by high temperature following DNB would occur only in very ductile cladding materials. Such failures have been seen only in tests with Zircaloy-clad fuel with nearly zero burnup and in Zr–1%Nb cladding used in Russian VVER fuel.

Because of the way plants are started up, the postulated reactivity accidents for both BWRs and PWRs would occur with coolant flowing through the core. Under those conditions, the onset of DNB would not occur until just above 100-cal/g fuel peak fuel-rod enthalpy, and cladding failure by overheating would not occur until well above that. This is significantly above the apparent failure threshold for PCMI for Zircaloy-clad fuel. Therefore DNB related failures are not expected for these reactivity accidents; this is in agreement with the observed PCMI failures seen in the tests.

LWR fuel with Zircaloy cladding fails by PCMI as the result of limited ductility. The PCMI failure threshold declines with increasing cladding oxidation and fluence because these processes progressively reduce cladding ductility. Cladding oxidation appears to be the more important of these two processes.

Zircaloy cladding that has a large accumulation of oxidation and has experienced spallation may contain hydride blisters and radially oriented hydrides. Such material exhibits very little resistance to PCMI failure. A similar effect might be expected for fuel rods with large gaps between pellets.

High-burnup fuel will experience pellet fragmentation and enhanced release of fission products during a reactivity transient. This is the result of the altered microstructure of high-burnup oxide fuel. Pellet fragments and fission products can be released into the coolant if the cladding fails.

Test conditions to date have not been prototypical, and this has had some effect on the results. The biggest effect is probably due to test temperature, which affects fracture toughness and ductility. A cold (20 °C) zero-power rod-drop accident is possible in a BWR, whereas a zero-power rod-ejection accident can only occur when a PWR is hot (>270 °C); tests have been performed one way or the other, and the results simply have been lumped together. The next biggest effect is probably due to pulse width. Pulse widths that are too narrow produce enhanced stresses in the cladding at a time when the cladding is cooler than it should be. Pulse widths may also introduce strain-rate effects, but the magnitude of such effects is not currently known.

Although the data trend is one of declining failure threshold with increasing cladding oxidation, the failure threshold for BWR and PWR high-burnup fuel should be approximately the same at around 100 cal/g fuel. This follows from making several observations about the trend line in Fig. 8. High-burnup PWR cladding may have 60 to 80 μm of uniform oxidation (without spallation), but the data trend line on that side of the figure was heavily influenced by tests conducted at room temperature. Because the PWR accident would be a hot accident, the failure threshold should be above the line. Conversely, BWR cladding does not develop as much uniform oxidation as PWR cladding, so attention should be focused on the left side of Fig. 8. This side of the trend line was influenced heavily by a high-temperature test. Because a cold BWR accident must be considered, the BWR threshold should be somewhat below the line. A more precise determination of failure threshold is probably not justified; the effects of corrosion nodules on BWR cladding have

not been tested at high burnup, there are large uncertainties in the existing data, and there is much variation in commercial cladding materials.

Realistic 3-D plant calculations have shown that fuel-rod enthalpies during rod-drop and rod-ejection accidents should not exceed 100 cal/g fuel. Because this is not greater than the approximate failure threshold, cladding failure should not occur for these accidents provided that fuel with spalling oxide or large pellet gaps is not present. With cladding integrity preserved, fuel fragments and fission products would remain within the fuel rods and should not have to be considered in the safety analysis for these accidents.

ACKNOWLEDGMENTS

Test data and photographs were provided by the Nuclear Protection and Safety Institute (IPSN, France), the Japan Atomic Energy Research Institute, and the Russian Research Centre (the Kurchatov Institute).

REFERENCES

1. U.S. Nuclear Regulatory Commission, *Reactivity Insertion Transient and Accident Limits for High Burnup Fuel,* NRC Information Notice 94-64, August 31, 1994.
2. D. J. Diamond and L. Neymotin, Analyzing the Rod Drop Accident in a BWR with High Burnup Fuel, in *Proceedings of the 1997 International Topical Meeting on Light Water Reactor Fuel Performance,* Portland, Oregon, March 1997, pp. 643-649, American Nuclear Society.
3. W. Wulff, H. S. Cheng, D. J. Diamond, and M. Khatib-Rahbar, *Description and Assessment of RAMONA-3B MOD.0 Cycle 4: A Computer Code with Three-Dimensional Neutron Kinetics for BWR System Transients,* Report NUREG/CR-3664 (BNL-NUREG-51746), January 1984. Documentation for RAMONA-4B has not yet been published.
4. S. Ray, D. H. Risher, B. J. Johansen, M. J. Hone, R. A. Holland, U. Bachrach, and G. E. Derylo, A Best-Estimate Assessment of Rod Ejection Fuel Duty in PWRs, in *Proceedings of the CSNI Specialist Meeting on Transient Behavior of High Burnup Fuel*, Report OCDE/GD(96)197, pp. 245-250, 1996.
5. C. L. Heck, R. A. Rand, G. A. Potts, J. F. Klapproth, R. Harrington, and J. G. M. Andersen, Realistic Evaluation of Reactivity Insertion Accidents in Boiling Water Reactors, in *Proceedings of the CSNI Specialist Meeting on Transient Behavior of High Burnup Fuel*, Report OCDE/GD(96)197, pp. 377-399, 1996.
6. L. J. Agee, A. F. Dias, L. D. Eisenhart, and R. E. Engel, Realistic Scoping Study of Reactivity Insertion Accidents for a Typical PWR and BWR Core, in *Proceedings of the CSNI Specialist Meeting on Transient Behavior of High Burnup Fuel*, Report OCDE/GD(96)197, pp. 291-304, 1996.
7. A. M. Garde, G. Smith, and R. C. Pirek, Effects of Hydride Precipitate Localization and Neutron Fluence on Ductility of Irradiated Zircaloy-4, in *Zirconium in the Nuclear Industry: 11th International Symposium,* ASTM STP 1295, pp. 407-429, G.P. Sabol (Ed.), American Society for Testing and Materials, Philadelphia, Pa., 1996.
8. H. M. Chung, F. L. Yaggee, and T. F. Kassner, Fracture Behavior and Microstructural Characteristics of Irradiated Zircaloy Cladding, in *Zirconium in the Nuclear Industry: 7th International Symposium,* ASTM STP 939, pp. 775-801, R. B. Adamson and L. F. P. Van Swam (Eds.), American Society for Testing and Materials, Philadelphia, Pa., 1987.
9. C. E. Beyer, D. D. Lanning, and L. J. Siefken, High Burnup Modeling Changes to NRC Fuel Performance Codes that Impact Reactivity Initiated Accidents, in *Proceedings of the CSNI Specialist Meeting on Transient Behavior of High Burnup Fuel*, Report OCDE/GD(96)197, pp. 533-549, 1996.
10. P. Menut, D. Lespiaux, and M. Trotabas, Cladding and Fuel Modifications of a 60-GWj/tM Irradiated Rod During a Power Transient Performed in the CABRI-Reactor, in *Proceedings of the CSNI Specialist Meeting on Transient Behavior of High Burnup Fuel*, Report OCDE/GD(96)197, pp. 127-135, 1996.
11. F. Schmitz, J. Papin, M. Heassler, and N. Waeckel, New Results from Pulse Tests in the CABRI Reactor, in *Proceedings of the Twenty-Third Water Reactor Safety Information Meeting*, Oct. 23–25, 1995, Report NUREG/CP-0149, Vol. 1 (CONF-9510156—Vol.1), pp. 33-43, March 1996.
12. F. Schmitz, C. Gonnier, and J. Papin, The Status of the CABRI Test Program Recent Results and Future Activities, in *Proceedings of the Twenty-Fourth Water Reactor Safety Information Meeting*, Report NUREG/CP-0157, Vol. 1, pp. 107-130, January 1997.
13. K. Ishijima, Y. Mori, T. Fuketa, and H. Sasajima, Postulated Mechanisms on the Failure of 50 MWd/kgU PWR Fuel in the NSRR Experiment and the Related Research Programs in JAERI, in *Proceedings of the CSNI Specialist Meeting on Transient Behavior of High Burnup Fuel,* Report OCDE/GD(96)197, pp. 87-105, 1996.
14. T. Fuketa, K. Ishijima, Y. Mori, H. Sasajima, and T. Fujishiro, New Results from the NSRR Experiments with High Burnup Fuel, in *Proceedings of the Twenty-Third Water Reactor Safety Information Meeting*, Oct. 23–25, 1995, Report NUREG/CP-0149, Vol. 1 (CONF-9510156—Vol.1), pp. 45-63, March 1996.
15. K. Ishijima and T. Fuketa, Progress of the RIA Experiments with High Burnup Fuels and Their Evaluation in JAERI, in *Proceedings of the Twenty-Fourth Water Reactor Safety Information Meeting*, Report NUREG/CP-0157, Vol. 1, pp. 93-105, January 1997.
16. B. A. Cook and Z. R. Martinson, *Reactivity Initiated Accident Test Series, Test RIA 1-4 Fuel Behavior Report*, Report NUREG/CR-3938 (EGG-2336), September 1984.
17. S. L. Seiffert, Z. R. Martinson, and S. K. Fukuda, *Reactivity Initiated Accident Test Series, Test RIA-1-1 (Radial Average Fuel Enthalpy of 285 cal/g) Fuel Behavior Report*, Report NUREG/CR-1465, EG&G Idaho, Inc., September 1980.
18. V. Asmolov and L. Yegorova, Development and Performance of a Research Program for the Analysis of High

Burn-Up Fuel Rod Behavior Under RIA Condition in the IGR Pulse Reactor, in *Proceedings of the CSNI Specialist Meeting on Transient Behavior of High Burnup Fuel*, Report OCDE/GD(96)197, pp. 155-165, 1996.

19. V. Asmolov and L. Yegorova, Recent View to the Results of Pulse Tests in the IGR Reactor with High Burn-Up Fuel, in *Proceedings of the Twenty-Third Water Reactor Safety Information Meeting*, Oct. 23–25, 1995, Report NUREG/CP-0149, Vol. 1 (CONF-9510156—Vol.1), pp. 65-80, March 1996.
20. V. Asmolov and L. Yegorova, Recent Results on the RIA Test in IGR Reactor, in *Proceedings of the Twenty-Fourth Water Reactor Safety Information Meeting*, Report NUREG/CP-0157, Vol. 1, pp. 131-139, January 1997.
21. P. E. MacDonald, S. L. Seiffert, Z. R. Martinson, R. K. McCardell, D. E. Owen, and S. K. Fukuda, Assessment of Light-Water-Reactor Fuel Damage During a Reactivity-Initiated Accident, *Nucl. Saf.*, 21(5): 582-602 (September–October 1980).
22. T. Fujishiro, K. Yanagisawa, K. Ishijima, and K. Shiba, Transient Fuel Behavior of Preirradiated PWR Fuels Under Reactivity Initiated Accident Conditions, *J. Nucl. Mater.*, 188: 162-167 (June 1992).
23. T. Nakamura, M. Yoshinaga, M. Sobajima, K. Ishijima, and T. Fujishiro, Boiling Water Reactor Fuel Behavior at Burnup of 26 GWd/tonne U Under Reactivity-Initiated Accident Conditions, *Nucl. Technol.*, 108(1): 45-60 (October 1994).
24. M. O. Marlowe, J. S. Armijo, B. Cheng, and R. B. Adamson, Nuclear Fuel Cladding Localized Corrosion, in *Topical Meeting on Light Water Reactor Fuel Performance*, Orlando, Fla., April 21–24, 1985, Report DOE/NE/34130-1-Vol.1 (CONF-850401—Vol.1), pp. 3.73–3.90.
25. R. S. Semken, S. Shiozawa, Z. R. Martinson, R. K. McCardell, P. E. MacDonald, J. A. Fernandez, and S. K. Fukuda, *Reactivity Initiated Accident Test Series, RIA Scoping Tests Fuel Behavior Report*, Report NUREG/CR-1360, April 1980.
26. B. A. Cook, S. K. Fukuda, Z. R. Martinson, and P. Bott-Hembree, *Reactivity Initiated Accident Test Series, Test RIA 1-2 Fuel Behavior Report*, Report NUREG/CR-1842, January 1981.
27. R. W. Miller, *The Effects of Burnup on Fuel Failure, Power Burst Tests on Fuel Rods with 13,000 and 32,000 MWd/MTU Burnup*, Report ANCR-1280, January 1976.
28. M. Sobajima and S. Katanishi, Effect of Cooling Conditions of Fuel Failure During Fast and Slow Power Transients, in *Proceedings of the 1st JSME/ASME Joint International Conference on Nuclear Engineering and Exhibition (ICONE-1)*, Tokyo, November 4–7, 1991, Report CONF-911135—Vol. 2, pp. 249-254.
29. G. P. Smith, Jr., R. C. Pirek, H. R. Freeburn, and D. Schrire, *The Evaluation and Demonstration of Methods for Improved Nuclear Fuel Utilization*, Report DOE/ET/34013-15 (CEND-432), August 1994.
30. C. E. Coleman, B. A. Cheadle, A. R. Causey, P. C. K. Chow, P. H. Davies, M. D. McManus, D. K. Rogers, S. Sagat, and G. van Drunen, Evaluation of Zircaloy-2 Pressure Tube from NPD, in *Zirconium in the Nuclear Industry: 8th International Symposium*, ASTM STP 1023, pp. 35-49, L. F. P. Van Swam and C. M. Eucken (Eds.), American Society for Testing and Materials, Philadelphia, 1989.
31. T. M. Link, A. T. Motta, and D. A. Koss, On the Issue of Zircaloy Ductility During a Reactivity-Initiated Accident, in *Proceedings of the Twenty-Fourth Water Reactor Safety Information Meeting*, Report NUREG/CP-0157, Vol. 1, pp. 141-149, January 1997.
32. R. O. Montgomery and Y. R. Rashid, *Evaluation of Irradiated Fuel During RIA Simulation Tests, Final Report*, Report EPRI-TR-106387, Electric Power Research Institute, August 1996.

French Studies on High-Burnup Fuel Transient Behavior Under RIA Conditions

By J. Papin, M. Balourdet, F. Lemoine, F. Lamare, J. M. Frizonnet, and F. Schmitz[a]

Abstract: *The Institute for Protection and Nuclear Safety (IPSN) approach to study high-burnup fuel behavior under reactivity-initiated accidents led to initiation of the CABRI REP-sodium (Na) experimental program and related support studies together with the development of the SCANAIR code. High-burnup effects, such as significant contribution of fission gases to early pellet–clad mechanical interaction loading, have been quantified, and fuel fragmentation, high fission gas release, and occurrence of transient oxide layer spallation have been highlighted. Validation of the SCANAIR code on the CABRI REP-Na tests and on the HBO-1 test at the Nuclear Safety Research Reactor has shown satisfying results. The extrapolation to reactor conditions, however, has underlined the need for more knowledge in the fields of clad mechanical properties (PROMETRA tests), cladding-to-coolant heat transfer (PATRICIA tests), and fission gas behavior, including the initial state of the rods, to allow for a reliable predictive capability.*

The evolution of the fuel management system in French pressurized-water reactors (PWRs), aimed at increasing the burnup up to 52 MWd/kgU, and the absence of an experimental basis for mixed-oxide (MOX) fuel rods have motivated the Institute for Protection and Nuclear Safety (IPSN) to initiate new studies, particularly in the framework of reactivity-initiated accidents (RIAs), such as control-rod ejection. This type of accident can produce energy injections of a duration of several tens of milliseconds in the fuel rods neighboring the ejected control-rod assembly and thus induce a rapid and significant increase of fuel enthalpy.

Up to the early 1990s, the available experimental data base [Special Power Excursion Reactor Test (SPERT), Power Burst Facility (PBF), and Nuclear Safety Research Reactor (NSRR) tests] has been restricted to fresh or low irradiated fuel (up to 30 MWd/kgU with UO_2) and has served as a basis for the establishment of the safety criteria considering that, for irradiated fuel, independently of the burnup level, an enthalpy limit of 200 cal/g fuel can guarantee the reactor safety against the risk of fuel dispersion into the coolant with a sufficient safety margin.

Specific aspects of the high irradiation level, however, may affect the fuel-rod behavior under RIA transients such as the following:

- The high fission gas retention of PWR fuel (1.6 cm^3/g at an average burnup of 60 MWd/kgU) linked to small release in operating conditions, which can lead, under overpower conditions, to fuel overpressurization and swelling and thus to strong pellet–clad mechanical interaction (PCMI) in the early phase of the transient.
- The important level of clad corrosion with possible high local hydrogen concentration caused by oxide spalling, which severely degrades the clad mechanical properties.
- The presence of the "rim" zone in the pellet periphery with high porosity and high local gas content and a very fine-grained structure (at mean burnup above 40 MWd/kgU).

These points underline the potential for early rod failure, which has been first confirmed by the NSRR experiments JM4 and JM5 in Japan, giving a clear indication of the PCMI failure mode and of reduction of the failure enthalpy threshold compared with fresh fuel.

Moreover, in the absence of early rod failure, the high gaseous retention inside the fuel can also enhance the internal pressure buildup after gas release with potential for clad ballooning after a clad temperature increase in the late phase of the transient caused by heat removal from the fuel to the cladding and coolant.

These considerations led to the initiation of the present in-pile CABRI REP-Na program performed with sodium coolant and focused on the study of the PCMI during the first phase of the power transient when clad–coolant heat exchange has a minor effect.

[a]Institute for Protection and Nuclear Safety, Cadarache, Commissariat à l'Energie Atomique, 13108 St. Paul Lez Durance, France.

This program is carried out in collaboration with Electricité de France (EdF) and with the financial participation of the U.S. Nuclear Regulatory Commission (NRC).

In parallel, IPSN is developing the SCANAIR code with the aim to predict the fuel-rod behavior under RIA transients in reactor conditions, especially for high-burnup fuel, on the basis of the physical knowledge gained through the CABRI REP-Na program and other experiments, such as NSRR tests available under the Japan Atomic Energy Research Institute (JAERI)/IPSN agreement. Additional out-of-pile support studies have also been undertaken to provide the necessary data base for implementation into the SCANAIR code. They concern the investigation of cladding transient mechanical properties and of cladding-to-coolant heat transfer under rapid heating.

In this article the CABRI REP-Na program and its main outcome, the SCANAIR code and its validation status, and the ongoing support studies together with a first extrapolation study of reactor conditions are presented.

THE CABRI REP-Na PROGRAM

General Characteristics

The transient rod behavior may be affected by the initial conditions from the base irradiation and by the pulse characteristics through several factors. Depending on the burnup and on the elevation along the fuel rod, corrosion of the cladding leads to hydrogen and oxygen buildup in the Zircaloy and thus results in altered mechanical properties with reduced ductility, especially under fast ramps; severe embrittlement may arise from the local accumulation of hydride precipitates following spalling of the outer oxide layer.

The burnup-dependent fission gas retention is the driving force of transient fuel swelling and thus of increased PCMI. Also, the rim effect increases strongly with burnup: the fine-grained and highly porous outer fuel zone with enhanced plutonium production and high fission gas content influences PCMI (see page 304). Fuel behavior, and hence clad loading, is affected by the ramp rate also through thermal and mechanical conditions. Nevertheless, even in case of slow RIA transients, the time scale of the transient and particularly of the heating phase with strong PCMI is too short to induce a cushioning effect of the rim, as observed in incidental transients (slow ramps of several minutes).

Finally, the transient response of MOX fuel must be studied: Because of the fabrication process, the major part of fissile material and subsequently the fission products are concentrated within small agglomerates of about 20-μm mean diameter (but much higher sizes are not infrequent) and of 30% Pu/M initial enrichment; this heterogeneity is smoothed down to some degree during the base irradiation because of the plutonium burning and fission-product recoil effect on one side and of the production of ^{239}Pu from neutronic capture by ^{238}U on the other side. Differences in the microstructure and the fission gas distribution still exist, however, as compared with standard uranium fuel, and may lead to a peculiar behavior, especially under fast ramp transient conditions.

Therefore the following parameters are considered in the test matrix (Table 1):

- The fuel burnup: either low (33 MWd/kgU without any rim formation) in REP-Na2, which provides a link to the international data base on RIAs; medium (53 MWd/kgU with about 100-μm rim thickness) in REP-Na3, which corresponds to the current base irradiation of four cycles; or high (64 MWd/kgU with about 200-μm rim thickness) in REP-Na1, REP-Na4, and REP-Na5, which corresponds to the target burnup after five cycles.
- The clad corrosion: either negligible (4-μm outer oxide thickness) in REP-Na2 caused by the Belgian reactor conditions (BR3), small (20 μm) in REP-Na5 in which a second span was used, medium (40 μm) in REP-Na3, high (80 μm) in REP-Na4 in which a fifth span was used, and high with more or less spalling in REP-Na1 and REP-Na8.
- The fuel type: REP-Na6, REP-Na7, and REP-Na9 aim at testing MOX fuel irradiated during three, four, and two cycles, respectively.
- The energy deposition: from about 100 cal/g fuel in most experiments to more than 200 cal/g fuel in REP-Na2.
- The pulse width: either short (9 to 10 ms) in REP-Na1, REP-Na2, REP-Na3, and REP-Na5 or broad (about 40 ms) in all other tests.

Except for REP-Na2, in which an entire BR3 rod with only a modified plenum pressure (0.1 MPa of helium) is used, all experiments are carried out with EdF rods, which must be adapted to dimensions compatible with CABRI: in the reconditioning process, a given span with adjoining grid regions is cut off from the parent rod; equipped with hafnium plugs, spring,

Table 1 Characteristics and Results of REP-Na and NSRR Tests with Commercial PWR Rods

	CABRI-REP (Flowing sodium at 0.5 MPa and 280 °C)							
Test	**REP-Na1**	**REP-Na2**	**REP-Na3**	**REP-Na4**	**REP-Na5**	**REP-Na6**	**REP-Na7**	**REP-Na9**
Fuel type	UO_2	UO_2	UO_2	UO_2	UO_2	MOX	MOX	MOX
Initial enrichment,[a] %	4.5	6.85	4.5	4.5	4.5	5.925	5.948	6.559
Internal pressure, MPa	0.1	0.101	0.31	0.301	0.302	0.302	0.3	*b*
Active length, mm	569.0	1000.0	440.0	567.6	563.5	553.5	554.2	*b*
Maximum burnup, MWd/kgU	63.8	33.0	52.8	62.3	64.3	47.0	55.0	28.0
Corrosion thickness,[c] μm	80.0 Spallation	4.0	40.0	80.0	20.0	40.0	50.0	12.0[d]
Energy deposition,[e] cal/g fuel (J/g)	110 (460.0)	211 (882.0)	120 (502.0)	97 (404.0)	105 (439.0)	165 (690.0)	175 (732.0)	228 (953.0)[d]
Pulse width, ms	9.5	9.5	9.5	64.0	9.0	~35.0	~40.0	~40.0
Peak fuel enthalpy, cal/g fuel (J/g)	115 (481.0)	209 (876.0)	125 (522.5)	96 (403.0)	115 (481.0)	145 (606.0)[d]	150 (628.0)[d]	200 (836.0)[d]
Maximum mean hoop strain, %	Early failure [30 cal/g (125 J/g)]	3.5	2.1	0.37	1.11	3.1	Failure [120 cal/g (501 J/g)]	*b*
Fission gas release, %		5.54	13.7	8.3	15.1	21.6		*b*
Helium release, mm^3/g		9.53	35.7	38.2	43.1	34.45		*b*
Helium released/(Xe + Kr) formed,[f] %		1.28	2.48	2.27	2.46	3.0		*b*

[a] $^{235}U/U$ for UO_2, Pu / (U + Pu) for MOX.
[b] Not yet available.
[c] Maximum value.
[d] Preliminary results.
[e] For fast ramps at 0.4 s. For slow ramps at 1.2 s.
[f] Calculated on total fissile length.

and end caps; and filled with new gas (0.3 MPa of helium except for REP-Na1, which has 0.017 MPa of xenon and 0.083 MPa of helium). The resulting test rod, with about 0.6-m fissile length, undergoes checks and nondestructive examinations (leak test, radiography, gamma spectrometry, eddy-current inspection of the clad soundness, eddy-current measurements of the outer oxide thickness, diameter measurements, and visual inspection); these, in addition to knowledge of the parent rod, help characterize the pretest condition.

Power excursion experiments are carried out in the CABRI reactor of the IPSN in Cadarache, France; the reactor has been used for years for testing fast breeder reactor (FBR) pins under transient overpower and coolant coastdown conditions. The single test rod is inserted into a test section where it is surrounded by a Zircaloy shroud [inside diameter (ID) × outside diameter (OD) = 14.2 × 17.2 mm], which is placed in the sodium loop in the center of the driver core with 0.8-m fissile height.

Initial conditions in the channel with 280 °C temperature and 4-m/s coolant velocity are intended to simulate hot zero power operation in a commercial reactor (except for the pressure level, which is 0.5 MPa at the inlet). Thermal neutrons, hence with a radial flux depression, are delivered to the test rod by the light-water CABRI driver core, which can be controlled by hafnium rods. Transient reactivity insertions can be triggered by voiding ^3He reservoirs.[1]

Many on-line diagnosis capabilities are provided by the CABRI facility which allow assessment of the sequence of events. The driver core power is measured by fission chambers; fuel motions, such as fissile stack elongations or important dispersals, can be detected by the hodoscope (a battery of neutron detectors aimed at the test rod); thermal and hydraulic conditions in the coolant channel can be measured by the test section instrumentation (Fig. 1). The following pieces of information can be gathered:

- Temperatures at several axial positions (thermocouples).
- Inlet and outlet sodium flow rates (flowmeters).
- Channel pressures below and above the rod (pressure sensors).
- Acoustic events allowing trace of the time and location of rod failure with an uncertainty of ±0.25 ms (microphones).

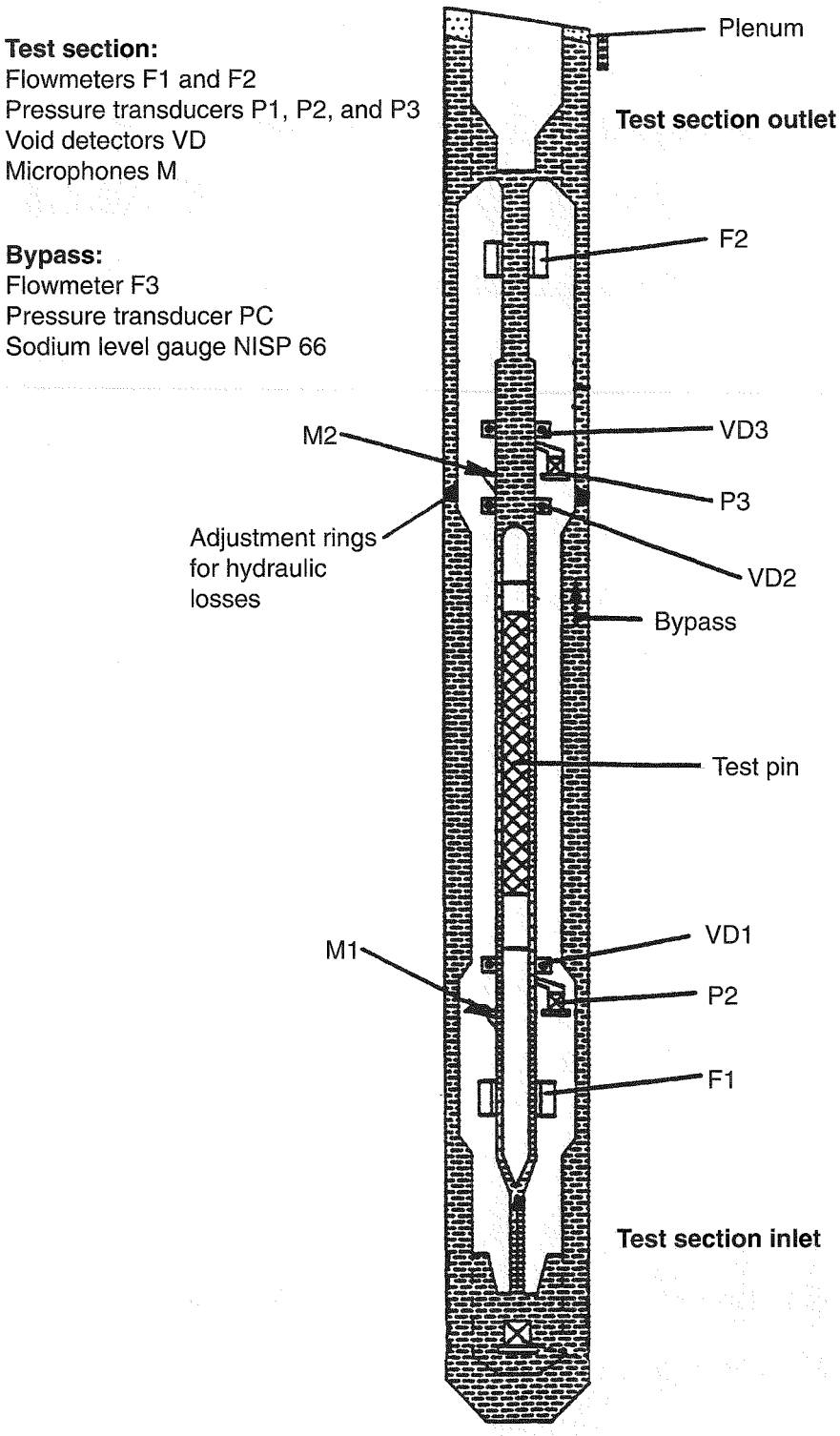

Fig. 1 Sketch of the CABRI test section with bypass and instrumentation.

- Rod elongation (displacement transducer).
- Channel voiding at the outlet (void detector).

Before the test the neutronic coupling factor between the core and rod power is determined, as well as the axial profile, during steady-state runs at reduced power levels. Transient linear powers are then deduced from the transient core power, as measured by fission chambers with the use of the coupling factor and the axial profile previously established. The energy input is thus determined within ±4% relative accuracy; the precision on timing is ±250 μs. Obviously, enthalpy values can only be estimated through code calculations. After the test indications on the final fuel mass distribution (elongation and dispersal) are given by the hodoscope during a low-power run.

In addition to hodoscope information, a first assessment of the final state is obtained by nondestructive examinations performed on the CABRI site before and after the test: X-ray, and sometimes neutron, radiography and gamma spectrometry give hints on geometrical changes and material redistributions. These serve as a basis for defining further, more-detailed, examinations.

Posttest examinations (PTEs) are carried out in hot cells of Commissariat à l'Energie Atomique (CEA)-DRN, mostly in Cadarache.[2] They are intended to provide qualitative and, if possible, quantitative information on phenomena of interest, principally PCMI and gas release. In case of rod failure (e.g., REP-Na1), PTEs consist of metallographic examinations, but in most cases nondestructive examinations can be performed with the following results from various techniques:

- Surface condition observed by visual inspection.
- Rod deformations measured by diameter measurements along several generating lines.
- Outer oxide thicknesses measured by eddy-current testing along several generating lines.
- Axial redistributions of materials estimated by gamma spectrometry.
- Cladding soundness or defects detected by eddy-current inspection.

These are supplemented by destructive examinations:

- Overall gas release rate and free plenum volume measured by rod puncturing, gas collecting, and analysis.
- Fuel and cladding structures observed, at 10 to 500 magnification, by optical microscopy of polished samples (radial and axial cuts).
- Fuel and cladding structures observed, possibly at a higher magnification and with high field depth, by fractography and scanning electron microscopy (SEM).
- Concentrations and distributions of fission products (xenon and neodymium) and other elements (uranium, plutonium, and cladding constituents) by electron probe microanalysis (EPMA).

These results are to be compared with the reference condition resulting from the base irradiation, as predicted by fuel behavior codes such as METEOR[3] and as observed by postirradiation examination (PIE) of a sibling rod or of another portion of the parent rod.

Main Outcome from CABRI Experiments

With the first five tests with uranium oxide fuel, four main features from PTE have been identified as most relevant to the understanding of transient rod behavior:

1. Response of the cladding (deformation and failure).
2. Fission gas release.
3. Fuel fragmentation and other structure changes.
4. Transient spalling.

However interesting they may be, postfailure phenomena are not considered in detail in this article because of lack of representativity of the sodium coolant.

Response of the Cladding. On every unfailed rod, the measured permanent hoop strains follow the axial power profile in CABRI but with differences in the magnitude and distribution (Table 1). The highest deformation has been recorded after REP-Na2 with up to 3% at midpellet locations and 4.1% between pellets (Fig. 2). It is the only instance where primary ridges have considerably increased (more than 50 μm radially), which gives evidence of strong PCMI with hourglass-shaped pellets; it is also the only case in which fuel pellet dishings (free volume at upper and lower pellet faces) have been completely filled up (Fig. 3). Primary ridges have been preserved during REP-Na4, but the peak deformation is small anyway (0.4%).

Conversely, primary ridges have been erased during REP-Na3 as the result of PCMI loading by pellets that have assumed a barrel shape as a consequence of the temperature field. Depending on the azimuth considered, the maximum deformation varies between 1.3 and 2.6%. Similar ovalizations with an axially constant

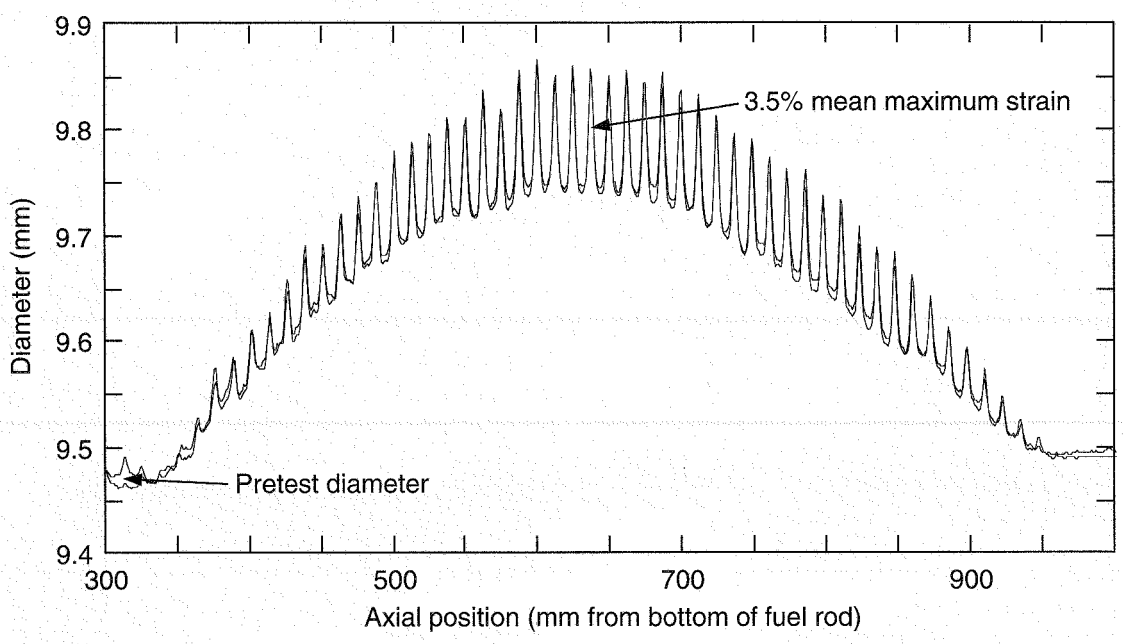

Fig. 2 REP-Na2 profilometry along 2 diameters showing hourglass-type PCMI.

orientation have been observed after REP-Na5 (Fig. 4) and REP-Na6. These last two tests led to mixed results with indications of both hourglass- and barrel-type interactions at the same axial position. Initial ridges have been kept everywhere except toward the azimuths with maximum deformation in peak power regions; here the deformation peaks at midpellet.

Except after REP-Na1, no crack has been observed in the cladding; also, no hint of a defective cladding has been detected by eddy-current inspection. Transient cracking and spalling of the outer oxide is discussed later in this report. The mean hydrogen content in the cladding remains unaffected by tests: concentrations measured after REP-Na1 and REP-Na3 are consistent with values of the pretest oxide thickness in view of the current relationship established on many PWR rods.

A particular feature is the modified hydride structure. The drastic redistribution with radially oriented hydride platelets, which occurred during REP-Na1, can be explained by the high temperatures experienced after rod failure, channel voiding, and dispersal of hot materials; however, limited redistributions took place also during nonfailure tests, especially in the outer third of the REP-Na5 cladding (Fig. 5) in spite of colder temperatures; here the stress field might be responsible.

Concerning UO_2 fuel, rod failure occurred only during REP-Na1 at a low level of energy input (about 15 cal/g fuel at peak power locations corresponding to 30 cal/g fuel pellet averaged enthalpy) [i.e., very early when the cladding was only slightly above 280 °C (Ref. 1)]. After the test, the rod appeared to be opened over the whole fissile length by several longitudinal cracks hinting at brittle behavior (Fig. 6). This has been confirmed on many transverse sections showing through-wall cracks running mostly perpendicular to the surface; in contrast with NSRR results in Japan in tests HBO-1 and HBO-5, there are only sparse examples of ductile shear. The failure hoop strain, roughly estimated from clad circumferences on these radial cuts, seems to be negligible. At several locations, sunburst-like hydride accumulations were found in the outer third of the clad thickness with many cracks from the outside, which suggests that failure was initiated in one of those accumulations (Fig. 7). SEM observations of cracks (Fig. 8) give evidence of clearly brittle aspects with cleaved hydrides at least in the outer clad layer and also toward the inner surface. Depending on the sample, a zone with shallow dimples may be found in which, at a higher magnification, brittle regions seem to be surrounded by ductile ligaments. These results suggest that crack propagation occurred by cleavage of hydrides ahead of the main crack tip. The presence of any defect (e.g., preexisting cracks) other than hydride accumulations can be excluded on the basis of pretest examinations.

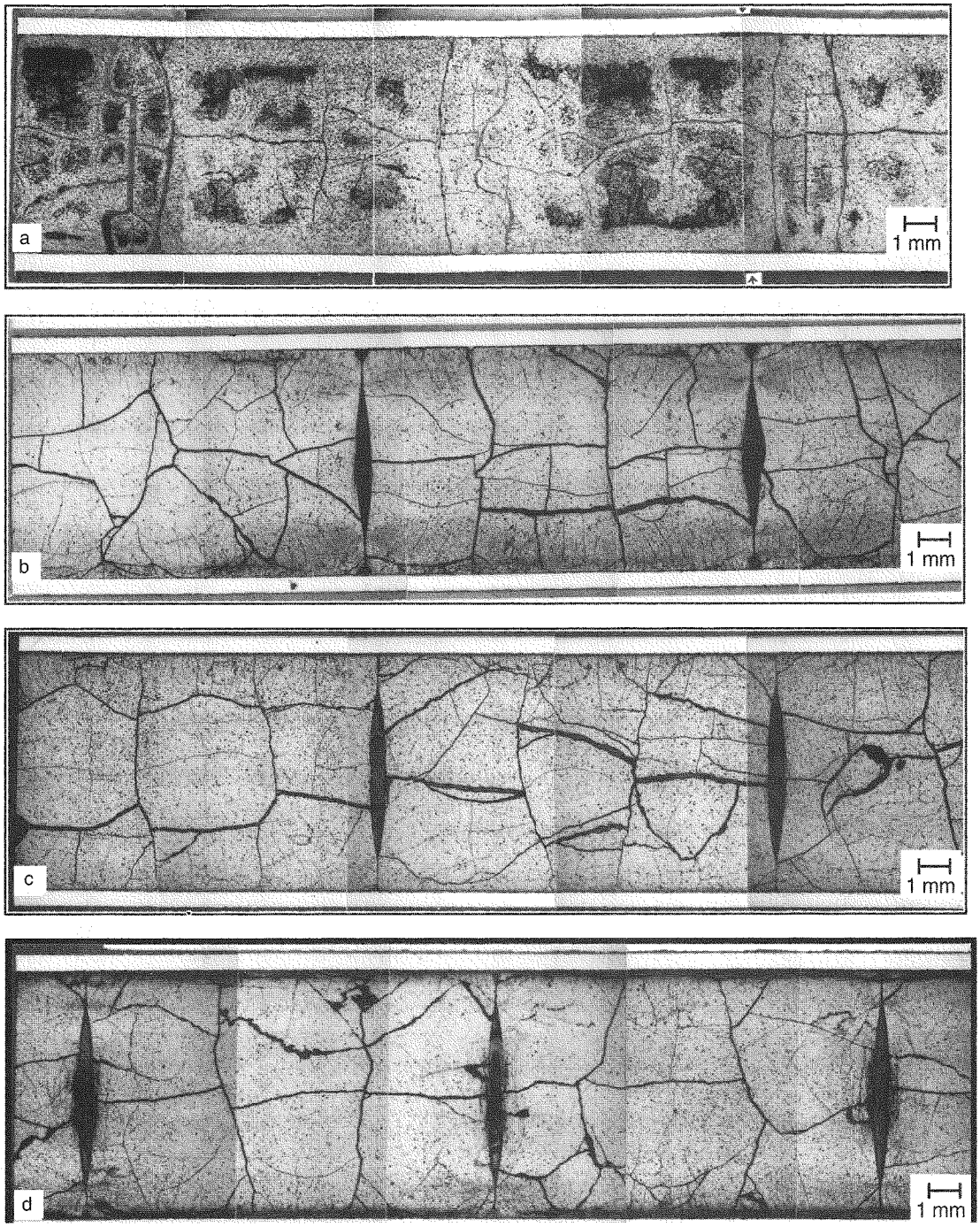

Fig. 3 Optical micrographs of axial cuts near peak power position: (a) REP-Na2, (b) REP-Na3, (c) REP-Na4, and (d) REP-Na5.

With MOX fuel, rod failure occurred during the REP-Na7 test while the energy deposition was 110 cal/g fuel, which led to a maximum average pellet enthalpy of 120 cal/g fuel. The analysis of the test is

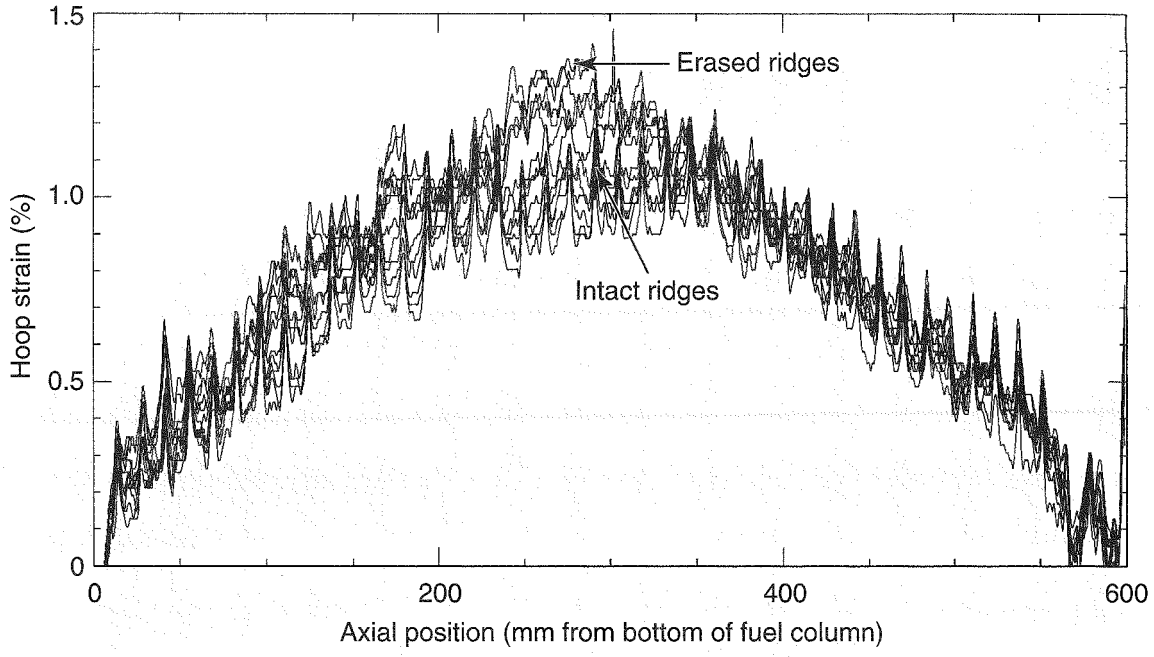

Fig. 4 REP-Na5 profilometry along 12 diameters showing hourglass- as well as barrel-type PCMI.

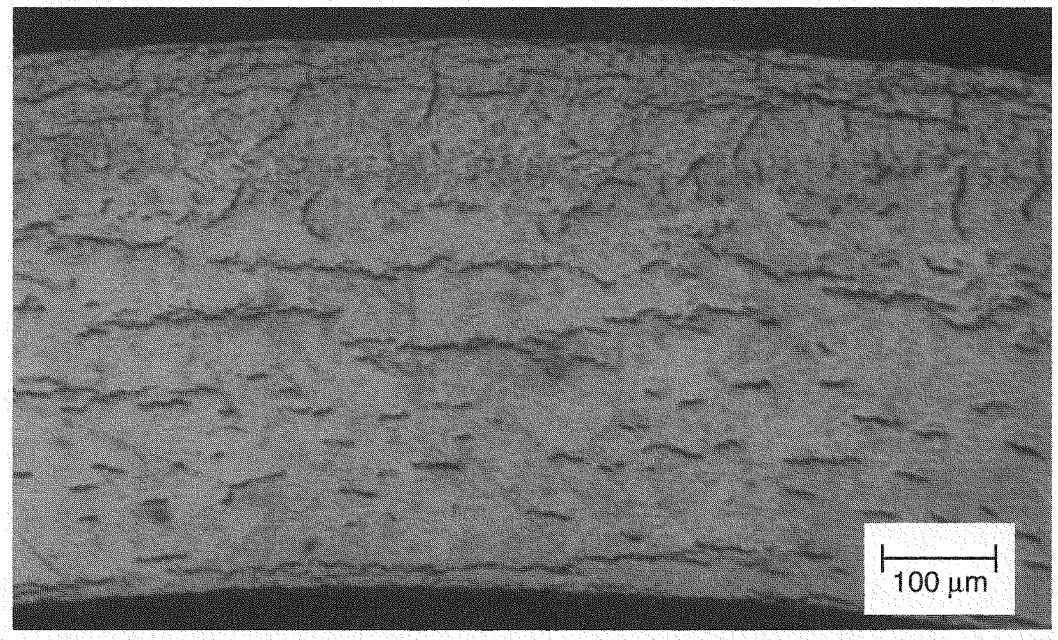

Fig. 5 REP-Na5 cladding with partial hydride redistribution.

still under way; however, note that, in contrast with REP-Na1, the cladding should not be affected by any defect caused by hydride accumulation as deduced from pretest examinations (neutronography).

Fission Gas Release. During the base irradiation, little fission gas is released, about 2% from UO_2 fuel after five runs or after only three runs from MOX fuel. Much higher values have been measured after CABRI

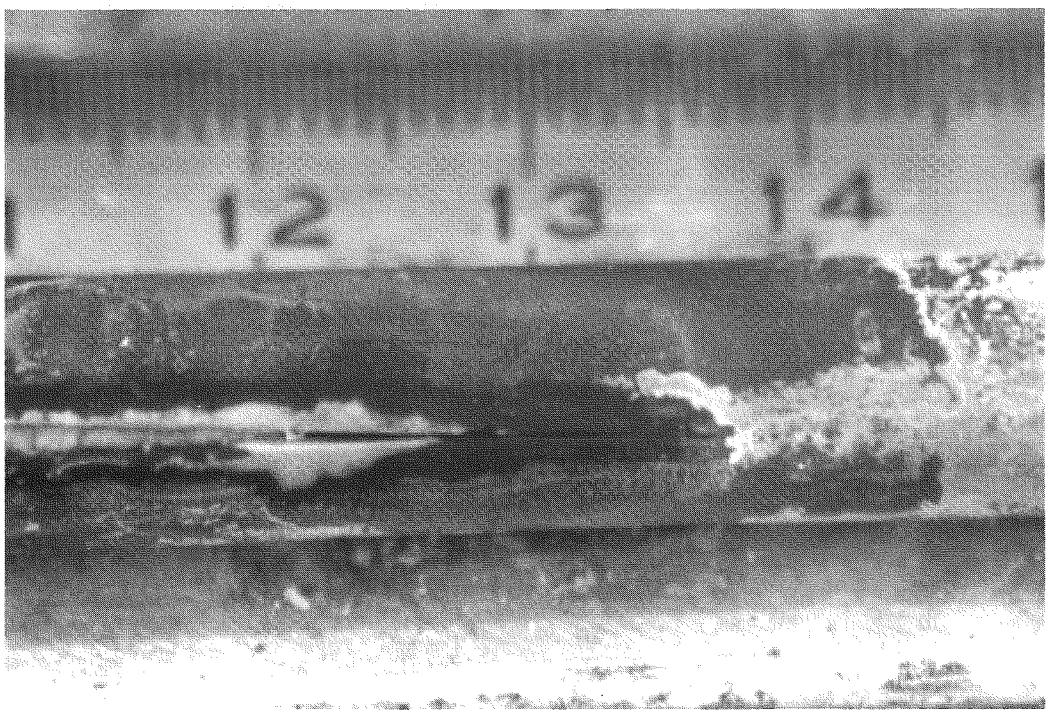

Fig. 6 Visual inspection of the REP-Na1 test rod near 500 mm/bfc with longitudinal crack in the cladding.

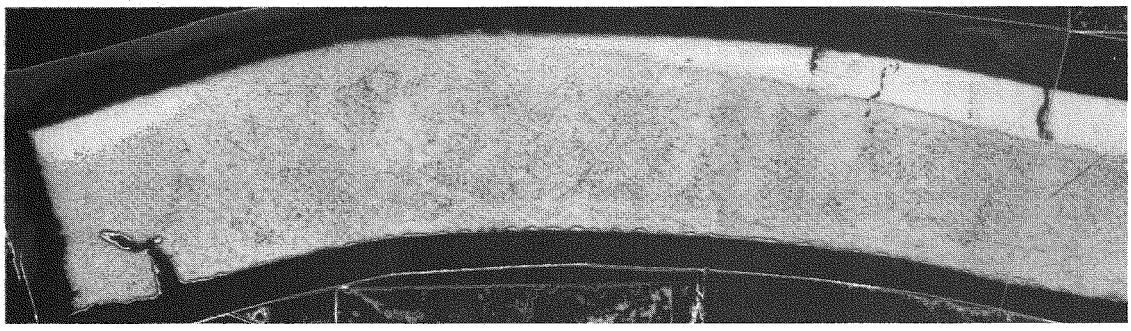

Fig. 7 REP-Na1 cladding at 168.5 mm/bfc with through-wall crack and hydride accumulations.

experiments (Fig. 9): about 13 to 15% for REP-Na3 and REP-Na5, respectively. Roughly speaking, transient fission gas release (FGR) rates seem to increase with burnup for a given fuel enthalpy as observed with NSRR too.[4] This hints at an important contribution from the rim region. REP-Na2 led to the lowest FGR, less than 6% in spite of twice the energy injection of other REP-Na tests with UO_2. Compared with REP-Na5, REP-Na4 with an intermediate FGR (8%) illustrates the influence of the pulse width (i.e., of the radial temperature distribution in the fuel and also of the clad deformation). From free volume measurements, it appears that closed pores were fully opened after REP-Na5 and only partly opened after REP-Na4. The REP-Na6 FGR (22%) is much stronger because of the higher peak fuel enthalpy, which could be attributed to the contribution from gas retained within the highly porous agglomerates.

In addition to the classical release of the fission gases xenon and krypton, an unexpected helium release was observed in the CABRI nonfailure tests (Table 1), which leads to the conclusion that a significant quantity of helium is trapped in the irradiated fuel. Helium in nuclear fuel results from two sources:

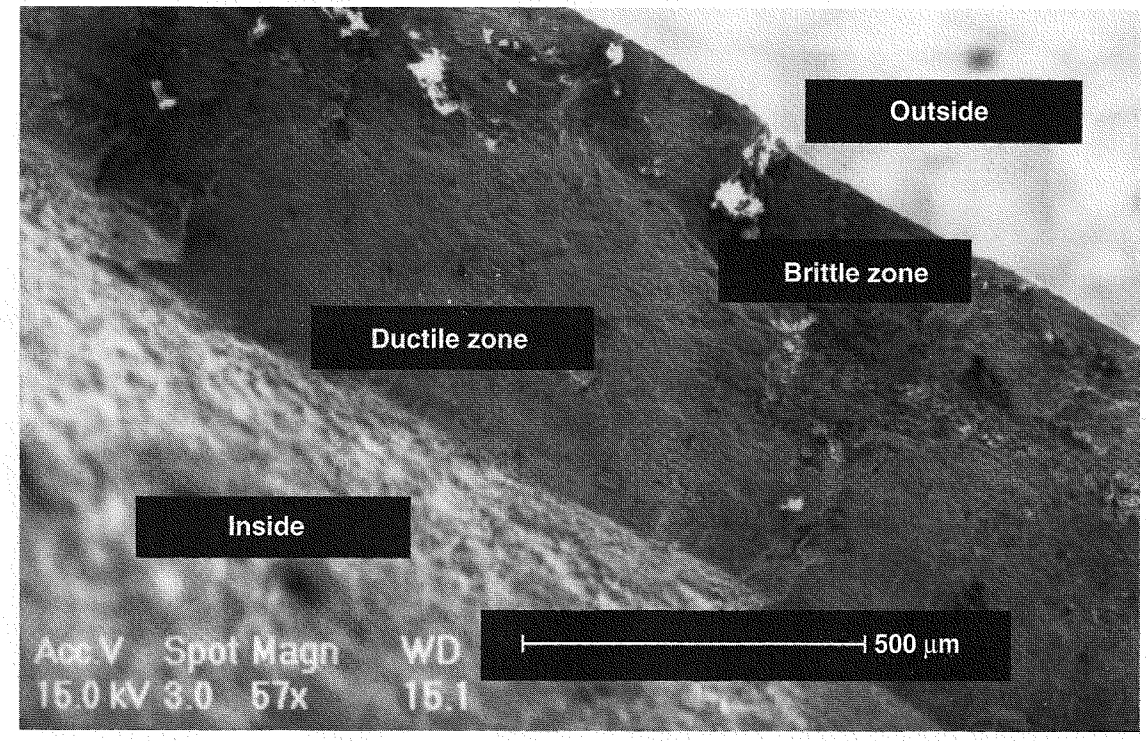

Fig. 8 Scanning electron microscopy examination of fracture surfaces in REP-Na1.

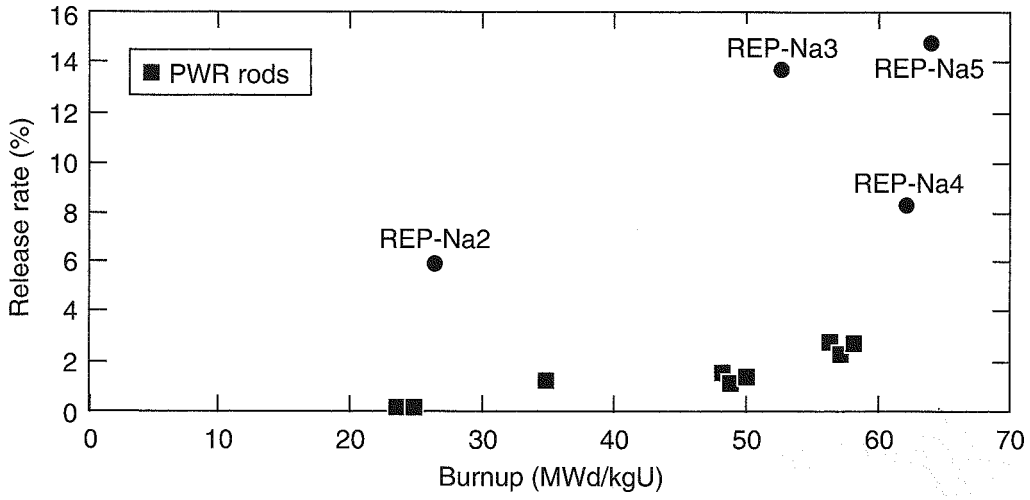

Fig. 9 Transient fission gas release rates in CABRI compared with release rates during PWR base irradiations.

(1) the filling gas and (2) production by ternary fissions, alpha-decay of heavy nuclides, and (n,α) reactions. The usual range of production in UO_2 is estimated to be 1 to 2% of the fission gas production. In high-burnup UO_2 fuel (~63 MWd/kgU), this leads to a value between 17.5 and 35 mm^3/g, lower than the helium release measured in REP-Na4 and REP-Na5. Thus some part of the helium contained in the fuel could originate from the filling gas because of implantation and diffusion processes via gap and cracks and the relatively important mobility of helium during reactor operating conditions. This assumption is

consistent with the quasi-systematically lower amount of helium measured after puncturing of the irradiated pin, as compared with the initial content deduced from the filling conditions (pressure and temperature) and from the calculated free volume. Helium reentry in the fuel has some impact on the plenum pressure evolution, even if this last one is not well-known because of the high uncertainty in the helium filling (about 15%).

Helium release in RIA could have some influence on the fuel-rod thermal behavior because its conductivity is better than that of the fission gases xenon and krypton, and it could contribute to the rod inner pressure increase (about 15% from the results of REP-Na4, REP-Na5, and REP-Na6). It is not taken into account in the present modeling because of insufficient knowledge of the base irradiation. Nevertheless, the volume of helium contained in the fuel is in the range of the fission gas release volume occurring during normal operating conditions and becomes significant in high-burnup fuel. Thus production and reentry of the filling helium should be considered.

Fuel Fragmentation and Other Structural Changes. Fuel de-densification is evidenced after all CABRI tests are completed by the observation of various cracks and of the grain boundary opening; the latter gives way to a darker ring or layer on optical macrographs of transverse (Fig. 10) or longitudinal (Fig. 3) sections cut in the peak power region.

A specific fragmentation aspect appears on radial cuts (Fig. 10). Indeed, in the case of REP-Na3, REP-Na4, and REP-Na5, two crack patterns can be recognized: (1) the main thick radial cracks crossing the whole pellet, probably as a result of the base irradiation; and (2) smaller and numerous radial cracks initiated from the periphery. These are caused by the test, and their lengths vary from roughly 400 μm in REP-Na3 to 3 mm in REP-Na4. These differences are related to the mechanical characteristics of the fuel and to the pulse parameters. Moreover, circumferential cracks are suspected on REP-Na3 and REP-Na5. Their presence, as shown later, is confirmed by micrographs. First results on MOX fuel with REP-Na6 (part e of Fig. 10) do not differ significantly from those of UO_2 rods. Crack patterns, especially, are intermediate between those of REP-Na4 and REP-Na5 (parts c and d of Fig. 10).

Concerning the REP-Na2 fuel, the radial macroscopic morphology observed is very different from the other tests. Only three main radial cracks about 3 mm long are initiated from the pellet center, and a sort of circular embrittled boundary where oxide grains have been separated appears, its diameter accounting for about 85% of the pellet diameter.

Axial cuts also exhibit, at the fuel periphery of REP-Na3, REP-Na4, and REP-Na5, thin radial cracks in addition to the main classical ones (Fig. 3). Moreover, in the case of REP-Na5, streamline fractures are noticed at the vicinity of the dishes, and at pellet contact locations the presence of another pattern of small cracks with several orientations is guessed. These features, already mentioned in similar works,[5] also exist on the REP-Na3 axial cut, but they are less distinct.

On REP-Na2 (part a of Fig. 3), fuel swelling produced by a high level of energy deposit is well pointed out since the dishes are completely filled. The presence of separated grain zones inside the pellets, previously observed on the radial cut, is confirmed.

Modifications of the grain structure are better investigated by optical microscopy (Fig. 11). First, for the completion of the fuel fragmentation description, micrographs taken on the REP-Na3 and REP-Na5 pellet edges (parts b and d of Fig. 11) clearly reveal the presence of circumferential cracks. Concerning more specifically the oxide microstructure at the periphery, a feature common to all tests except REP-Na4 is detected: it is the occurrence of grain separation or, in other words, the opening of grain boundaries. In the REP-Na2 test, this phenomenon occurs mainly according to a preferential radial orientation, whereas in REP-Na3 and above all in REP-Na5, the openings seem to follow a preferential tangential orientation. In REP-Na2, the whole radius is affected, whereas in REP-Na3 and REP-Na5 this event stays located inside the outer rings, 0.8 and 0.4 mm in thickness, respectively. For REP-Na4, micrographs of the periphery do not suggest drastic microstructural evolution, no grain separation is detected, and the porous so-called rim zone seems to have kept its integrity.

Concerning the rim zone, thickness values have been estimated in the first place from optical micrographs (Table 2). As expected with low-burnup MOX fuel, no optical rim could be observed on REP-Na6 samples. In view of the uncertainties, no great thickness variations generated by the CABRI test seem to be observed in comparison with those observed after PWR irradiation for identical burnups.[6] It is even worth underlining the presence of azimuthal inhomogeneity in these measurements and hence the wide range of results.

The investigation was then carried on at a microscopic scale by SEM examination and focused on

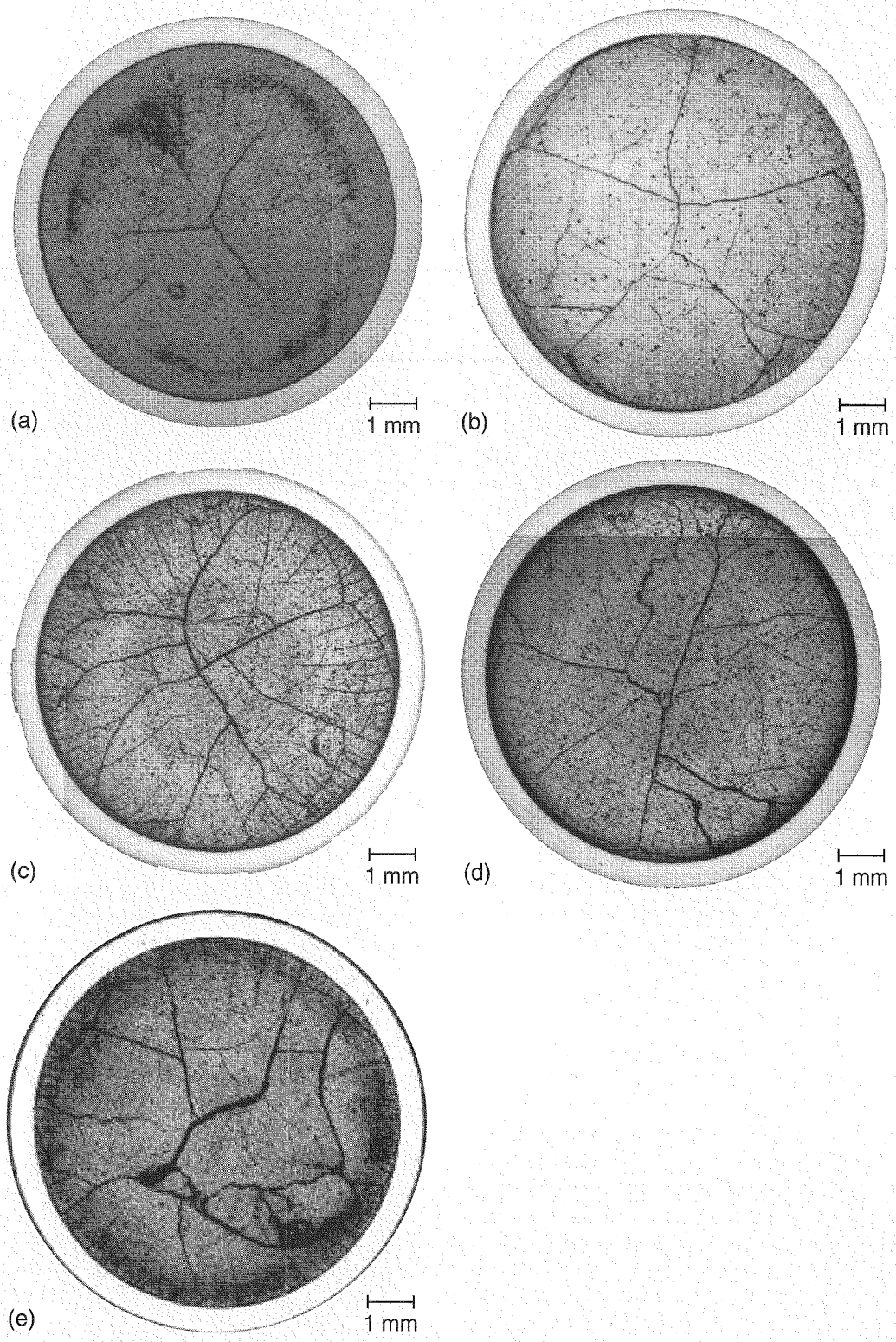

Fig. 10 Optical macrographs of radial cuts at peak power location (a) REP-Na2, (b) REP-Na3, (c) REP-Na4, (d) REP-Na5, and (e) REP-Na6.

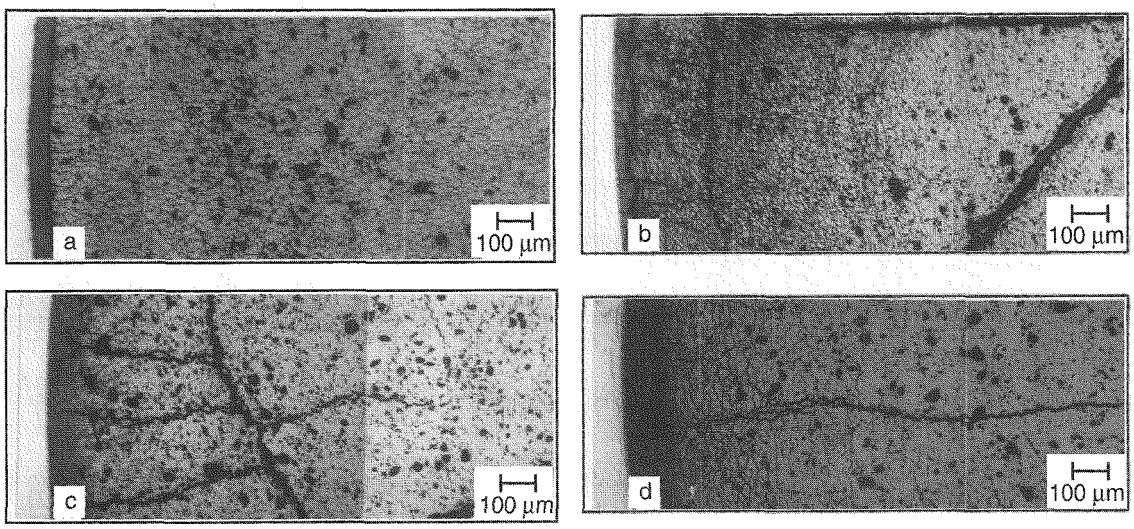

Fig. 11 Optical micrographs of radial cuts at peak power location: (a) REP-Na2. (b) REP-Na3. (c) REP-Na4. (d) REP-Na5.

Table 2 Optical Rim Thickness Assessments

Test rods	Rim size, μm
REP-Na2	0
REP-Na3	20 to 60
REP-Na4	100 to 200
REP-Na5	60 to 100
REP-Na6	0

REP-Na4 and REP-Na5 with views of the fuel periphery on radial fresh fracture surfaces (Fig. 12). At medium magnification (parts a and c of Fig. 12 for REP-Na4 and REP-Na5, respectively), a paving-like fragmentation of the rim is clearly evidenced in REP-Na 5, whereas no fracture is exhibited in the REP-Na4 rim. Conversely, photographs taken at higher magnification (parts b and d of Fig. 12 for REP-Na4 and REP-Na5, respectively) do not reveal any difference in the rim microstructure because in both cases the same common morphology with submicronic-faceted grains and high-porosity density is observed.

The rim characterization has been pursued with the use of EPMA, the xenon distribution in the REP-Na5 fuel periphery being illustrated by X-mapping (Fig. 13). The photograph highlights a sort of outer depleted zone corresponding to the loss of xenon detection in the rim related to the occurrence of large porosity. On the radial xenon content profile (Fig. 14), in addition to the rim effect observed from the pellet–cladding interface up to nearly 250 μm, a great discrepancy between detection and the calculated creation curve is also recorded from about 2000 μm up to the pellet center. This second depleted zone is also due to the gas release and precipitation occurring during base irradiation in the PWR reactor. If this result is compared with the examination of a usual PWR rod with a similar burnup[6] (Fig. 15), no striking difference is observed. Therefore, on the basis of these EPMA observations, the assertion can be made that rapid RIA pulse, close to 100 cal/g fuel, does not change the intragranular fission gas distribution.

Transient Spalling. Except for REP-Na2, in which a rod with almost no corrosion is used, all CABRI tests have resulted in some damage of the outer oxide layer with consequences (e.g., cracks, spalling) increasing apparently with the pretest oxide thickness. It is least pronounced in REP-Na5 with the occurrence of radial and circumferential cracks in the oxide. In REP-Na6, limited spalling, with the departure of a few millimeters long oxide fragments, can be observed near peak power regions as well as numerous small pits toward both test-rod ends, which might represent an incipient spalling. In REP-Na3 and REP-Na4, large oxide patches have disappeared (Fig. 16). Finally, very few oxide remnants were seen in the metallographic samples of REP-Na1, but oxide scales could be found among debris collected by the test section upper filter.

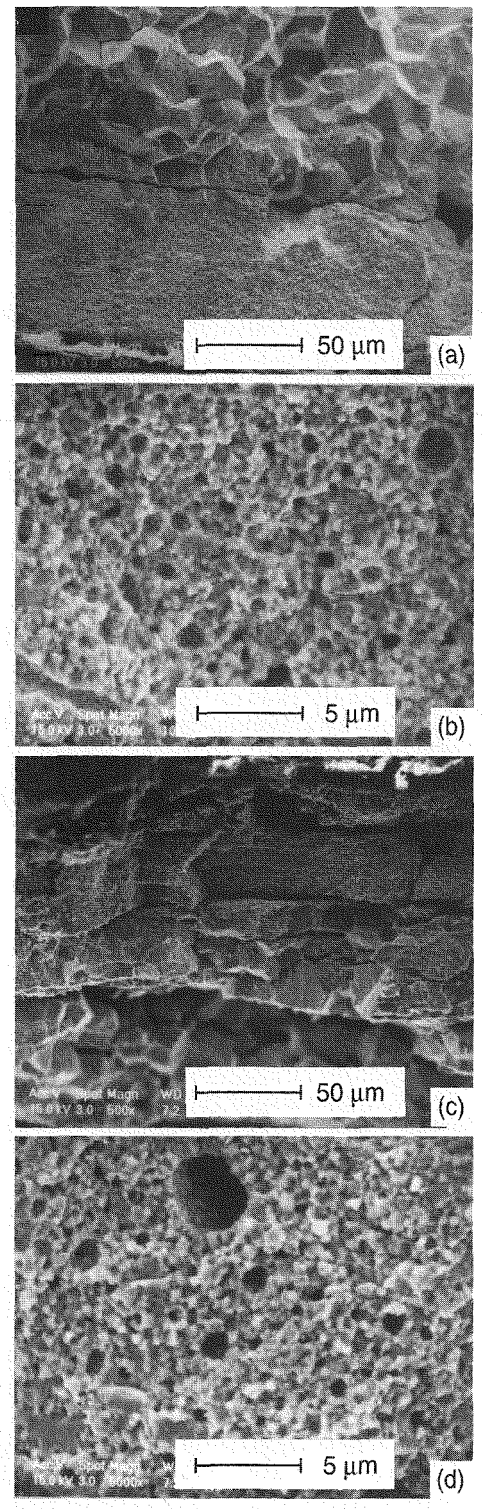

Fig. 12 Scanning electron micrographs of the rim zone at different magnification in (a) and (b) REP-Na4 and (c) and (d) REP-Na5.

The fact that a thick oxide layer cannot withstand the slightest transient deformation of the cladding has been further evidenced by out-of-pile clad tensile tests of the PROMETRA program during which transient spalling occurred except on fully brittle samples that failed with zero elongation. Thus the phenomenon must take place quite early, during the PCMI phase, but there is no indication of the time when oxide fragments drift in the coolant; in any case, transient spalling is liable to alter the channel coolability and to change suddenly the cladding to coolant heat transfer, which would result, under reactor conditions, in an earlier departure from nucleate boiling (DNB) in comparison to case without any spalling.

Understanding of Fuel Transient Behavior. A schematic view of the irradiated fuel behavior under RIA transient conditions is shown in Fig. 17 (Ref. 7). Different phases can be considered in the transient development. For each phase, the role of fission gases is clearly identified. Thus, induced by the fuel thermal history, and in addition to the thermal expansion, different modes of clad loading occur. The clad deformation and/or risk of failure can be assessed, depending on its thermal evolution and mechanical behavior.

Figure 17 also shows the domain of the CABRI REP-Na test representativity. The fuel–cladding thermal and mechanical history is correctly simulated during the early transient phase. Nevertheless, there is some restriction concerning the pressure conditions caused by the absence of pressurization of the CABRI Na loop. In the later phases, the fluid–cladding heat transfers do not correspond to reactor conditions. Inside the early loading phase, however, the CABRI tests provide important data[8] that are characteristic of the high-burnup fuel-rod behavior under RIA conditions.

Each of the major results from CABRI REP-Na tests (rod failure, clad straining, and final FGR) can be roughly correlated with a transient phase as described in Fig. 17. The analysis of these results allows identification of the specific aspects of high-burnup fuel and the transient conditions that enhance the risk of failure in each step of an RIA transient.

Early Transient Phase: Fission Gas Contribution to PCMI Loading. An RIA in cold or hot standby condition is characterized by a rapid increase of fuel temperature (10^4 to 10^5 K/s) in quasi-adiabatic conditions. So the thermal level is rapidly overpassing the end-of-life (EOL) fuel temperatures, which are

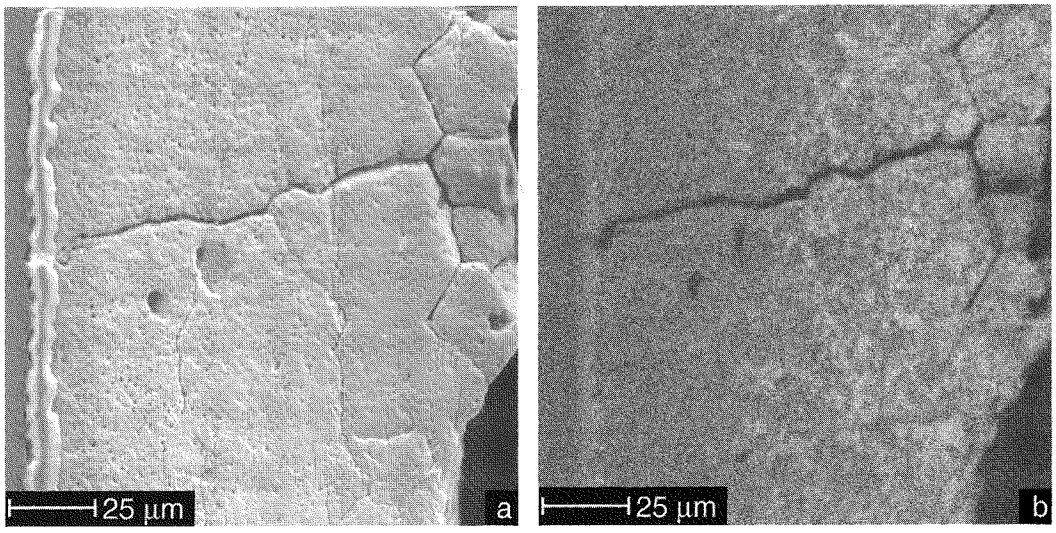

Fig. 13 Scanning electron micrograph of REP-Na5 in (a) fuel periphery and (b) corresponding xenon X-mapping.

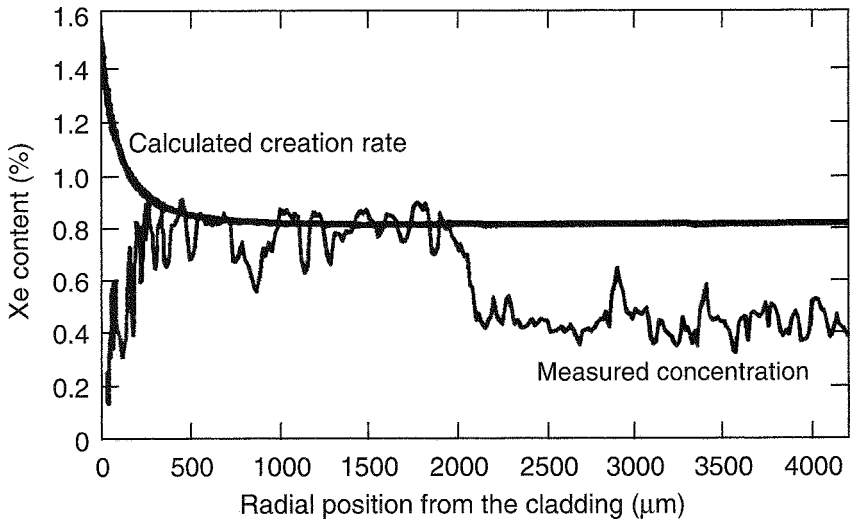

Fig. 14 Electron probe microanalysis radial xenon (Xe) profile for REP-Na5.

relatively low in high-burnup fuel (from about 650 K at the surface to 1100 K in the center). During a short time scale, the radial profile inside the fuel pellet is very close to the radial power profile, so the relative temperature increase is more important in the outermost region of the pellet and all the more because the pulse width is shorter and the burnup is higher (effect of ^{239}Pu buildup).

This fast heating rate induces an important overpressurization inside fission gas bubbles, which can be assumed to be in thermomechanical equilibrium inside the fuel in stationary hot conditions. Indeed, over the pulse time scale, insufficient time is available to activate vacancy diffusion phenomena and to relieve the overpressurization by bubble swelling, even at relatively high temperatures. Consequently high stress fields can be obtained inside the fuel. If the fracture stress is exceeded, brittle fracture will occur in the fuel. Clear evidence of this "brittle" fuel fracture along grain boundaries has been obtained from the SILENE experiments in France with liquid-metal-reactor (LMR) fuel, which leads to an energetic fuel dispersal in the absence of any significant fuel restraint.[4]

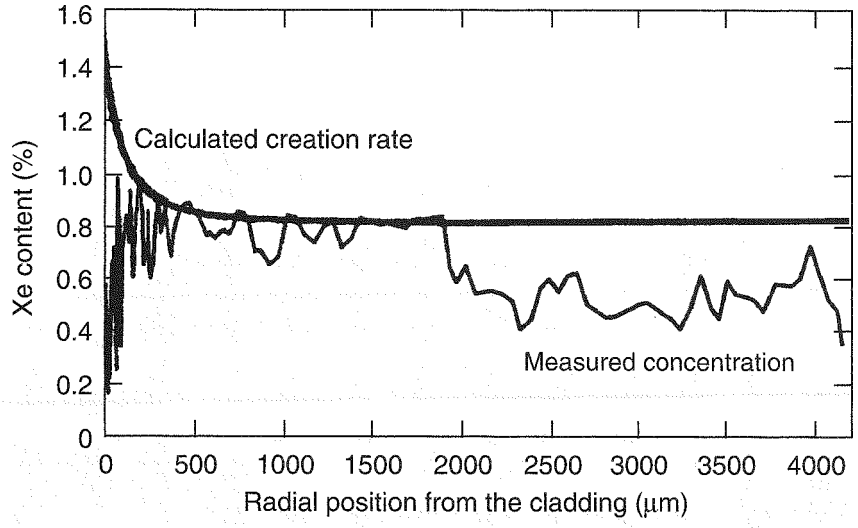

Fig. 15 Electron probe microanalysis radial xenon (Xe) profile after five-run PWR base irradiation.

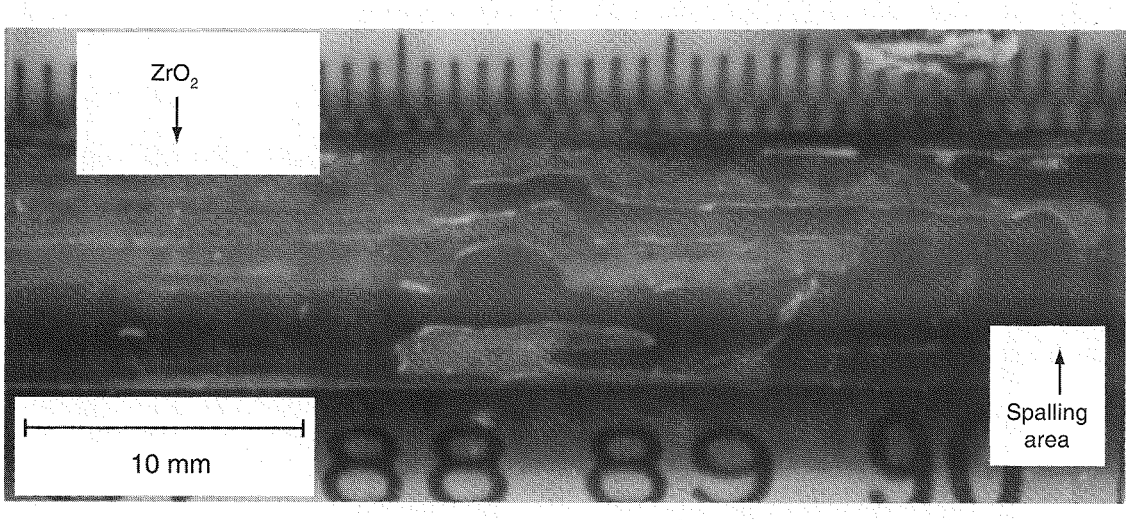

Fig. 16 Visual inspection of the REP-Na4 test rod showing transient spalling.

This fuel fragmentation mechanism is also postulated to explain the grain boundary separation observed in the outer zones of the NSRR and REP-Na tests (Fig. 18). The parameters involved are the relative increase of temperature between EOL and transient condition, the initial state of grain boundary bubbles (pressure and coverage fraction), the fuel fracture stress, and the fuel hydrostatic pressure.

In high-burnup fuel, a particular microstructure change occurs at the periphery of LWR fuel pellets above a local burnup of about 70 MWd/kgU (average burnup of ~40 MWd/kgU). When the burnup peaks at 100 to 120 MWd/kgU locally, the thin "rim" region is characterized by the following:[4]

- Extremely fine-grained structure (grain size 0.02 to 1 μm).
- Depletion of matrix fission gas deduced from EPMA, up to 80 to 90%.
- High local gas content.
- Increased porosity (15 to 20%) containing the major part of the retained gases, thus as large micrometer-size overpressurized pores.
- Nanometer-size bubbles coating the grain boundaries.[9,10]

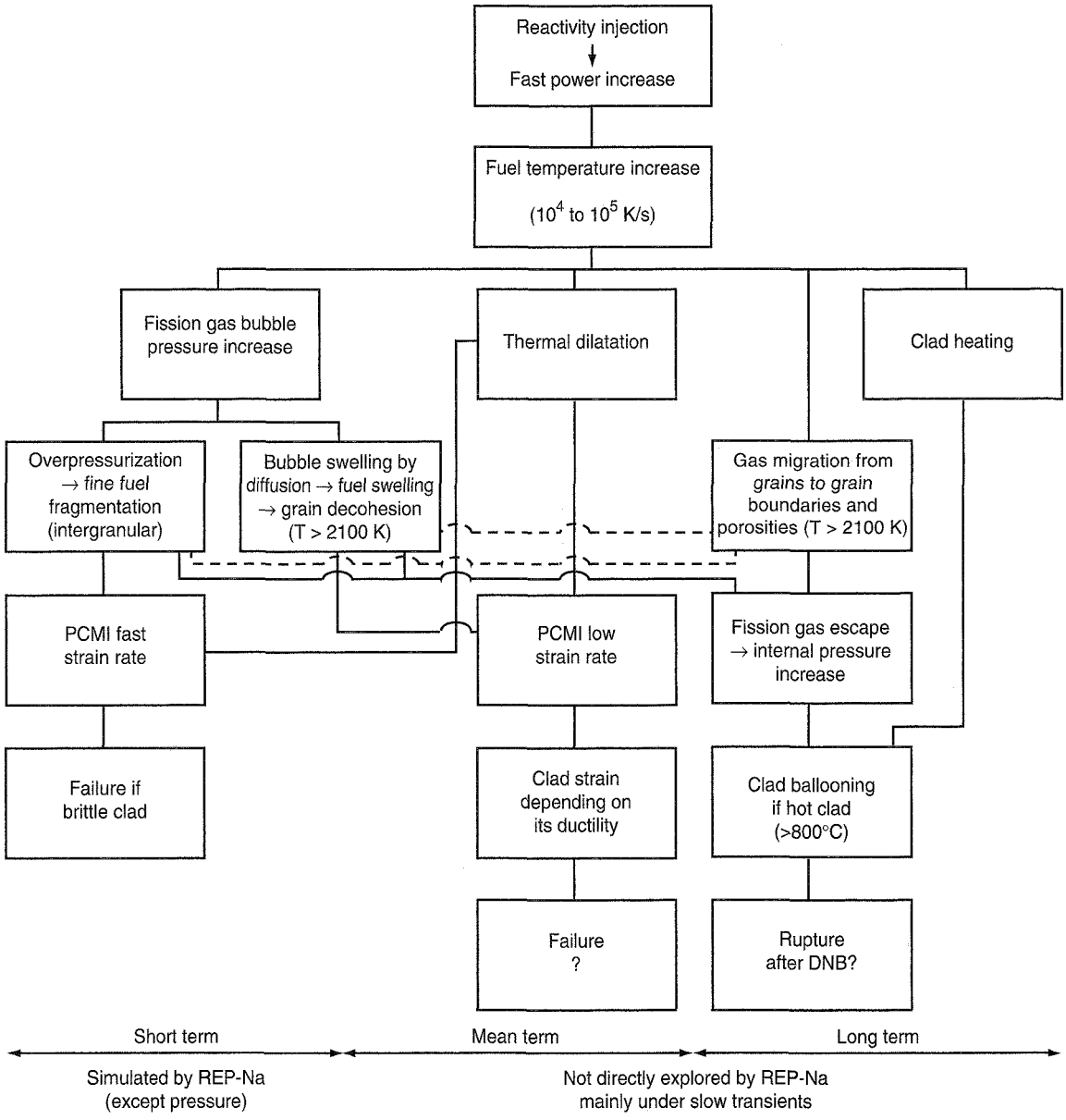

Fig. 17 Schematic view of irradiated fuel behavior under reactivity-initiated accident transient conditions.

Between this final state and the initial structure of irradiated fuel, intermediate steps can be observed, characterized by a progressive depletion of the soluble gas as seen by EPMA and an increase of porosity under the form of inter- and intra-granular bubbles containing the "invisible" gas.

As a consequence of this porosity increase, the fuel fracture stress is decreased, and lower fragmentation thresholds can be expected in terms of fuel temperature. In contrast with values of 1300 to 1500 K estimated in the outer zones, excluding the rim region, it seems possible to obtain a grain boundary cracking in the rim at about 900 to 1000 K.[4,11–13]

This fuel fragmentation mechanism has different consequences:

- It is the necessary condition for a fast liberation of the energy stored in intergranular bubbles and pores.

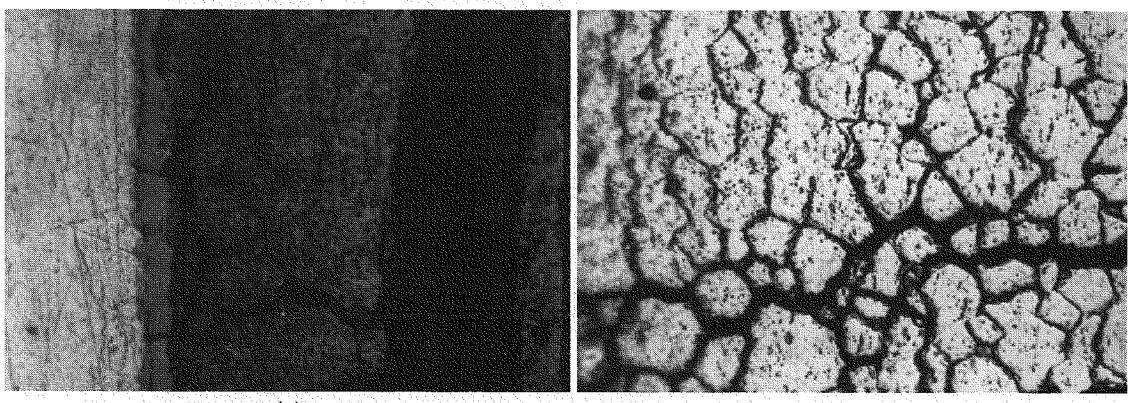

(a) (b)

Fig. 18 High-burnup fuel after RIA transient (REP-Na5). (a) Rim. (b) ~0.95 outside radius.

• In case of clad failure, it can lead to an ejection of a fuel–gas mixture and to an interaction of fine-grained fuel with the coolant.

• In the absence of clad failure, it allows the gas to escape to the free volumes if the grain boundary opening is sufficient.

The most important aspect that must be considered is the possible contribution of the liberated fission gases to the PCMI loading, consequently with an enhancement of the risk of clad failure. This can be determined by performing an energy balance, assuming no fuel strength after grain boundary failure and no gas escape (justified by the time scale of the pulse). The work from expanding gases is transformed into clad deformation and the condition for clad rupture is roughly given by:

$$S_c \sum_i P_{bi}\, g_i\, Log \frac{P_{bi}}{P_r} > S_g \int_{\varepsilon_{th}}^{\varepsilon_r} \sigma d\varepsilon$$

where σ_r = rupture stress of the cladding, equivalent to an internal hydrostatic pressure
P_r = $(2\, e_g/d_g)\, \sigma_r$
ε_r = corresponding rupture strain
S_c = fragmented fuel area
S_g = clad section
e_g, d_g = cladding thickness and mean diameter
P_{bi} = bubble pressure of group i at fragmentation time or at a later time during the heating phase
g_i = relative volume of bubbles
ε_{th} = contribution of fuel–cladding differential thermal expansion to clad deformation

The integral on the right-hand side introduces the concept of strain energy density (SED), now used in the analysis of RIA experiments.[14] The determination of this term will be considered later.

A necessary condition for an effective contribution of fission gases to clad loading is that the term on the left-hand side must be significant. Some evaluations have been made for UO_2 fuel (Table 3) considering three levels of average burnup: 40 MWd/kgU just before the rim formation, 65 MWd/kgU with a relatively well-established rim microstructure as described previously, and 52 MWd/kgU with an intermediate state of the rim. The study is focused on the peripheral zone where the effect of burnup is the most important, and the grain fragmentation occurs first during a fast pulse. The characteristics of grain boundary gas (lenticular intergranular bubbles and large pores) are issued from experimental examinations and theoretical considerations. The values of the associated stored energy at EOL give some idea of the potential energy available from fission gases, which increases strongly with burnup. The potential action during the heating phase has been calculated at the estimated fragmentation temperature (900 K for the higher burnup, 1500 K for the others) and at a higher temperature (2900 K) near the UO_2 melting point. A value of P_r = 80 MPa has been taken as a rupture condition, which corresponds to current laws for irradiated cladding.

From the results of Table 3, some important conclusions can be drawn:

1. The contribution of fission gases to PCMI loading is negligible as far as a medium burnup is concerned (≤ 40 MWd/kgU).

2. This contribution increases with burnup and rim formation, correlated to the fission gas accumulation in

Table 3 Evaluation of Potential Energy Available from Grain Boundary Gas in Fuel Outer Pellet After Fragmentation (UO_2 Fuel)

	Average pellet burnup					
	40 MWd/kgU		52 MWd/kgU		65 MWd/kgU	
End-of-Life State						
Local burnup, MWd/kgU	57		92		120	
Fission gas content, mm^3/g	1767		2446		2795	
Fuel temperature, K	673		673		673	
Bubble Population						
	Intergranular bubbles	Large pores	Intergranular bubbles	Large pores	Intergranular bubbles	Large pores
Gas content, mm^3/g	5.83	157.0	483.0	157.0	191.0	2185.0
Relative volume, %	0.019	4.5	2.4	4.5	0.5	19.5
Internal pressure, MPa	496.6	10.0	103.3	10.0	1228.4	40.2
Stored energy, J/g	0.0135	0.064	0.352	0.064	0.877	1.119
Total, J/g	**0.0778**		**0.416**		**1.996**	
Transient Behavior (P_r = 80 MPa)						
Fuel temperature, K	1500		1500		900	
Internal pressure, MPa	1106.8	22.3	230.2	22.3	1642.7	53.7
Expansion work, J/g	0.0526	–0.122	0.555	–0.122	2.364	–0.398
Total, J/g	**0.07**		**0.433**		**1.966**	
Fuel temperature, K	2900		2900		2900	
Internal pressure, MPa	2140.0	43.09	445.1	43.09	5293.3	173.1
Expansion work, J/g	0.127	–0.114	1.746	–0.114	10.67	2.48
Total, J/g	**0.013**		**1.632**		**13.15**	

intergranular bubbles and large pores, strongly increasing the risk of clad failure during the heating phase at a low fuel enthalpy level; this risk also depends on the clad mechanical properties and on the SED at failure.

Rough evaluations can be made in case of fully brittle behavior, which is the case of the first failure in REP-Na1 for a fuel temperature of about 900 K. If clad failure at yield stress is assumed, a value of 9.77 J/m can be obtained for the linear energy required for clad failure ($\varepsilon_{th} = 6 \times 10^{-3}$), which must be compared with the energy available from gas expansion in the rim zone (about 5% of fuel section): 53.4 J/m. The REP-Na1 failure can be explained by such results. The nonfailures in the other CABRI REP-Na tests with similar burnups are consistent with this approach and can be explained by the following factors: low clad corrosion and residual ductility in REP-Na5, absence of local hydride accumulations, lower strain rate (factor of 50), and higher clad temperature in REP-Na4.

Similar energetic considerations could be made for MOX fuel, considering the potential energy available from fission gases in agglomerates. Indeed, the local burnup in these last ones is much higher than the mean fuel burnup [depending on the initial enrichment, the size of agglomerates, and the burnup: up to about 3 with an initial content of 0.06 in plutonium/(uranium + plutonium) at an average mean burnup of 55 MWd/kgU]. Typical microstructures, very similar to the rim region of UO_2 fuel, can be observed in the plutonium agglomerates of the outer part of the high-burnup MOX fuel pellet: a porous and fine-grained structure with a high local gas content undetectable with EPMA. Nevertheless, the experimental data on high-burnup MOX fuel presently available are insufficient to allow precise evaluation of potential work available from fission gases.

Contribution of Fission-Gas-Induced Swelling to Clad Straining. Bubble swelling is caused by vacancy diffusion induced by the increase in bubble pressure (Fig. 17). This phenomenon is thermally activated, and it is significant for fuel temperatures above about 2100 K and if sufficient time is available (higher

temperatures imply shorter times). Bubble swelling depends also on the initial bubble size: it is more important for small bubbles, but the absolute effect is low.

The mechanisms are relatively well known and are taken into account in the SCANAIR modeling.[15] Clear evidence of the contribution of the fission-gas-induced swelling has been demonstrated in the interpretation of the REP-Na3 and REP-Na2 tests.[8] Fuel thermal expansion is not sufficient to explain the measured clad strains. In REP-Na3 with a relatively low energy injection, swelling occurs only in the outer zones where the thermal level is highest and leads to a barrel-type deformation of the pellet as evidenced on the clad deformation after test. In REP-Na2 with a high energy injection, swelling occurs also in the innermost zones and leads to the hourglass shape of the pellet as observed on the cladding after test. In most of the cases, the swelling is mainly intragranular. Intergranular swelling is limited in the modeling once grain fragmentation or bubble interconnection is calculated to occur. Nevertheless, it is not possible, from the posttest examinations presently performed, to have experimental confirmation of the origin of swelling.

Indeed, common features from the base irradiation are more or less found after the tests: submicronic intragranular bubbles in the inner zones, revealed mainly after etching, and porosities or "pitches" inside grains in the outer zones; however, the current magnifications used in the examinations (500 with optical microscopy, 5000 with SEM) do not allow observance of nanometer-size bubbles. The large grain boundary opening observed in most of the REP-Na tests,[2] which increases with the clad strain, is probably not the cause but the consequence of this strain. Fuel fragmentation occurs at the beginning of the PCMI phase so that the opening must be limited because of the clad constraint. Grain boundary opening becomes possible during the cooling-down phase when the stress decreases and preferentially in the direction of lower stress and if sufficient volume is available (because of the clad strain or the dishes). This explains the preferential tangential orientation of the opened grain boundaries in REP-Na3 and REP-Na5 (parts b and d of Fig. 11) and the absence of any visible opening in REP-Na4 (part c of Fig. 11), which is not, however, a proof of nonfragmentation. The rather homogeneous opening of grain boundaries observed in REP-Na2 (part a of Fig. 11) is probably due to the high temperature level and to the hydrostatic fuel behavior.

In conclusion, the grain boundary opening observed in the outer zones seems to result from the cooling-down phase, and it is different from the classical intergranular swelling caused by vacancy diffusion in the hot state. It does not contribute to the clad strain except by some dynamic effect during fragmentation; however, this is not really significant outside the rim zone.

Fission Gas Release Mechanisms. Two phenomena are correlated to the fission gas release: internal pressure increase and degradation of the fuel-to-cladding thermal transfer. Thus not only the final release is important but also the gas release kinetics during the transient. Experimental results give access only to the first point; kinetic aspects can only be deduced from correlations with microstructural changes.

High fission gas releases, increasing with fuel burnup, have been observed in the NSRR and CABRI tests, up to 20% even with a low energy deposition (Table 1). The temperature threshold for intragranular gas migration is about 2100 K (Fig. 17), depending, in fact, on the duration of the hot state and also on the thermal gradient and grain size. In RIA transients, this corresponds to a fuel enthalpy of about 107.5 cal/g fuel (450 J/g). Thus in all the NSRR tests this mechanism is not or only slightly activated. In the CABRI tests, this mechanism occurs in the most energetic tests (REP-Na2 and REP-Na6), and it is less pronounced in REP-Na3. REP-Na5 is at the limit, and intragranular migration is probably limited to a small ring at the internal part of the rim zone (~0.95 to 0.975 of the radius R) where the intragranular gas is still significant and the temperature is sufficiently high. This conclusion is consistent with results of the SCANAIR code, which calculates a small contribution of the intragranular gas to the final release, and with EPMA observations (Figs. 14 and 15), which show no striking difference before and after the test except in a small ring between 100 and 250 μm from the outer fuel surface.

Consequently, one can conclude that the high gas release observed in the high-burnup fuel tests stems mainly from porosities and grain boundary bubbles. The intergranular gas concentration (grain faces) is limited by the specific area of the grains and represents less than 1% of the retained gas outside the rim region. Thus the high gas release is the proof that a significant quantity of gas is accumulated in porosities in irradiated fuel: as-fabricated porosities in which fission gases have been released or corner pores formed

during irradiation. Below 40 MWd/kgU, this quantity increases with the burnup (Fig. 9) probably in correlation with the overall gas release in the pin. Above 40 MWd/kgU, the contribution of the rim zone becomes significant and increases with burnup, as do the rim width, the porosity volume, and the quantity of gas inside. At 65 MWd/kgU, the contribution of grain-boundary gas (intergranular bubbles and porosities) inside and outside the rim region is of the same order: 7 to 8% of the total retention. For this estimation, outside the rim region, large pores in equilibrium with the plenum pressure for high-burnup fuel at EOL are assumed. Indeed, this assumption leads to a good agreement with experimental results.[4,8,11]

In addition to the burnup effect, other parameters that influence the fission gas release have been identified from the experimental results (Table 1):

- The energy deposition increases the intragranular migration.
- The pulse width: the results of HBO tests in the NSRR in Japan and of REP-Na4 and REP-Na5 in the CABRI in France show that the gas release increases when the pulse width decreases; furthermore, in the case of REP-Na4 and REP-Na5, correlations have been established between maximum clad strain, free volume, and final gas release, which leads to the conclusion that this effect is due to the level and location of the maximum fuel temperature and to their consequences on clad strain and microcracking in outer zones during the cooling phase.
- The height of the refabricated fuel rod: the characteristic time for gas flow along the gap is proportional to the square of the mean flow length. There is a factor of about 4 between REP-Na and HBO; this feature can explain the higher gas release in HBO than in REP-Na tests.
- The fuel state at EOL: gas release is issued mainly from porosities; thus the gas content depends on the porosity volume (fuel-fabrication characteristics, densification, and porosity evolution under irradiation) and on the rod inner pressure (with the assumption of equilibrium with plenum). This can also contribute to the higher gas release in HBO than in REP-Na tests.
- The fuel type: in MOX fuel, the gas release seems higher than in UO_2; this gas is issued in major part from the high gas content inside the relatively important porosity in plutonium agglomerates. In addition to this effect of initial heterogeneous structure and its consequence on fission gas repartition, however, there is also some influence of the pulse characteristics: higher enthalpy with large pulse (which increases fuel temperature in inner zones).

Nevertheless, even though the mechanisms of fission gas release and the influence of the different parameters are relatively well understood, it is more difficult to obtain the release kinetics. This aspect is the most important because it influences the thermal and mechanical fuel rod behavior all along the transient. Especially during the later phase, the combination of plenum pressure increase (or local peak pressures in the gap) and of clad temperature history can cause clad ballooning and subsequent clad failure in case of a significant increase of clad temperature (≥800 °C) after DNB with loss of mechanical strength. Thus it is of major importance to know the different steps that govern the fission gas escape from the fuel to the plenum: transfer from the fuel to the gap inside the more or less interconnected porosity network and final transfer via the gap to the plenum. The correct description of these physical processes is a necessary condition for an accurate interpretation of the REP-Na4 and REP-Na5 tests and for a reliable modeling of an RIA transient. Presently, only qualitative assessments can be made: if it can be assumed that some gas escape from porosities takes place during the heating-up phase, the major transfer occurs probably during the cooling-down phase by fuel cracking and stress relaxation. Quick cooling down in outer zones occurs relatively soon in the transient and induces radial microcracks, which creates paths for gas transfer from the fragmented zones to the closed gap. The overall gas release, however, is obtained rather by fuel cracking and/or gap reopening during the later cooling-down stage.

Posttest examinations in cold state are insufficient to access the knowledge in hot state. Except for the macrostructural and microstructural changes (large cracks, fine microcracking, and grain separation) that occur during the cooling phase as a consequence of the thermal and mechanical fuel–cladding behavior, there is no physical trace left by fission gas release. In particular, apart from some circumferential cracks in REP-Na3 and REP-Na5, the rim structure seems to be unchanged despite a well-established conclusion that this spongy structure has lost its gases. More-refined examinations, like transmission electron microscopy (TEM), could be useful.

THE SCANAIR CODE MODELING: STATUS OF VALIDATION AND EXTRAPOLATION TO REACTOR CONDITIONS

The SCANAIR code[15,16] is a 1.5-D code that describes the fuel and cladding thermomechanical behavior during fast power transients. The initial fuel-rod conditions correspond to end of irradiation conditions as calculated by either the TOSURA-REP (IPSN) or METEOR (CEA/DRN) code.[3] This "t_0 state" is mainly characterized by fuel and clad geometry, fission gas content and spatial distribution, internal rod pressure, and clad corrosion level. The geometry considered is a single-rod geometry cooled by a flowing fluid (water or sodium) surrounded by an external shroud and a bypass that represents the experimental design. This part is neglected in reactor calculations. The simulation of such fast power transients involves the following aspects:

- The fuel and clad mechanical behavior.
- The fission gas transient behavior.
- The thermic qualities of the different materials (fuel, clad coolant, and shroud if any).

All of these aspects are closely related, as illustrated in Fig. 19.

The Physical Modeling

Rod Mechanics. The structural mechanics modeling has already been presented in detail in Ref. 15. We recall here the basic assumptions:

- Axisymmetric conditions consider only axial and radial displacements.
- Fuel and cladding are considered as long cylinders.

This leads to diagonal stress and strain matrixes and then to simplified equations. The total strain is assumed to be the sum of elastic, plastic, thermal, cracking, and swelling strains (only the first three for the cladding). The elastic strains are given by Hooke's law.

Fuel and clad plasticity is treated, and the plastic strains are given by Prandtl–Reuss laws. The mechanism of fuel and clad creep has been neglected so that no description of the clad ballooning is presently available. Concerning the fuel, the fuel creep at high temperature is roughly simulated by way of a softening temperature at which the yield stress is set to zero.

The thermal expansion of fuel and cladding is based on correlations giving the change in volume as a function of temperature. The cracking strains (Fig. 20) are generated in the plane normal to the tangential and axial directions assuming that the fuel, initially cracked after irradiation, does not offer tensile resistance (the resulting stress is set to zero). Such a modeling is derived from the TRANSURANUS code.[17] Its main outcomes are a realistic stress distribution (which has an impact on the fission-gas-induced swelling) and a better simulation of the average fuel volume expansion (without local effects).

Fuel expansion caused by the presence of the fission gases is described on the basis of the transient evolution of the bubbles given by the fission gas modeling and on the fuel hydrostatic pressure (one third of the trace of the stress tensor): this induces a strong numerical coupling between fission gases and mechanical modeling. The fuel and cladding are discretized in axial slices, each of them being split in radial meshes, and the numerical method used to solve the equation of radial equilibrium is the finite-element method.

The clad mechanical laws (σ_{ys} function of temperature) are issued from a first tensile test campaign on irradiated cladding now being complemented by the PROMETRA program[7] from which a clad failure criterion is expected to be derived for implementation in SCANAIR.

Fission Gas Behavior. The fission gases retained in the fuel matrix are described under three kinds of population with the following assumptions:

1. The intragranular bubbles move toward the grain boundary and coalesce under thermal gradient and Brownian diffusion movement; overpressurized by the temperature increase and their coalescence, they can grow by the capture of a vacancy flux from the UO_2 lattice, which leads to intragranular fuel swelling.
2. The intergranular bubbles are motionless and located at the grain boundaries and can grow by vacancy diffusion as the result of overpressurization induced by heatup and intragranular influx; this population is embedded in the porosities when the grain fragmentation occurs, linked to saturation or fracture caused by overpressurization and based on the fuel fracture stress (which can be very low in the rim zone).
3. The quantity of the porosity gases is initially defined from the t_0 state and evolves as the result of the intergranular flux and migration to free volumes according to Darcy's law.

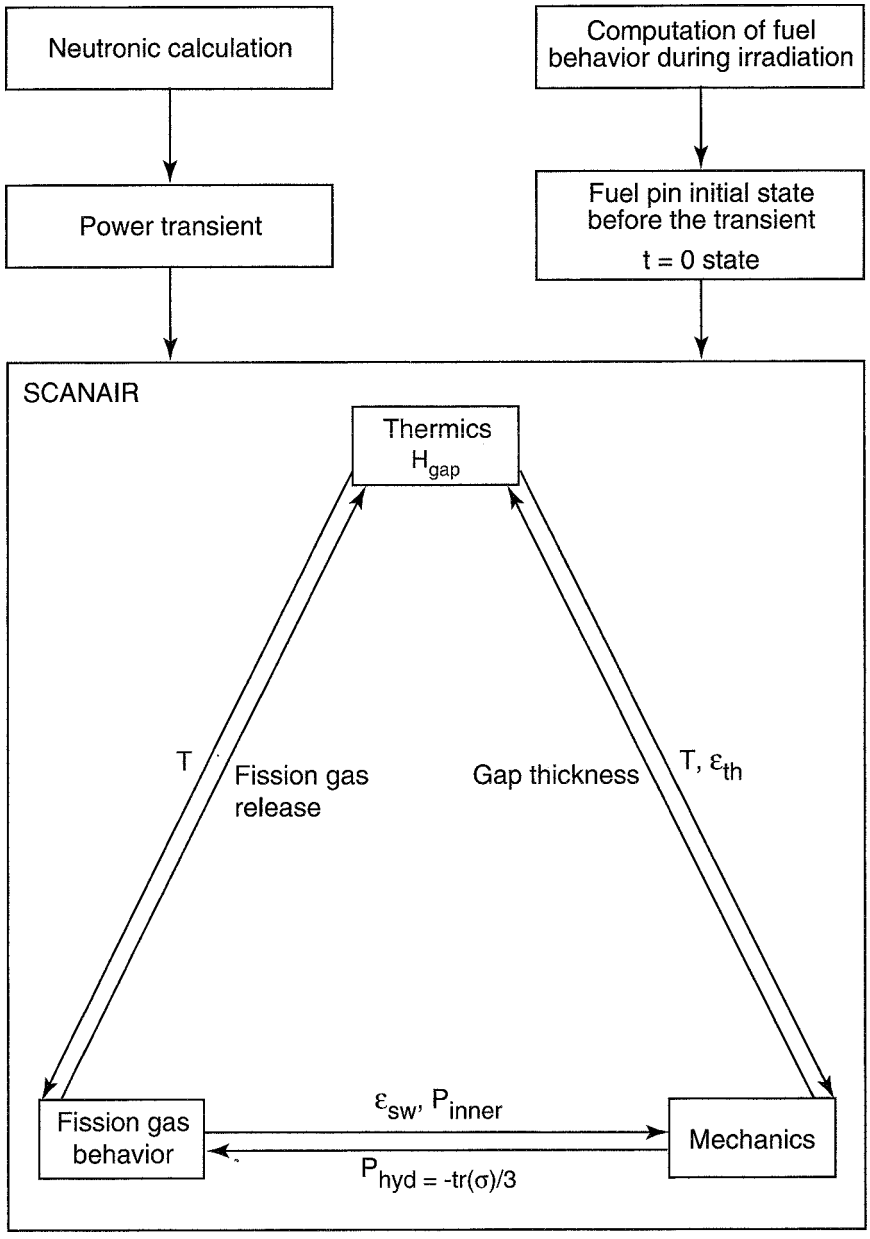

Fig. 19 SCANAIR general modeling process. t, time; T, temperature; ε_{th}, deformation due to thermal expansion; ε_{sw}, deformation due to fuel swelling; P_{inner}, internal pressure; P_{hyd}, hydrostatic fuel pressure; t_r, tensor trace; σ, stress; H_{gap}, gap conductance.

Transient Modeling of the Rim Zone. The external part of the higher burnup fuel rod, the so-called "rim," is characterized by a high level of plutonium concentration, gas content, burnup, and porosity in an annular zone of 100- to 200-μm thickness together with a very small grain size (<1 μm).

Under fast transients and because of the rapid heatup of this porous zone, early grain fragmentation may lead to direct loading of the gas pressure onto the cladding and thus result in rod failure in case of low clad mechanical resistance as the result of embrittlement (see the REP-Na1 failure). Such a

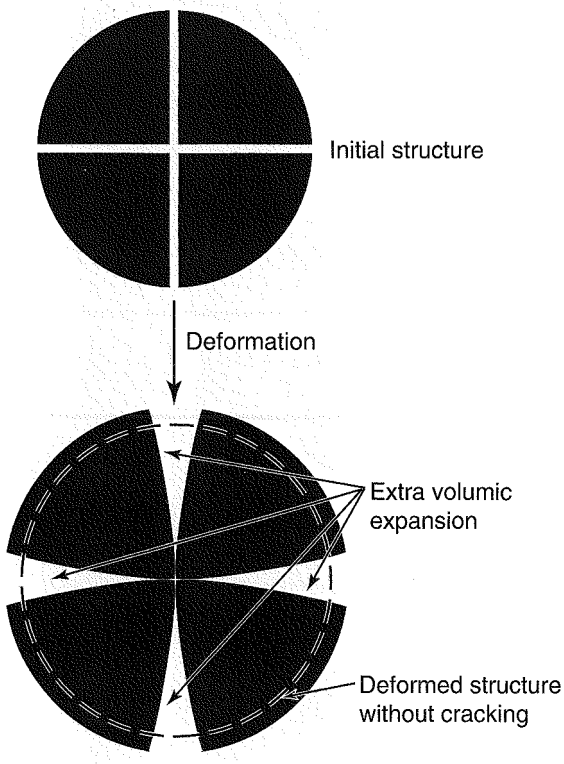

Fig. 20 Influence of the cracking strains.

behavior is modeled in SCANAIR under the option assuming that, in zones with high porosity (>10%) and after grain fragmentation, the pressure in the porosity instantaneously balances the fuel hydrostatic pressure ($P_{hyd} = - tr(\sigma)/3$, σ = stress tensor) and that the fuel behaves as a mixture of gas and powder (hydrostatic behavior).

Thermal Dynamic Aspects. Radial conduction is taken into account in the fuel, cladding, and shroud as well as radiative heat transfer through the fuel–cladding gap. The axial coupling is realized by the coolant flow (convection, 1-D) assumed in liquid phase and with imposed inlet flow.

The gap conductance takes into account the radiative heat transfer between fuel and cladding and the conduction through a gas layer function of the evolution of the gas composition and considering contact roughness in case of PCMI.

The heat transfer between cladding and coolant is modeled by heat-exchange laws established from steady-state analysis with the following assumptions:

- Dittus–Boelter law in single phase.
- DNB based on temperature of minimum film boiling issued from Groeneveld-Stewart law.
- Film boiling regime using the modified Bromley law.
- No description of nucleate boiling or of transition phases.

The zirconia oxide layer is simulated by its thermal behavior (low conductibility) but is assumed to have no tensile mechanical resistance (like the fuel).

Validation on Experiments

The SCANAIR code is being validated on the CABRI REP-Na tests and on some of the NSRR experiments.[8,15] Concerning the REP-Na tests, the SCANAIR results showed a satisfying description of the clad elongation and of the mean radial clad straining (Fig. 21), which follows the axial power profile (Fig. 22). The calculations show that, depending on the energy injection level, the clad straining results not only from fuel thermal expansion but also from fission-gas-induced swelling (REP-Na2 and REP-Na3). Indeed, in the REP-Na2 test, the energetic power transient (211 cal/g fuel injected at 0.4 s) led to high fuel temperature levels (almost reaching melting), which allowed activation of the mechanisms of bubbles swelling by diffusion in the innermost zones while the fuel thermal expansion contributed to a clad straining of only 1.6% (to be compared with an experimental mean maximum value of 3.5%). The calculated value of the maximum clad plastic hoop strain of 6.1% in REP-Na2 can be reduced to 4.1% if the collapse of the porosities and the filling of the dishings at high temperature are taken into account.

In REP-Na3 test calculations, taking into account the relatively low energy injection (120 cal/g fuel at 0.4 s), the fission-gas-induced swelling is found in the fuel outer zones where the temperatures are the highest. The different localizations of the fuel zones responsible for fuel swelling explain the differences in the pellet deformation (barrel type in REP-Na3 and hourglass type in REP-Na2), although such three-dimensional effects are not described with SCANAIR.

The effect of the energy injection rate has been evaluated by the analysis of the REP-Na4 and REP-Na5 tests with the use of rods with similar burnups but with different clad corrosion thickness and submitted to power transients with pulse half-widths of 64 and 9 ms for a similar total energy injection (95 cal/g fuel at 1.2 s).

The SCANAIR results showed that, in opposition to a rapid ramp that heats the fuel adiabatically, with a

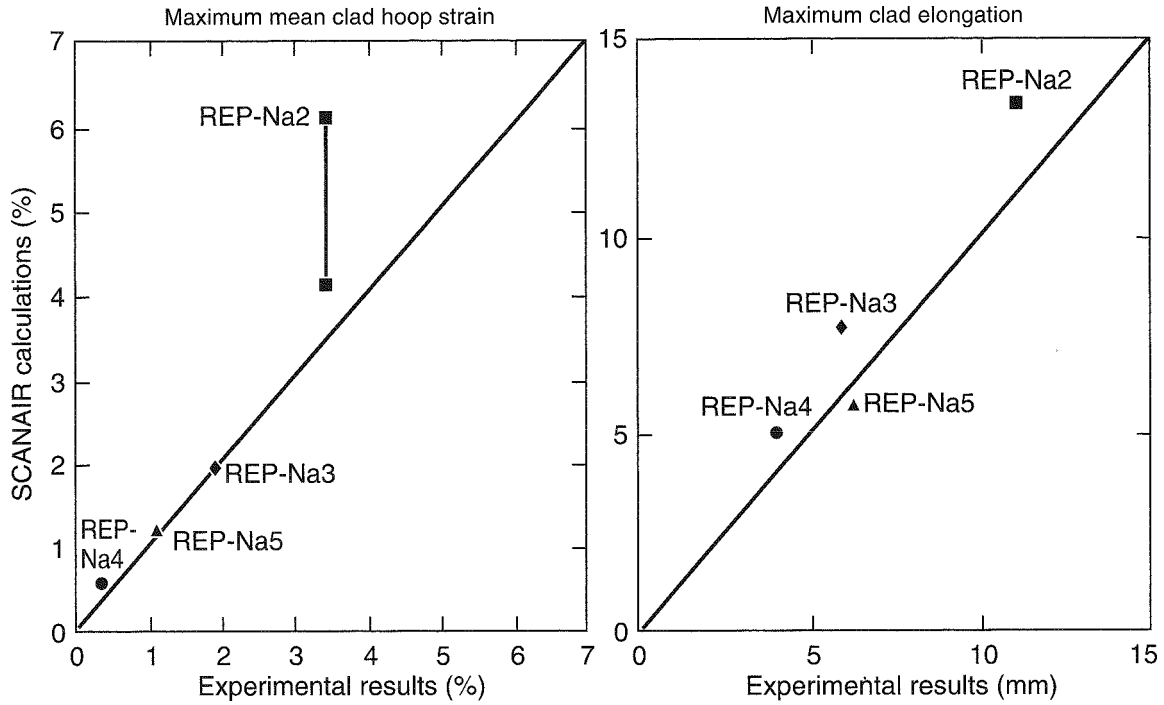

Fig. 21 SCANAIR results compared with experiments.

slower energy injection rate, the fuel temperature increase is affected by the rod-to-coolant heat transfer; thus the temperature increase rate and the maximum temperature reached in the fuel are reduced. The stresses in the outer part of the fuel are reduced, and thus the strains are decreased. Such an effect is consistent with the maximum clad deformations obtained in REP-Na4 (0.4%) and REP Na5 (1.1%) tests and are well reproduced by the SCANAIR results (0.58% and 1.2%, respectively). The high fission gas release rate increasing with burnup and fuel enthalpy level is correctly described with SCANAIR; the main contribution is assumed to come from the intergranular bubbles and from the porosity gases initially in pressure equilibrium with the plenum at EOL conditions for high-burnup fuel with the rim zone (Fig. 23).

For the REP-Na4, the calculated result was overestimated because of partial opening of the porosities (not presently modeled in SCANAIR) related to limited clad deformation. In opposition to the other test results, a significant contribution of the intragranular bubbles on the total gas release is calculated in REP-Na2 consistently with the high fuel enthalpy level, which allows thermal activation for gas migration; however, no conclusion on the kinetics of gas release, which may affect the rod internal pressure increase and the fuel–cladding heat transfer, can be drawn because of the lack of experimental knowledge.

The occurrence of grain boundary failure caused by gas-bubble overpressurization early in the rim zone and contributing to high gas release is described in SCANAIR as the result of a fast heating rate in the early phase of the transient, high stress field buildup, and reduced fracture stress in the porous rim zone of high-burnup fuel. In the case of the REP-Na1 test, such an effect is likely to have contributed to clad failure by sudden increase of the loading of the already embrittled cladding (caused by oxide spalling), and it is simulated using the rim transient modeling. In effect, in REP-Na1 at experimental failure time (74 ms), the maximum fuel temperature reached only 600 °C at peak power node in the outer rim of the pellet with no clad heatup. At such a temperature level, the classical fission-gas-induced fuel swelling mechanism is not activated and cannot contribute to clad loading, and clad deformation caused by fuel thermal expansion is evaluated at 0.06% only.

The SCANAIR code has also been applied to the NSRR HBO-1 test[5] whose rod characteristics are the following: 50.2-MWd/kgU burnup, 45-μm oxide thickness, 90-μm rim thickness, mean gas retention of 1.38 cm^3/g standard temperature and pressure (STP),

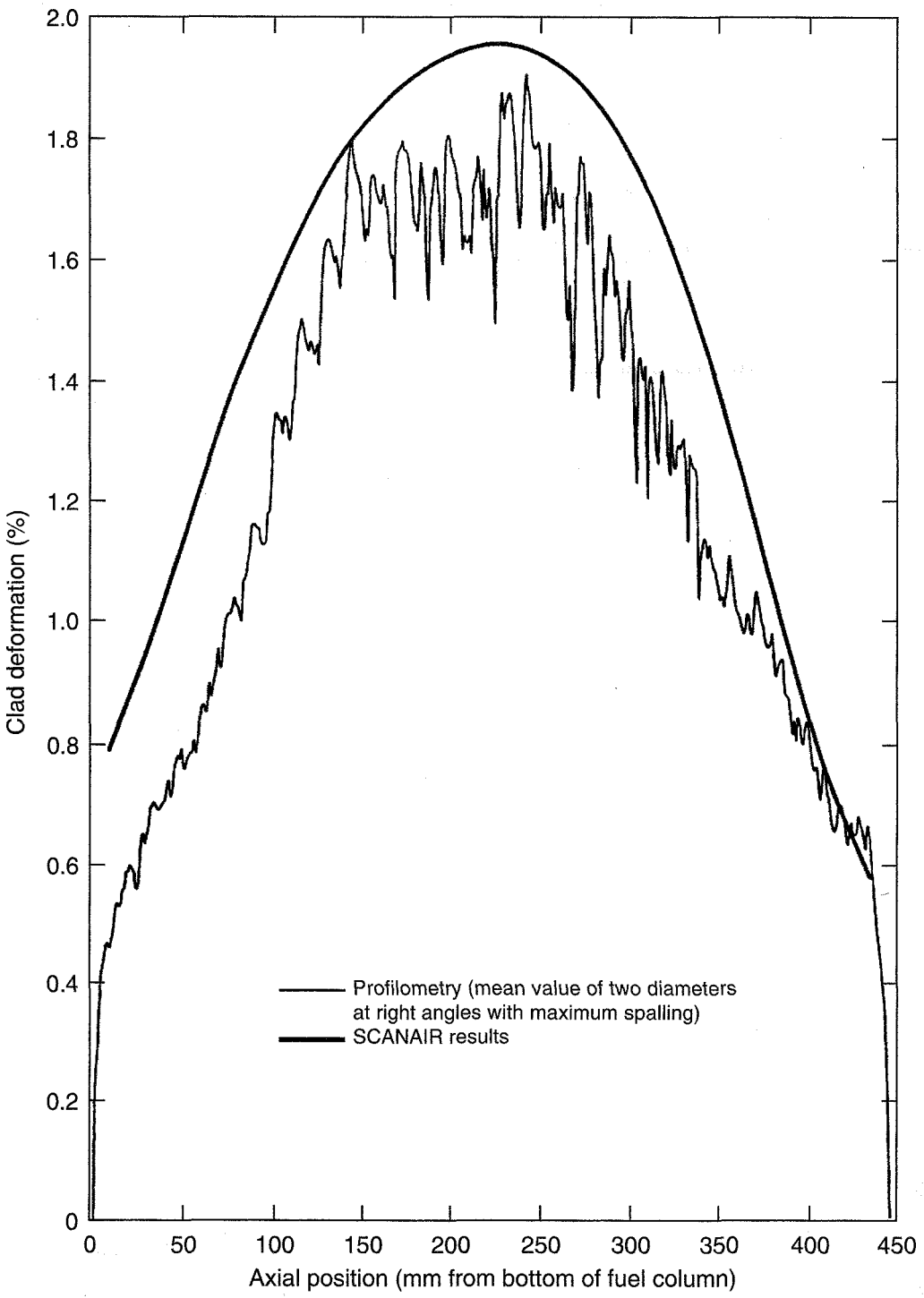

Fig. 22 Axial profile of clad plastic hoop strain and SCANAIR results for REP-Na3.

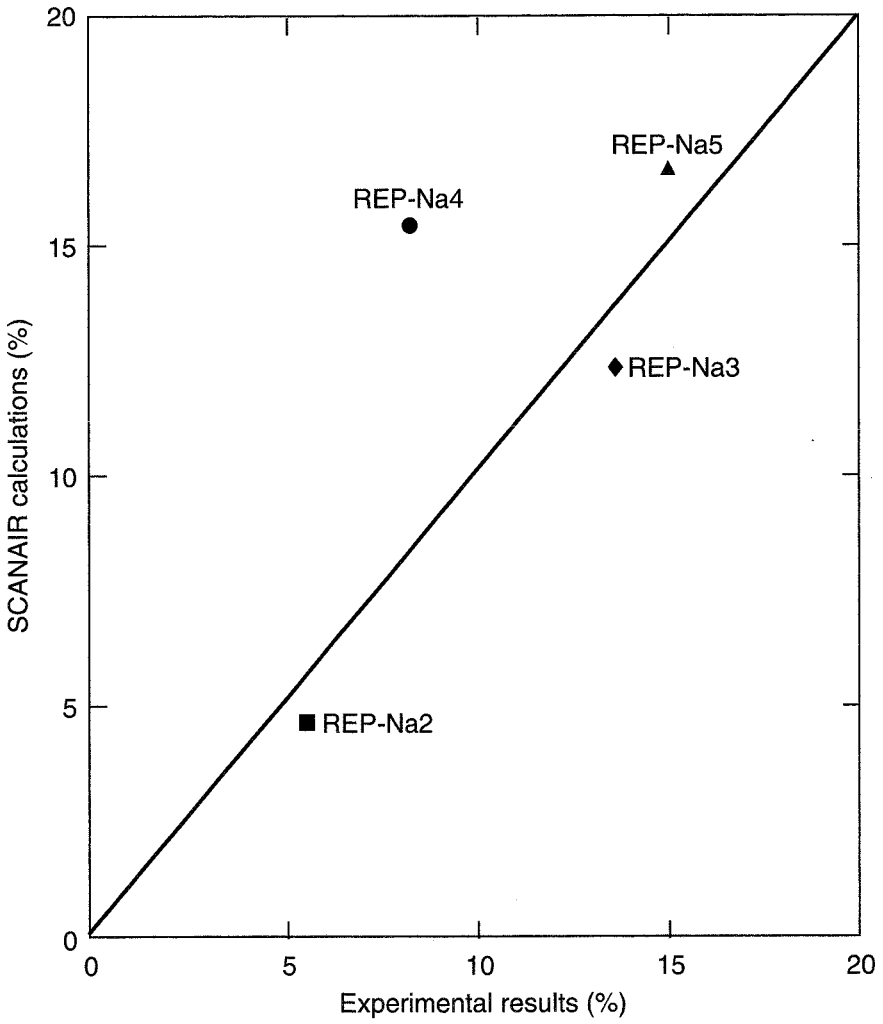

Fig. 23 SCANAIR results compared with experiments: transient gas release rate.

gap filled with helium at 0.1 MPa, and radial power depression P_{out}/P_{center} = 2.8. The test rod is cooled by stagnant water at 25 °C, 0.1 MPa. The fast power pulse (4.4-ms half-width) led to a maximum fuel enthalpy of 73 cal/g fuel.

The calculation has been made without activation of the rim option and with the use of the clad mechanical laws derived from Ref. 18 ($\sigma_{yield\ stress}$ = 698 MPa at 25 °C) and the standard clad–fluid heat transfer of SCANAIR. The maximum fuel temperature is 1650 °C (at 206.5 ms), and clad plastification is obtained at 203.5 ms, which corresponds to the experimental failure time: this is fully consistent with the assumption of clad brittleness caused by concentration of hydrides in the peripheral part of the cladding and enhanced by the low initial temperature. At failure time, the maximum clad hoop strain is evaluated to be 0.3%, and the mean fuel enthalpy is 51 cal/g fuel.

Such a result indicates that the rod failure is due to PCMI related to fuel thermal expansion without any significant effect of the rim transient behavior in opposition to the CABRI REP-Na1 failure mode, which involves the contribution of the pressurization of the gases in the rim on clad loading. This low effect of the rim zone is also consistent with the understanding of the CABRI REP-Na3 (four-cycle rod) performed at about the same burnup as the HBO-1 test but with a higher energy injection.

Beyond failure time, the calculation indicates that DNB is reached (220 ms) with a maximum radially average fuel enthalpy of 73 cal/g fuel. Such a result cannot be directly compared with the HBO-1 test because of rod failure; however, it seems consistent with the result of the nonfailed test HBO-3 performed with a similar rod (lower span) and same energy injection, which showed DNB occurrence.

Extrapolation to Reactor Conditions

Reactivity injection transients have been calculated by considering a fuel rod at high burnup (62 MWd/kgU) and highly oxidized (80 μm in zirconia thickness, nonspalled) similar to the rod used in the REP-Na4 test but placed in a pressurized-water environment.

The initial conditions of the CABRI REP-Na4 rod were adjusted so as to reproduce the state at EOL of the corresponding PWR rod (plenum volume adjusted to rod section, composition, quantity, and pressure of gases in the free volumes; coolant conditions: T = 280 °C, P = 15.5 MPa, and v = 4 m/s). These calculations were intended to evaluate the effects of some physical parameters on the main results during the accident sequence.

Two power pulses based on PWR 900-MW transients starting at zero power and leading to the same maximum fuel enthalpy of 80 cal/g fuel (envelope case) were calculated with two different half-widths: 75 ms [slow pulse (SL) case] and 20 ms [fast pulse (FT) case], which led to different total energy depositions (Fig. 24). The rapid transient could correspond to the simulation of an RIA in UO_2–MOX fuel management.

Study of the Initial Phase (PCMI). Comparison of the results has shown that, at the same maximum enthalpy reached in the fuel, a rapid energy injection plays the part of an envelope in the initial phase of the transient. Indeed, the energy deposit is increased in the rim zone because of the radial power profile ($P_{out}/P_{center} \sim 3$), which leads to a high temperature in the pellet periphery (Fig. 25) and thus to a strong PCMI under high strain rate and with cold cladding. In case of embrittlement by hydriding at a high corrosion level, such conditions have been shown to be penalizing (CABRI REP-Na1 rod failure). These results are also consistent with the different clad strainings obtained in CABRI REP-Na4 and REP-Na5 performed with slow and fast pulses.

Figure 26 shows that, in case of a rapid transient, the strain energy density (SED = $\int_t \sigma_i d\varepsilon_i$, only tensile stresses) is much higher in the first milliseconds than with a slower transient in spite of similar maximum values reached later. Considerations on the SED could be used for failure evaluation provided that critical SED values are established for the cladding material as a function of temperature, strain rate, and corrosion level; such data are expected from the PROMETRA program but are not yet available for use in SCANAIR.

Late Phase with Cladding Heatup. Figure 26 also shows that for both transients considered the external clad temperature does not increase after the first milliseconds because no DNB was detected in those calculations (standard laws of SCANAIR); however, a tendency toward higher clad temperature is found with the slow pulse.

The influence of the cladding–coolant heat transfer has been studied with the use of a DNB criterion based on a critical heat flux of 1.8 MW/m^2 and the correlation of Bishop–Sandberg–Tong after DNB. The results have shown that the use of this correlation leads to DNB occurrence for a lower fuel enthalpy (60 to 66 cal/g fuel in slow and fast pulses) than the one given by the standard correlation of SCANAIR (95 to 100 cal/g fuel for slow and fast pulses). In case of DNB, the clad temperature increase (and thus the reduction of its mechanical resistance) is associated with a high plenum pressure linked to important fission gas release; such effects enhance the risk of a delayed rod failure. The strong influence of the correlations used on the results underlines the need for a better knowledge of heat-transfer conditions under fast transients. The out-of-pile PATRICIA experimental program devoted to the determination of heat-exchange laws should reduce the uncertainty in this field.

The CABRI REP-Na tests have shown the occurrence of oxide spallation during the RIA transients under the effect of clad deformation: very important spalling in REP-Na4 with an 80-μm oxide layer but also with lower oxide thickness as in REP-Na3 and REP-Na6 (tests with MOX fuel). Such an effect has been simulated in the case of a fast power pulse, in which the oxide spalling was assumed to occur at the onset of the transient (with no zirconia layer). Compared with the FT case, DNB is reached very early and leads to high cladding heatup [$T_{cl,\,max}$ = 913 °C instead of 353 °C in the FT case (Fig. 27)] as a result of the disappearance of the oxide layer, which increases the heat transfer to the coolant.

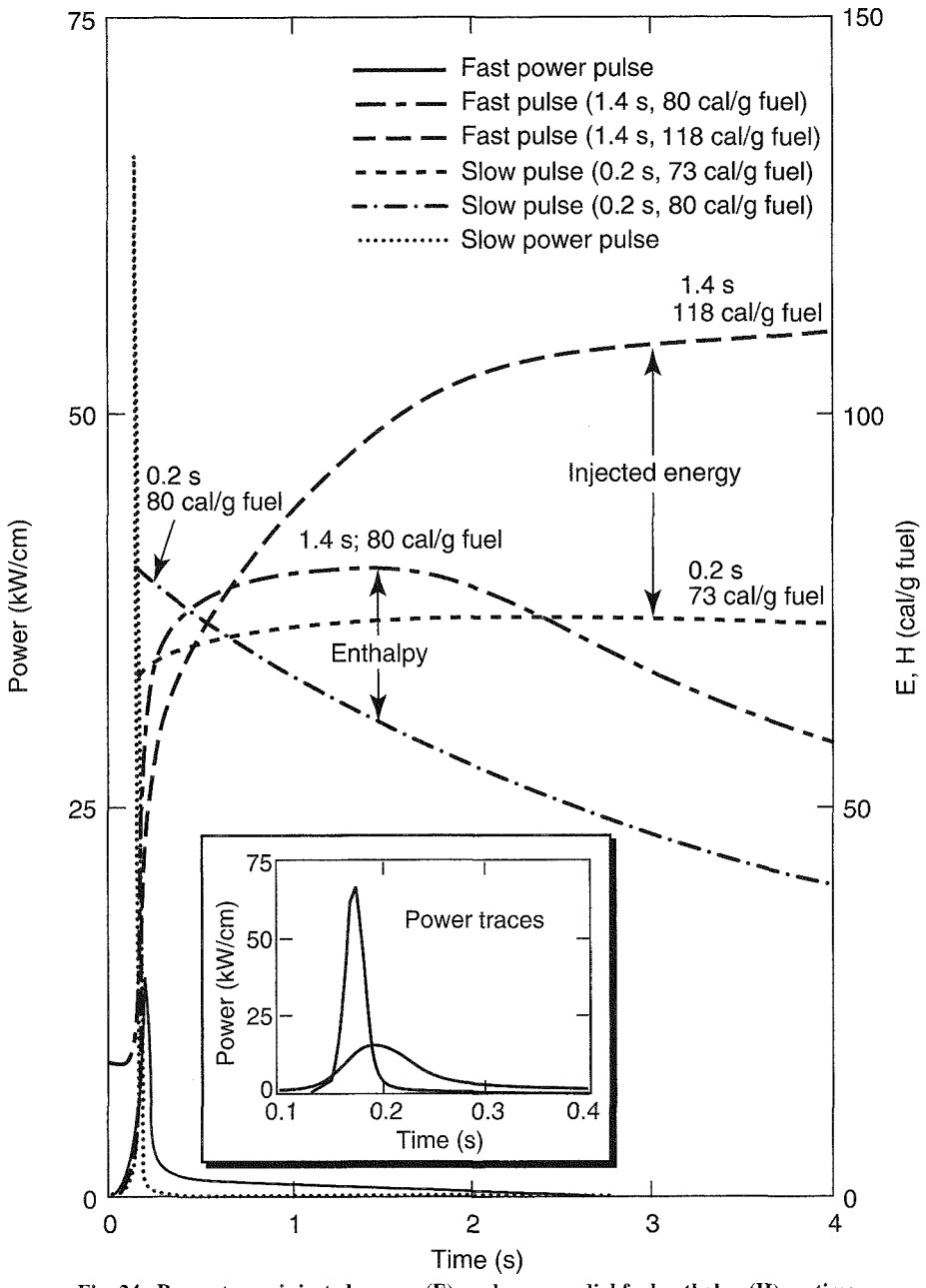

Fig. 24 Power trace, injected energy (E), and mean radial fuel enthalpy (H) vs. time.

Similar to the previous results, the evolution of the internal rod pressure as the result of high fission gas release and associated with the high clad temperature level (Fig. 27) may enhance the risk of delayed rod failure. Moreover, because of the reduction of the heat transfer, the cooling down of the fuel is much slower, and in case of rod failure with fuel ejection, violent water vaporization may occur.

Another parameter that influences the clad heatup is the gap conductance. This can be seen in Fig. 28 by the comparison of the calculations of the HBO-1 rod (four-cycle rod, 3% of fission gas in the gap) and the REP-Na4 rod (five-cycle rod, 12% of fission gas in the gap) in reactor conditions under fast power pulses with similar maximum fuel enthalpy (HBO-1 rod: 30-ms half-width, H_{max} = 73 cal/g fuel; REP-Na4 rod: 20-ms half-width, H_{max} = 80 cal/g fuel).

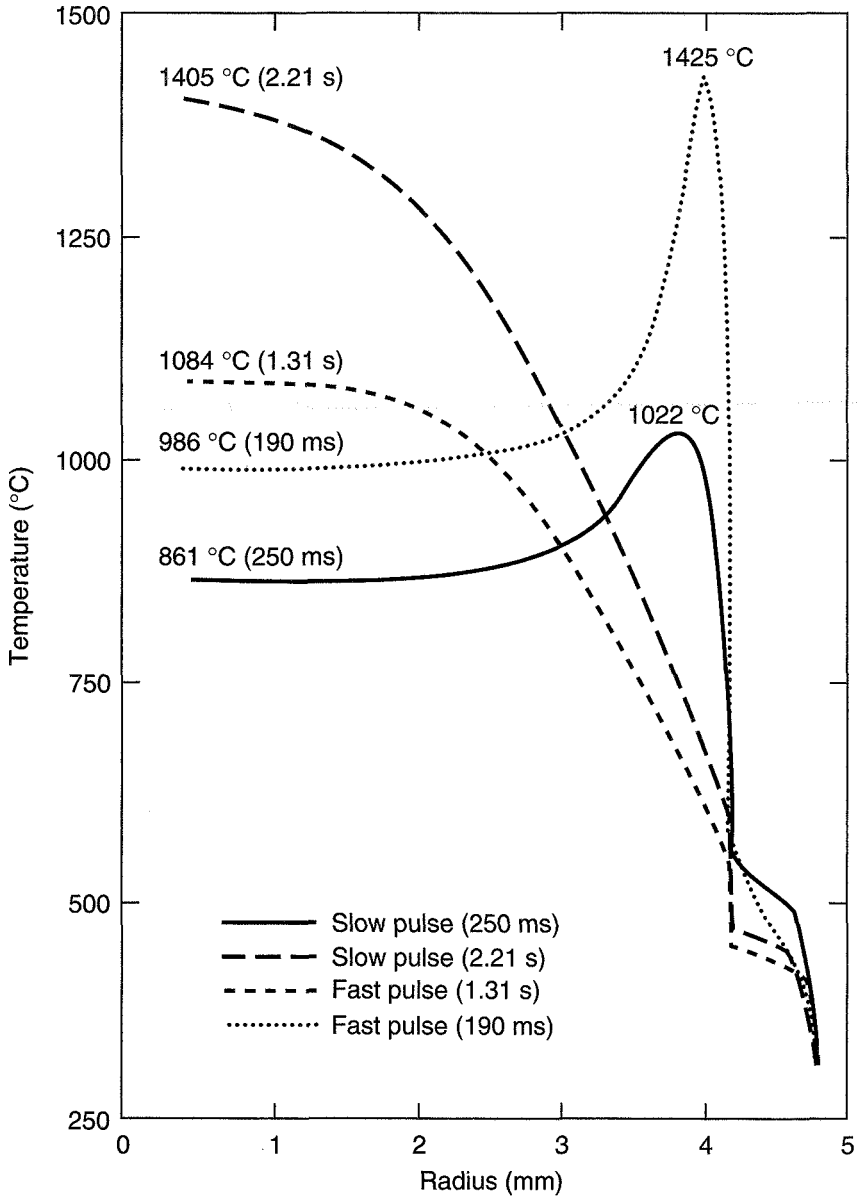

Fig. 25 Comparison of radial temperature profiles for slow and fast pulses.

Indeed, the previous study has shown that, with the standard laws of SCANAIR for the cladding–coolant heat transfer, the DNB occurrence is found for a fuel enthalpy of 100 cal/g fuel, whereas it is calculated for 73 cal/g fuel with the HBO-1 rod. This is related to the higher gap conductance value in a four-cycle rod caused by lower fission gases concentration (higher helium rate) at the end of irradiation compared with a five-cycle rod. This difference is not erased by the transient fission gas release and the gap closure, and it underlines the importance of a good knowledge of the initial state of the rod after irradiation.

THE OUT-OF-PILE RELATED STUDIES

Cladding Mechanical Properties

Scope of the PROMETRA Program. Loading conditions encountered by the cladding during an RIA are far from those addressed by surveillance programs

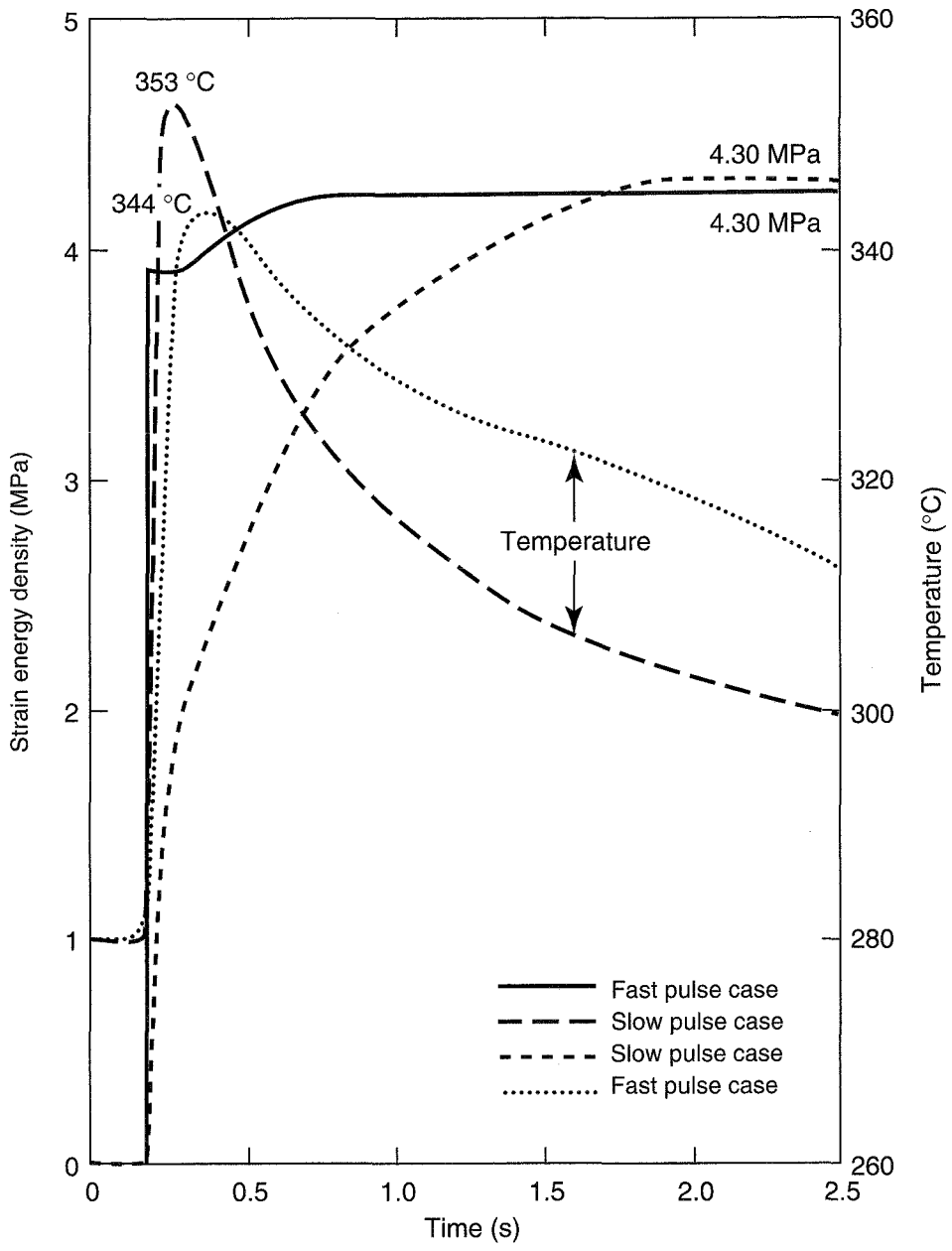

Fig. 26 Comparison of the external clad temperature and strain energy density evolution for slow and fast pulses.

of the clad mechanical properties: the strain rate is much higher (typically 1 s^{-1} instead of 3×10^{-4} s^{-1}), especially during the first stage dominated by PCMI; also, the heatup rate (of the order of 103 $K \cdot s^{-1}$) is very fast. Relevant temperatures for the reactor case vary between 280 and 1482 °C; however, rather cold temperatures are of interest to the interpretation of CABRI REP-Na experiments and even room temperature for NSRR. Therefore out-of-pile tests had to be programmed to investigate transient mechanical properties of the irradiated cladding; the objective is to set up a data base to be used by accident codes such as

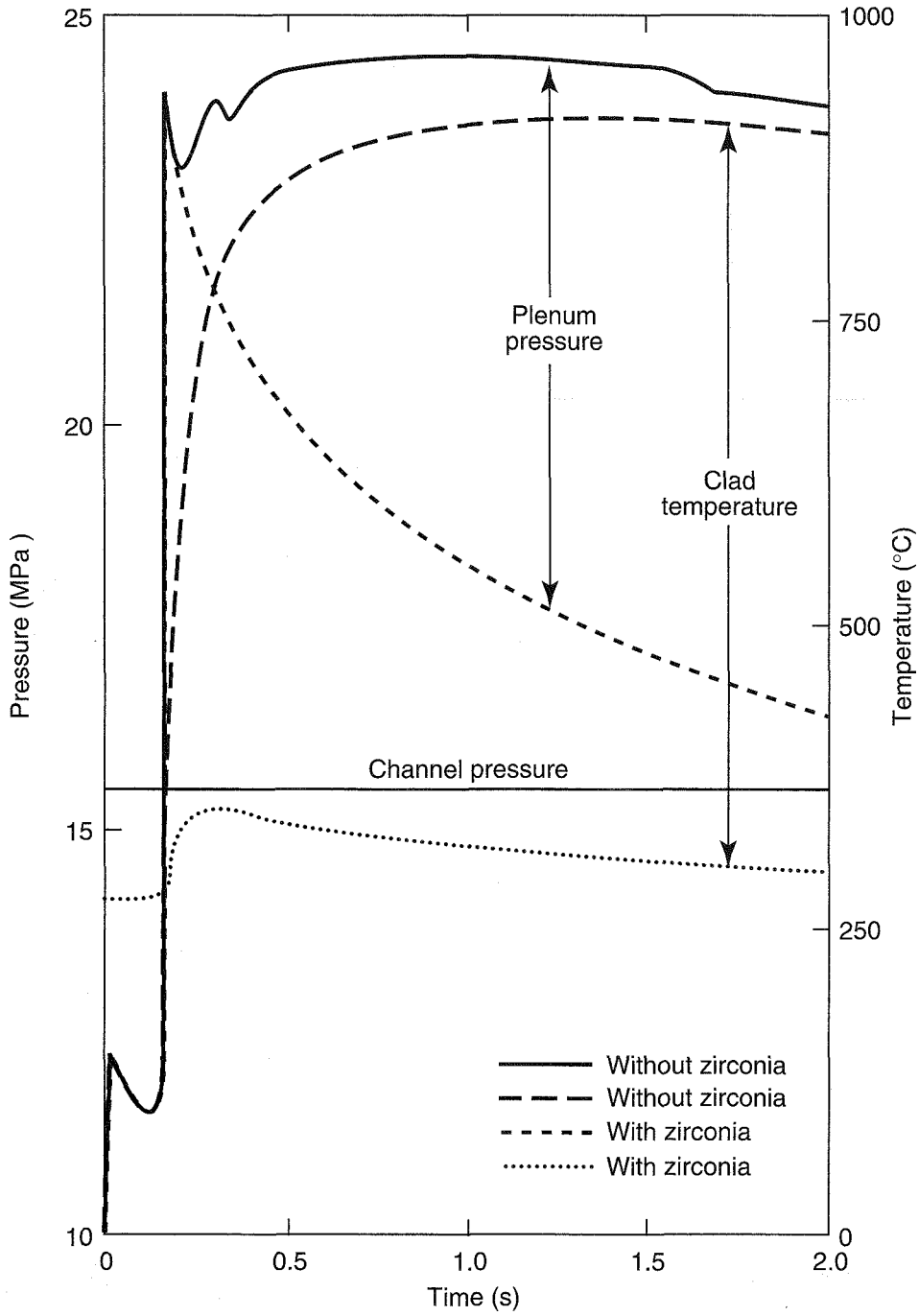

Fig. 27 Influence of the oxide layer spallation on the clad temperature and internal rod pressure.

SCANAIR for calculating the transient response of the cladding. Also, a failure criterion must be established, for instance, in terms of strain energy density.

The premature failure in CABRI REP-Na1 has put to light the previously unexpected circumstance that stresses may develop early when the cladding is still cold and brittle; then ample evidence of clad embrittlement has been provided by posttest examinations. Similar, less-severe results were obtained afterward in the NSRR. Therefore some knowledge of the

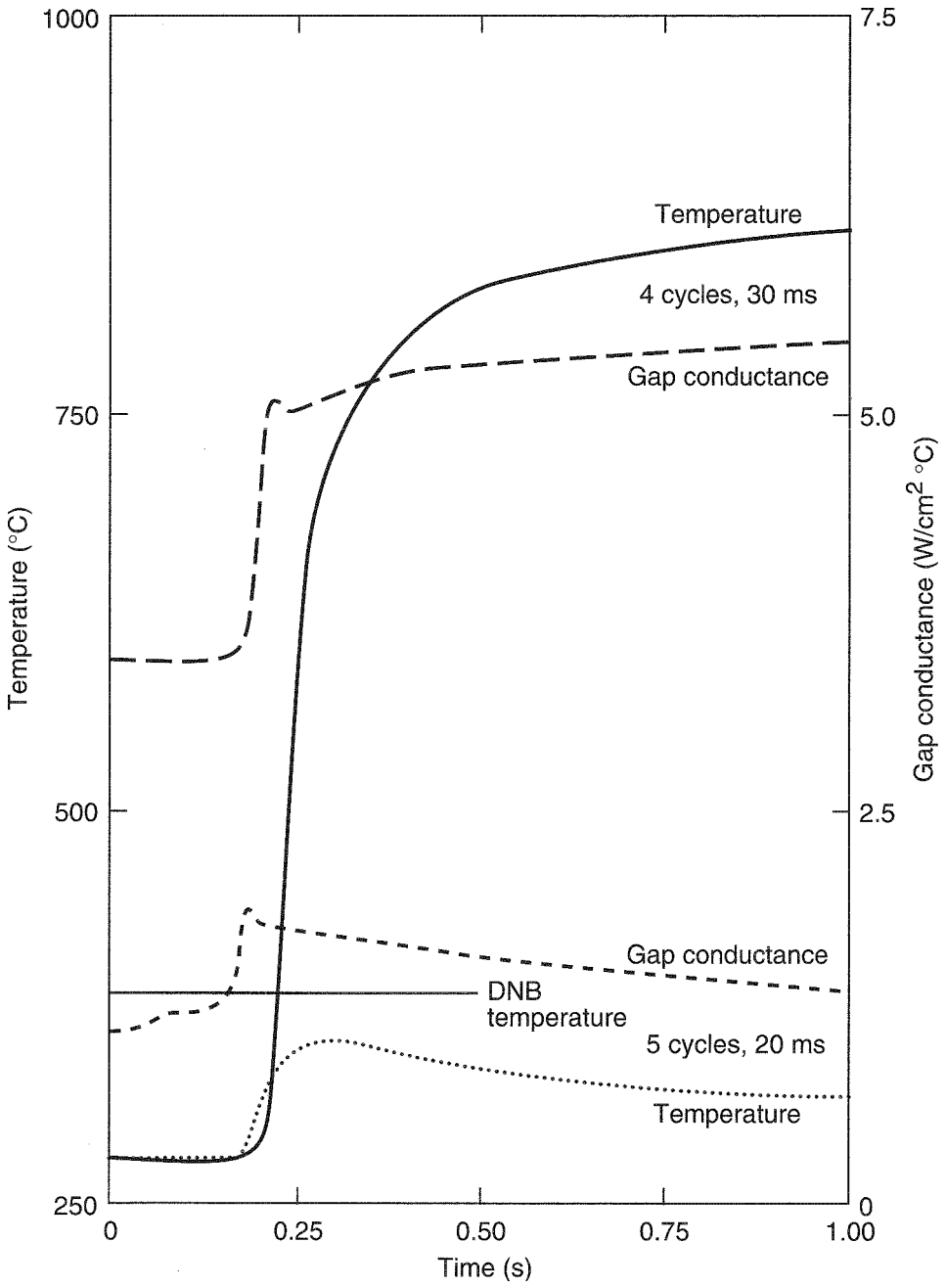

Fig. 28 Comparison of the external clad temperature and gap conductance evolutions of four-cycle and five-cycle rods under fast pulses (20 to 30 ms).

ductile-to-brittle transition (DBT) of irradiated Zircaloy-4 is needed.

Mechanical properties are affected by the base irradiation through many factors: neutron dose, possibly some mechanical damage linked with load-follow operation, microstructure, and composition changes with hydrogen and oxygen uptake; however, the dominant influence is exerted by the hydride precipitates so that mechanical properties should be studied as a function of hydriding, which is determined by the corrosion state.

The typical state of the irradiated cladding in upper spans (4, 5, 6) of a 60-MWd/kgU rod is characterized

by a thick outer ZrO_2 layer (80 to 90 μm) and by a significant hydrogen buildup with 700 to 800 ppm mean content and with a concentration gradient toward the outside. At the low temperatures of interest to NSRR or CABRI experiments (20 to 280 °C), the hydrogen solubility is negligible, and it has precipitated as circumferentially oriented platelets of hydride. Such is the situation that is currently encountered and that has been tested in CABRI REP-Na4 with a broad power pulse applied to a nonspalled rod. Much less typical characteristics may arise if the base irradiation of a cladding with an already spalled ZrO_2 is pursued, giving way locally to drastic changes; hydrogen migrates toward the colder spalled zones and thus forms "sun-burst"-like hydride accumulations. This is obviously the case for rods of an older design, such as the one tested in CABRI REP-Na1 with a narrow power pulse and the one to be tested in REP-Na8 with a broad pulse. Also, compared with the rod tested in REP-Na4 and REP-Na5, those rods had spent a longer time under load-follow operation, which may have contributed to their considerable degree of spalling.

In principle, measuring tensile properties under RIA conditions should provide the set of data needed for accident codes, at least as far as normal or regular rods are concerned (i.e., without any spalling). This is the objective of a first series of tests performed at CE-Saclay. The question of rods with randomly distributed local defects (i.e., spalled rods where hydride accumulations may be suspected) may not be managed so straightforwardly. As a preliminary step, it seems worth while to investigate the DBT of irradiated and possibly spalled cladding. This issue is addressed by a second series of tests launched at CE-Grenoble.

First Series of Tests: Establishing a Data Base. Presently, CABRI REP-Na tests aim at simulating the first phase in an accident starting from hot zero power conditions. Therefore the main interest is in cold temperatures, between 280 °C (even room temperature is of interest for the interpretation of NSRR experiments) and about 600 °C.

Different initial conditions, however, starting from nonzero power, may be addressed by future tests; therefore higher temperatures have to be investigated, too, up to 1100 °C (above that, measurements are useless). In the fast CABRI ramps, PCMI leads to rapid loading with roughly 1-s^{-1} strain rate [indeed, with the use of sodium flow expulsions measured during nonfailure tests (for example, REP-Na2), strain rates can be estimated to be of the order of 5 s^{-1}]. During a later phase, slower but still high strain rates can be expected, typically 0.01 s^{-1}; slower CABRI ramps such as REP-Na4 or the reactor case fall in between. PCMI results in hoop and axial stresses with any possible value of the σ_z/σ_θ ratio. Therefore mechanical properties in the transverse as well as in the rolling directions are needed, especially in the colder temperature range where anisotropy is expected. Depending on the temperature reached, the heatup rate may be of importance; thus transient heating must be accounted for, at least above 600 °C (from preliminary tests, it appeared that 100 $K \cdot s^{-1}$ was enough for simulating higher heating rates).

The pretest condition addressed corresponds, after five runs, to a target burnup of about 60 MWd/kgU locally with up to 100-μm oxide thickness. This will be used as the relevant characteristic because other parameters, hydriding and oxygen uptake, go along with corrosion, and mostly one neutron dose is considered.

Thus the issue of the data base for the more typical cladding hopefully can be resolved by measuring tensile properties as a function of the following parameters:

- Hydriding (i.e., corrosion) (ZrO_2 = 0 to 80 μm).
- Temperature history (transient or slow heating).
- Loading direction (axial or hoop).
- Temperature (280 to 1100 °C).
- Strain rate (0.01 to 5 s^{-1}).

Tensile specimens have been spark machined, with well-defined gauge lengths, either in the rolling or in the transverse direction of chemically defueled samples from up to 63 MWd/kgU burnup rods. These two-wing specimens are similar to those used for years for testing stainless steel cladding except that the outer oxide layer of irradiated samples must be removed before machining. Only samples without spalling have been selected to avoid local effects. In consequence, the effect resulting from local hydride accumulations is not reflected in the test results.

Results in the high-temperature range (400 to 1100 °C) and at three strain rates (0.01, 0.2, and 5 s^{-1}) were obtained in 1992 and 1993 on fresh and high-burnup cladding (26 tests each) tensile tested in the rolling direction.[19] All samples, either fresh or five-cycle irradiated in the Gravelines reactor, corresponded to the standard FRAGEMA design (i.e., stress-relieved Zircaloy-4 with 1.5% tin). Tests above 700 °C have been performed with the use of specimens with a shorter gauge length (5 mm), which allows for

transient heating at 100 $K \cdot s^{-1}$ by an electric current passing through the sample. Below 800 °C, specimens with a longer gauge length (15 mm) have been tested after slow furnace heating at about 0.1 $K \cdot s^{-1}$; this may result in some recrystallization above 600 °C. All tests have been performed under air.

Tests in the low-temperature range (280 to 600 °C) and at two strain rates (0.01 and 5 s^{-1}) have been carried out in 1996 in the transverse and rolling directions (respectively, 48 and 22 tests) of four- and five-cycle irradiated cladding, including some samples with an improved design (low tin); as a further reference, a few fresh samples have been tested. According to the oxide thickness, either measured by eddy currents or surmised from the sample position, different corrosion levels could be identified: very feeble (<20-μm ZrO_2 on four-run irradiated samples), feeble (~30 μm), medium (50 to 55 μm), and strong (65 to 85 μm). Only specimens with a longer gauge length have been used for the axial tests. Rings machined for hoop tests have a 3-mm gauge length. Again, tests have been triggered after slow furnace heating. As shown by metallographic examination, hydride precipitates in irradiated specimens tested at 600 °C have been homogeneously redistributed with no preferential orientation. As far as axial tests are concerned, results of the 1996 campaign are consistent with those of 1993 in the overlapping temperature range.

In the rolling direction, the yield stress (YS) and the ultimate tensile strength (UTS) of fresh and irradiated cladding are observed to decrease with increasing temperature and with decreasing strain rate. Irradiation results in increased strengths (YS and UTS) compared with the as-fabricated condition. Strengths of samples with the thickest oxide layer are reduced with respect to less corroded ones. Corrosion results also, especially at high strain rate, in a decrease of the uniform elongation (UE) and of the total elongation; however, some ductility is maintained (UE > 2%).

Variations with strain rate and with corrosion are apparently less pronounced in the transverse direction. The UE of samples with the strongest corrosion is significantly reduced, down to <1% mainly at high strain rate (Fig. 29). Much higher elongations are observed toward 600 °C as a result of recrystallization and, possibly, of hydride redistribution. No striking anisotropy can be found when results from hoop and axial tests are compared.

Even though low ductility values have been recorded, no fully brittle result has been obtained even at 280 °C and 5 s^{-1}. It must be stressed that these results hold true only for rods without any local defect such as spalling. By integrating the recorded tensile curves, SED values at failure can be obtained readily, but such raw results, including elastic contributions from the apparatus, can only be quoted on a differential basis. Thus SED values of samples with maximum corrosion tested at high strain rate are 15 MPa lower than those of less corroded ones. Finite-element analyses with the CASTEM 2000 code are under way; by modeling stress and strain fields within samples, local values (for instance, of the maximum SED) will be estimated, and possible artifacts as the result of specimen design will be assessed.

Two burst tests on 120-mm-long tube samples have been performed at 350 °C with nearly 0.01-s^{-1} strain rate: results are consistent with those from uniaxial tests.

Second Series of Tests: DBT Studies. A special series of tests was started in 1996 to investigate the DBT as a function of the relevant parameters:

- Hydriding (limited, corresponding to 30 μm ZrO_2, up to the most severe one with spalling).
- Temperature (20 to 350 °C).
- Strain rate (3×10^{-4} to 5 s^{-1}).

Here the ductility is estimated from tensile tests on simple rings (i.e., with an ill-defined gauge length) cut from mechanically defueled samples taken on span 6 of the rod tested in CABRI REP-Na1. From previous tests, it appeared that consistent results were obtained assuming a 5-mm gauge length; this value has been confirmed by testing an unirradiated ring with an engraved pattern. Because of difficulties encountered with mechanical defueling at high burnup, only six tests with reliable results have been performed. Test temperatures are too close (280 and 350 °C) for differences to be observed; however, there is a marked influence of the strain rate. Two rings tested at 5 s^{-1} failed with a negligible elongation by a brittle-like straight crack (Fig. 30): this supports the REP-Na1 result. At 0.01 s^{-1}, two rings failed with about 10% elongation by ductile shear, but two other rings, ruptured with a negligible ductility, exhibited a mixed behavior: brittle cracking through spalled regions and ductile shear over the remaining sample width (Fig. 30).

These first observations, especially the correlation between embrittlement and spalling, are confirmed by SEM examinations. Ductile structures with dimples are

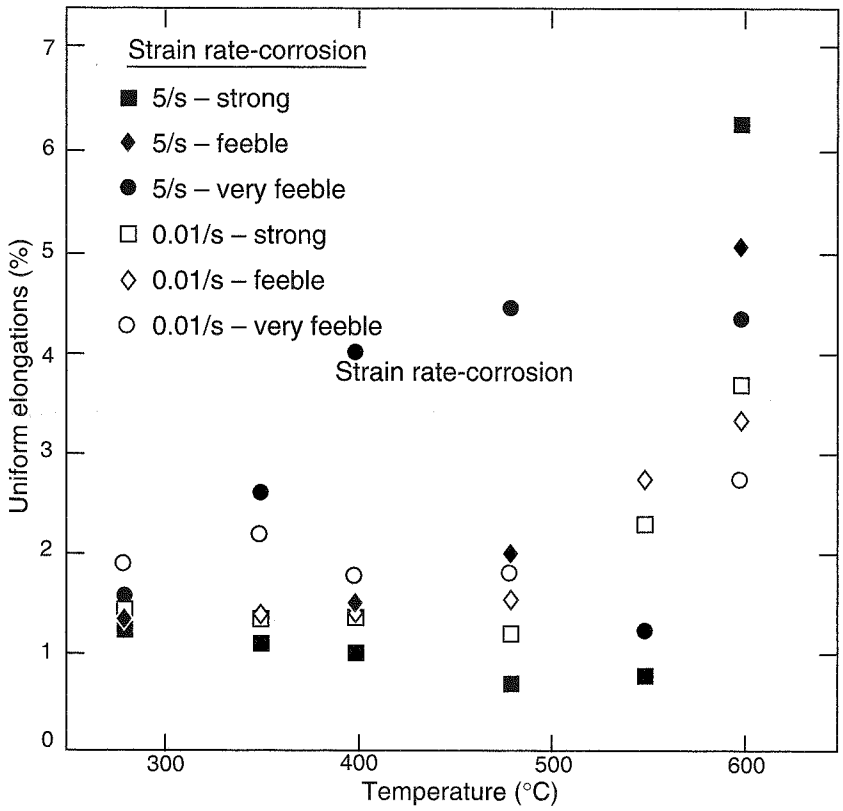

Fig. 29 Uniform elongations in the transverse direction vs. temperature (nonspalled cladding).

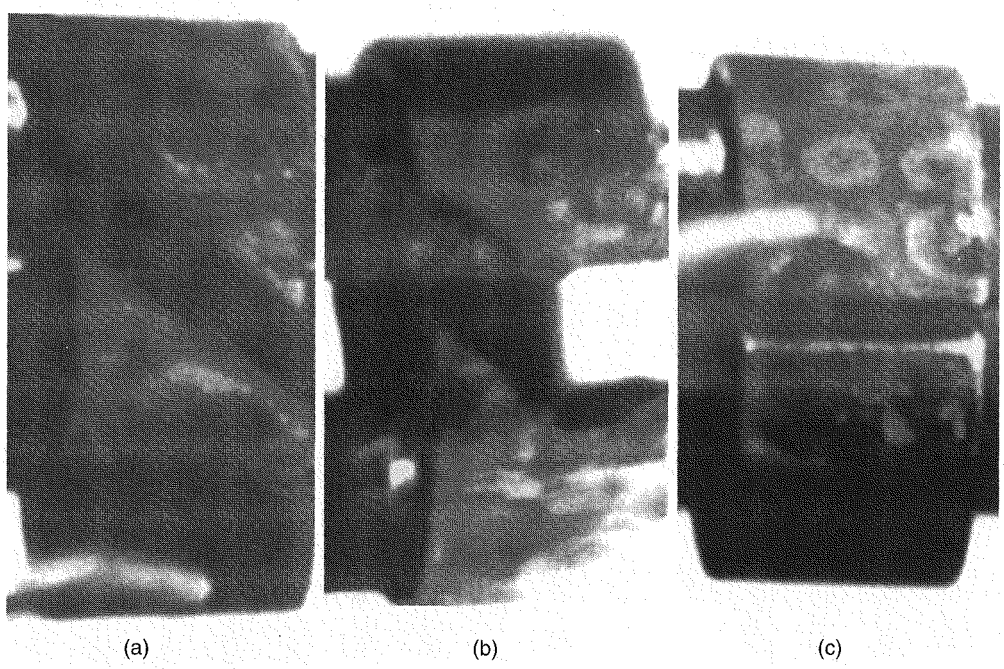

Fig. 30 Spalled rings after tensile tests. (a) 280 °C and 0.01 s^{-1}, 12% uniform elongation—ductile. (b) 350 °C and 0.01 s^{-1}, 1.5% uniform elongation—mixed. (c) 280 °C and 5 s^{-1}, 0% uniform elongation—brittle.

evidenced in regions with shear failure (everywhere on the most ductile samples and partially on samples with a mixed failure); brittle zones are seen elsewhere, but these are surrounded by ductile ligaments. The structure variation through the clad thickness is noticed on samples with brittle and mixed failure—from ductile toward the inside to rather brittle in the outer rim. Similar observations have been made after REP-Na1.

The mean hydrogen content can be estimated from the ZrO_2 thickness measured by an eddy-current technique. On three specimens, local concentrations will be measured after test by heating and gas chromatography with the use of small samples taken near the failure site and in the opposite direction. Optical micrography of the other three specimens is under way to characterize hydride distributions by image analysis; also, hydrogen profiles should be measured by secondary ion mass spectrometry (SIMS). On the first micrographs, features resembling those obtained after REP-Na1 are found, which further confirms the correlation between brittle failure and hydride accumulations (Fig. 31).

From these six tests, the DBT of spalled cladding seems to pass through 0.01 s^{-1} and 300 °C; tests are still to be carried out at lower strain rates and colder temperatures. In view of results from the first series in Saclay, investigations at high strain rates (0.01 to 5 s^{-1}) and cold temperatures (20 to 150 °C) will be pursued in 1997 on nonspalled cladding. Finite-element analysis, aimed at assessing geometrical artifacts and estimating local maximum SED values at failure, is under way also.

Failure Criterion. Mechanical behavior laws for computer use will be built up on the basis of the first series of tests and also on low strain-rate tensile tests from the surveillance program (hoop and axial), thus covering a wide range of loading conditions. Results from tests on spalled cladding (second series) will be included as far as SED is concerned. In principle, any criterion (for example, the UTS) could be employed by the accident code for failure prediction. Nevertheless, most benefits are expected from using the SED at failure (critical SED): a sort of cumulative damage, including contributions from various loads, can thus be computed at every time step. Margins to failure can be estimated by simply comparing the potential work from fission gases with the strain energy limit of the cladding. This might offer a means of dealing with rods suffering from local defects such as spalling. Experimental SED values can also be compared with results from other sources, for example, EPRI.[14]

Cladding-to-Coolant Heat Transfer

The objective of this out-of-pile program (PATRICIA) is to determine the cladding-to-coolant heat transfer laws under RIA-type transients on the basis of experimental results. Indeed, up to now, the available thermal–hydraulic correlations have been established in steady-state or loss-of-coolant-accident (LOCA) conditions, far from RIA heating rate conditions. The strong influence of the cladding–fluid heat transfer on the evolution of rod behavior in the late phase of the accident has underlined the need for better knowledge in this field, in

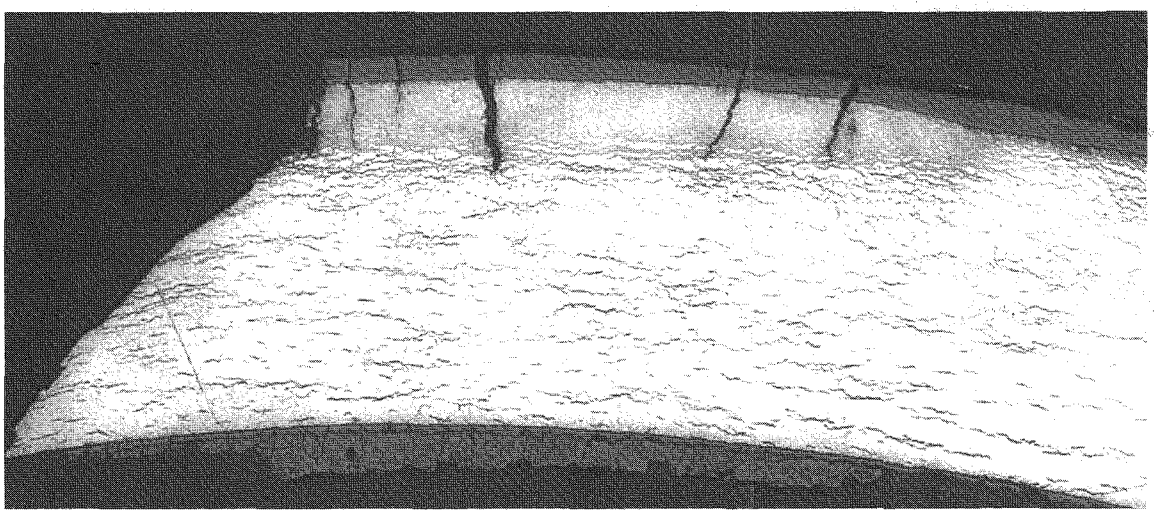

Fig. 31 Spalled ring tested at 350 °C and 0.01 s^{-1}, 1.5% uniform elongation.

particular for the determination of DNB thresholds. The main aspects to be studied are the fast kinetics with the presence of steep transient thermal gradients near the cladding (vapor film instability) and the state and/or nature of the clad surface with the presence of an oxide layer.

The tests are foreseen with electrically heated 1-m-long rods (direct heating in the cladding tube made of Inconel) with realistic thermal–hydraulic conditions such as pressure, initial temperature, flow rate, and power transient in the cladding resulting from fast and slower power pulses (10- to 80-ms half-widths) as predicted by SCANAIR calculations.

The program has been defined with three main steps:

1. Realization of tests under steady-state conditions for verification of the consistency of the obtained results with the classical laws.
2. Realization of a basic test matrix with flow, pressure, inlet temperature, and power transient as variable parameters.
3. Complementary tests for evaluation of the influence of heated rod length, hydraulic diameter, and surface state using Zircaloy rods.

The first tests are being performed, but interpreted results are not yet available.

CONCLUSIONS

The evolution of the fuel-management system in French PWRs, aimed at increasing the burnup to 52 MWd/kgU, as well as the absence of an experimental basis for MOX rods has motivated the IPSN to initiate new studies, particularly in the framework of RIAs such as control-rod ejection.

The CABRI REP-Na experimental program performed with high-burnup UO_2 and MOX fuel rods, its interpretation, and the SCANAIR code-related studies have led to a better understanding of fuel behavior under RIAs. By comparison with fresh fuel, two main features characterize the high-burnup fuel behavior under RIAs:

1. The increasing amount of fission gases with burnup, which generates a high potential for fuel swelling and expansion under rapid heating conditions.
2. The clad embrittlement caused by hydrogen buildup and the possibility of local hydride accumulation with degradation of the clad mechanical properties resulting in possible early failure as in the REP-Na1 experiment.

The unfailed REP-Na tests underlined the ability of a cladding without oxide layer spalling to withstand the significant PCMI caused by such a fuel loading. Other phenomena, such as fuel fragmentation, modifications in the microstructure, large fission gas release, and transient oxide spallation, were evidenced and underlined the importance of knowledge of the initial state (gas retention and rim characteristics) and of the kinetics aspects under transient conditions (dynamic loading and gas release).

The interpretation of the experiments with the SCANAIR code has shown a satisfying status of validation; however, the extrapolation to reactor conditions has underlined the high influence of the cladding–fluid heat transfer on the risk of delayed rod failure as the result of clad temperature increase associated with internal rod pressure, especially in the case of transient oxide layer spallation.

The ongoing test programs PATRICIA (cladding-to-coolant heat transfer) and PROMETRA (clad mechanical properties and failure criterion) should bring the relevant information to be implemented in SCANAIR and reduce the uncertainties on these points. Although important knowledge has been gained through the CABRI REP-Na experiments, they were not devoted to the study of the whole phenomenology of high-burnup rods submitted to RIA transients because clad temperatures typical of the reactor situation cannot be achieved. Such aspects underline the need already expressed by the authors[8,20,21] of an extension of the analysis under a representative water environment before any conclusions can be derived for safety issues.

ACKNOWLEDGMENTS

The authors feel indebted to Messrs. Breton, Cazalis, and Rigat (IPSN) for the interpretation of the CABRI tests and reactor calculations, to Messrs. Lespiaux and Noirot (DRN) for posttest examinations at CE Cadarache, and to Messrs. Piron and Royer for mechanical testing at Grenoble and Saclay.

REFERENCES

1. M. C. Anselmet et al., The Experimental Test Program for the Study of High-Burnup PWR Rods Under RIA Conditions in the CABRI Core, in *Proceedings of the CSNI Specialist Meeting on Transient Behavior of High Burnup Fuel,* Cadarache, France, September 12–14, 1995, Report NEA/CSNI/R(95) 22, 1996.

2. D. Lespiaux et al., Post-Test Examinations of High Burnup Fuels Submitted to RIA Transients in CABRI Facility, in *Proceedings of the International Topical Meeting on Light Water Reactor Fuel Performance,* Portland, Oregon, March 2–6, 1997, American Nuclear Society.
3. C. Struzik, M. Moyne, and J. P. Piron, High Burnup Modelling of UO_2 and MOX Fuel with METEOR-TRANSURANUS Version 1.5, in *Proceedings of the International Topical Meeting on Light Water Reactor Fuel Performance,* Portland, Oregon, March 2–6, 1997, American Nuclear Society.
4. F. Lemoine, High Burnup Fuel Behavior Related to Fission Gas Effects Under RIA Conditions, in *Proceedings of IEQES-96,* Mito, Japan, August 21–23, 1996.
5. K. Ishijima, Y. Mori, T. Fuketa, and H. Sasajima, Postulated Mechanisms on the Failure of 50 MWd/kgU PWR Fuel in the NSRR Experiment and the Related Programs in JAERI, in *Proceedings of the CSNI Specialist Meeting on Transient Behavior of High Burnup Fuel,* Cadarache, France, September 12–14, 1995, Report NEA/CSNI/R(95) 22, pp. 87-105, 1996.
6. P. Guedeney, M. Trotabas, M. Boschiero, C. Forat, and P. Blanpain, in *Proceedings of the ANS Topical Meeting on Light Water Reactor Fuel Performance,* Avignon, France, April 21–24, 1991, p. 639.
7. F. Lemoine and M. Balourdet, RIA Related Analytical Studies and Separate Effect Tests, in *Proceedings of the International Topical Meeting on Light Water Reactor Fuel Performance,* Portland, Oregon, March 2–6, 1997, American Nuclear Society.
8. J. M. Frizonnet, J. P. Breton, H. Rigat, and J. Papin, The Main Outcomes from the Interpretation of the CABRI REP-Na Experiments for RIA Study, in *Proceedings of the International Topical Meeting on Light Water Reactor Fuel Performance,* Portland, Oregon, March 2–6, 1997, American Nuclear Society.
9. L. E. Thomas, C. E. Beyer, and L. A. Charlot, Microstructural Analysis of LWR Spent Fuels at High Burnup, *J. Nucl. Mater.,* 188: 80-89 (1992).
10. K. Nogita and K. Une, Irradiation-Induced Recrystallization in High Burnup UO_2 Fuel, *J. Nucl. Mater.,* 226: 302-310 (1995).
11. F. Lemoine and F. Schmitz, Impact of Fission Gas on Irradiated PWR Fuel Behavior at Extended Burnup Under RIA Conditions, in *Proceedings of the CSNI Specialist Meeting on Transient Behavior of High Burnup Fuel,* Cadarache, France, September 12–14, 1995, Report NEA/CSNI/R(95) 22, 1996.
12. S. R. Pati, A. M. Garde, and L. J. Clink, Contribution of Pellet Rim Porosity to Low-Temperature Fission Gas Release at Extended Burnups, in *Proceeding of the International Topical Meeting on Light Water Reactor Fuel Performance,* Williamsburg, Virginia, April 17–20, 1988, p. 204.
13. J. T. A. Roberts and Y. Ueda, Influence of Porosity on Deformation and Fracture of UO_2, *J. Am. Ceram. Soc.,* 55(3): 117-123 (March 1992).
14. O. Ozer et al., Evaluation of RIA Experiments and Their Impact on High Burnup Fuel Performance, in *Proceedings of the CSNI Specialist Meeting on Transient Behavior of High Burnup Fuel,* Cadarache, France, September 12–14, 1995, Report NEA/CSNI/R(95) 22, 1996.
15. J. Papin, H. Rigat, F. Lamare, and B. Cazalis, The SCANAIR Code for the Description of PWR Fuel Rod Behavior Under RIA: Validation on Experiments and Extrapolation to Reactor Conditions, in *Proceedings of the International Topical Meeting on Light Water Reactor Fuel Performance,* Portland, Oregon, March 2–6, 1997, American Nuclear Society.
16. J. C. Latché, F. Lamare, and M. Cranga, Computing Reactivity Initiated Accidents in PWRs, in *Transactions of the 13th International Conference on Structural Mechanics in Reactor Technology,* Porto-Alegre, Brazil, August 13–18, 1995, pp. 33-44.
17. K. Lassmann and H. Blank, Modelling of Fuel Rod Behaviour and Recent Advances of the TRANSURANUS Code, *Nucl. Eng. Des.,* 106(3): 291-313 (March 1988).
18. F. Nagase, K. Ishijima, and T. Furuta, Influence of Locally Concentrated Hydrides on Ductility of Zr-4, in *Proceedings of the CSNI Specialist Meeting on Transient Behavior of High Burnup Fuel,* Cadarache, France, September 12–14, 1995, Report NEA/CSNI/R(95) 22, 1996.
19. M. Balourdet and C. Bernaudat, Tensile Properties of Irradiated Zircaloy 4 Cladding Submitted to Fast Transient Loading, in *Proceedings of the CSNI Specialist Meeting on Transient Behavior of High Burnup Fuel,* Cadarache, France, September 12–14, 1995, Report NEA/CSNI/R(95) 22, 1996.
20. J. Papin, H. Rigat, and J. P. Breton, The Behavior of Irradiated Fuel Under RIA Transients: Interpretation of the CABRI Experiments, in *Proceedings of the CSNI Specialist Meeting on Transient Behavior of High Burnup Fuel,* Cadarache, France, September 12–14, 1995, Report NEA/CSNI/R(95) 22, 1996.
21. F. Schmitz, Update of High Burnup Fuel Issues, in *Proceedings of the OECD/CSNI–PWG1 Specialist Meeting on Nuclear Fuel and Control Rods,* Madrid, Spain, November 5–7, 1996.

NSRR/RIA Experiments with High-Burnup PWR Fuels

By T. Fuketa,[a] F. Nagase,[a] K. Ishijima,[a] and T. Fujishiro[b]

Abstract: *Results obtained in the Nuclear Safety Research Reactor (NSRR) power burst experiments with irradiated pressurized-water-reactor (PWR) fuel rods with fuel burnup up to 50 MWd per kilogram of uranium (kgU) are described and discussed in this article. A series of experiments with irradiated PWR fuel rods was performed with the use of pulse irradiation capability of the NSRR. Fuel failure did not occur in the seven experiments, and fuel integrity was demonstrated at peak fuel enthalpy below 108 cal/g fuel (453 J/g fuel) for fuel burnup of 42 MWd/kgU or lower (tests OI-1, OI-2, MH-1, MH-2, MH-3, GK-1, and GK-2). In subsequent experiments with higher burnup fuels (tests HBO-1 through HBO-7) cladding failed at the relatively low energy deposition level for two tests (tests HBO-1 and HBO-5). This energy deposition level is lower than the provisional failure threshold [85 cal/g fuel (356 J/g fuel)] defined in the current Japanese guidelines. These results suggest that pellet–cladding mechanical interaction with reduced cladding integrity as the result of hydrogen absorption leads to the cladding failure. In the high-burnup fuel experiments, fission gas release to the fuel rod plenum reached 22.7% at maximum in the experiments for 50 MWd/kgU PWR fuels.*

For longer refueling cycles, the fuel burnup limit for Japanese pressurized-water reactors (PWRs) has been increased from 39 to 48 MWd per kilogram of uranium (kgU) for plants most recently licensed. A further increase of the limit to 55 MWd/kgU is being considered for plants undergoing licensing review. Analyses and operating experience show that the performance of the high-burnup fuel is acceptable under normal operating conditions; however, the behavior of the fuel under transient conditions, in particular during reactivity-initiated accidents (RIAs), requires careful consideration. Experimental programs at CABRI and at the Nuclear Safety Research Reactor (NSRR) appear to indicate that cladding failures may occur at enthalpy values lower than would be expected.[1–8] Results from two experiments [i.e., CABRI REP-Na1 at the Institute for Protection and Nuclear Safety (IPSN) and HBO-1 at the NSRR] raised concerns that existing licensing criteria could be inappropriate beyond a certain level of burnup. The failure that occurred in test HBO-1 suggests that pellet–cladding mechanical interaction (PCMI) with reduced cladding integrity as the result of hydrogen absorption (hydride-assisted PCMI) leads to the cladding failure. This article presents results from the NSRR/RIA experiments with irradiated PWR fuel rods, including recently performed tests HBO-5 to HBO-7.

A current Japanese safety evaluation guideline (Nuclear Safety Commission, "Evaluation guideline for reactivity-initiated events in power-producing light water nuclear reactors," 1984) for reactivity-initiated events defines an absolute limit of fuel enthalpy as 230 cal/g fuel (963 J/g fuel) to avoid generating destructive forces. As shown in Fig. 1, this guideline also defines an allowable limit of fuel enthalpy for fuel design as 65 to 170 cal/g fuel (272 to 712 J/g fuel) as a function of the difference between rod internal and external pressures. When fuel-rod internal pressure is lower than external pressure, as it is in PWRs, the limit is 170 cal/g fuel (712 J/g fuel). The guideline was established by the Nuclear Safety Commission of Japan in 1984 on the basis of mainly the results of the NSRR experiments, but all the NSRR data used were limited to those derived from the experiments with fresh, unirradiated fuel rods. For this reason, the current guideline adopted the energy deposition at the cladding failure of 85 cal/g fuel (356 J/g fuel) in the Special Power Excursion Reactor Test (SPERT) 859 experiment as a provisional failure threshold of preirradiated fuel rods; this failure threshold is used to evaluate the number of failed preirradiated fuel rods and to assess the source term resulting from the fission gas released in a postulated RIA. For commercial light-water-reactor (LWR) plants to be licensed in Japan, the safety evaluation must show that the events yield acceptable consequences (i.e., fuel failures are acceptable as long as the amount of fission gas released is within certain limits).

[a]Department of Reactor Safety Research, Japan Atomic Energy Research Institute, Tokai, Ibaraki 319-11 Japan.

[b]Oarai Research Establishment, Japan Atomic Energy Research Institute, Oarai, Ibaraki 311-13 Japan.

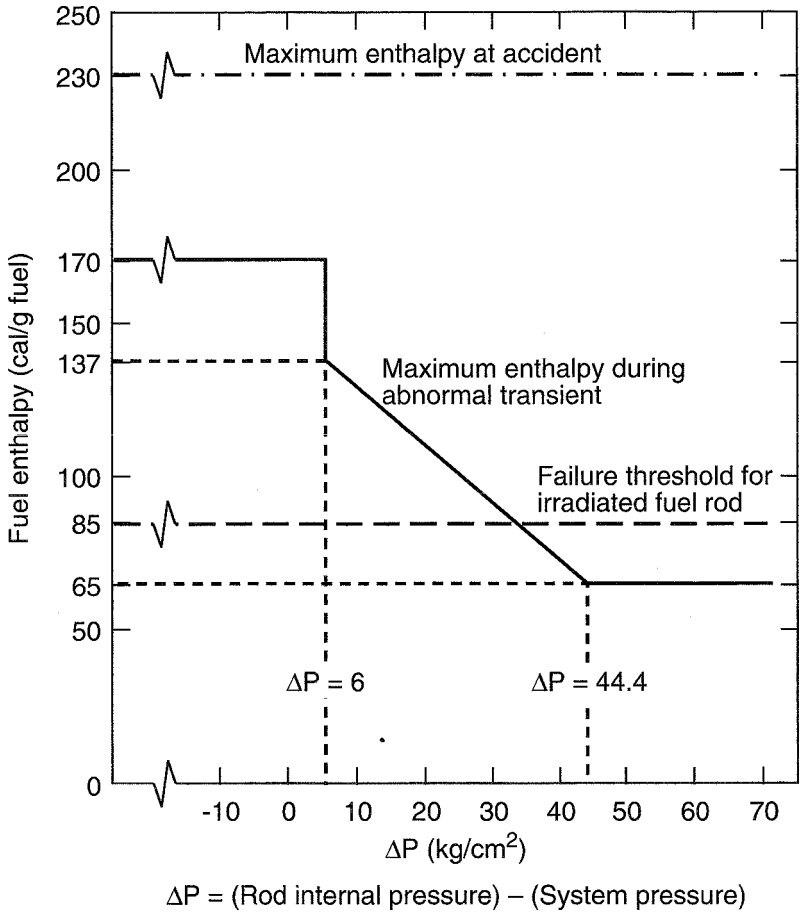

Fig. 1 Current Japanese guideline for reactivity-initiated events.

PULSE IRRADIATION EXPERIMENTS IN THE NSRR

The NSRR is a modified TRIGA-ACPR (Annular Core Pulsed Reactor). Salient features are the large pulsing power capability and large (22-cm-diameter) dry irradiation space located in the center of the reactor core, which can accommodate a sizable experiment. The shape of the NSRR power history depends on the amount of reactivity inserted; the smaller the pulse, the broader it is. For example, the full width at half maximum for a \$4.6 pulse is 4.4 ms, that for a \$3.0 pulse is 6.9 ms. The capsule used in the pulse irradiation experiment is a double-container system for the irradiated fuel-rod test in the NSRR. The inner capsule is a sealed pressure vessel with 72-mm inside diameter (ID) and 680-mm height. The capsule contains an instrumented test fuel rod with stagnant coolant water at atmospheric pressure and ambient temperature. During a pulse irradiation experiment, cladding surface temperatures at three elevations, coolant water temperature, and capsule internal pressure at the bottom of the inner capsule are measured. In some experiments, sensors for axial elongation of the pellet stack and cladding tube are also instrumented.

In a series of irradiated PWR fuel experiments, five different test fuels were refabricated from full-size commercial reactor fuels and subjected to pulse irradiation in the NSRR. These are MH, GK, OI, HBO type A, and HBO type B. The MH, GK, and HBO type A fuels were manufactured by Mitsubishi Heavy Industries, Ltd. (MHI), and the OI and HBO type B fuels were manufactured by Nuclear Fuel Industries, Ltd. (NFI). Fuel burnup and linear heat generation rate (LHGR) during the base irradiation (the irradiation in each commercial reactor) are listed in Table 1. Before the extension of the PWR fuel burnup limit from 39 to 48 MWd/kgU, the lead use program of high-burnup

fuel was performed in the Ohi Unit 1 reactor. The HBO test fuels had been irradiated in this program, and the fuel burnup reached 50 MWd/kgU. In the early four experiments of the HBO test series, tests HBO-1 to HBO-4, test fuel rods sampled from HBO type A fuel with a burnup of 50.4 MWd/kgU were subjected to pulse irradiation. Conversely, three recent HBO experiments, HBO-5 to HBO-7, used HBO type B fuel with a burnup of 44 to 49 MWd/kgU. Note that both HBO fuels were not newly designed and manufactured for the high-burnup application. The radial distance between the cladding inner surface and the fuel pellet (P/C gap) listed in the table is obtained from metallography for the arbitrary horizontal cross section (round slice). As shown in Table 1, the P/C gap for the HBO test fuels is smaller than that for the other test fuels because creepdown of the cladding is greater and the linear heat generation rate in the last irradiation cycle is lower in the high-burnup HBO test fuels. Because of the limitation of the NSRR pulsing capability and the low residual fissile content in the irradiated commercial reactor fuel, the maximum fuel enthalpy in the experiments with the irradiated commercial reactor fuels is limited to 120 cal/g fuel (500 J/g fuel) or lower. In addition to the irradiated PWR fuel experiments, short-size fuel rods with initial enrichment of 10 or 20% were preirradiated in the Japan Materials Testing Reactor (JMTR), Japan Atomic Energy Research Institute (JAERI), and were subjected to pulse irradiation experiments (JM test series).[4,9] This relatively high initial enrichment of the JM test fuel results in higher fuel enthalpies during the pulse irradiation in the NSRR.

The details of the NSRR, the test scheme, and the test fuel rods were previously reported in the literature.[1,9] As-fabricated fuel-rod specifications and the pulse-irradiation conditions, including the energy deposition and peak fuel enthalpy, are listed in Tables 2 and 3, respectively. Whereas the uncertainty of the energy deposition and peak fuel enthalpy values listed in Table 3 is evaluated as within 6%, the values for tests HBO-5 through HBO-7 are from preliminary evaluations and have about 10% uncertainty for its energy deposition and peak fuel enthalpy values.

RESULTS AND DISCUSSION

Cladding Failure

Test HBO-1 in the NSRR and REP-Na1 in the CABRI experiment exhibited energy deposition at fuel failure of 60 cal/g fuel (250 J/g fuel) for 50.4 MWd/kgU PWR fuel and 30 cal/g fuel (125 J/g fuel) for 63.8 MWd/kgU fuel.[1–8] Parts a and b of Fig. 2 summarize the existing data of in-pile RIA experiments. Part a of Fig. 2 shows peak fuel enthalpy during transients as a function of fuel burnup of test fuels. Conversely, in part b of Fig. 2, data from experiments resulting in fuel failure are plotted with energy

Table 1 Base-Irradiation Conditions

Test ID	Reactor	Initial enrichment, %	Irradiation cycle	Fuel burnup, MWd/kgU	LHGR at last cycle, kW/m	Radial P/C gap,[b] mm
HBO	Ohi 1	3.2	4	44 to 50.4	15.4[a]	<0.01[a]
OI	Ohi 2	3.4	2	39.2	20.5	0.02
MH	Mihama 2	2.6	4	38.9	19.3	0.02
GK	Genkai 1	3.4	3	42.1	19.8	0.02

[a]Values for tests HBO-1 to HBO-4; values to be determined for HBO-5 to HBO-7.
[b]The radial P/C gap is the radial distance between the cladding inner surface and the fuel pellet.

Table 2 As-Fabricated Fuel-Rod Specifications

		Cladding, mm		Fuel pellet, mm			
Fuel ID	Fuel type	OD	ID	Thickness	OD	Height	Shape
HBO(A)	17 × 17	9.5	8.36	0.57	8.19	13.5	Dished
HBO(B), OI	17 × 17	9.5	8.22	0.64	8.05	9	Dished, chamfered
MH, GK	14 × 14	10.72	9.48	0.62	9.29	15.2	Dished

Table 3 Pulse-Irradiation Conditions

Test ID	Fuel burnup, MWd/kgU	Sampling position,[a] span	Rod internal pressure, MPa	Inserted reactivity, $	Energy deposition, cal/g fuel (J/g fuel)	Peak fuel enthalpy, cal/g fuel (J/g fuel)	Remarks
HBO-1	50.4	3/8	0.1	4.6	93 (390)	73 (305)	Failed at 60 cal/g fuel (250 J/g fuel)
HBO-2	50.4	4/8	5.1	3.0	51 (215)	37 (157)	FGR: 17.7%[b]
HBO-3	50.4	5/8	0.1	4.6	95 (397)	74 (310)	FGR: 22.7%
HBO-4	50.4	6/8	0.1	3.6	67 (279)	50 (211)	FGR: 21.1%
HBO-5[c]	44	2/8	0.1	4.6	103 (430)	79 (330)	Failed at 72 cal/g fuel (300 J/g fuel)[d]
HBO-6[c]	49	4/8	0.1	4.6	103 (430)	79 (330)	FGR: (9)%
HBO-7[c]	49	3/8	0.1	4.6	103 (430)	79 (330)	
OI-1	39.2	3/8	0.1	4.5	136 (571)	106 (444)	
OI-2	39.2	4/8	0.1	4.6	139 (581)	108 (453)	FGR: 10.2%
MH-1	38.9	3/6	4.6	3.4	63 (262)	47 (196)	FGR: 3.5%
MH-2	38.9	3/6	4.6	3.8	72 (301)	54 (228)	
MH-3	38.9	3/6	4.6	4.3	87 (363)	67 (280)	FGR: 4.0%
GK-1	42.1	3/6	4.3	4.3	121 (505)	93 (389)	FGR: 12.8%
GK-2	42.1	3/6	0.1	4.2	117 (490)	90 (377)	FGR: 7.0%

[a]Span of 1/6 or 1/8 denotes the highest.
[b]FGR is fission gas release.
[c]Fuel burnup, energy deposition, and peak fuel enthalpy values are from preliminary evaluations.
[d]Value is preliminary.

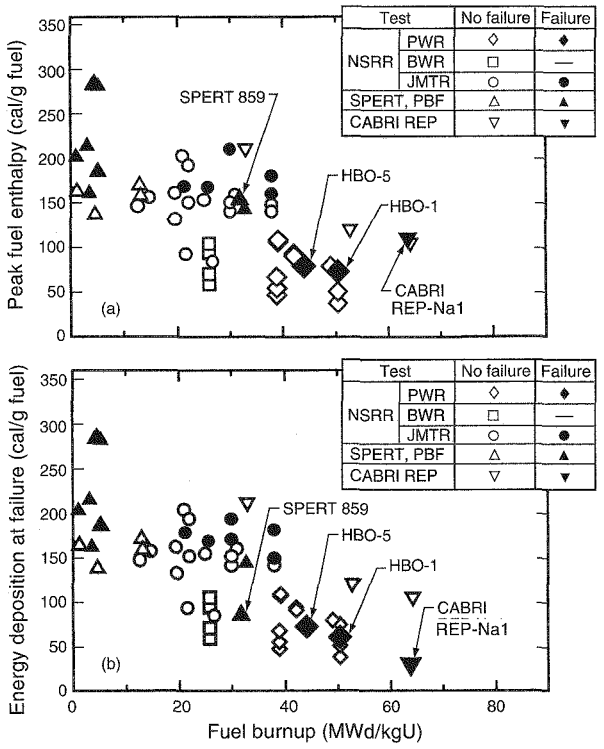

Fig. 2 (a) Peak fuel enthalpy as a function of fuel burnup of test fuels and (b) energy deposition at fuel failure as a function of fuel burnup of test fuels.

deposition at failure instead of peak fuel enthalpy. Because the PCMI failure tends to occur in the early stage of the transient, the energy deposition at failure is lower than the peak fuel enthalpy in most of the experiments that resulted in fuel failure. The points representing the data of tests HBO-1 and REP-Na1 suggest a decreased failure threshold in the high-fuel-burnup region.

A total of 42 experiments, including 20 commercial LWR fuel tests and 21 JMTR preirradiated fuel tests, were performed in the NSRR. Fuel failure occurred in 8 of the 42 experiments. The eight experiments that resulted in fuel failure are the six JM test series, which had the relatively high energy deposition levels, and two of the HBO experiments with high-burnup PWR fuels (tests HBO-1 and HBO-5). Figure 3 shows the posttest appearance of the fuel rod in test HBO-5. Axial cracking of the cladding corresponds to the entire region of the fuel stack—this occurred also in test HBO-1. In the case of the HBO-1 rod, two axial cracks were generated perpendicular to the thermocouples welded at the surface. The important finding in test HBO-5 is that the crack runs along the side where the three thermocouples were spot-welded to measure cladding surface temperature evolution during the transient. In test HBO-5, a number of instances of local spalling

of the oxide film were observed. (Note that some of these spallings were already found before the pulse irradiation.) The rod in the subsequent experiment HBO-6 showed no significant damage as the result of the pulse irradiation.

Figure 4 shows horizontal cross sections in the vicinity of the cracking observed in tests HBO-1 and HBO-5. In these test fuel rods, significant hydride deposition below the oxide film was generated in the cladding outer surface. The crack shows ductile fracture in the inner region and brittle fracture in the outer region where a number of hydride clusters are deposited. In test HBO-5, typical brittle/ductile fractures very similar to those of test HBO-1 were observed.

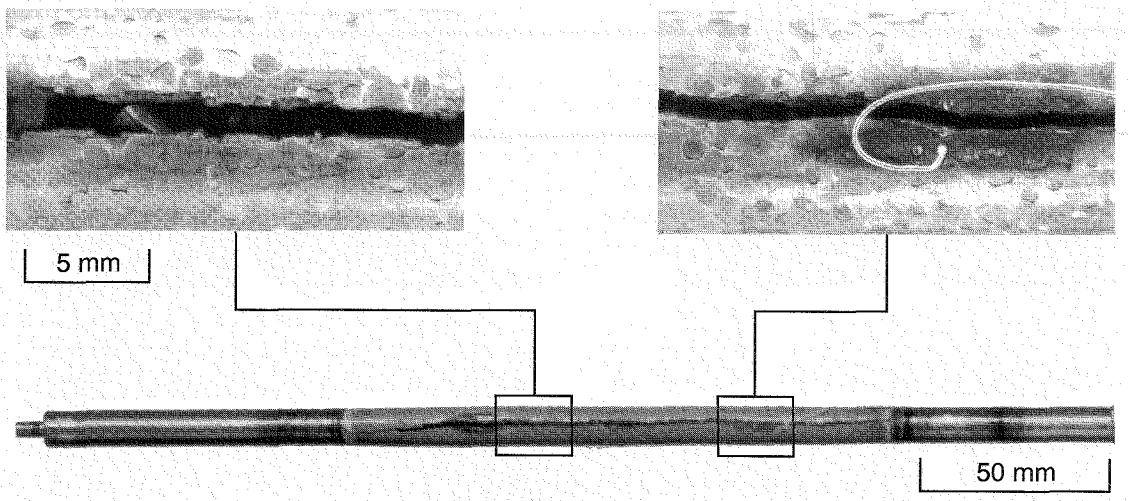

Fig. 3 Posttest appearance of the HBO-5 test fuel.

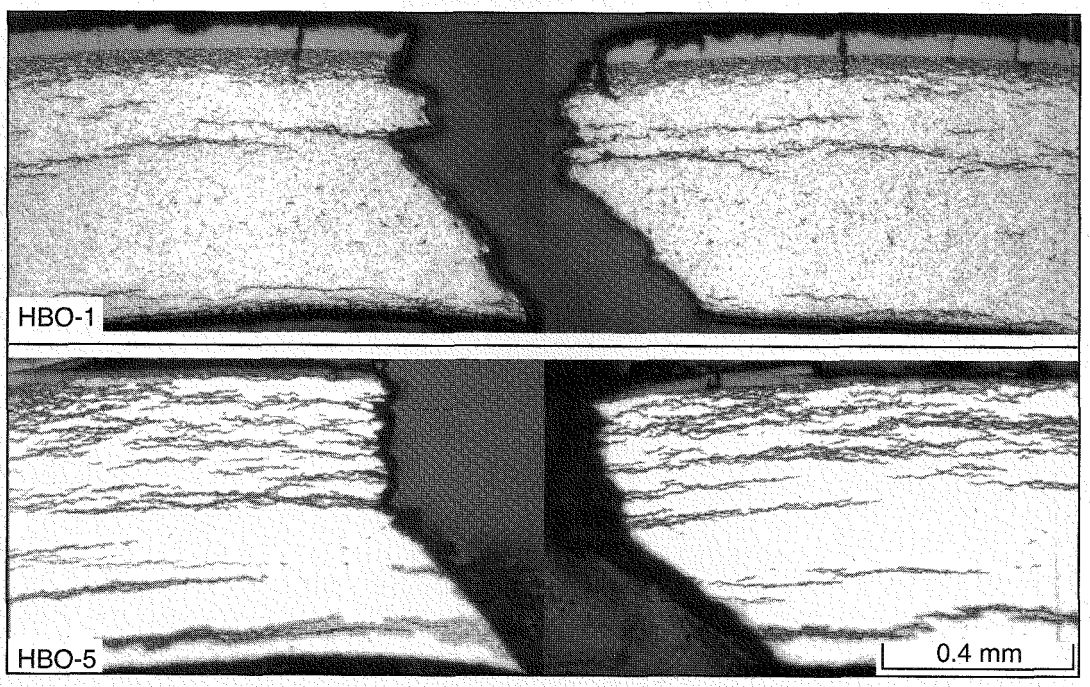

Fig. 4 Horizontal cross section of through-wall cracks observed in tests HBO-1 and HBO-5.

Only in test HBO-5, however, did the axial crack go through the region heat-affected by the thermocouple welding. In the vicinity of the thermocouples, a crack penetrated through the heat-affected region. The failure mechanism of test HBO-5 is hydride-assisted PCMI, but the effects of thermocouple welding on the occurrence of the failure cannot be neglected. The thermocouple attachment may lead to earlier cracking and result in a low-energy deposition level at failure.

In tests HBO-1 and HBO-5 resulting in fuel failure, a number of small cracks perpendicular to the surface were observed in the posttest cladding. The through-wall crack could originate from one of these crack tips. Small cracks in the oxide and hydride layers were observed also in test HBO-6, which resulted in no failure. Figure 5 shows the small cracks observed in tests HBO-5 and HBO-6. Figure 6 illustrates the elevation where the test fuel rod was sampled in each experiment and the occurrences of fuel failure and microcrack generation.

Fuel failure occurred in the experiments with test fuel rods from the highest elevation (HBO-1 and HBO-5), and microcrack generation in oxide and hydride layers was observed in the experiments with rods from the higher level (HBO-1, HBO-5, HBO-6, and HBO-7). The small cracks observed in test HBO-6 are expected to be a precursor to cladding failure. It can be naturally accepted that occurrence of fuel failure in the HBO experiments correlates with the sampling elevation and, accordingly, with thickness of oxide film[10] and severity of hydrogen deposition of the tested fuel rod. Although some measurements on oxide film thickness and hydrogen concentration of the specimens sampled from the mother rods were conducted, it is a little premature to present quantitative data here. The data will be released after careful reexamination. Conversely, oxide film thickness and hydrogen concentration were measured in the sibling rod extracted from the same fuel assembly from which the HBO-5 to HBO-7 test fuels were sampled. Figure 7 shows axial profiles of hydrogen concentration and oxide layer thickness in the sibling rod. Both profiles have peaks at an elevation in the second grid span where the HBO-5 test fuel was sampled. The hydrogen concentration reaches about 380 ppm at the peak, whereas it is less than 200 ppm in the lower half.

Hydrogen deposition, in particular, could have critical importance in the high-burnup PWR fuel behavior during an RIA. The effect of hydride deposition cannot be described by concentration averaged at cross section, and the effects of radial and circumferential localization of the hydride clusters are very important.[11] Figure 8 shows a radial cross section of the cladding in the second grid span of the sibling rod. So that the extent of radial localization of hydrides could be evaluated, the distribution in the cross section was measured with photo-image analysis. The hydrogen concentration was evaluated under the assumption that the cross-sectional area of hydride is proportional to hydrogen concentration and all of the hydrides are in the delta phase. Figure 8 shows the result of the evaluation on the radial cross section. The hydrogen concentration in the outer 20-μm-thick region reaches about 2600 ppm. Even if the assumptions may not provide precise evaluation especially for very high hydrogen concentration, the result indicates that the local hydrogen concentration in the cladding outer region reaches some thousands of parts per million. The photo-image analysis for radial distribution of hydride clusters and hydrogen composition measurements is to be performed also on pretest and posttest cladding. The influence of the radially localized hydride layer on the

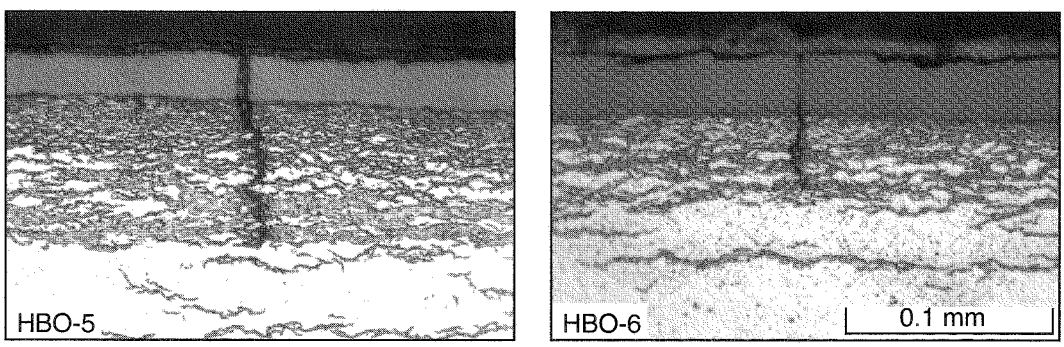

Fig. 5 Microcracks observed in tests HBO-5 and HBO-6.

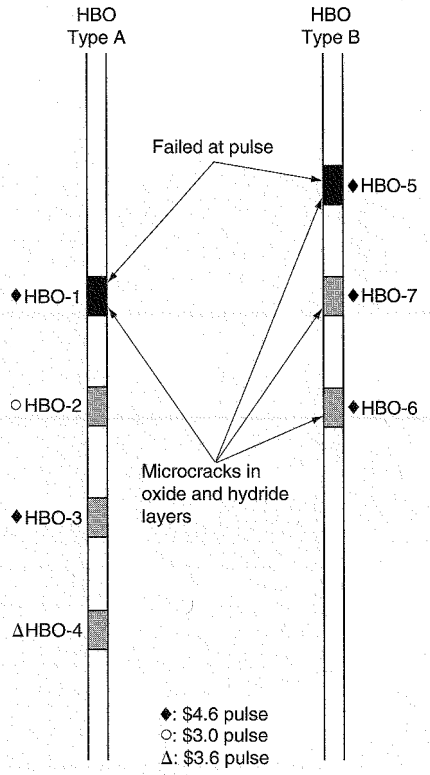

Fig. 6 Correlation between sampling elevation of the test fuel rods and occurrences of cladding failure and/or microcracks. [The test fuel rods are 316 mm long and 135 mm in the fuel stack (active) region.]

cladding mechanical integrity is being examined also in out-of-pile, separate-effects testing at JAERI.

Reduction of hydride embrittlement has been shown in the range of relatively low hydrogen concentration with long duration in elevated temperature.[12,13] In accidental conditions of PWRs with the higher coolant temperature and the slower power transient (typical value of the full width at half maximum expected in PWRs is about 30 ms), the cladding temperature becomes higher than that in the NSRR test conditions; however, the radially localized hydride layer was observed in the high-burnup fuel cladding as shown in Fig. 8, and the concentration of hydrogen in the outer 0.1-mm region reached 900 ppm or higher. Even in accident conditions of a PWR with high-temperature coolant and the slower transient, cladding temperature in the outer 0.1-mm region does not exceed 730 K,[14] and the interval from onset of the event to cladding failure is much less than 0.1 s. Compared with the high concentration of hydrogen in the outer region, solubility of hydrogen into the matrix is very limited at this temperature level. Annealing of the hydride layer cannot be expected during this short time.[11] These facts indicate that the decreased ductility as the result of the radially localized hydride layer has a significant influence on an occurrence of cladding failure even under the conditions that exist in a PWR. The reduced ductility of the cladding with localized hydride is demonstrated also in tube burst, tube tensile, and ring

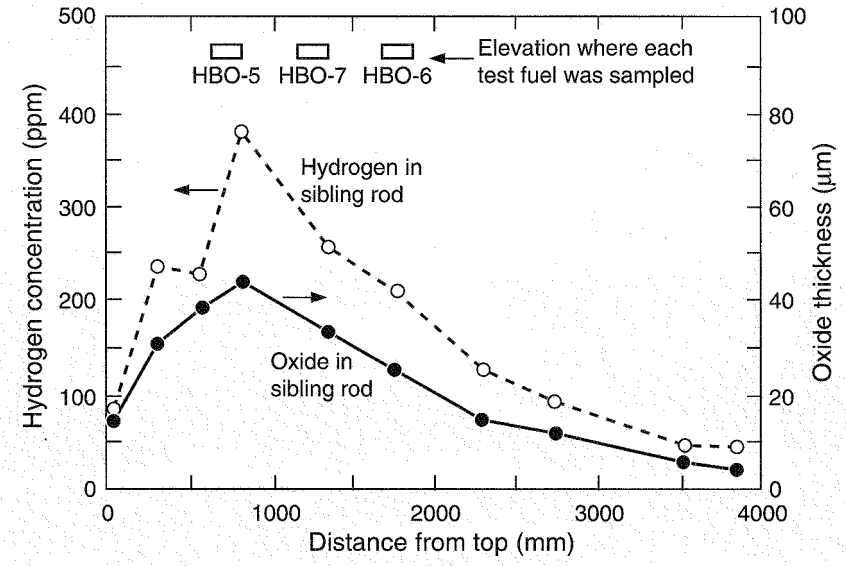

Fig. 7 Axial profiles of hydrogen concentration and oxide layer thickness in HBO type B sibling fuel rod. [The sibling fuel rod is 316 mm long and 135 mm in the fuel stack (active) region.]

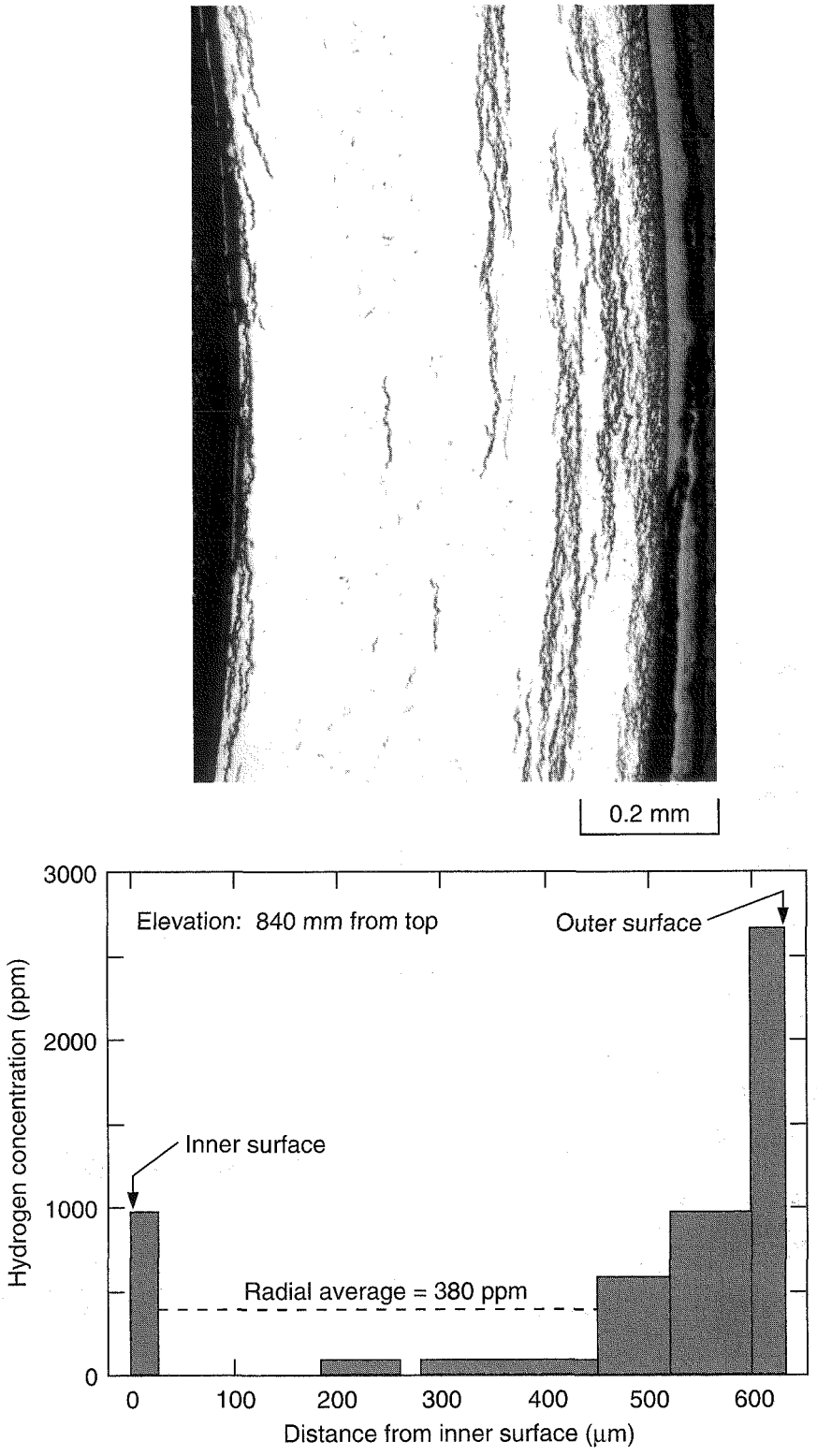

Fig. 8 Radial profile of hydrogen concentration at 840 mm below top in HBO type B sibling fuel rod. [The test fuel rod is 316 mm long and 135 mm in the fuel stack (active) region.]

tensile tests in the temperature range of 313 to 673 K.[15] These tests were performed with relatively low strain rate, and further reduction of ductility could be expected in the faster strain as expected in an RIA. Physical property data of the hydrided cladding tube, including data regarding the transition temperature of a brittle-to-ductile state, should be accumulated with separate-effects tests to investigate the influences of hydrogen concentration, hydrogen radial and circumferential distribution, strain rate, and temperature.

Fuel dispersion occurred only in test HBO-1. All the fuel pellets were found as finely fragmented particles after test HBO-1. More than half of the fragmented fuel particles are smaller than 50 μm. In test HBO-5, however, most of the fuel pellets remained inside the cladding tube, and only a very small amount of fuel powder was recovered from the coolant water.

Cladding Surface Temperature

Figure 9 shows the transient histories of the cladding surface temperature measured during the pulse irradiation of tests HBO-3, HBO-5, and HBO-6. In the HBO experiment series, three thermocouples are attached at the cladding surface of test fuel rods except in test HBO-7. One or two thermocouples failed during each pulse irradiation, so only the five records shown in Fig. 9 are available from tests HBO-3, HBO-5, and HBO-6. Only the thermocouple attached 40 mm below the fuel active center in test HBO-3 showed temperature elevation up to about 400 °C. The rest of the data did not show any indication of departure from nucleate boiling. In the latest HBO-7 experiment, thermocouples for cladding surface temperature and sensors for fuel stack and cladding axial elongation were not instrumented. Instead of elongation sensors, a coolant water column movement sensor was installed on the test capsule to evaluate the generation of mechanical forces; however, no notable signal was recorded during the pulse irradiation because the experiment resulted in no failure. Figure 10 shows the maximum cladding surface temperature as a function of the peak fuel enthalpy. This figure also indicates that the temperature in test HBO-3 reached 400 °C at a relatively low peak fuel enthalpy level.

Fuel Deformation

Figure 11 shows the axial profile of the cladding outer diameter before and after the pulse irradiation of tests HBO-3, HBO-4, HBO-6, and HBO-7. Posttest dimensional measurements could not be performed because of cladding failure in tests HBO-1 and HBO-5. Diametrical change between pretest and posttest was negligible in test HBO-2 because peak fuel enthalpy in the experiment was only 37 cal/g fuel (157 J/g fuel). In tests HBO-3, HBO-6, and HBO-7, the test fuel rods were subjected to pulse irradiation with inserted reactivity of $4.6, and fuel enthalpy reached 74 to about 84 cal/g fuel (310 to about 350 J/g fuel) at maximum. Inserted reactivity and peak fuel enthalpy in test HBO-4 were $3.6 and 50 cal/g fuel (211 J/g fuel). Figure 12 shows residual hoop strain of posttest cladding as a function of peak fuel enthalpy. The strain becomes larger as the peak fuel enthalpy increases. For the fresh, unirradiated fuel rod, the residual hoop strain remains <0.5% at 191 cal/g fuel (800 J/g fuel). As seen in Fig. 12, the strains in the experiments with irradiated PWR fuels are much larger than those with fresh fuels because the expansion of the fission gas accumulating in the irradiated fuel pellets accelerates the fuel swelling. In the relatively low peak fuel enthalpy range, 60 cal/g fuel (250 J/g fuel) or lower, HBO tests resulted in larger strain than those in the MH tests, as was expected from the narrower prepulse P/C gap in the HBO test fuel. The test fuel rods of tests HBO-2, MH-1, and MH-2 were prepressurized as listed in Table 3, but the effect of the prepressurization on the strain could be neglected for the relatively low cladding temperature in the range of the fuel enthalpy. At the higher enthalpy level, the strains of tests HBO-3, HBO-6, and HBO-7 are in the same range as those of tests MH-3, GK-1, and GK-2. Note that test HBO-7 with a fuel burnup of 49 MWd/kgU resulted in no failure, although the strain in this experiment exceeded 2%. Because of the relatively high cladding temperature during the transient, test OI-2 resulted in no failure with a strain of 4.8%.

Fission Gas Release

After the pulse irradiation, rod-averaged fission gas release was destructively measured for the test rod by rod puncture and gas analysis. The fission gas release during the pulse irradiation as a function of the peak fuel enthalpy is shown in Fig. 13. Although fission gas release from the mother rod (type A) of tests HBO-1 to HBO-4 during the base irradiation was only 0.49%, significant fission gas release occurred in the pulse irradiation of tests HBO-2, HBO-3, and HBO-4. Fission

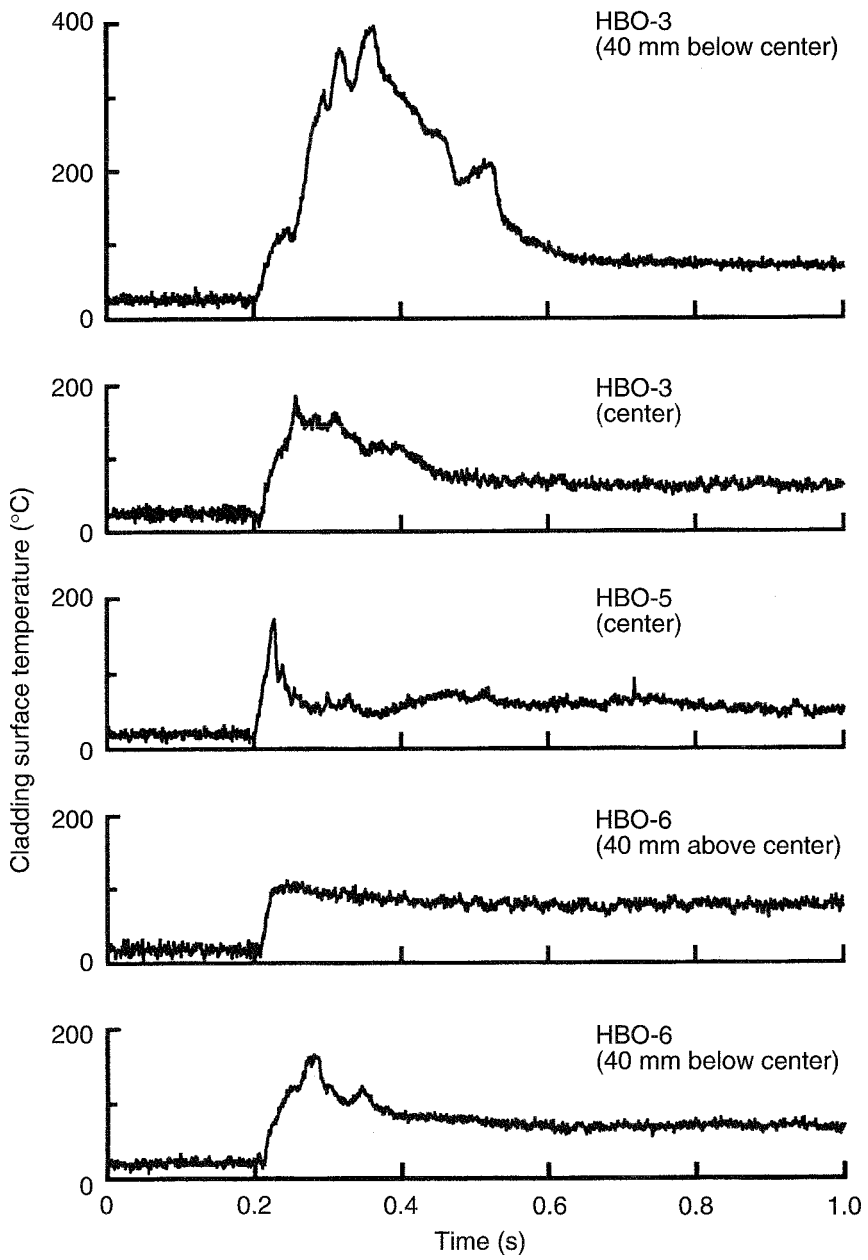

Fig. 9 Transient histories of the cladding surface temperature in tests HBO-3, HBO-5, and HBO-6. [The test fuel rods are 316 mm long and 135 mm in the fuel stack (active) region.]

gas release is 17.7% even in test HBO-2 with the peak fuel enthalpy of 37 cal/g fuel (157 J/g fuel), and it reaches 22.7% in test HBO-3 [peak fuel enthalpy of 74 cal/g fuel (310 J/g fuel)]. The fission gas release in test HBO-2 is higher than that in test GK-1 with the peak fuel enthalpy of 93 cal/g fuel (389 J/g fuel). Figure 14 shows the relationship between fission gas release and residual hoop strain of posttest cladding. As shown in Fig. 14, the significant fission gas release occurred in tests HBO-2, HBO-3, and HBO-4 with the HBO type A test fuels with relatively small fuel swelling. Conversely, fission gas release obtained from a preliminary evaluation for test HBO-6 with the HBO type B test fuel is about 9%, and it is much lower than the

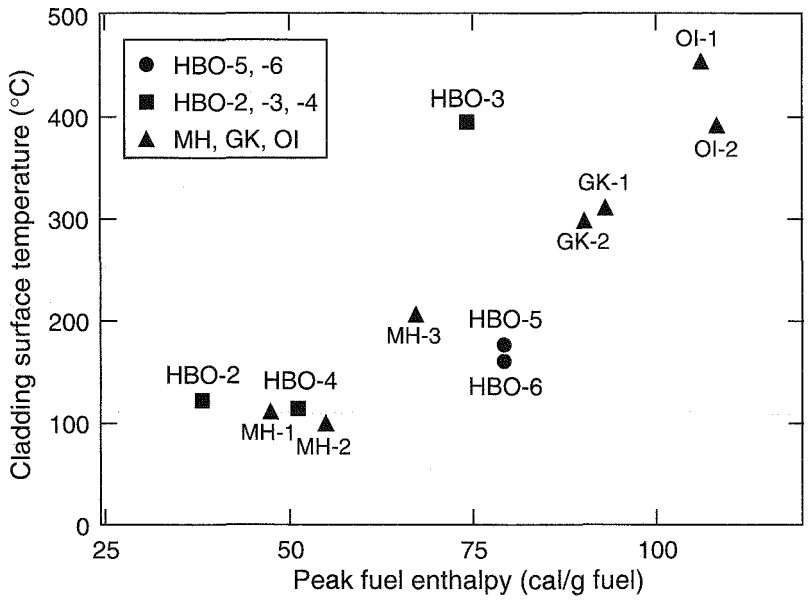

Fig. 10 Maximum cladding surface temperature as a function of peak fuel enthalpy.

three experiments with the HBO type A test fuels. The pretest state of fission gas accumulation (for example, radial distribution of accumulated gas, ratio of intergranular and intragranular inventories, and rim effect) is expected to be different between the type A and type B fuels. Detailed examination of sibling samples from the mother rods is in the planning stage.

Analytical Approach

In the analysis, a new version of the FRAP-T6 code was used. The code is based on the FRAP-T6 code version 22 provided from the Idaho National Engineering and Environmental Laboratory and includes a gas bubble swelling model developed at JAERI. The deformation behavior of irradiated PWR fuels undergoing an RIA could not be simulated with the original FRAP-T6 code because it has simple thermal expansion models for the fuel swelling. Thus a fission gas-induced deformation model was developed and included in the code.[16] Some fission gases are generated in fuel grains and migrate to grain boundaries during base irradiation in power reactors. The pressure of these gases could increase and cause grain boundary separation during the pulse irradiation. The fission gas swelling model assumes that the grain boundary separation would occur above a temperature threshold, which is fixed at 1100 °C as an assumption in the current model. The swelling would result in fission gas pressure loading of the cladding. The fission gas would be released to the fuel-rod plenum after release paths have formed with grain boundary separation and cladding deformation. In the current model, it is also assumed that an amount of fission gas contributing to the swelling is equivalent to that of fission gas released during the pulse irradiation.

Because a number of models regarding the prepulse state of fission gas (fission gas release, degradation of fuel thermal conductivity as the result of swelling, heat-transfer model for the cooling conditions in the NSRR experiment, etc.) do not describe existing conditions, the present analysis remains in a preliminary stage. Figure 15 shows the plastic hoop strain of cladding from the calculations for a pulse irradiation of $4.6 reactivity insertion to the HBO type A fuel, corresponding to tests HBO-1 and HBO-3. Although the FRAP-T6 version 22 underestimates the strain, the code with the gas swelling model predicts a little larger strain.

SUMMARY

The NSRR experiments suggest a possible reduction of the failure threshold for high-burnup fuels, and indicate that PCMI with swelling of the fuel pellets

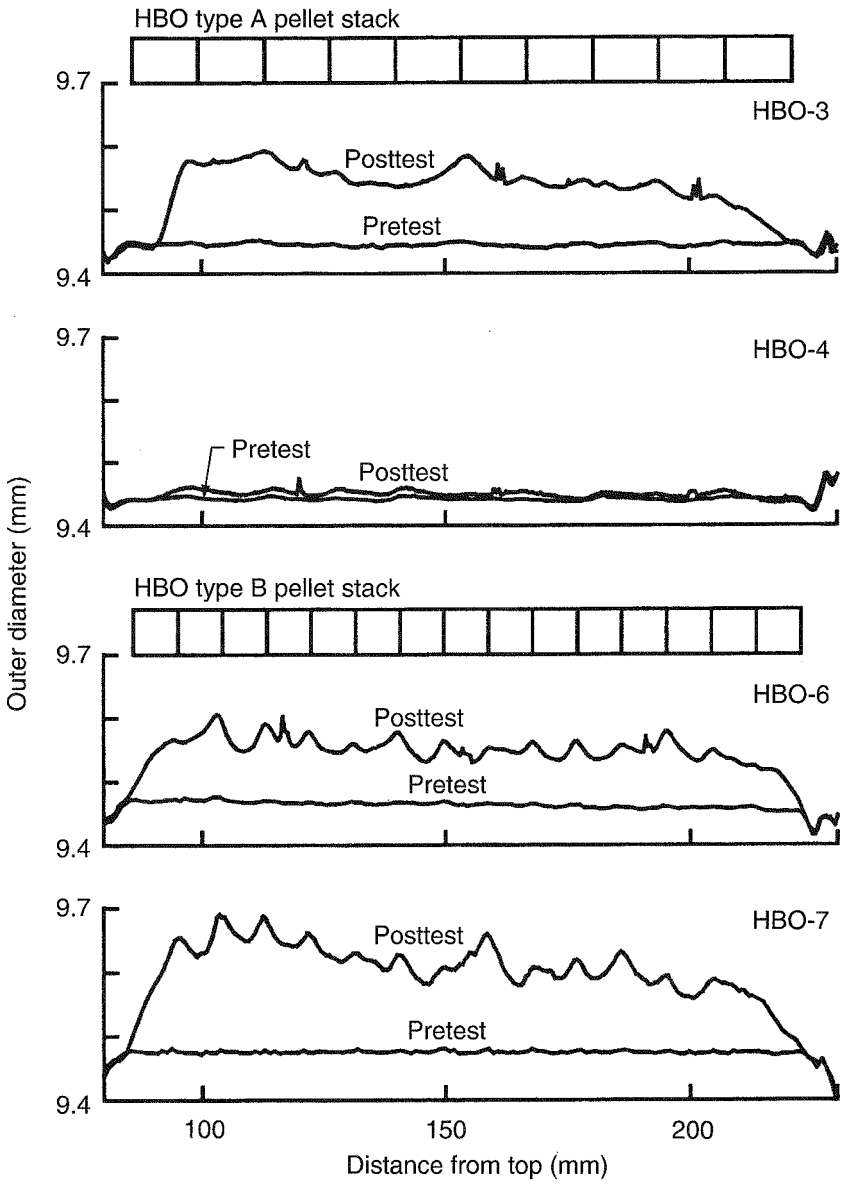

Fig. 11 Axial profiles of pretest and posttest cladding outer diameter in tests HBO-3, HBO-4, HBO-6, and HBO-7. [The test fuel rods are 135 mm long in the fuel stack (active) region—10 pellets of type A and 15 pellets of type B.]

and decreased cladding integrity lead to the failure. A preexisting hydride layer in the cladding played an important role in the failure of the rods. Recent experiments HBO-5 and HBO-6 with the test fuel rods sampled from relatively higher elevations resulted in fuel failure and microcrack generation, respectively. Occurrence of fuel failure in the HBO experiments correlates with the thickness of the oxide film and the severity of hydrogen deposition of the fuel rod. Small cracks in oxide and hydride layers were observed in tests HBO-1 and HBO-5, which resulted in fuel failure, and also in tests HBO-6 and HBO-7. The cracks in the HBO-6 and HBO-7 rods could be a precursor of cladding failure. Significant fission gas release up to 22.7% occurred in the previous experiments with HBO type A fuels. Conversely, the fission gas release in test

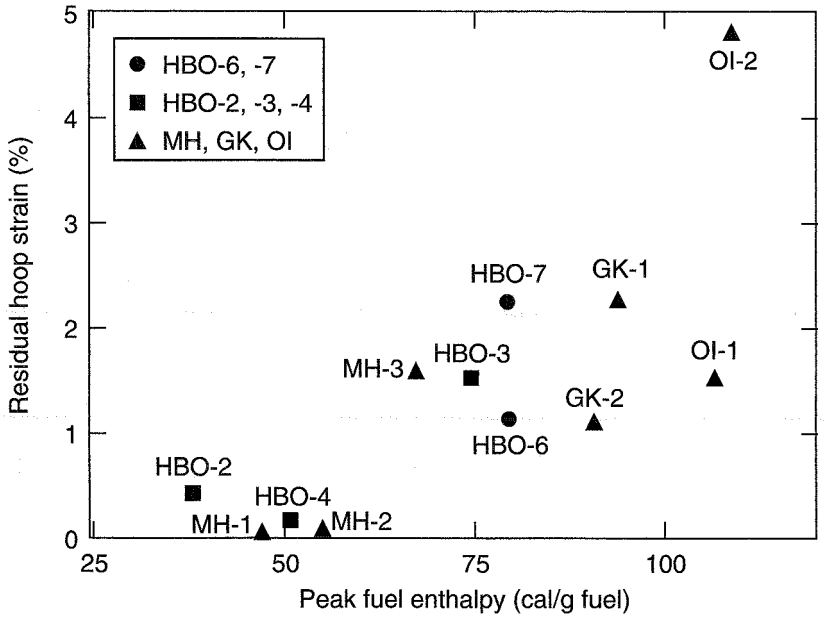

Fig. 12 Posttest residual hoop strain as a function of peak fuel enthalpy.

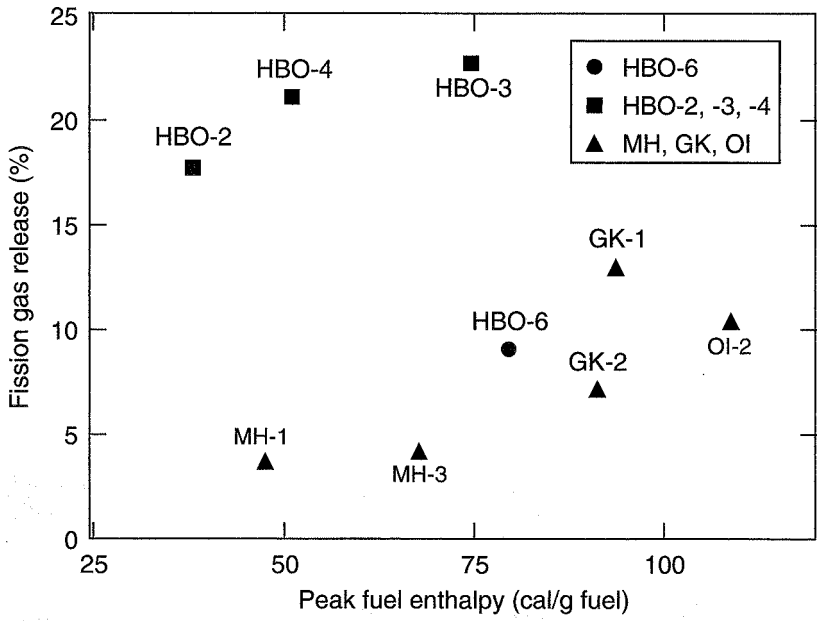

Fig. 13 Fission gas release during transients as a function of peak fuel enthalpy.

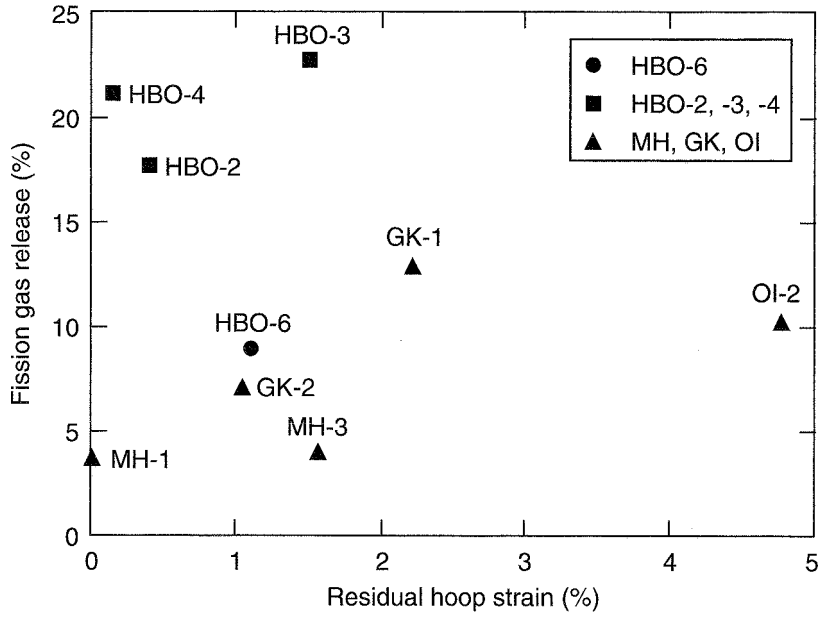

Fig. 14 Relation between fission gas release and residual hoop strain.

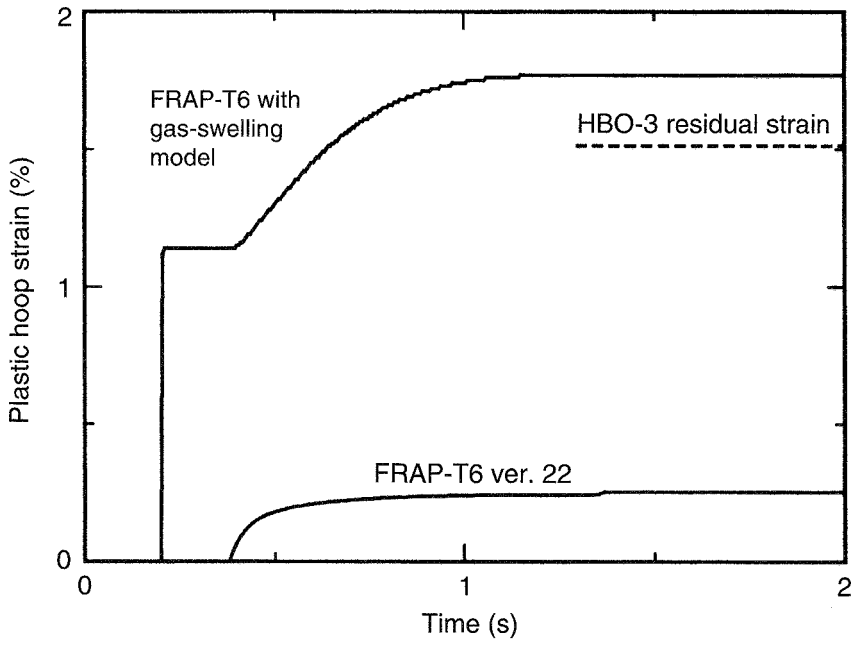

Fig. 15 Plastic hoop strain in preliminary analyses with FRAP-T6 code (version 22).

HBO-6 remained about 9%. The pretest state of fission gas accumulated in the fuels and, accordingly, the fabrication scheme of the fuel pellets may have a strong influence on the amount of fission gas released during the transients. As for the analytical prediction for fuel failure in the test conditions and in the power reactor conditions, extensive data on the physical properties of the cladding are needed as well as the ability to model a variety of phenomena (for example, fission gas release).

ACKNOWLEDGMENTS

The authors would like to acknowledge and express their appreciation for the efforts devoted by numerous engineers and technicians in the Department of Reactor Safety Research and the Department of Hot Laboratories, JAERI. Particular thanks are due to Dr. Hiroshi Uetsuka, Mr. Hideo Sasajima, and Mr. Takehiko Nakamura of JAERI; Mr. Yukihide Mori of Nuclear Development Corporation; and Mr. Yoshihiro Tsuchiuchi of NFI for their contributions to the project. The HBO test series has been performed as a collaboration between JAERI and MHI (for tests HBO-1 to HBO-4) and between JAERI and NFI (for tests HBO-5 to HBO-7) by using fuel rods transferred from Kansai Electric Power Company, Inc.

REFERENCES

1. T. Fuketa, Y. Mori, H. Sasajima, K. Ishijima, and T. Fujishiro, Behavior of High Burnup PWR Fuel Under a Simulated RIA Condition in the NSRR, in *Proceedings of the CSNI Specialist Meeting on Transient Behavior of High Burnup Fuel*, Cadarache, France, September 12–14, 1995, Report NEA/CSNI/R(95)22, pp. 59-85, 1996.
2. K. Ishijima, Y. Mori, T. Fuketa, and H. Sasajima, Postulated Mechanisms on the Failure of 50 MWd/kgU PWR Fuel in the NSRR Experiment and the Related Research Programs in JAERI, in *Proceedings of the CSNI Specialist Meeting on Transient Behavior of High Burnup Fuel*, Cadarache, France, September 12–14, 1995, Report NEA/CSNI/R(95)22, pp. 87-105, 1996.
3. T. Fuketa, K. Ishijima, Y. Mori, H. Sasajima, and T. Fujishiro, New Results from the NSRR Experiments with High Burnup Fuel, in *Proceedings of the Twenty-Third Water Reactor Safety Information Meeting*, Bethesda, Maryland, Oct. 23–25, 1995, Report NUREG/CP-0149, Vol.1 (CONF-9510156—Vol.1), pp. 45-63, March 1996.
4. T. Fuketa, H. Sasajima, Y. Mori, and K. Ishijima, Fuel Failure and Fission Gas Release in High Burnup PWR Fuels Under RIA Conditions, *J. Nucl. Mater.*, 248: 249-256 (1997).
5. K. Ishijima and T. Fuketa, Progress of the RIA Experiments with High Burnup Fuels and Their Evaluation at JAERI, in *Proceedings of the Twenty-Fourth Water Reactor Safety Information Meeting*, Bethesda, Maryland, October 21–23, 1996, Report NUREG/CP-0157, Vol. 1, pp. 93-105, January 1997.
6. T. Fuketa, H. Sasajima, Y. Tsuchiuchi, Y. Mori, T. Nakamura, and K. Ishijima, NSRR/RIA Experiments with High Burnup PWR Fuels, in *Proceedings of the International Topical Meeting on Light Water Reactor Fuel Performance*, Portland, Oregon, March 2–6, 1997, pp. 669-676.
7. F. Schmitz, J. Papin, M. Haessler, and N. Waeckel, New Results from Pulse Tests in the CABRI Reactor, in *Proceedings of the Twenty-Third Water Reactor Safety Information Meeting*, Bethesda, Maryland, October 23–25, 1995, Report NUREG/CP-0149, Vol.1 (CONF-9510156—Vol.1), pp. 33-43, March 1996.
8. F. Schmitz, Ch. Gonnier, and J. Papin, The Status of the CABRI Test Program: Recent Results and Future Activities, in *Proceedings of the Twenty-Fourth Water Reactor Safety Information Meeting*, Bethesda, Maryland, October 21–23, 1996, Report NUREG/CP-0157, Vol.1, pp. 107-130, January 1997.
9. T. Fuketa, H. Sasajima, Y. Mori, K. Homma, S. Tanzawa, K. Ishijima, S. Kobayashi, H. Kamata, and H. Sakai, *Behavior of Pre-irradiated Fuel Under a Simulated RIA Condition [Results of NSRR Test JM-5]*, Report JAERI-Research 95-078, November 1995.
10. R. O. Meyer, R. K. McCardell, and H. H. Scott, A Regulatory Assessment of Test Data for Reactivity Accidents, in *Proceedings of the International Topical Meeting on Light Water Reactor Fuel Performance*, Portland, Oregon, March 2–6, 1997, pp. 729-744.
11. F. Nagase and H. Uetsuka, Hydride Morphology and Hydrogen Embrittlement of Zircaloy Fuel Cladding Used in NSRR/HBO Experiment, in *Proceedings of the International Topical Meeting on Light Water Reactor Fuel Performance*, Portland, Oregon, March 2–6, 1997, pp. 677-684.
12. J. Bai, C. Prioul, J. Pelchat, and F. Barcelo, Effect of Hydrides on the Ductile-Brittle Transition in Stress-Relieved, Recrystallized and Beta Treated Zircaloy-4, in *Proceedings of the International Topical Meeting on Light Water Reactor Fuel Performance*, Avignon, France, April 21–24, 1991, pp. 233-241.
13. J.-H. Huang and S.-P. Huang, Effect of Hydrogen Contents on the Mechanical Properties of Zircaloy-4, *J. Nucl. Mater.*, 208:166-179 (1994).
14. R. O. Montgomery and Y. R. Rashid, *Evaluation of Irradiated Fuel During RIA Simulation Tests, Final Report*, Report EPRI TR-106387, August 1996.
15. A. M. Garde, G. P. Smith, and R. C. Pirek, Effect of Hydride Precipitate Localization and Neutron Fluence on the Ductility of Irradiated Zircaloy-4, in *Zirconium in the Nuclear Industry: 11th International Symposium*, Report ASTM STP 1295, pp. 407-430, E. R. Bradley and G. P. Sabol (Eds.), American Society for Testing and Materials, 1996.
16. T. Nakamura, H. Sasajima, T. Fuketa, and K. Ishijima, Fission Gas Induced Cladding Deformation Under Reactivity Initiated Accident Conditions, *J. Nucl. Sci. Technol.*, 33(12): 924-935 (December 1996).

The Russian RIA Research Program: Motivation, Definition, Execution, and Results

By V. Asmolov and L. Yegorova[a]

Abstract: *This article describes a research program to study fuel-rod behavior of Russian pressurized-water reactors (PWRs) under reactivity-initiated accident (RIA) conditions; presents the main results of reactor tests of fresh fuel rods, of high-burnup fuel rods, and of fuel rods with preirradiated cladding and fresh fuel; and analyzes in a preliminary way the obtained results to determine failure thresholds and fuel-element failure mechanisms.*

In 1983 the Russian Research Centre "Kurchatov Institute" (RRC KI) started a research program to experimentally validate the behavior of VVER fuel elements under reactivity-initiated accident (RIA) conditions.

It was not a simple task to correctly define the framework of the program, especially initially, because general trends in the validation of reactor safety in pre-Chernobyl Russia and the limited capabilities of computer codes for analysis of possible RIA scenarios prevented illumination of the real range of problems in this research area. Another limiting factor was a lack of methods, procedures, technologies, and specialists required to implement this type of program. This is why the program was expanded to include tests of the entire spectrum of VVER fuel elements for a maximally broad range of varying factors that determine RIA scenarios. At the same time the program was designed to allow a step-by-step increase in the complexity of investigations as the experimental procedure improved.

The main cycle of RIA experiments conducted under this program was completed in 1992. It included reactor tests and posttest examinations of more than 200 VVER fuel rods. Tests were performed under conditions of pulse changes of the fuel-rod power. In addition to design characteristics of fuel rods, the following parameters that determine the RIA scenario were varied:

- Energy deposition in the fuel rod.
- Pulse half-width.
- Initial pressure drop across the cladding.
- Burnup of the fuel.
- Type of coolant.

The final stage of the program was a series of tests intended to study burnup effects on the threshold characteristics of fuel-rod failure. Refabricated fuel rods manufactured from commercial fuel elements irradiated up to 48 MWd per kilogram of uranium (kgU) were used for tests performed during the period 1990 to 1992.

Unfortunately, because of the economic situation in Russia at the beginning of the 1990s, this research was frozen before posttest studies were completed. The revival of this research was spurred by a need to validate Russian and world safety standards and by unexpected results of experiments with high-burnup fuel conducted at the CABRI reactor in France as part of the corresponding Institute for Protection and Nuclear Safety (IPSN) program in 1993 and 1994. This work was restarted in 1995 to update the data base on the behavior of Russian pressurized-water-reactor (PWR) fuel elements with high-burnup fuel under RIA conditions. Beginning in 1995 the research was done under agreements that RRC KI made with the U.S. Nuclear Regulatory Commission (NRC), IPSN (France), AO Mashinostroitelny Zavod (AO MZ) (Electrostal), Imatran Voima Osakeyhtio (IVO, Finland), and with the financial support of the Russian Ministry of Science.

The research was carried out at RRC KI in collaboration with specialists from other institutes:

- Research Institute of Atomic Reactors (RIAR), Dimitrovgrad, Russia: refabrication of test fuel rods and pretest and posttest examinations.

[a]Nuclear Safety Institute, Russian Research Centre "Kurchatov Institute," Kurchatov Square, Moscow.

• Institute of Atomic Energy of the National Nuclear Center of Kazakstan Republic (IAE), Semipalatinsk, Kazakstan: RIA simulating reactor tests.

• Scientific Industrial Association (Lutch) (SIA), Podolsk, Russia: development and mounting of sensors to measure temperature and pressure.

OUTLINE OF VVER RIA RESEARCH PROGRAM

Possible scenarios of RIAs in vessel-type light-water reactors (LWRs) can be divided into two types: RIAs from reactor cold-start conditions and RIAs from reactor hot-start conditions.

Typical initial conditions for RIAs from a cold start are the following:

• Practically no coolant flow rate.
• Coolant and fuel-rod temperatures of about 20 °C.
• Coolant pressure of about 0.1 MPa.
• Gas pressure inside the fuel rod of at least 0.1 MPa.

RIAs from a hot start are characterized by the following initial parameters:

• Coolant flow rate.
• High coolant pressure.
• Coolant and fuel-element cladding temperatures of about 300 °C.

Another parameter that characterizes the features of RIA scenarios is the fuel burnup because the accident can occur at any time during the power operating cycle. In other words, the analysis of RIA scenarios should include their consideration as a function of the average burnup in the range of 0 to 50 MWd/kgU.

Thus the optimal program of experimental research on the behavior of VVER fuel elements under RIA conditions should provide for studies of failure mechanisms and failure thresholds in relation to the entire set of RIA conditions; however, the practical implementation of this approach is impossible.

Studying the failure mechanisms and failure thresholds in relation to the entire set of RIA conditions would require a time comparable to that required to develop new generations of nuclear power plants. This means that, by the time experimental results were obtained, they would be unusable because other design, processing, and operating parameters would characterize initial and boundary conditions for RIA analyses.

The current set of RIA scenarios is in continuous development in accordance with the development and improvement of the safety analysis methodology for nuclear power plants. The result is that the matrix of initial and boundary conditions for RIA scenarios is poorly stipulated. Therefore efforts to use elements of this matrix as technical requirements for the experimental program to study the behavior of fuel elements under RIA conditions can lead to errors of presently unassessable scale.

The majority of countries that conducted these studies used another approach to develop experimental programs of RIA investigations. The essence of the approach is to obtain the test data base under the simplest test conditions while adhering to the following principles:

• Conservativeness of results obtained.
• Maximum possible full dimensionality of the data set on failure mechanisms and thresholds.
• The amount of data obtained should be sufficient for computer codes to use to determine and validate parameters of fuel-element failure under RIA initial and boundary conditions.

This approach allowed us to develop and implement the experimental program aimed at the validation of VVER fuel-element behavior under RIA conditions. The program was carried out within the framework of the following considerations:

1. The set of key factors to be studied that influence fuel-element behavior was determined on the basis of the analysis of physical processes accompanying RIA scenarios from cold and hot starts.

2. The purpose of testing was to determine failure thresholds and mechanisms of VVER fuel elements as a function of the set of key factors. The failure threshold is characterized by the peak fuel enthalpy value for each of the two types of fuel-element failure: fuel-element cladding rupture and fuel-element cladding fragmentation. In this case the peak fuel enthalpy is determined as the radially averaged enthalpy at the axial elevation of the fuel element with the peak power.

3. As a rule, the program did not include studies of coolant behavior under RIA conditions. Thus tests were conducted under rather simple and easily reproducible initial and boundary coolant conditions.

A set of key factors was defined for this program:

• Energy deposition in the fuel (peak fuel enthalpy).
• Pulse half-width.

• Initial pressure drop across the cladding of the fuel element.

• Fuel burnup.

In a subtle way, variations of processing and design characteristics of fuel elements were present as test parameters. In certain cases the influence of these characteristics was also checked. In general, however, their total effects can be assessed on the basis of the spread of failure thresholds with a fixed value set of key factors.

The entire range of varying the key factors is shown schematically in Fig. 1. The logic of investigations was designed to study the influence of each key factor at three stages of the study.

The task of the first stage was to determine failure mechanisms and failure thresholds of fresh fuel rods as a function of the pulse half-width and initial pressure drop across the cladding for RIA from a cold start. Characteristics of the first stage of the test are shown in parts a and c of Fig. 1. In general, this stage of studies allowed us to get a statistically convincing set of results to use as the data base for comparing the effects of other key factors.

The second stage of investigations covered the influence of burnup effects on the behavior of fuel elements under RIA conditions. As shown in part b of Fig. 1, these tests were conducted in a narrower range of pulse half-width and only for the burnup that corresponds to the end of the power operating cycle. This approach was used because of two circumstances. First, the cycle of investigations performed at the first stage did not reveal a significant influence of the pulse half-width on failure thresholds and failure mechanisms. Second, a specific feature of VVER high-burnup fuel elements (unlike PWR high-burnup fuel elements) is a practically complete absence of oxidation and hydriding in the process of the power operating cycle. The result is that claddings of VVER fuel elements preserve plastic properties until the end of the power operating cycle. The combination of these two circumstances allowed us to assume that, unlike PWR high-burnup fuel elements, in which pellet–cladding mechanical interaction (PCMI) mechanisms are responsible for the cladding failure (in this case the failure threshold is a function of the burnup), the mechanism for failure of VVER high-burnup fuel elements is identical to that for fresh fuel elements and takes place at approximately the same levels of peak fuel enthalpy. This assumption was verified within the framework of test modes, shown in part b of Fig. 1.

The third stage of investigations covered the influence of conditions of hot-start variants. Test parameters of this stage are shown in part d of Fig. 1. Note that, in terms of fuel-element deformation behavior, the main parameter determining RIA from hot-start features is the presence of high pressure up to 16 MPa, which results in changes in fuel-element failure mechanisms and therefore in changes in failure thresholds. This is why corresponding investigations were conducted to study the influence of this parameter.

MAIN PROVISIONS OF TEST PROGRAM AND TEST PARAMETERS

In general, this experimental program was characterized by the following distinctive features:

• Test type: reactor capsule tests of VVER fuel rods.

• Method to simulate RIA: reactor burst with preset pulse half-width.

• Method to simulate other RIA conditions: variations by energy deposition, burnup, initial pressure drop across the cladding, etc.

Shortened fuel rods of VVER type were used as the test objects. High-burnup fuel rods were refabricated from commercial fuel elements from the Novo Voronezh nuclear power plant.

In all the studies the test fuel rod was positioned in a capsule filled with coolant, principally water. In some cases air was used as the coolant to obtain the data necessary to validate computer codes. A characteristic feature of this test data base is very simple boundary conditions on the surface of the fuel rod. The coolant pressure in the capsule was varied from 0 to 16 MPa. The initial coolant temperature was about 20 °C, and the flow rate was 0 g/s. Two research pulse reactors [GIDRA and Impulse Graphite Reactor (IGR)] were used to implement this program. The use of two reactors allowed us to significantly expand the range of the pulse half-width (see Fig. 2). The test procedure for VVER fuel rods is shown schematically in Fig. 3.

Special technologies were developed and applied to measure fuel-rod test parameters, including:

• Fuel temperature.

• Cladding temperature.

• Temperature of the gas plenum in the fuel rod.

• Pressure in the fuel rod.

• Temperature and pressure of the coolant.

• Energy deposition in the fuel.

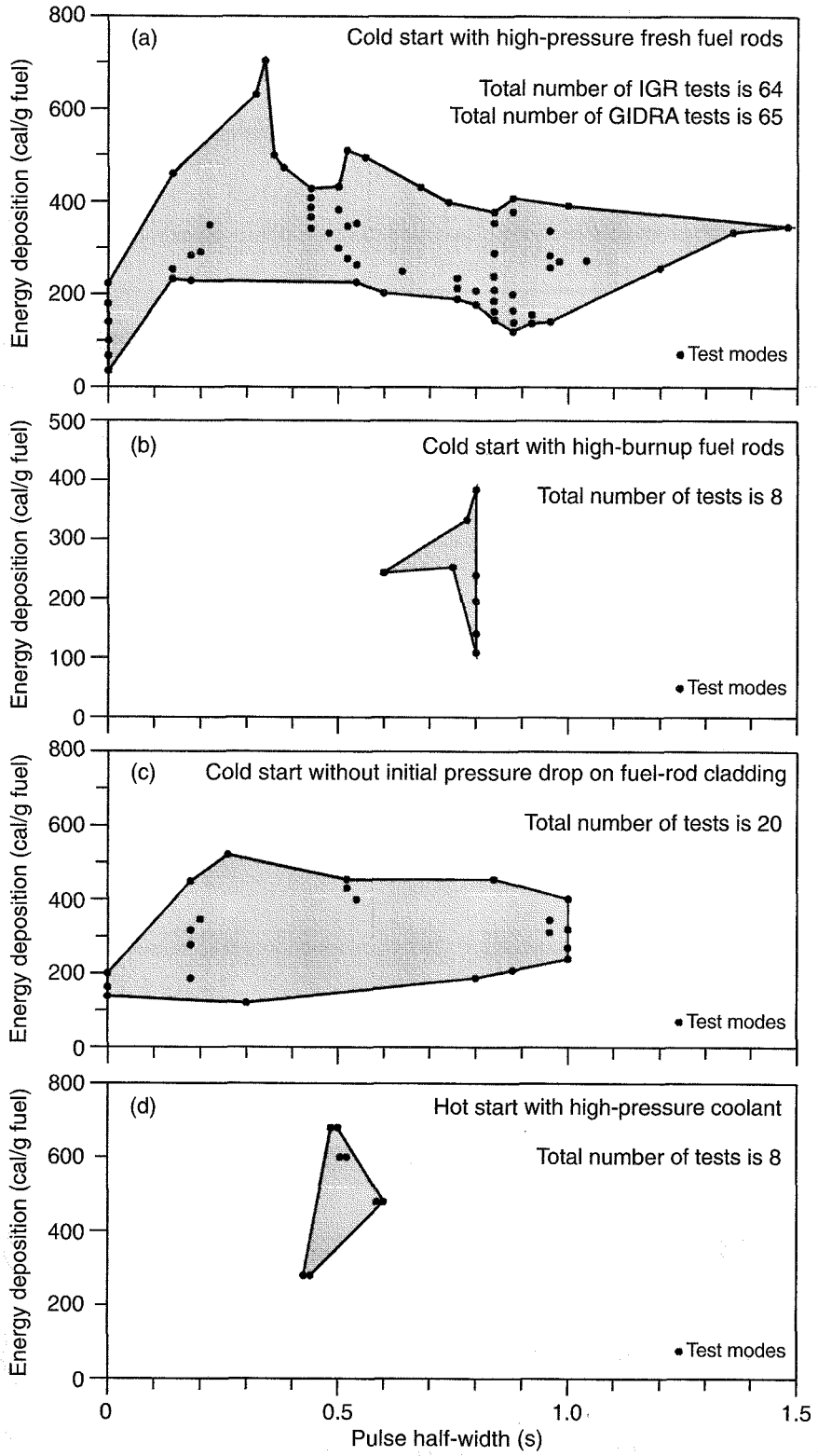

Fig. 1 Key variables and testing logic of VVER RIA tests.

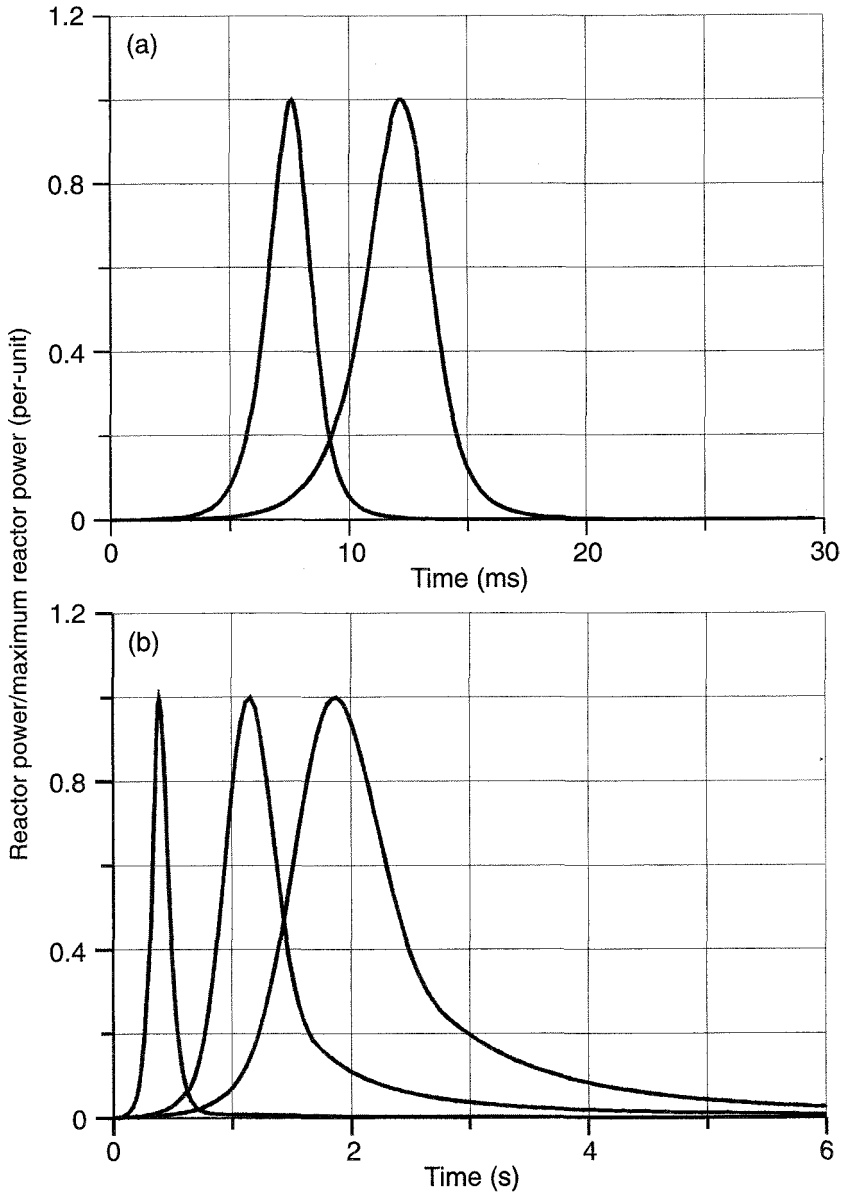

Fig. 2 Reactor power shapes for the GIDRA (a) and IGR (b) reactors.

When developing test procedures, special attention was paid to methods for posttest examinations. This allowed us to obtain a large data base to characterize processes that occur under RIA conditions:

- Geometric size.
- Cladding oxidation.
- Cladding–fuel chemical interaction.
- Melting of the fuel rod.
- Strain parameters of the fuel and cladding.
- Measurement of the number of fissions in the fuel.

These methods allowed us to identify the sequence of physical processes that form various scenarios of fuel-rod failure under RIA conditions, to determine absolute values of failure parameters, and to develop the data base necessary to validate computer codes for calculating VVER fuel-element behavior under RIA conditions.

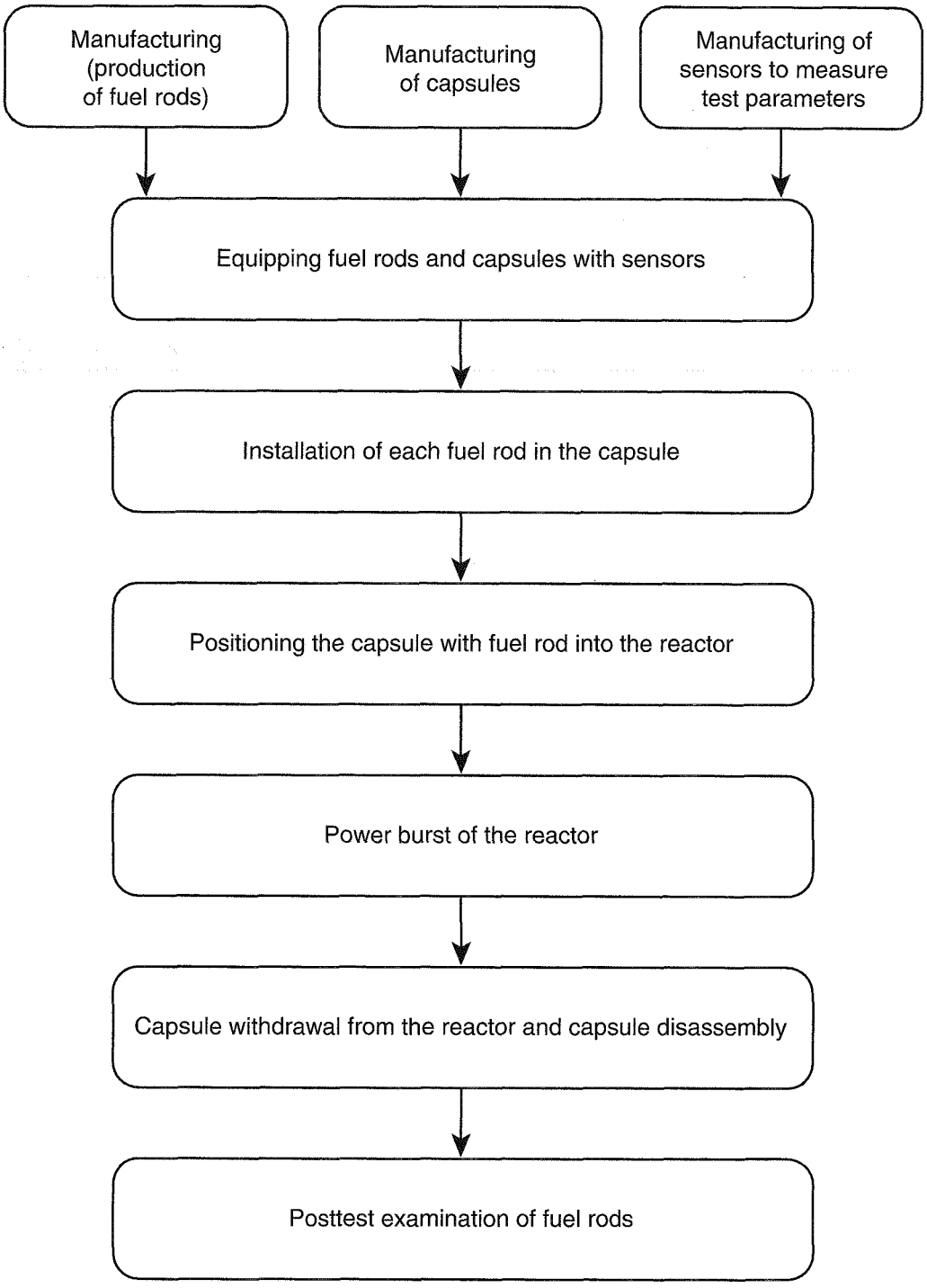

Fig. 3 Main stages of the procedure to test VVER fuel rods under RIA conditions.

In terms of test parameters, all the program investigations can be divided into three groups:

1. *Tests of fresh fuel rods at the GIDRA reactor.* These tests used extremely small values of the pulse half-width (about 2 to 3 ms), standard initial conditions of the coolant (20 °C, 0.1 MPa), and an initial pressure drop across the cladding of about 0.0 to 2.2 MPa.

2. *Tests of fresh fuel rods at the IGR reactor.* These tests were conducted at pulse half-widths from 0.14 to 1.5 s. The initial coolant conditions were of two types: (1) standard or close-to-standard conditions (20 °C; 0.1 to 0.5 MPa) and (2) high coolant pressure (20 °C; 16 MPa). The initial pressure in fuel rods was varied from 0.1 to 2.3 MPa depending on test tasks.

3. *Tests of high-burnup fuel rods at the IGR reactor.* These tests were performed at pulse half-widths of 0.6 to 0.8 s. Initial coolant conditions were standard. Initial pressure in the fuel rods was about 1.7 MPa. The fuel burnup reached 50 MWd/kgU.

FRESH FUEL-ROD TEST CONDITIONS AT THE GIDRA REACTOR

Two types of VVER fuel rods (Fig. 4) were tested at the GIDRA reactor. There were no differences in the materials or design of the active parts of the two types of fuel rods. The difference was in the sealing method of the fuel-rod cladding. One type was sealed by butt resistance welding (part a of Fig. 4); the other was sealed by electron-beam welding (part b of Fig. 4).

Different sealing methods result in different designs for the lower and upper caps. These two types of fuel rods were used because of the desire of the VVER fuel-rod developers to check the influence of the welding type on the operational capability of fuel elements under RIA conditions. Both types of fuel rods were manufactured by AO MZ (Electrostal, Moscow region, Russia) in accordance with the requirements of the processing cycle for VVER fuel elements. Fresh fuel rods consist of cladding made of Zr–1%Nb alloy, fuel

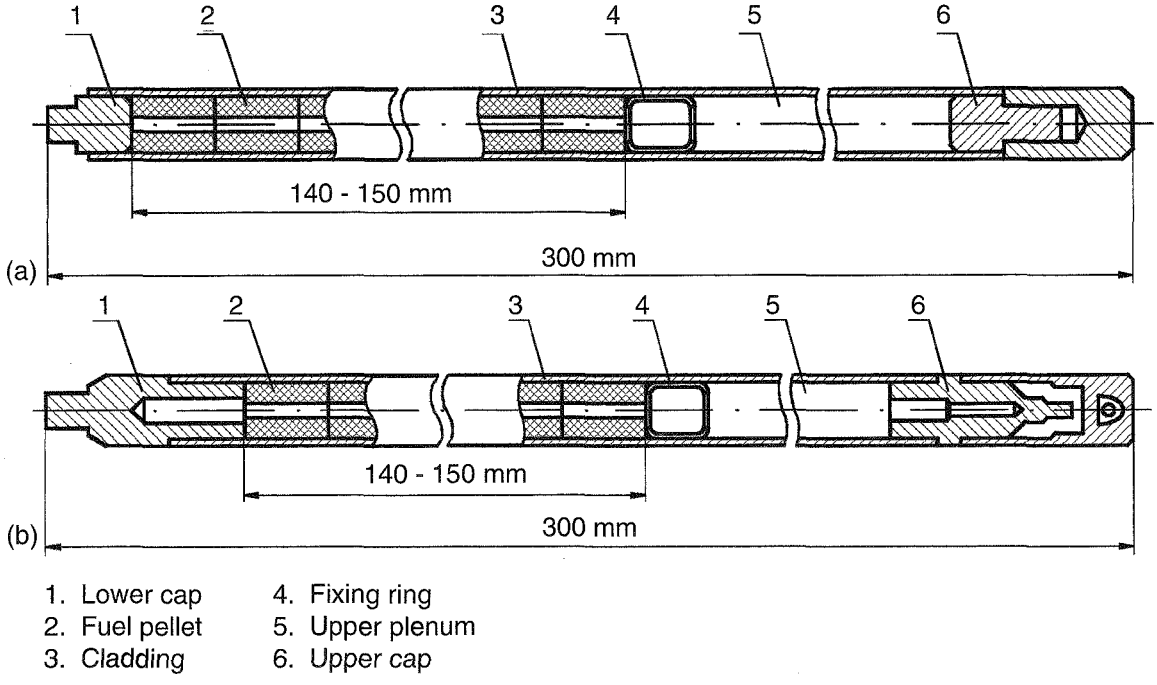

Fig. 4 Scheme of fuel rod sealed by butt resistance welding (a) and electron-beam welding (b).

stack, fixing ring, upper plenum, and caps. The fuel rods were filled with helium. Fuel pellets of fuel rods were made of UO_2 with 4.4% and 10% enrichment and had the standard 1.4-mm-diameter central hole. The characteristics of fuel rods tested in the GIDRA reactor are shown in Table 1.

Table 1 Representative Characteristics of VVER Fresh Fuel Rods Tested at GIDRA Reactor

Characteristic	Value
Fuel (UO_2)	
Enrichment, %	4.4, 10
Pellet outer diameter, mm	7.50
Density, g/cm^3	10.6
Cladding (Zr–1%Nb)	
Cladding outer diameter, mm	9.14
Cladding thickness, mm	0.63
Fuel rod	
Initial fill pressure, MPa	2.0 to 2.5
Gas composition	He
Fuel–cladding gap, mm	0.22

The GIDRA is a pulse research reactor of the water-solution-enriched type (Fig. 5). Twenty liters of water solution of UO_2SO_4 in a steel vessel form the reactor core. Four absorber rods, three control rods, the shim rod, and the start-up rod are located inside the reactor. Start-up and shim rods are thin-walled hollow cylinders positioned coaxially relative to the central reactor axis. The central reactor channel intended for housing test devices is located inside the shim rod. The power burst of the reactor with the required pulse half-width is produced with the use of a set of corresponding procedures and finally is ensured by the withdrawal of the start-up rod from the reactor with the help of the pneumatic drive.

Tests of VVER fuel rods were carried out in the self-quenching power-burst mode. In this case the reactor power burst is suppressed by the negative reactivity coefficient that includes two components: (1) the negative temperature reactivity coefficient of UO_2SO_4 water solution and (2) the negative void reactivity coefficient resulting from the radiolytic decomposition of UO_2SO_4 water solution.

The main characteristics of the GIDRA reactor[1] are shown in Table 2.

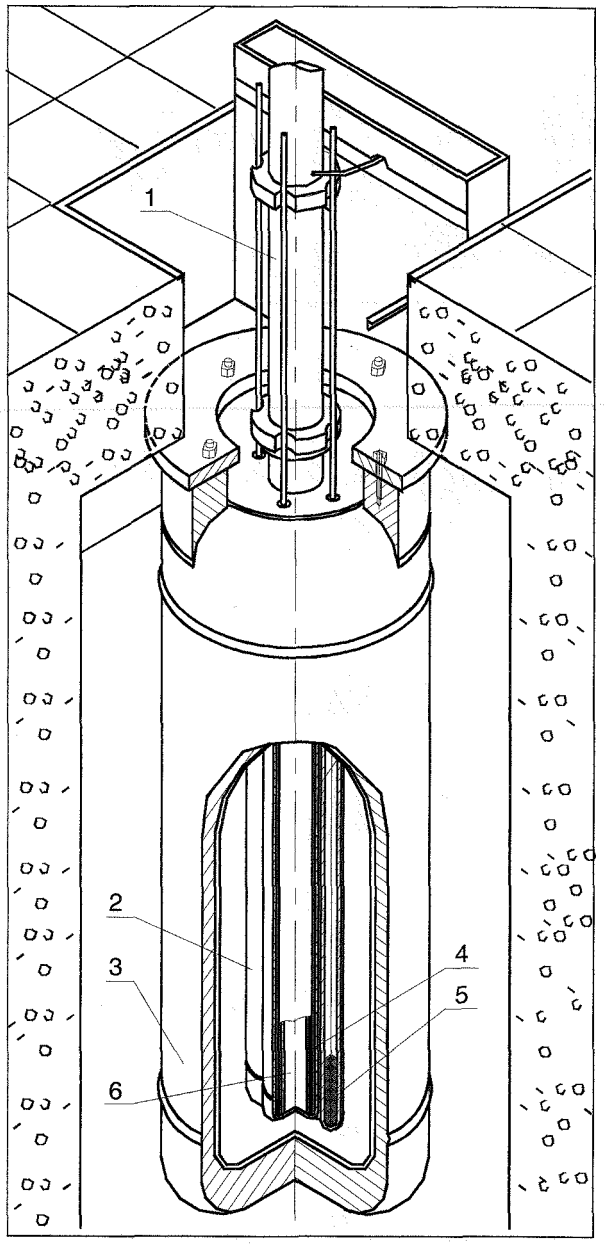

1. Pneumatic actuator of start-up
2. Channel for absorber rod
3. Reactor vessel
4. Start-up rod
5. Control rod
6. Central experimental channel

Fig. 5 Axial section of GIDRA reactor.

The test procedure of VVER fuel rods at the GIDRA reactor consisted of the following stages:[2]

- Installing the fuel rod in the test capsule.
- Positioning of the test capsule with the fuel rod in the central channel of the reactor.

Table 2 Main Characteristics of GIDRA Reactor

Parameter	Value
Material of reactor core	UO_2SO_4
Material of reactor vessel	Stainless steel
Inner diameter of reactor vessel, mm	392
Thickness of reactor vessel, mm	30
Material of reflector	Graphite
Material of control rods	B_4C
Outer diameter of control rods, mm	35.2
Material of start-up rod	B_4C
Thickness of start-up rod, mm	5
Outer diameter of central experimental channel, mm	75
^{235}U concentration in the solution, g/L	179.2
Reactivity maximum initial excursion, β_{eff}	7.5
Effectiveness of control rods, β_{eff}	9.5
Volume coefficient of reactivity, β_{eff}/L	1.6
Prompt neutron lifetime, ms	1.84
Efficient fraction of delayed neutrons, β_{eff}	0.0075

- Power burst of the reactor.
- Removing the capsule from the reactor.
- Neutronic radiography of the capsule with the fuel rod.
- Removing the fuel rod from the capsule.
- Posttest examinations.

The test capsule (Fig. 6) had a vessel made of aluminum alloy with an inner diameter of 30 mm. Before the test, the capsule was filled with water under standard conditions (20 °C, 0.1 MPa).

The test fuel rod was positioned along the axis of the test capsule. Parameters of the reactor power pulse for fuel rods tested near the failure threshold were as follows: pulse half-width of 2 to 3 ms and initial excursion of reactivity of 4.0 to 5.5 β_{eff}.

FRESH FUEL-ROD TEST CONDITIONS AT THE IGR REACTOR

The types of fuel rods tested in the IGR reactor were the same as those tested in the GIDRA reactor. Additionally, some design characteristics were varied. For example, in addition to fuel rods with cylindrical fuel pellets with the inner hole diameter of 1.4 mm, fuel rods were tested that had fuel pellets with chamfered edges. The inner hole of these pellets was 2.3 mm in diameter. Also, the initial pressure in the fuel rods was varied in these tests from 0.1 to 2.5 MPa. The main characteristics of fresh fuel rods tested in the IGR reactor are shown in Table 3. A special group of

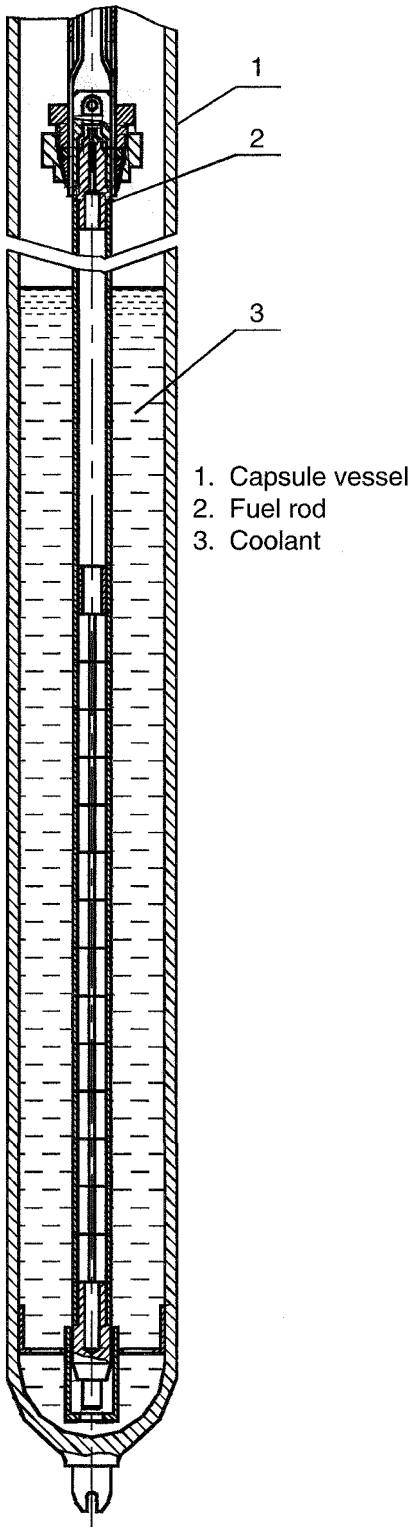

Fig. 6 Scheme of capsule vessel for the GIDRA reactor.

Table 3 Representative Characteristics of VVER Fresh Fuel Rods Tested at IGR Reactor

Characteristic	Value
Fuel (UO_2)	
Enrichment, %	4.4
Pellet outer diameter, mm	7.56
Density, g/cm^3	10.6
Cladding (Zr–1%Nb)	
Cladding outer diameter, mm	9.12
Cladding thickness, mm	0.63
Fuel rod	
Initial fill pressure, MPa	0.1 to 2.5
Gas composition	He
Fuel–cladding gap, mm	0.2

fuel rods tested in the IGR reactor included fuel rods equipped with sensors to measure test parameters.

The IGR is a pulse uranium–graphite self-quenching reactor of thermocapacity type.[2] Figures 7 and 8 show cross and axial sections, respectively, of the IGR reactor. The reactor core consists of graphite blocks impregnated with uranium salt. The side reflector and top and bottom edge reflectors consist of the same graphite blocks (but without uranium). The reactor core is located in the leak-tight reactor vessel filled with helium. The reactor vessel with the core is located in the water-filled tank.

The heat generated during reactor operation is accumulated in the reactor core and then is gradually transferred to the coolant circulating in the water tank. Control rods positioned in special holes in the reactor core are used to control the reactor power. Four lateral rods in the reactor are also located in holes in the reactor core. Reactor power is monitored with the use of a group of ionization chambers installed at a certain angle along the circumference of the water tank. In addition, in-core sensors of the neutron flux are used in some cases. These sensors are installed in the central plenum of the reactor. This part consists of a graphite insert with the central hole, which contains the central experimental channel of the reactor. Test objects (in our case, the capsule with fuel rods) are positioned in the central cavity of the central experimental channel.

The two main types of reactor power modes are the uncontrolled power pulse and the controlled power pulse. The uncontrolled power pulse mode is implemented by withdrawing a required group of control rods to a required height. This results in the introduction of the initial positive reactivity of up to 10 β_{eff} and thus in the formation of the forward front of the reactor power pulse. The power pulse is suppressed without the use of control rods because of the negative temperature reactivity coefficient.

The controlled power pulse is implemented with the use of the automatic regulator of the reactor power. It is possible to implement practically all reactor power profiles as a function of time. Both types of reactor power modes were used during tests of VVER fuel rods. Note that another specific method was used to study VVER fuel-rod behavior for modes with pulse half-widths in the range of 0.17 to 0.3 s. Because the power burst of the IGR reactor in this range results in fuel-rod melting and fragmentation (as the result of high values of peak fuel enthalpy that are typical for this range), the test procedure was somewhat changed: boric acid was added to the coolant surrounding the test fuel rod to reduce its peak fuel enthalpy.

The main characteristics of the IGR reactor are shown in Table 4.

Four types of capsules were used to test VVER fresh fuel rods at the IGR reactor. One of the capsule types was also used to test high-burnup fuel rods and is discussed in the next section of this article. The design schemes of three other types of capsules are shown in Fig. 9.

The capsule shown in part a of Fig. 9 was made of aluminum alloy and had an inner diameter of 83.4 mm; it was intended for tests of single fuel rods. The test fuel rod was positioned along the central axis of the capsule. A fixing device ensured free movement of the rod in the axial direction to compensate for temperature-related expansion during the test. Water or water with boric acid was used as the coolant. The initial coolant conditions were standard (20 °C, 0.1 MPa). The second type of capsule, shown in part b of Fig. 9, was intended for simultaneous testing of two fuel rods. In this case, the fuel rod equipped with sensors to measure test parameters was positioned along the central axis of the capsule, thereby displaying the standard fuel rod from the capsule center. The capsule vessel was made of aluminum alloy; the inner capsule diameter was 80 mm. The capsule was filled with the coolant (H_2O or air) at 20 °C at 0.1 to 0.5 MPa. Sensors to measure coolant parameters were also provided in the capsule.

The third type of capsule, shown in part c of Fig. 9, was made of zirconium alloy and was intended for tests of fuel rods at high coolant pressure, up to 16 MPa. The inner diameter of the capsule vessel was 110 mm. Fuel rods within the capsule were arranged

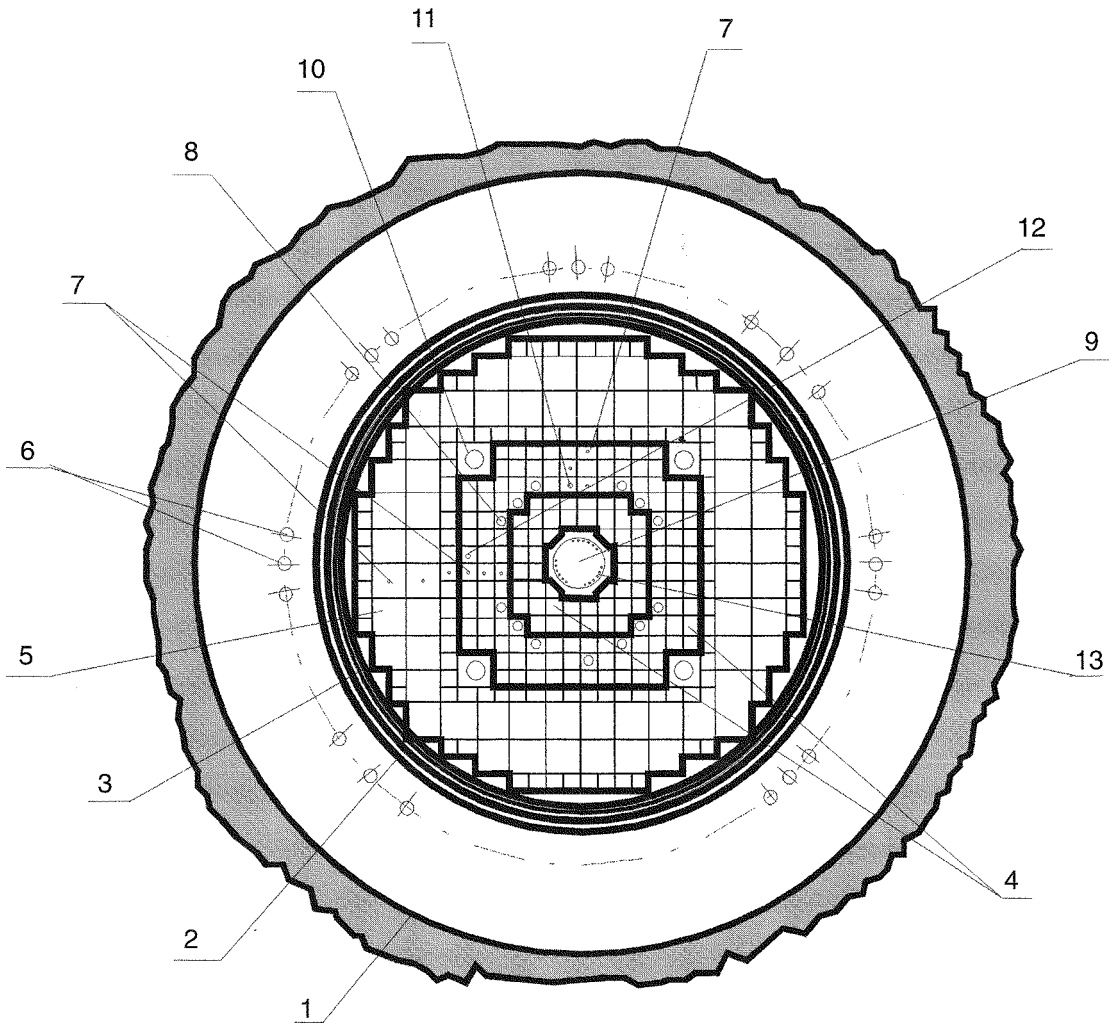

1. Water tank
2. Reactor vessel
3. Thermal shield
4. Reactor core
5. Side reflector
6. Ionization chamber channel
7. Temperature sensor channel
8. Control rod channel
9. Central experimental channel
10. Side experimental channel
11. Physical measurement channel
12. Neutron source channel
13. In-core monitoring detector channel

Fig. 7 Cross section of IGR reactor.

according to the scheme shown in part b of Fig. 9. The test procedure of VVER fresh fuel rods at the IGR reactor consisted of the following stages:[2]

- Installing fuel rod in the test capsule.
- Positioning the test capsule with the fuel rod in the central channel of the IGR reactor.
- Connecting test parameter measurement sensors to the recording system.
- Reactor power burst.
- Removing capsule from the reactor and fuel rod from the capsule.
- Posttest examinations.

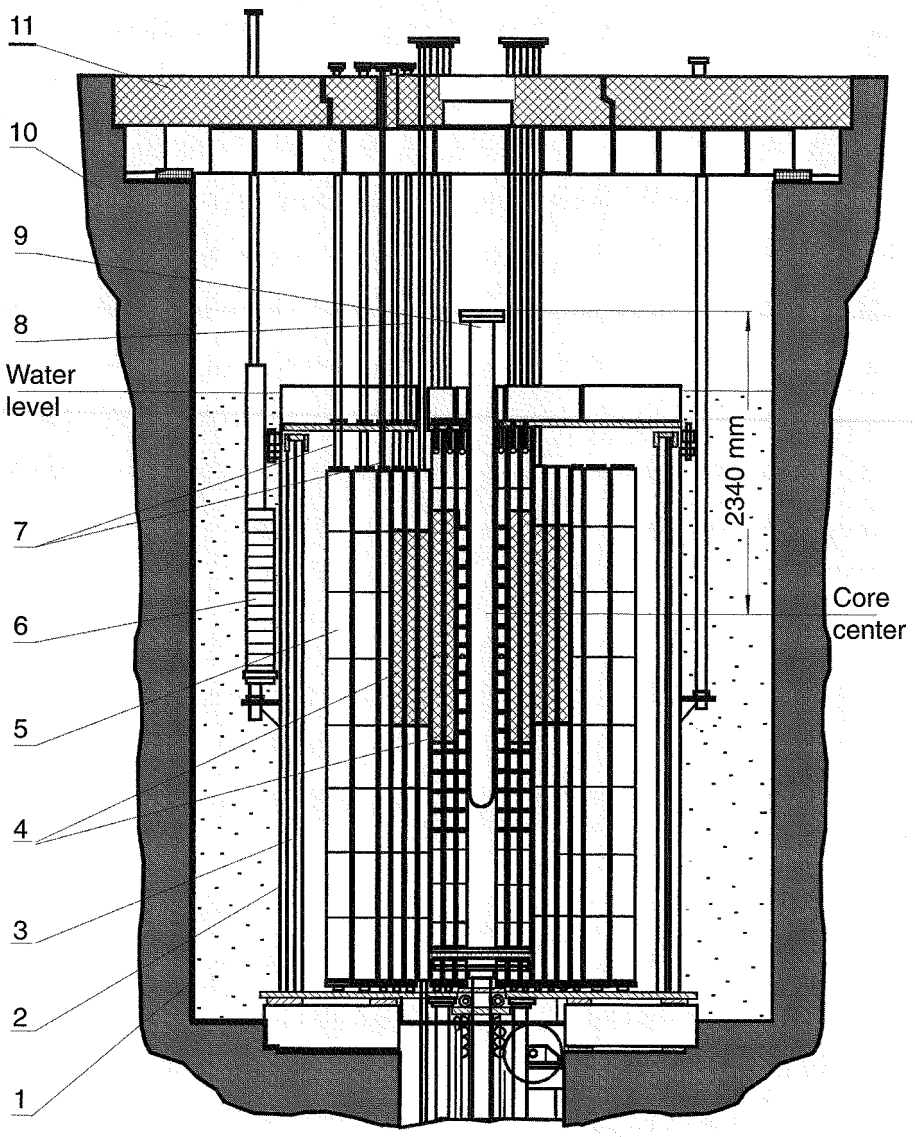

1. Water tank
2. Reactor vessel
3. Thermal shield
4. Reactor core
5. Side reflector
6. Ionization chamber channel
7. Temperature sensor channel
8. Control rod channel
9. Central experimental channel
10. Biological shield
11. Ceiling

Fig. 8 Axial section of IGR reactor.

The test parameter range of VVER fresh fuel rods near failure thresholds was as follows:

- Pulse half-width for fuel rods with the initial pressure drop across the cladding of about 1.8 to 2.2 MPa: 0.14 to 1.5 s.
- Pulse half-width for fuel rods with the initial pressure drop across the cladding of about 0 to 0.5 MPa: 0.18 to 1 s.
- Pulse half-width for fuel rods tested at high coolant pressure: 0.44 to 0.6 s.

Table 4 Main Characteristics of IGR Reactor

Characteristic	Value
Approximate overall dimensions of the reactor core, mm	$1400 \times 1400 \times 1400$
Outer diameter of the central experimental channel, mm	270
Material of fuel elements of the reactor core	Graphite impregnated with uranyl sulfate
U^{235} mass in the reactor core, kg	9
Fuel enrichment in U^{235}, %	90
Nuclear ratio, carbon/uranium	8040
Moderator material	Graphite
Reflector material	Graphite
Maximum thermal neutron flux density in the reactor central experimental channel, neutrons/cm$^2 \cdot$ s	7×10^{16}
Maximum thermal neutron fluence in the central experimental channel, neutrons/s^2	3.7×10^{16}
Excess reactivity, β_{eff}	31.6
Effective fraction of delayed neutrons, β_{eff}	0.00685
Temperature reactivity coefficient, β_{eff}/K	–0.03
Maximum permissible temperature of the reactor core, K	1400

HIGH-BURNUP FUEL-ROD TEST CONDITIONS AT THE IGR REACTOR

Two types of fuel rods were designed and manufactured for these tests: refabricated high-burnup fuel rods and refabricated fuel rods with preirradiated cladding and fresh fuel. The two types of fuel rods were used with the aim to identify key factors in the failure mechanism and threshold of high-burnup fuel rods under RIA conditions.

Refabricated High-Burnup Fuel Rods

Refabricated high-burnup fuel rods were manufactured from commercial fuel elements preirradiated up to 48 MWd/kgU at Novo Voronezh nuclear power plant. The nonuniformity coefficient of the burnup along the segment height of the VVER fuel element used for refabricated fuel rods was 1.04. The design of this type of fuel rod is shown in Fig. 10.

The fuel rod contained the active part (fuel stack and cladding), which was part of a commercial fuel element, and special components such as the fixing ring, connector, upper plenum, and upper and lower caps. All special components of the fuel rod were made of nonirradiated materials. The fuel-rod cladding was Zr–1%Nb alloy, fuel-rod pellets were cylindrical, and there was a 1.4-mm-diameter hole along the pellet axis. The source fuel material was UO_2. The internal plenum of the fuel rod was filled with helium under pressure of about 1.7 MPa. Representative characteristics of high-burnup fuel rods are shown in Table 5.

Refabricated Fuel Rods with Preirradiated Cladding and Fresh Fuel

This type of refabricated fuel rod contains, in the active part, a segment of the cladding from commercial fuel elements from Novo Voronezh nuclear power plant and a fuel stack with nonirradiated fuel. The design of the fuel rod is analogous to the one shown in Fig. 10.

Fuel pellets were cylindrical with chamfered edges with a hole along the pellet axis. The internal environment of the fuel rod was helium under 1.7-MPa pressure. Characteristics of fuel rods are shown in Table 6.

The special capsule design developed to test high-burnup fuel rods is shown in Fig. 11. Two fuel rods were tested simultaneously in this capsule: the refabricated fuel rod and the fresh fuel rod. The steel vessel of the capsule was filled with water under standard initial conditions (20 °C, 0.1 MPa). The fuel-rod fixing device in the capsule ensured the possibility of its free movement in the axial direction during the process of thermal expansion. Twenty-three refabricated fuel rods were tested in the pulse half-width range of 0.5 to 0.8 s.

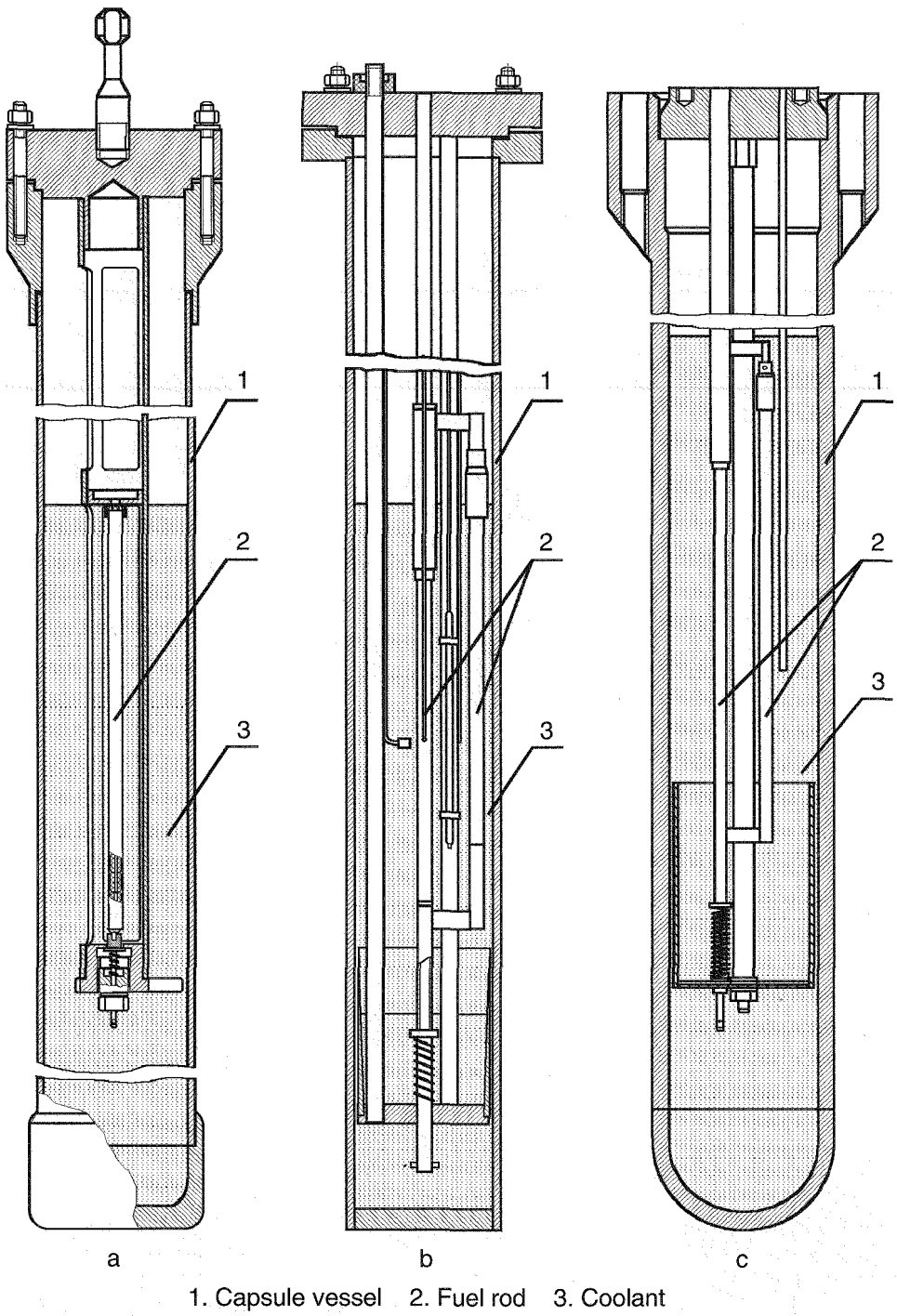

Fig. 9 Schemes of capsules to test one (a) or two (b) fresh fuel rods at low coolant pressure and (c) two fresh fuel rods at high coolant pressure.

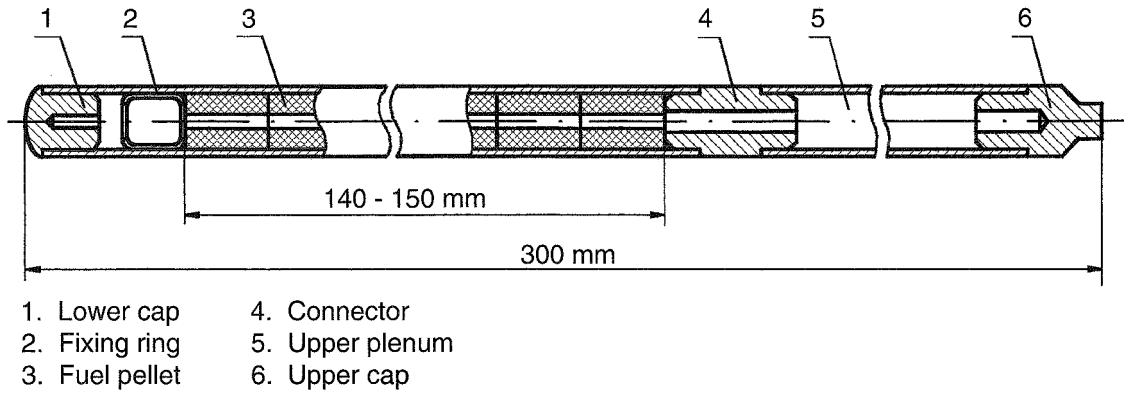

Fig. 10 Scheme of high-burnup fuel rod.

Table 5 Representative Characteristics of VVER High-Burnup Fuel Rods

Characteristic	Value
Fuel (UO_2)	
Burnup, MWd/kgU	41 to 49
Pellet outer diameter, mm	7.55 to 7.60
Density, g/cm^3	10.31 to 10.32
Cladding (Zr–1%Nb)	
Cladding outer diameter, mm	9.1
Corrosion thickness, μm	5 to 6
H_2 content in the cladding, wt %	3 to 6×10^{-3}
Fuel rod	
Initial fill pressure, MPa	1.7
Gas composition	He
Free volume, cm^3	6.11
Fuel–cladding gap, mm	0.03 to 0.07

Table 6 Representative Characteristics of VVER Fuel Rods with Fresh Fuel and Preirradiated Cladding

Characteristic	Value
Fuel (UO_2)	
Enrichment, %	4.46 to 4.47
Pellet outer diameter, mm	7.56
Density, g/cm^3	10.5 to 10.6
Cladding (Zr–1%Nb)	
Outer diameter, mm	9.11
Corrosion thickness, μm	5 to 6
H_2 content in cladding, wt %	3 to 6×10^{-3}
Fuel rod	
Initial fill pressure, MPa	1.7
Gas composition	He
Free volume, cm^3	5.8
Fuel–cladding gap, mm	Not measured

MEASUREMENTS OF THERMOPHYSICAL PARAMETERS

The development of procedures to measure thermophysical parameters of RIA tests was a special investigation area because sensors measuring the temperature and pressure must conform to the following requirements:

- Must not disturb the thermomechanical behavior of fuel rods.
- Have no significant error related to response to neutron and gamma flux.
- Have small dimensions and ensure maximum contact with the surface, the temperature of which is to be measured.
- Have a small inertia to be able to measure fast transient processes.
- Have high limits of temperature measurements (2100 °C for the fuel-rod cladding and 2500 °C for the fuel).
- Be made of materials that do not chemically react with fuel-rod materials.

Sequential stages of investigation allowed us to develop unique technologies that yielded the following test parameter measurements:

- Temperatures of the fuel, fuel-rod cladding, upper plenum, and coolant.
- Pressure in the fuel rod and in the coolant.
- Time of fuel-rod failure.

Figure 12 shows the appearance of the VVER fuel rod with sensors to measure test parameters.

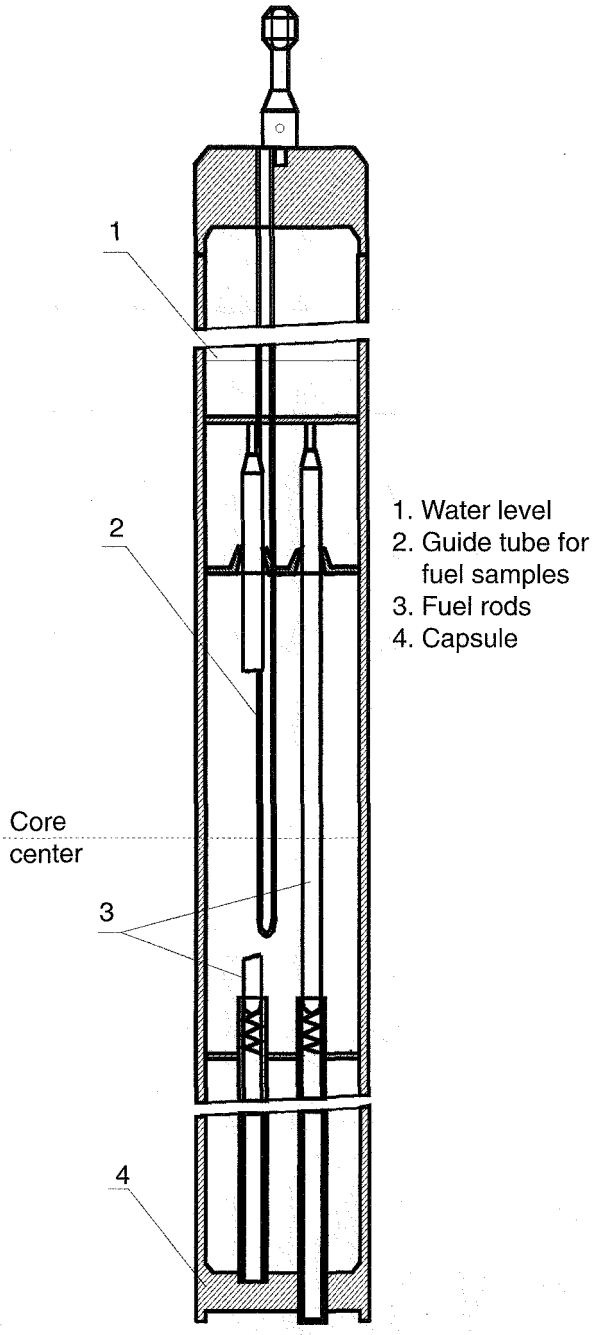

Fig. 11 Scheme of the capsule to test high-burnup fuel rods.

DETERMINING POWER SHAPE AND ENERGY DEPOSITION IN FUEL RODS

Reactor power shapes were used to determine the set of power shapes in VVER fuel rods. Reactor power shape changes vs. time were measured with the use of the ionization chambers of the IGR and GIDRA reactors. The final stage of the procedure to get the distribution of fuel-rod power vs. time is the differentiation of the energy deposition in the fuel rod using the curve of the reactor power shape. This approach requires a very accurate description of the reactor power shape for the area of the residual heat (i.e., near zero reactor power). Special scoping tests were conducted at the IGR and GIDRA reactors to obtain a corresponding test data base; special calculation methods to simulate these procedures were developed and verified. These calculation methods were used to adjust the reactor power shape near zero reactor power for each test. In addition to measurements of the fuel-rod power vs. time, the fuel-rod power vs. the fuel-pellet radius vs. the axial elevation were calculated from the data base of fuel-pellet measurements and by using computer codes to describe these distributions in each of the tested fuel rods.

The energy deposition in VVER fuel rods was measured by an indirect method in three steps: (1) measurement of the number of fissions in the fuel, (2) determination of the distribution of fissions in the fuel rod, and (3) determination of r,z,t distribution of energy depositions in the fuel rod.

Measurement of the number of fissions in VVER fuel rods tested at the GIDRA reactor can be described as follows:[2]

- Determination of the ratio between the number of fissions in a fuel pellet of a VVER fuel rod and the activity of the special detector made of sulfur (S detector) using special scoping tests.
- Measurement of S detector activity after each test of VVER rods in the GIDRA reactor.

Thus the procedure is based on the experimentally determined ratio between the number of fissions in VVER fuel and the activity of the S detector, which was installed at the same point in the reactor for each test. The number of fissions in VVER fuel was determined with the use of spectrometric measurements of the activity of ^{140}La and ^{95}Zr isotopes, which are uranium fission products. S detector activity was measured on the basis of the induced activity of ^{32}P produced as a result of the reaction ^{32}S(n,p)^{32}P. Measurements were performed at a β-counting facility. The ratio obtained was used to determine the number of fissions in VVER fuel on the basis of the activity measured after each test with the S detector installed in the same point in the reactor.

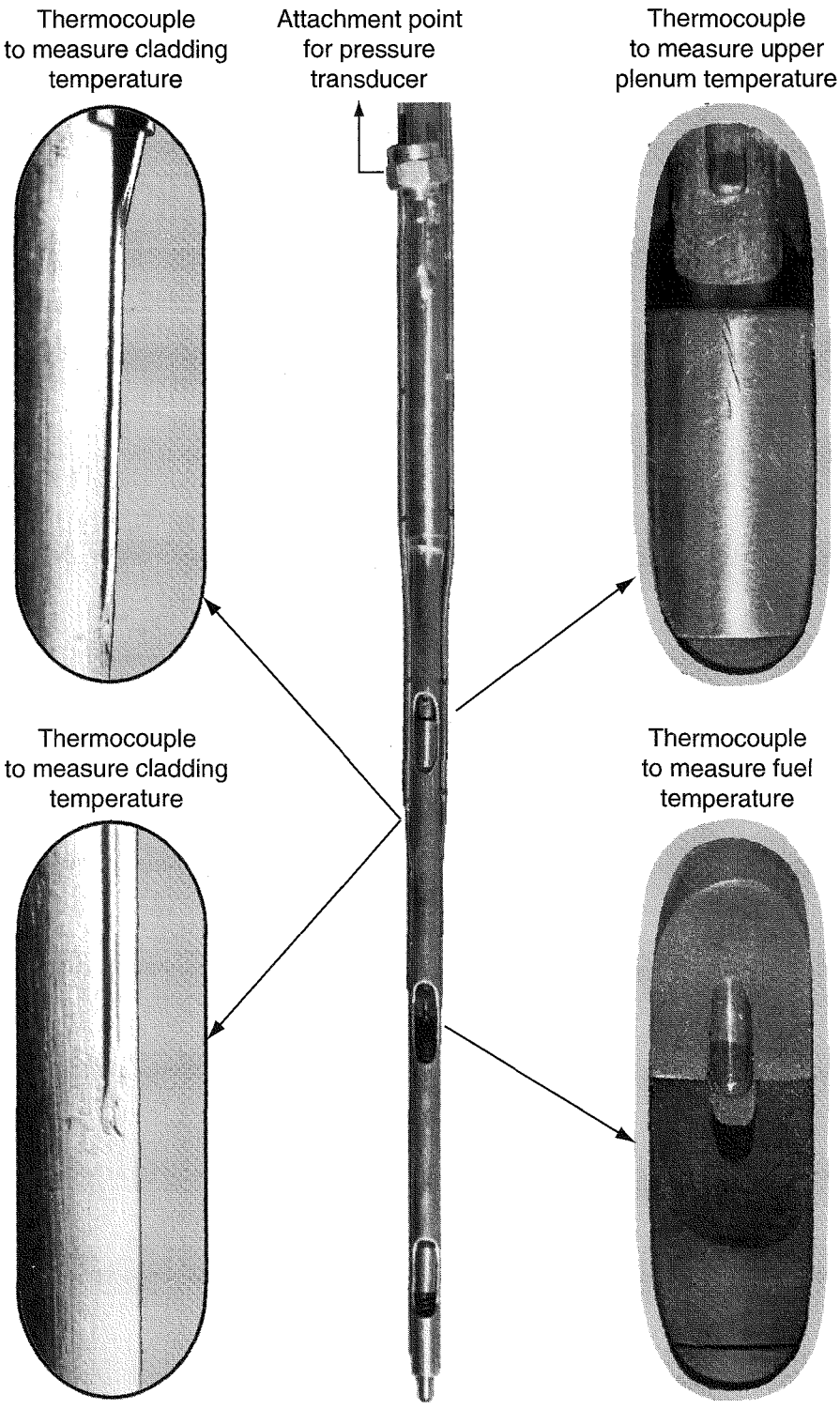

Fig. 12 Appearance of VVER fuel rod with sensors to measure test parameters.

The method used to determine the number of fissions in VVER fresh fuel rods tested at the IGR reactor is based on the experimental determination of the ratio between the number of fissions in a VVER fuel pellet and the number of fissions in a special uranium-containing detector (special fuel sample). Special fuel samples (Fig. 13) were installed at the same point in the reactor for each test. Measurements of the number of fissions in VVER fuel pellets and the number of fissions in special fuel samples were performed on the basis of measurements of ^{140}La and ^{95}Zr isotope activity by gamma spectrometry. It was necessary to determine the ratio of the number of fissions in VVER fuel to special fuel samples for all types of capsules that were used in the IGR reactor with all types of coolant (H_2O, air, and H_2O with various concentrations of H_3BO_4).

The development and validation of the procedure to determine the number of fissions in high-burnup fuel rods tested at the IGR reactor was a very complicated problem that involved a set of calculational, methodological, and experimental studies. The main provisions of this procedure are:

- Determination of the burnup spatial distribution in each fuel rod.
- Determination of the spatial distribution of the isotopic composition in fuel rods.
- Determination of the axial distribution of the fuel mass.
- Measurement of the number of fissions in special fuel samples installed inside the capsule with the high-burnup fuel rod.
- Implementation of three-dimensional computer neutronics codes to perform calculations of the system "IGR reactor—capsule—fuel rod—special fuel sample" and determination of the ratio of the number of fissions in the special fuel sample to the number of fissions in the fuel rod for each fissile isotope.
- Determination of the fuel-rod energy deposition with the use of thermal equivalents of one fission event of various isotopes, taking into account specific features that depend on the contribution of prompt and delayed radiation components in fuel rods and in the reactor.

All stages of this procedure were carefully verified by conducting special experimental studies.

A test data base was used for verification, which included isotopic concentrations vs. burnup, isotopic distributions vs. fuel radius, and IGR reactor power vs. time. The relation between the number of fissions in fresh and high-burnup fuels was obtained in a special reactor test. The Monte Carlo codes were also used to verify the neutronic codes.

DETERMINATION OF PEAK FUEL ENTHALPY

The peak fuel enthalpy is used as the licensing criterion to indicate the failure threshold of fuel elements under RIA conditions. The peak fuel enthalpy cannot be measured directly but can be determined with the use of a computer code.

One of the most well-known and well-developed codes used to describe fuel-element behavior under transient processes is FRAP-T6.[3] This code is widely used to analyze experimental results at the Power Burst Facility (PBF), the Nuclear Safety Research

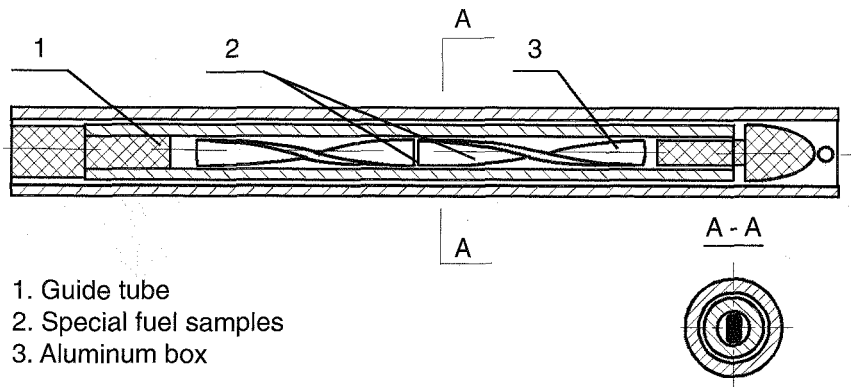

Fig. 13 Special fuel samples.

Reactor (NSRR), and other facilities, which is why version 21 of the code was selected to simulate VVER-type fuel-rod behavior under RIA conditions.

A challenge in this task was the fact that the FRAP-T6 code is not adapted to VVER fuel-element geometry or to VVER-type materials. Solving this problem required special investigations by RRC KI specialists. As a result of these investigations, a working version of the FRAP-T6 code was used to calculate peak fuel enthalpies in VVER fuel rods, and adaptation of the FRAP-T6 code to VVER conditions is under way. Estimates show that uncertainties of the calculated enthalpies do not exceed 10 to 15 cal/g fuel.

FAILURE THRESHOLDS AND MECHANISMS VS. PULSE HALF-WIDTH FOR HIGH-PRESSURE FRESH FUEL RODS

Analysis of the obtained experimental data set shows that the failure mechanism of high-pressure fuel rods is ballooning-type plastic deformation of the fuel-rod cladding as the result of internal pressure with subsequent cladding burst in the region of maximum hoop strain. A typical view of this deformation is shown in Fig. 14.

Analysis of posttest examination results and measurements of the fuel-rod cladding temperature demonstrate that fuel rods fail when the cladding temperature reaches about 900 °C. This temperature happens to be the temperature of the phase transformation in Zr–1%Nb alloy, which is accompanied by a sharp increase in stress and deformation of the cladding material. Typical behavior of a highly pressurized fuel rod under IGR test conditions is characterized by the parameters shown in Fig 15. According to measurements, the cladding burst when it reached about 1200 K (Fig. 15a) and the pressure drop across the cladding was 2.3 MPa (Fig. 15b).

The first stage of the procedure to determine the failure threshold of this fuel-rod type vs. the pulse half-width was computer modeling with the use of FRAP-T6 to determine the peak fuel enthalpy for each fuel rod. Calculation results are shown in Fig 16. The second stage was to determine the upper and lower boundaries of the failure threshold area. This area is limited by:

- Maximum peak fuel enthalpy values at which no fuel-rod failure was recorded on one side.
- Minimum peak fuel enthalpy values at which the fuel-rod failure was detected on the other side.

As shown in Fig. 16, the area of failure thresholds for high-pressure fuel rods is in the range of 160 to 180 cal/g fuel. These results show no notable influence of the pulse half-width on the failure threshold of high-pressure fresh fuel rods. Thus a conservative interpretation of the results should take the failure threshold of this type of fuel rods to be 160 cal/g fuel.

FAILURE THRESHOLD FOR LOW-PRESSURE FRESH FUEL RODS

The failure mechanism of these fuel rods is local melting of cladding. The fuel that is melted in the central part of the fuel stack percolates through a crack or axial gap between pellets to the internal side of the cladding. The interaction between melted fuel and cladding creates a hole in the cladding. Then the melted fuel flows into the coolant. Figure 17 illustrates this failure mechanism. It is possible that the appearance of a hole in the cladding occurs at a temperature somewhat lower than the melting point of Zr–1%Nb alloy because of eutectic dissolution of Zr–1%Nb by UO_2.

Unfortunately, the data set characterizing the behavior of these fuel rods is not representative enough to reliably determine the failure threshold vs. the initial pressure drop across the cladding; however, the available results allow us to make a conservative recommendation.

Data show that, in fuel rods with an initial pressure drop across the cladding of 0.4 to 0.9 MPa, the temperature of the cladding increases to 1680 to 1950 K, which automatically results in a failure enthalpy increase of up to 220 to 250 cal/g fuel. Note that these results were obtained for fuel rods with special features to accommodate the sensors of the test parameter measurement system. Thus, despite the fact that these results are absolutely reasonable from the physical viewpoint, the failure threshold of these fuel rods should be considered to be the same as the conservative estimate for the failure threshold of high-pressure fuel rods.

FAILURE THRESHOLDS AND MECHANISMS FOR FRESH FUEL RODS WITHOUT INITIAL PRESSURE DROP ACROSS THE CLADDING

It seems reasonable that the failure mechanism of fresh fuel rods should be similar to that of

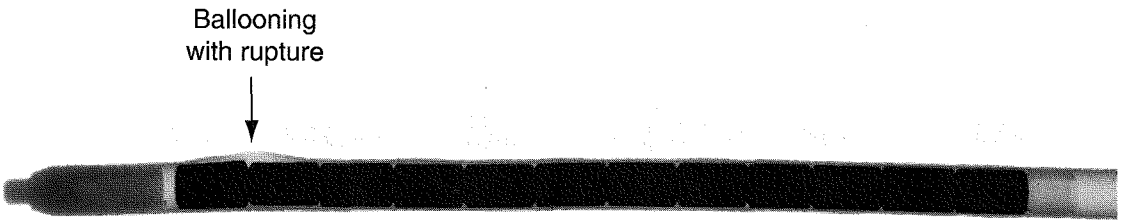

Fig. 14 Failure mechanism for high-pressure fresh fuel rod.

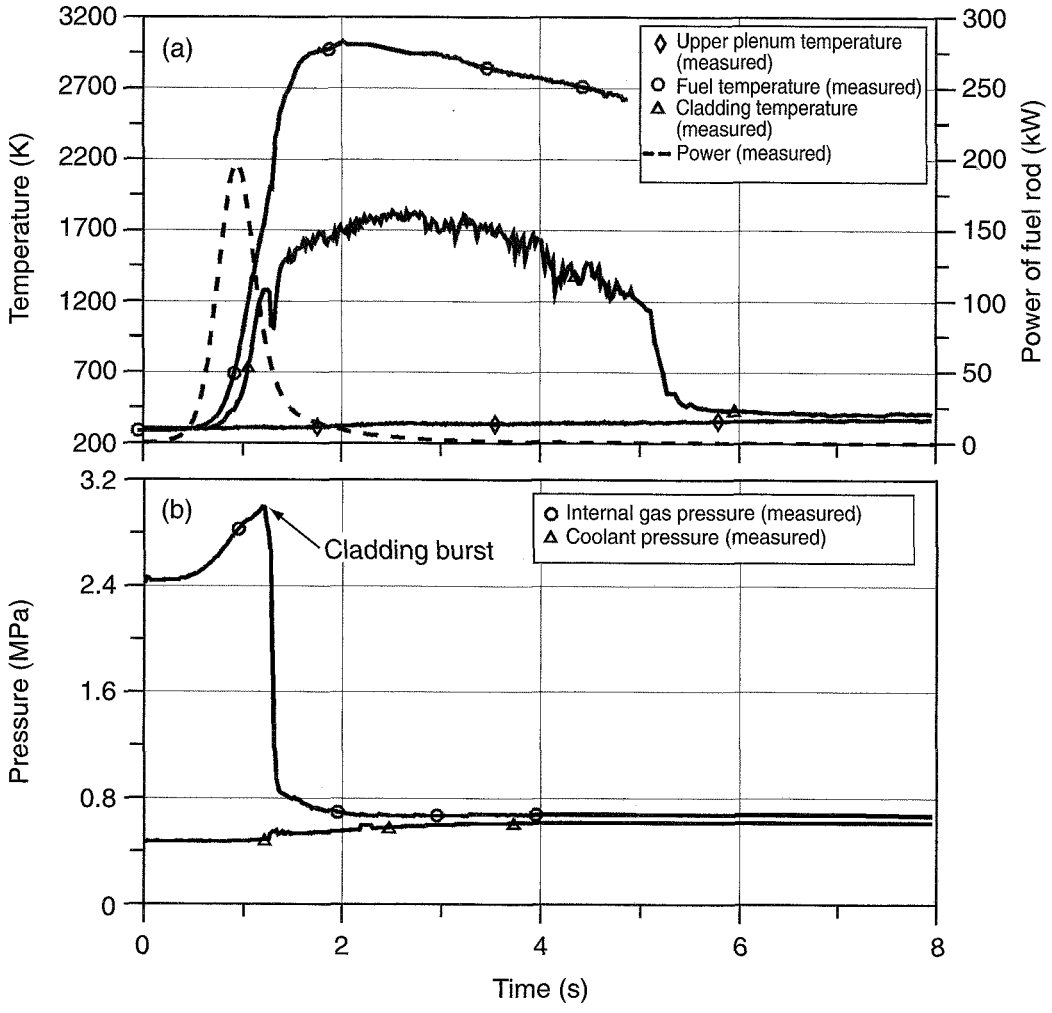

Fig. 15 Set of parameters to characterize failure threshold for high-pressure fuel rod tested at IGR reactor.

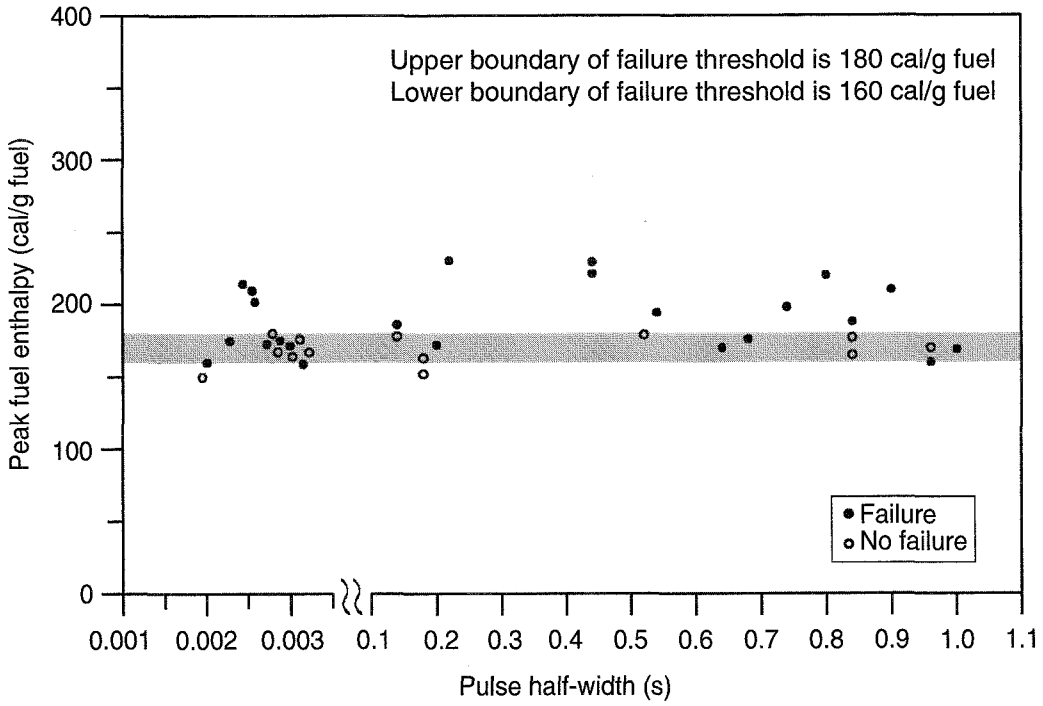

Fig. 16 Test data base to determine failure threshold vs. pulse half-width for high-pressure fresh fuel rods.

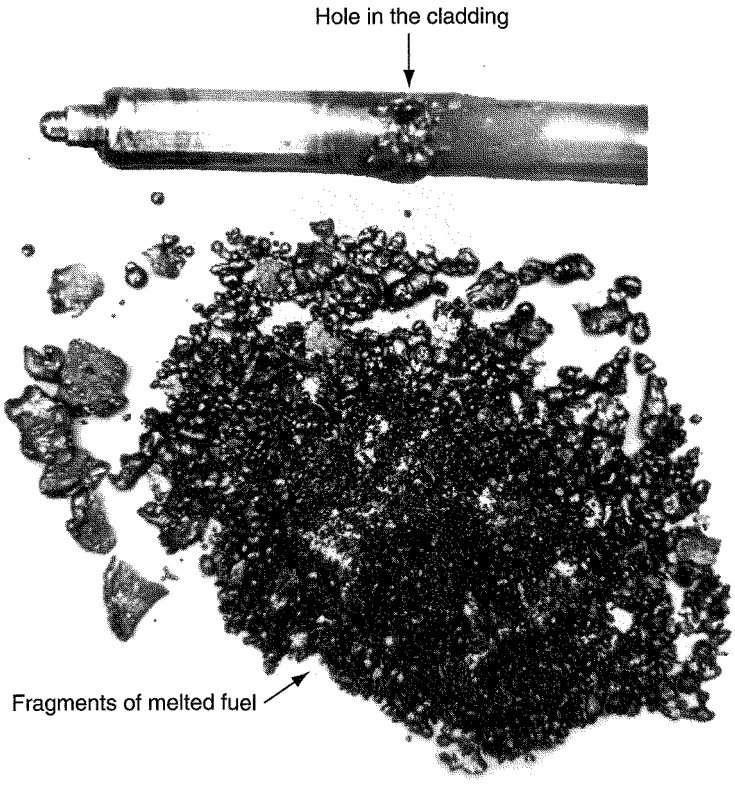

Fig. 17 Failure mechanism for low-pressure fresh fuel rods.

low-pressure fuel rods. If the peak fuel enthalpy is just above the failure threshold, the failure scenario is as follows:

- Melting of the bulk of the fuel.
- Local melting of the cladding.
- Escape of the fuel into the coolant.
- Strong oxidation of the fuel-rod cladding as the result of its temperature increase to 1500 °C and above.
- Fuel–cladding fragmentation in the cooling phase as the result of the tensile stress in the fuel-rod cladding and reduction of its plastic properties as the result of oxidation.

Test results have shown that all fuel rods failed consistent with this scenario. Figure 18 illustrates the processes that accompany this failure mechanism.

The calculation modeling of the behavior of a group of representative fuel rods with the use of the FRAP-T6 code yielded the peak fuel enthalpy values shown in Fig. 19. The data show that (1) the lower value of the peak fuel enthalpy for which fuel-rod failure was observed is about 300 cal/g and (2) the maximum value of the peak fuel enthalpy at which the fuel rod did not fail is about 260 cal/g.

In this case, note that the amount of experimental data characterizing the realistic failure threshold is not enough. Again, the failure of this type of fuel rod occurs when the fuel temperature exceeds the UO_2 melting point. The peak fuel enthalpy is about 250 cal/g at this point. Therefore, on the basis of conservative interpretation, this value of 250 cal/g can be adopted as the failure threshold for fresh fuel rods.

FAILURE THRESHOLDS AND MECHANISMS FOR FRESH FUEL RODS TESTED AT HIGH COOLANT PRESSURE

Tests of this type demonstrated that the increase in the cladding temperature to 900 °C results in its plastic deformation (as the result of external pressure) in the form of cladding collapse (see Fig. 20). Significantly, the deformed cladding preserves its integrity along the fuel stack height up to peak fuel enthalpy values that result in the fuel melting in the central part of the fuel rods. The analysis of posttest examination results shows that, unlike all other test types, in this case the deformation of critical scale and finally the cladding failure occur at the interface of fuel pellets where axial peak powers of fuel rods are in the area of the first and last fuel pellets.

Thus, in this location a cladding collapse of a peculiar type occurs, and a closed crack is formed when a certain value of the peak fuel enthalpy is obtained. The crack formation takes place, apparently, during the cooling phase when the cooling of the fuel rod causes tensile stresses. Note that this effect was observed in fuel rods equipped with the test parameter measurement system, but not standard fuel rods. The failure mechanism for standard fuel rods was the formation of a peculiar ballooning (Fig. 20) in the area of the top fuel pellet and the cladding melting through.

Data in Fig. 21 illustrate the relation between the peak fuel enthalpy and fuel-rod conditions after tests of this type. One test mode also measured test parameters vs. time (Fig. 22). These results show that the experimentally recorded value of the failure threshold is 250 cal/g fuel; however, the formation of closed cracks in the area of maximum hoop strain of the cladding was also observed at a lower value of peak fuel enthalpy. Thus, from a conservative viewpoint, the lowest experimental value of the peak fuel enthalpy, namely, 170 cal/g fuel, can be adopted as the failure threshold.

FAILURE THRESHOLD AND MECHANISM FOR HIGH-BURNUP FUEL RODS

The following phenomena are important to the analysis of the behavior of high-burnup fuel rods under RIA conditions: mechanism of cladding failure, scale of cladding deformation, and features of fuel-rod behavior above the cladding failure threshold.

According to the tests, ballooning was the threshold failure mechanism for all types of fuel rods. Figure 23 contains photographs of each type of tested fuel rod. Tests of high-burnup, pressurized fuel rods show that, as in fresh fuel rods, the basic mechanism of failure is the ballooning-type deformation of the cladding with subsequent cladding burst in the area of maximum hoop strain. Figure 23 compares the appearance of fresh fuel rods, fuel rods with preirradiated cladding and fresh fuel, and high-burnup fuel rods at the failure threshold.

An important factor in the analysis of fuel-rod failure as the result of ballooning is the cladding hoop strain. The study of this strain can be based on the comparison of the scale of the circumferential deformation for two fuel-rod groups: (1) high-burnup fuel

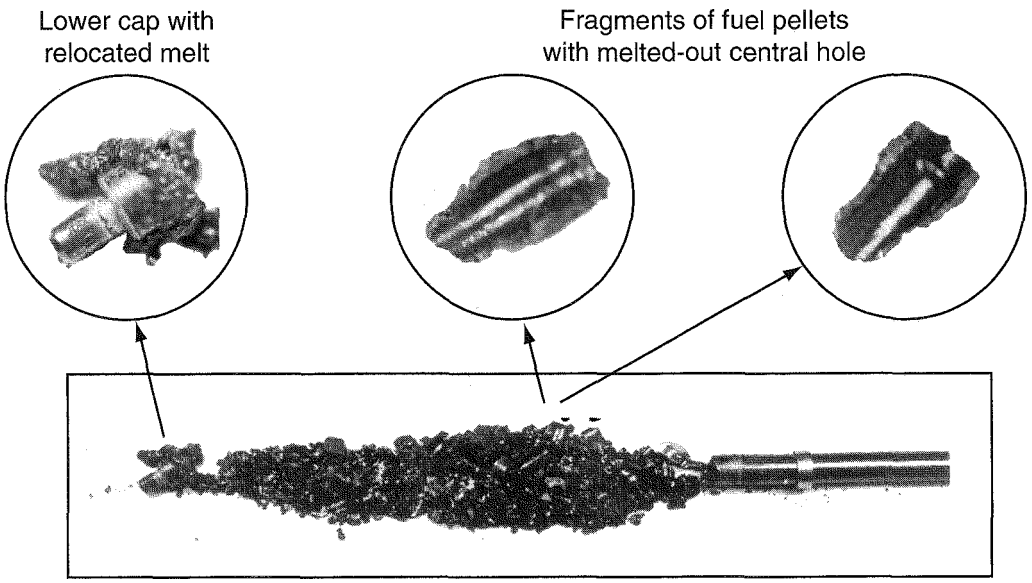

Fig. 18 Failure mechanism for fuel rod without initial pressure drop on the cladding.

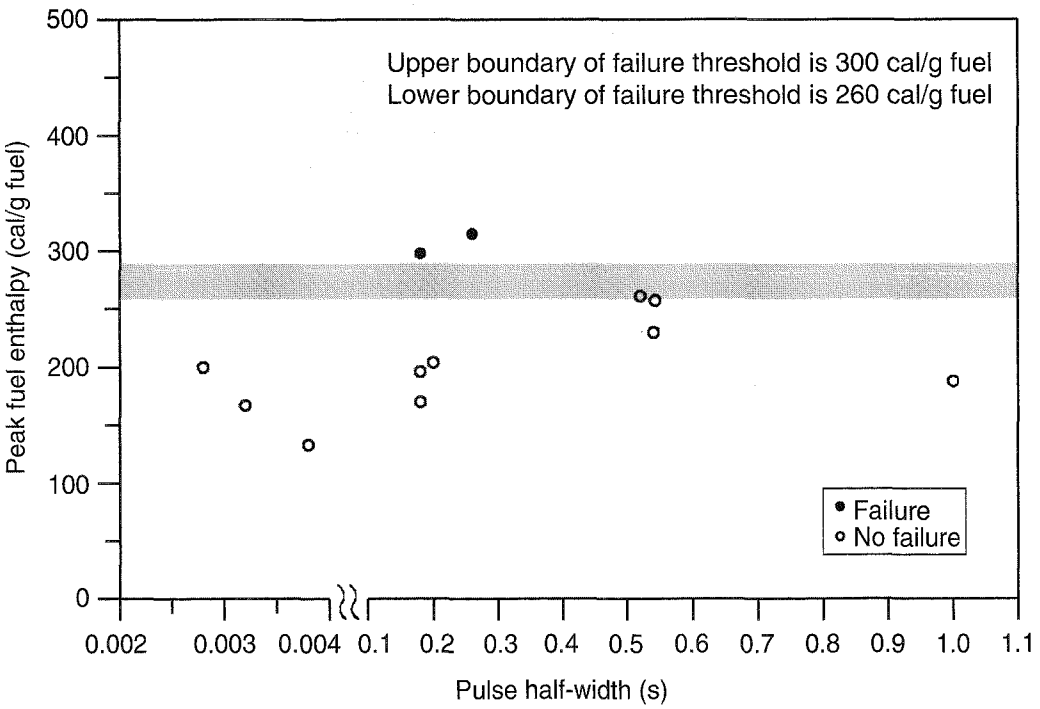

Fig. 19 Test data base to determine failure threshold for fuel rods without initial pressure drop on the cladding.

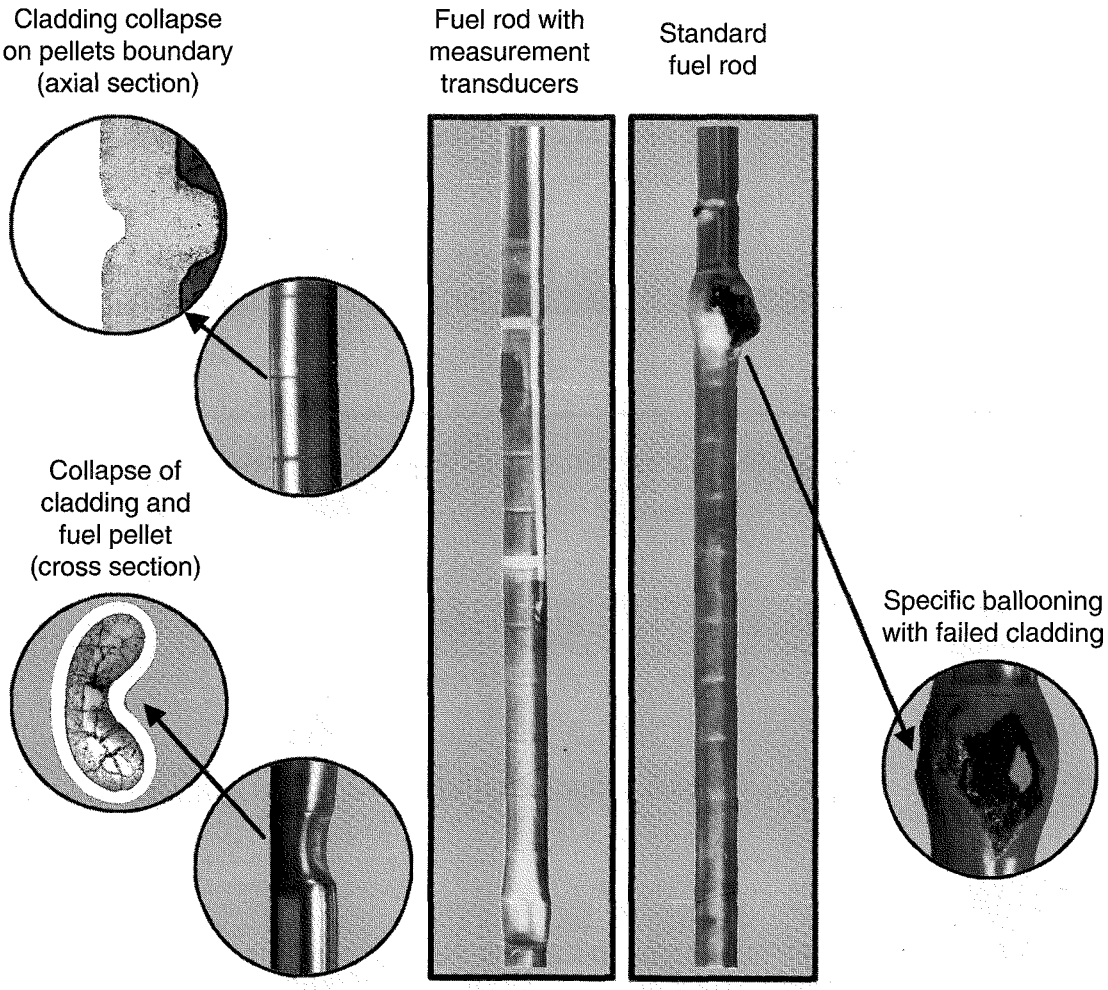

Fig. 20 Failure mechanisms for fuel rods tested at high coolant pressure.

rods compared with fresh fuel rods and (2) fuel rods with preirradiated cladding and fresh fuel compared with fresh fuel rods.

The comparison of results in the first fuel-rod group allows us to identify the effect of differences in mechanical properties of nonirradiated and preirradiated claddings. The measurements demonstrate that the circumferential deformation of the nonirradiated cladding is 25% higher than that of the preirradiated cladding. This result is illustrated in Fig. 24.

The comparison of results of similar measurements for the second group of fuel rods revealed a certain paradox. In spite of a number of differences in material properties and in the initial fuel-rod geometry, the maximum circumferential cladding deformation of these fuel rods was about 13%. The studies to explain these results are far from complete; even so it is appropriate to note one phenomenon observed during high-burnup fuel-rod tests.

Figure 25 is a photograph of the active part of a failed high-burnup fuel rod. The fuel rod has two balloonings that ruptured instead of one. This effect was detected in two out of three high-burnup fuel rods that failed near the failure threshold. The presence of two cladding ruptures indicates that the cladding deformation in each ballooning was probably caused by the gas that accumulated in two volumes isolated from each other. This effect was not observed in any of the tens of tests of fresh fuel rods. As for effects observed in fuel rods tested above the failure threshold, it is important to note that, first, the temperature of fuel melting was reached in one of the fuel rods. This

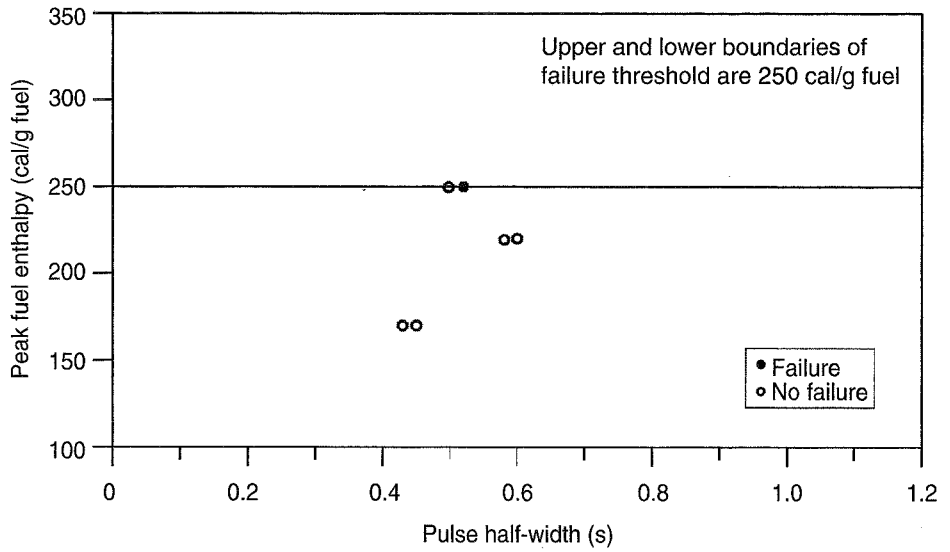

Fig. 21 Test data base to determine failure threshold for fuel rods tested at high coolant pressure.

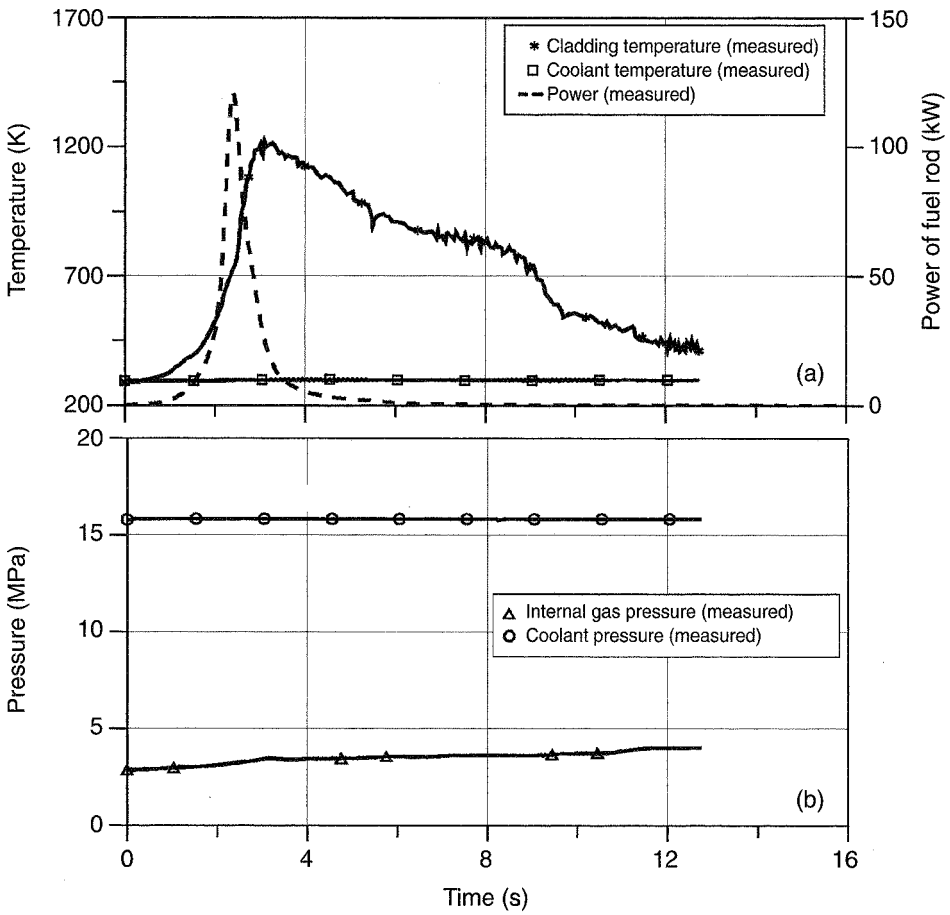

Fig. 22 Test parameters to characterize fuel-rod behavior at high coolant pressure.

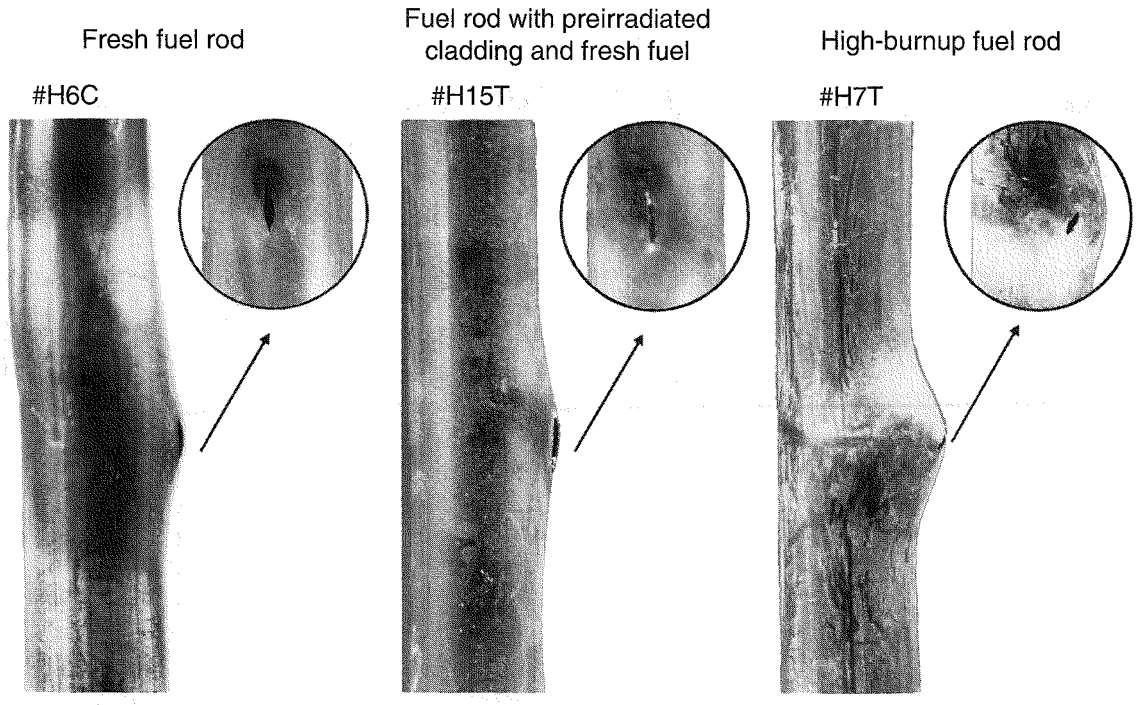

Fig. 23 Failed fuel rods of different types.

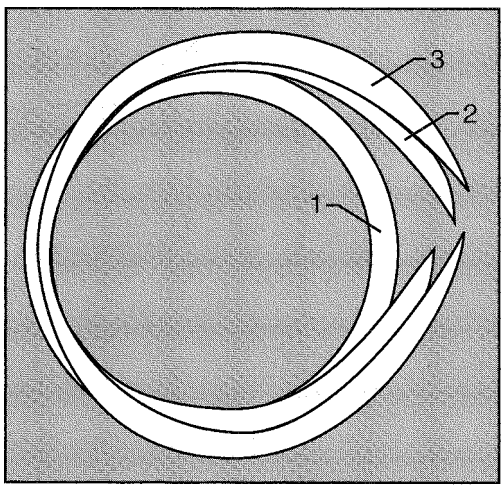

1. Cladding without radial hoop strain
2. Preirradiated cladding
3. Fresh cladding

Fig. 24 Test data base to determine failure threshold for high-burnup fuel rods.

induced a partial melting through of the fuel-rod cladding and in significant oxidation of its surface up to 105 μm. Nevertheless, there was no fragmentation of the cladding. The second effect is related to an atypical form of cladding rupture in the ballooning zone (see Fig. 26). The dimensions of these ruptures are much larger than those of typical ones (see Fig. 23). Moreover, they have a longitudinal orientation. The initial visual examination could lead to an assumption that these ruptures were formed in the cooling phase as a result of the oxidized cladding cracking; however, the results of the posttest examinations in Fig. 26 show that these ruptures were probably caused by the plastic deformation of the cladding. A brittle crack was detected at the area boundary; however, as shown in the photographs, this crack did not develop beyond the ballooning area. A key problem in characterizing the behavior of high-burnup fuel rods under RIA tests is determining their failure thresholds (i.e., a corresponding peak fuel enthalpy). The results that characterize threshold failures of VVER fuel rods have already been obtained.[4,5] The analysis of these results shows that the lower value of peak fuel enthalpy characterizing the failure threshold of VVER high-burnup fuel rods practically coincides with the lower boundary of the failure threshold of VVER fresh fuel rods and is equal to 160 cal/g fuel. The uncertainty analysis for the set of energy deposition values and expert judgment of

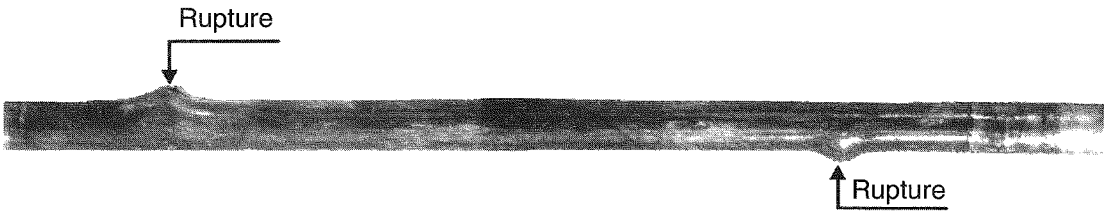

Fig. 25 Photograph of high-burnup fuel rod after IGR test.

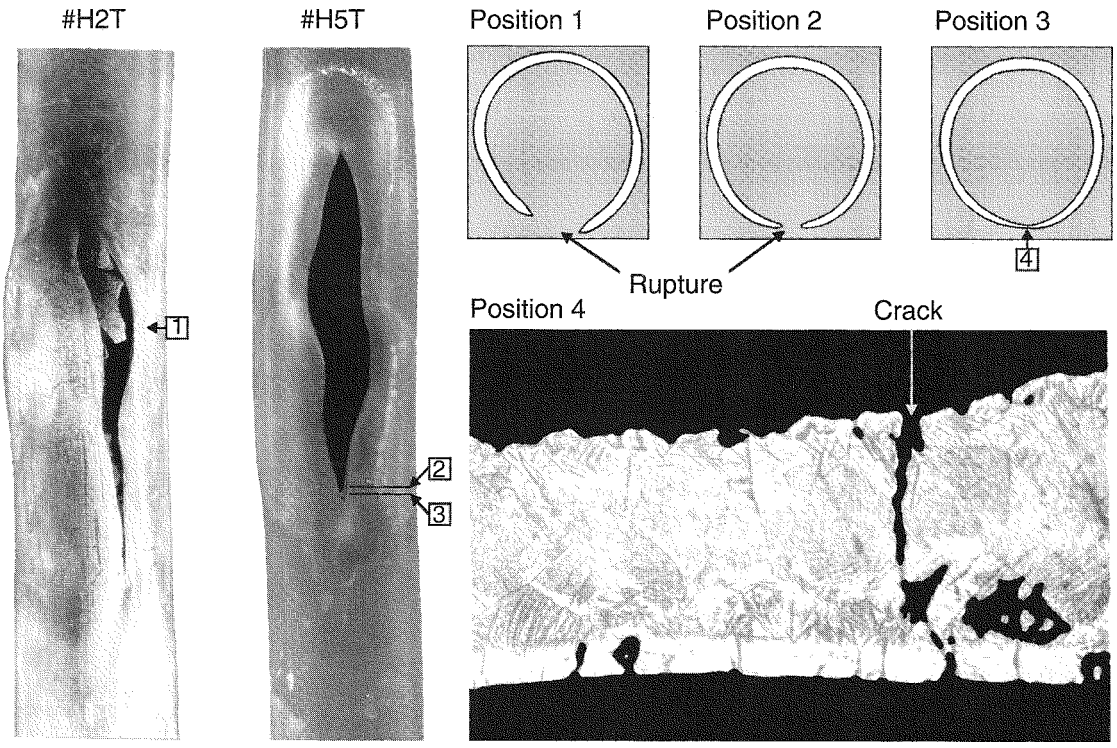

Fig. 26 Specific ruptures in high-burnup fuel rods.

the uncertainty level in determining peak fuel enthalpy lead us to believe that, in its final form, the failure threshold value for these types of fuel rods can be adjusted by not more than ±15 cal/g fuel.

Input data to determine the failure threshold of high-burnup fuel rods are shown in Fig. 27. Test results show that the low peak fuel enthalpy value for failed fuel rods and the high value for nonfailed fuel rods coincide and are about 160 cal/g fuel. Thus the failure threshold and the failure mechanism for VVER fuel rods are not a function of the burnup. (This was obvious because the operating cycle does not lead to significant oxidation and hydriding of the cladding. This, in turn, allows the cladding to preserve its highly plastic properties.)

CONCLUSIONS

Various types of tests were conducted to study the behavior of fresh and high-burnup VVER fuel rods under RIA conditions.

According to the test results for highly pressurized fuel rods, ballooning is the cladding failure mechanism (with no difference between fresh and

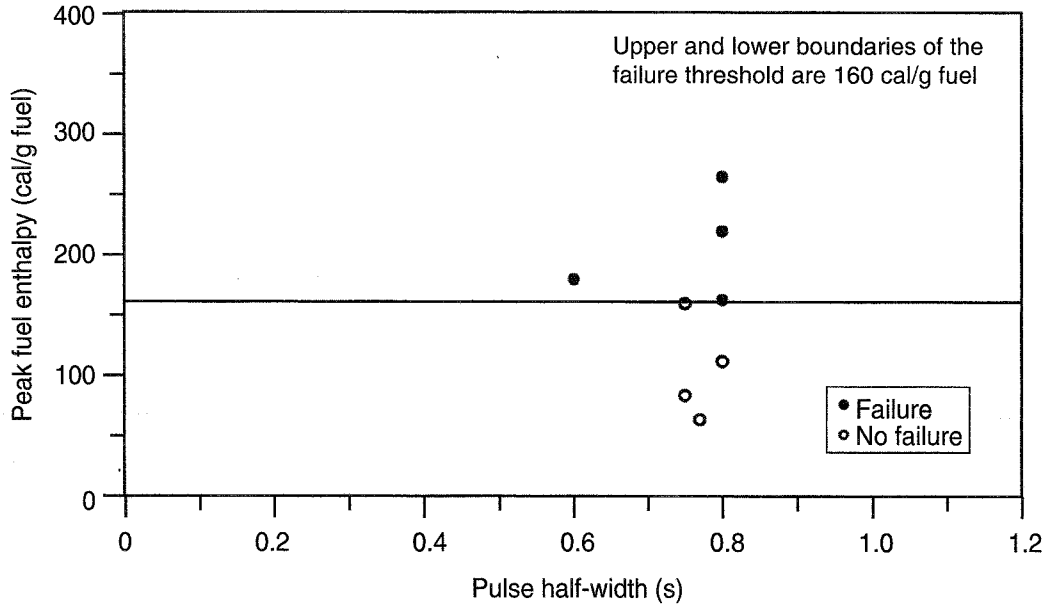

Fig. 27 Test data base to determine the failure threshold for high-burnup fuel rods.

high-burnup fuel types). This type of fuel rod demonstrated the lowest failure threshold under RIA conditions. Peak fuel enthalpies that correspond to the lower failure boundary for fresh and high-burnup fuel rods are practically the same and are equal to 160 cal/g fuel. These tests did not reveal any effect of burnup up to 50 MWd/kgU.

The behavior of fresh fuel rods without an initial pressure drop across the cladding is characterized by cladding melting and possible fragmentation in the cooling phase of the tests. No fuel–cladding fragmentation was observed in any test with a peak fuel enthalpy below 260 cal/g fuel.

Tests of fresh fuel rods at high coolant pressures show that one of the failure mechanisms is cladding collapse and failure in the area of maximum hoop strain. Another failure mechanism is a type of local ballooning accompanied by cladding melt-through. The observed failure threshold for these failures was around 250 cal/g; however, the formation of closed cracks in the area of maximum hoop strain was found at conditions as low as 170 cal/g.

All of the tests with fresh fuel were conducted with a wide range of pulse widths (2 ms to 1 s). No effect of pulse width was seen.

Although high-burnup fuel rods were tested only with broad pulse widths and high pressurization, its behavior under different conditions is expected to be the same as fresh fuel because Zr–1%Nb retains a large amount of ductility at high burnup.

Further studies to analyze the results of these tests should be focused mainly on the following:

- Development of a data base characterizing the properties of original VVER materials.
- Careful computer simulation of the behavior of different types of fuel rods under RIA conditions, including a special effort to verify codes and to improve certain models.
- Confirmation of the ability of VVER high-burnup fuel to survive PCMI conditions with narrow pulse widths.
- Organization and assessment of the entire test data base and development, with the use of that data base, of the phenomenology of fuel-rod behavior under RIA conditions and with dependence on key parameters.

ACKNOWLEDGMENTS

The authors would like to emphasize that specialists such as Prof. V. Sidorenko, Dr. V. Pavshook, Dr. G. Lunin (RRC KI), and Dr. Yu. Bibilashvili (ARSRIIM, Moscow) began the work that is presented in this article.

Important contributions to successful testing at the GIDRA and IGR reactors were made by Dr. Khvostinov, Dr. V. Pavshook (RRC KI, Moscow), V. Pahnits, and A. Vurim (IAE NNC, Kazakstan).

The procedure for posttest examinations of tested fuel rods was developed in cooperation with the specialists of RIAR (Dimitrovgrad, Russia). For this we would like to thank Dr. V. Smirnov and Dr. A. Goryachev, who also developed and implemented the procedure for refabrication of VVER commercial fuel elements.

Design and development of transducers for measuring fuel-rod parameters, as well as equipping fuel rods with these detectors, were performed by SIA Lutch (Podolsk, Russia) under the leadership of Dr. V. Nalivaev.

Development of calculation and experimental procedures to obtain the data base characterizing fuel behavior under testing conditions at IGR and GIDRA was carried out in close cooperation with several groups of specialists. This work was led by A. Bortash, Dr. V. Malofeyev, and Dr. L. Mayorov (RRC KI).

Implementation of the FRAP-T6 code for test conditions was done by A. Shestopalov and K. Lyutov (RRC KI).

Analysis and integration of experimental data files was accomplished by the efforts of many specialists. The authors wish to extend their gratitude to G. Abyshov, E. Kaplar, N. Jouravkova, A. Konobeyev, A. Bortash, V. Polivanov, A. Zvyagin, A. Avvackumov, and V. Malofeyev (RRC KI); A. Goryachev (RIAR, Dimitrovgrad); and V. Pahnits, S. Koltyshev, A. Vurim, and Yu. Istomin (IAE NNC, Semipalatinsk, Kazakstan).

The authors would also like to acknowledge Dr. F. Schmitz (IPSN, France), Dr. R. Meyer (NRC, USA), and Dr. Mackardel (INEL, USA) for invaluable advice, comments, and attention to this work.

Special gratitude should be expressed to those who provided financial support for these investigations: N. Ermakov (Minatom, Russia), E. Chuckardin (Ministry of Science and New Technologies, Russia), Dr. A. Panyuschkin and Dr. V. Tsybulia (AO Mashinostroitelny Zavod, Electrostal, Russia), Dr. O. Koskivirta (IVO, Finland), Dr. S. Speis and Dr. T. King (NRC, USA), and Dr. M. Livolant and Dr. M. Gomolinsky (IPSN, France).

REFERENCES

1. A. Smirnov, V. Talyzin, and V. Hvostinov, *Water-Solution Enriched Reactor for Activation Analysis*, Preprint of IAE Kurchatov Institute No. 1962, 1968.
2. L. Yegorova et al., *Analysis of Capsule Dynamic Tests with VVER-1000 Fuel Rods at IGR and GIDRA Reactors*, Report 30/694186, IAE Kurchatov Institute, 1986.
3. L. J. Siefken, Ch. Allison, M. Bohn, and S. Peck, *FRAP-T6: A Computer Code for the Transient Analysis of Oxide Fuel Rods*, Report NUREG/CR-2148 (EGG-2104), May 1981.
4. V. Asmolov and L. Yegorova, Recent View to the Results of Pulse Tests in the IGR Reactor with High Burn-Up Fuel, in *Proceedings of the Twenty-Third Water Reactor Safety Information Meeting*, Bethesda, Maryland, October 23–25, 1995, Report NUREG/CP-0149, Vol. 1 (CONF-9510156—Vol.1), pp. 65-80.
5. V. Asmolov and L. Yegorova, Recent Results on the RIA Tests in the IGR Reactor, in *Proceedings of the Twenty-Fourth Water Reactor Safety Information Meeting*, Bethesda, Maryland, October 21–23, 1996, Report NUREG/CP-0157, January 1997.

Assessment of RIA-Simulation Experiments on Intermediate- and High-Burnup Test Rods

By R. O. Montgomery,[a] Y. R. Rashid,[a] O. Ozer,[b] and R. L. Yang[b]

Abstract: *A critical assessment has been conducted of reactivity-initiated accident (RIA) simulation experiments with the use of preirradiated test rods. Included in this assessment are the Special Power Excursion Reactor Test-Capsule Driver Core (SPERT-CDC), the Nuclear Safety Research Reactor (NSRR), and the CABRI REP sodium (Na) experimental programs. Information was collected describing the base irradiation, test rod characterization, and test procedures and conditions. The representativeness of the test rods and test conditions with respect to anticipated light-water-reactor (LWR) RIA conditions is evaluated with the use of analysis results from detailed transient fuel behavior simulations. This assessment shows that the pulse characteristics and coolant conditions of the experiments are significantly different from those anticipated in LWR RIA conditions. Furthermore, the unrepresentative test conditions are found to exaggerate the mechanisms that caused cladding failure in the experiments.*

The licensing limits for a reactivity-initiated accident (RIA), as stated in NUREG-0800, were established with the use of RIA-simulation experiments with test rods that had either zero or very low burnup.[1] The test rod failure modes observed in these experiments were either clad melting or brittle fracture induced by quenching after reaching near-melting temperatures during departure from nucleate boiling conditions. Therefore the current licensing limit, intrinsically implying cladding failure, is primarily a thermal limit (i.e., high cladding temperatures). During irradiation, however, important material and behavioral changes occur that can affect the response of the fuel and cladding during an RIA event. These changes can impact pellet–cladding mechanical interaction (PCMI) and, under certain situations, activate mechanisms that can result in cladding failure. Such behavior has been observed recently in RIA-simulation experiments conducted on test rods that had been preirradiated to intermediate and high burnup. A small subset of these experiments resulted in cladding failure by PCMI-controlled processes at fuel enthalpy levels well below the current licensing limit.[2,3] Concerns about low-enthalpy failures have prompted regulatory agencies to reassess current licensing criteria and suspend consideration of all burnup extension applications.[4]

In response to this issue, the Electric Power Research Institute (EPRI) initiated a program to evaluate fuel-rod behavior during an RIA event with emphasis on intermediate- and high-burnup RIA-simulation tests.[5] The focus of the EPRI program was to understand the mechanisms that produced the observed test rod behavior. This understanding was then used to assess whether the RIA-simulation test results are representative of in-reactor conditions or if the results require further interpretation before being used to judge light-water-reactor (LWR) fuel behavior. This article summarizes the findings of the EPRI evaluation of the RIA-simulation experimental results.

RIA SIMULATION DATA BASE ON IRRADIATED TEST RODS

Four major programs have been conducted with the use of instrumented test rods to evaluate the behavior of irradiated fuel rods during a rapid power pulse simulating an RIA in an LWR. The RIA-simulation tests that are included in the present review are the Special Power Excursion Reactor Test (SPERT)-Capsule Driver Core (CDC) series,[6] the Nuclear Safety Research Reactor (NSRR) test series,[3] and, most recently, the CABRI REP sodium (Na) series.[2] The Power Burst Facility (PBF) RIA series was previously reviewed by McCardell.[7]

Over 50 RIA-simulation tests have been performed on test rods irradiated to burnups greater than 3 MWd/kgU as part of the PBF-RIA, SPERT-CDC, NSRR, and CABRI experimental programs. Figure 1 shows the maximum change in radially

[a]ANATECH Corp., 5435 Oberlin Drive, San Diego, California 92121.

[b]Electric Power Research Institute, P. O. Box 10412, Palo Alto, California 94303.

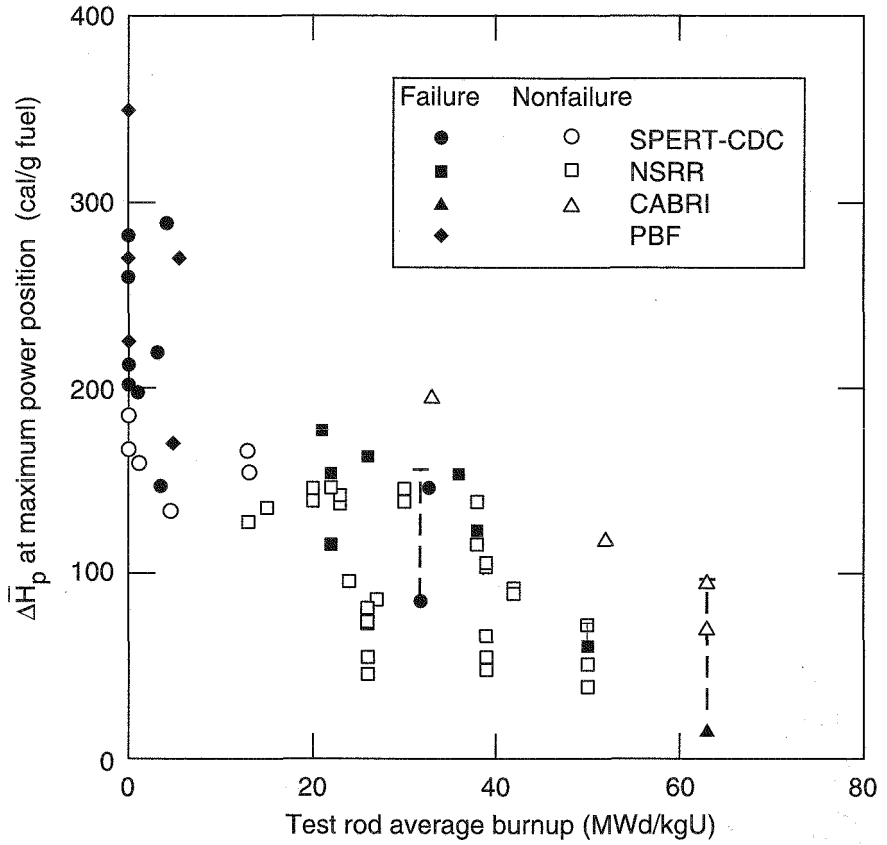

Fig. 1 Data base of RIA-simulation tests performed on LWR-type fuel rods. ($\Delta\overline{H}_p$ is the maximum change in radially averaged fuel enthalpy for each test rod; the vertical dashed lines represent the continuation of the tests after failure.)

averaged fuel enthalpy ($\Delta\overline{H}_p$) for each test rod as a function of test rod average burnup. The open symbols indicate a successful test, and the solid symbols indicate rod failure. Figure 1 includes test results from both nonirradiated (zero burnup) and preirradiated test rods. Because $\Delta\overline{H}_p$ governs the fuel-rod PCMI response, this quantity was chosen as the key attribute to compare the RIA-simulation tests.

As can be seen, a majority of preirradiated test rods survived with minimal consequences after experiencing maximum fuel enthalpy changes that ranged from 40 to 200 cal/g fuel. A total of 12 test rods failed during or at the completion of power pulses that produced maximum fuel enthalpy changes in excess of 120 cal/g fuel. Nine of these rods exhibited small cladding cracks at multiple locations. Three tests, SPERT-CDC 859, NSRR HBO-1, and CABRI REP-Na1, failed before reaching the end of the power pulse at fuel enthalpy changes below 85 cal/g fuel. The power pulses used for these three tests continued beyond failure, as indicated by the dashed lines in Fig. 1. A general trend observed in Fig. 1 is that the maximum change in fuel enthalpy during the test tends to decrease with average burnup. It is important to point out that this decreasing trend does not indicate a decrease in test rod integrity but rather indicates the decrease in test rod reactivity with burnup.

A failure threshold exists between the failed and surviving unirradiated test rods; however, a similar separation is not observed when the peak radially averaged fuel enthalpy is correlated with burnup for the preirradiated test rods. The correlation shows that the failures are interspersed among the surviving test rods. The existing RIA-simulation data base can only be used to construct a failure threshold from the failed preirradiated test rods if the failures are statistically representative of the surviving test rods. An analogy can be drawn from boiling-water-reactor (BWR) PCMI failure statistics where the PCMI failure threshold for BWR cladding is defined in terms of power level

vs. burnup.[8] In the BWR case, test rods were ramp-tested to various power levels to produce cladding failure. The power level achieved in the ramp was correlated with burnup, and a separation was observed between the failed and surviving test rods. Because of the representative test conditions and test rods used in the BWR PCMI irradiation program, the failures are a statistical representation of the fuel-rod behavior exhibited by all the test rods and therefore were used to define a PCMI failure threshold for BWR fuel rods. In contrast, the absence of similar separation in the RIA-simulation tests raises questions about the preirradiated test rod failures. These failures do not appear to represent the expected behavior of the surviving test rod population. Because of this, the circumstances regarding the test conditions and the test rod characteristics were reviewed to evaluate the representative nature of each test.

As already discussed, failure by thermal processes for unirradiated test rods can lead to a well-defined failure threshold, whereas such a threshold is not as clearly defined in the preirradiated test rods as the behavior transitions from thermal processes to those driven by PCMI. Several mechanisms have been postulated as the cause of the apparent burnup dependence of the observed low-enthalpy failures. Some authors have attributed the cause to the uncontrolled expansion of fission gases residing in the outer periphery of the fuel pellet.[2] This hypothesis is not borne out by the data, however, as this article will show. It is well known that irradiation affects the cladding mechanical properties and consequently could impact the cladding behavior during an RIA simulation test. Similarly, the buildup of hydrogen in the cladding from waterside corrosion as burnup increases can potentially impact the mechanical response. The influence of hydrogen on cladding ductility depends on the hydrogen concentration, the hydride morphology (hydride concentration and orientation), and cladding temperature, and the effects can vary over a wide range. Therefore a thorough understanding of both the irradiation and hydrogen effects is essential to properly interpret the fuel-rod behavior in the RIA tests. This review focused on quantifying these different effects for each failed test rod to evaluate the role of hydrogen.

Summary of Data Base Review

A majority of the preirradiated test rods shown in Fig. 1 were reviewed in the EPRI program.[5] The review focused on collecting sufficient information to enable the accurate modeling of test rods selected from each of the different experimental programs and to aid in the interpretation of the observed experimental results.

The review found that none of the test facilities simulated conditions resembling an LWR environment during a hypothetical RIA event. The SPERT-CDC and NSRR tests used stagnant water at atmospheric conditions [1.0×10^5 Pa (1 bar), 20 °C] as coolant, and the CABRI tests were performed in 3.0×10^5 Pa (3 bar) flowing sodium at 280 °C. In a majority of the tests, the pulse widths were less than 10 ms. The coolant conditions and the pulse width affect both the energy transfer from the test rod and the cladding temperature during the test. The influence of these test parameters should be evaluated before results derived from such tests are applied to LWR fuel behavior. The impact of these nonstandard test conditions was assessed as part of the EPRI program.

Most test rods used were of typical BWR or pressurized-water-reactor (PWR) geometry and enrichments but were less than 1 m in length. In some cases, refabrication was used to extract the test rod segments from full-length fuel rods, and in other cases, such as in the JM-NSRR and SPERT-CDC experiments, test rods were specifically designed and manufactured for the tests. Background information describing the fuel and cladding material characteristics, fabrication process, and base irradiation was reviewed to assess the representative nature of each test. In the case of the JM-NSRR test rods, impurities introduced during manufacturing produced incipient cladding defects during the base irradiation that are inconsistent with nominal LWR fuel. Similarly, the SPERT-CDC test rods were manufactured with the use of cladding material that is uncharacteristic of modern BWR cladding. The performance of these test rods during the base irradiation was also contrary to nominal BWR fuel rods. The most representative test rods used were those refabricated from commercial PWR fuel rods. Even in these cases, however, incipient defects may have been introduced during the refabrication process which could have influenced the test results. All these factors must be considered when reviewing the RIA simulation data base.

References 1 and 7 contain a detailed review of the SPERT-CDC tests, reference 9 contains the NSRR program results, and reference 2 contains the CABRI REP-Na test results.

FUEL BEHAVIOR ANALYSIS

The fuel behavior analysis of the RIA-simulation tests consists of three parts: (1) best-estimate analysis of the test rod behavior using the FREY-01 computer code, (2) sensitivity analyses to evaluate the effects of pulse width and coolant conditions, and (3) detailed pellet rim thermomechanical analysis using a local effects model.

Test Rod Analysis With the Use of FREY-01

A total of 12 test rods were selected for detailed fuel behavior analysis to evaluate the possible circumstances that resulted in test rod failure. The selected cases included the three low-enthalpy failures, CABRI REP-Na1, NSRR HBO-1, and SPERT-CDC 859, as well as companion rods from each of the individual test series. A list of the test rods analyzed is shown in Table 1. The analysis of the surviving companion rods served as a validation of the analytical approach.

The FREY-01 fuel behavior analysis focused on the evolution of the test rod response during and following the power pulse. Analysis of this type requires proper initialization of the pretest rod conditions and an analytical capability that can appropriately model the integral transient thermal and mechanical behavior of the test rod during the experiment. Also, for the evaluation of the integrity of a test rod during an RIA-simulation experiment, a mechanistic cladding integrity limit is required that considers the effects of the initial cladding state as well as the test conditions.

Analysis Approach and Cladding Integrity Model. FREY-01 is a finite-element-based best-estimate analysis program designed to compute the transient thermal and mechanical behavior of an LWR fuel rod during both normal and off-normal events.[10] Because PCMI is more dominant for high-burnup fuel behavior, an important capability provided by FREY-01 was the robust pellet–cladding thermal and mechanical interaction modeling during rapid transient events. This capability allows for the proper synergism between the pellet expansion, which produces cladding stresses and pellet–cladding heat conduction, which results in higher cladding temperatures and ultimately affects cladding mechanical properties. Test rod initial conditions after base irradiation were obtained for several test rods with the use of the ESCORE steady-state fuel performance program.[11]

A two-dimensional (r-z) geometric model was constructed that included the entire fuel column and cladding, the upper and lower plena, and the end caps. The model consisted of eight-node quadrilateral elements for the fuel and cladding and two-node line elements for the fuel–cladding gap and plenum regions. In the radial direction, an expanding mesh was used with fine detail in the 1-mm rim region near the pellet periphery and a coarse mesh was used in the remainder of the fuel pellet. The cladding contained two elements

Table 1 Selected RIA Simulation Test Rods for Analysis

Test	Test rod	Test rod average burnup, MWd/kgU	Peak radially averaged fuel enthalpy, cal/g fuel	Maximum change in fuel enthalpy at failure, cal/g fuel
CABRI	REP-Na1	63.8	100	15[a]
	REP-Na2	33.0	196	
	REP-Na3	52.8	118	
	REP-Na4	62.3	~70	
	REP-Na5	62.3	100	
NSRR	HBO-1	50.4	73	60
	HBO-2	50.4	37	
	HBO-3	50.4	74	
	HBO-4	50.4	50	
	JM-3	19.6	132	
	JM-4	21.6	177	177
SPERT-CDC	859	32.0	158	85

[a]The 15-cal/g fuel enthalpy increase at peak power locations corresponds to 30-cal/g fuel pellet averaged enthalpy (i.e., very early when the cladding was only slightly above 280 °C).

through the thickness to account for the nonlinear temperature profile during the beginning of the power pulse. The axial nodalization ranged between 10 and 14 elements and depended on the length of the test rod. Because of the quadratic interpolation functions used for the temperature and displacement profiles across an element, the level of discretization accuracy is quite high.

Modifications were incorporated into FREY-01 to address high-burnup specific fuel behavior, including the TUBRNP model for the fuel–pellet radial power distribution[12] and the effect of local burnup and porosity on the pellet thermal conductivity.[13–15]

A cladding integrity model for application to high-burnup RIA transients was developed with the use of data from mechanical property tests on irradiated cladding samples. The integrity model is based on a strain energy density (SED) approach and is applicable during the power pulse of an RIA event when PCMI forces dominate.[16] The data base of mechanical properties included irradiated cladding samples with fluences between 1×10^{25} and 12×10^{25} neutrons/m^2 (E > 1 MeV) and hydrogen contents between 100 and 760 ppm. These samples were obtained from fuel rods irradiated in commercial PWRs to burnups of 63 MWd/kgU. At the higher corrosion locations, these rods had considerable oxide spallation and nonuniform hydride distributions.[17]

The SED at material failure of a uniaxial tension test (U_f) is given by the area under the stress–strain curve and can be calculated by

$$U_f(T, \varphi t, \mathrm{H}) = \int_0^{\varepsilon_t(T,\varphi t,\mathrm{H})} \sigma d\varepsilon \qquad (1)$$

where σ and ε are the measured stress and strain responses, respectively, and ε_t is the strain at failure. U_f represents the critical SED and can be a function of temperature (T), fast fluence (φt), and hydrogen content (H). Analysis of the mechanical properties data base with the use of Eq. 1 resulted in specific relationships for U_f with hydrogen content and fast fluence. Because of limitations in the data base, a single expression combining the effects of temperature, fast fluence, and hydrogen content could not be developed for the critical SED. Even though an explicit temperature dependence was not developed, U_f would be expected to increase with increasing temperature.

The following provides the critical SED as a function of either fast fluence for low hydrogen content (H < 300 ppm) or as a function of high hydrogen content (H > 300 ppm):

$$U_f^1(\mathrm{H}) = 83.013\ e^{-2.6615\times10^{-3}\mathrm{H}} \quad (\text{for H} > 300\ \text{ppm}) \qquad (2)$$

and

$$U_f^2(\mathrm{H}) = 100.28\ e^{-1.114\times10^{-26}\varphi t} \quad (\text{for H} > 300\ \text{ppm}) \qquad (3)$$

These relationships are applicable at hot reactor coolant temperature conditions.

In FREY-01, the cladding SED response is given by

$$U(t) = \int_0^t \sigma_{ij}(t) \times \dot{\varepsilon}_{ij}(t)\, dt \qquad (4)$$

Equation 4 is calculated throughout the cladding as a function of time during the transient event. The calculated response is then compared with the critical SED, and failure is assumed possible when $U(t) \geq U_f$.

Test Rod Response During RIA-Simulation Tests. The fuel behavior analysis calculated the thermal and mechanical response during and following the power pulse. The parameters of interest included the pellet and cladding temperature history and distribution, the cladding stress and strain responses, and the pellet–cladding thermomechanical interaction processes. An important evaluation parameter was the residual cladding hoop strain or deformation, which could be compared with measured values from posttest examinations.

The analysis indicates that the narrow pulses used in RIA-simulation tests produce almost complete adiabatic heating of the fuel pellet during the power deposition. As a consequence, the temperature profile across the pellet radius is proportional to the radial power density, with the peak fuel temperatures occurring near the pellet periphery. The magnitude of the temperature peaking is governed by the radial power distribution and the power deposition rate. For high-burnup fuel, the maximum pellet periphery temperature was found to be as high as 1.6 times the fuel centerline temperature. An example of the pellet radial temperature profile for three time points during the power pulse is shown in Fig. 2 for CABRI REP-Na1. The temperature peaking in the pellet periphery is clearly evident with a maximum near 2500 K (4040 °F) at 87 ms. A characteristic parabolic temperature distribution is established about 2 s after the power pulse

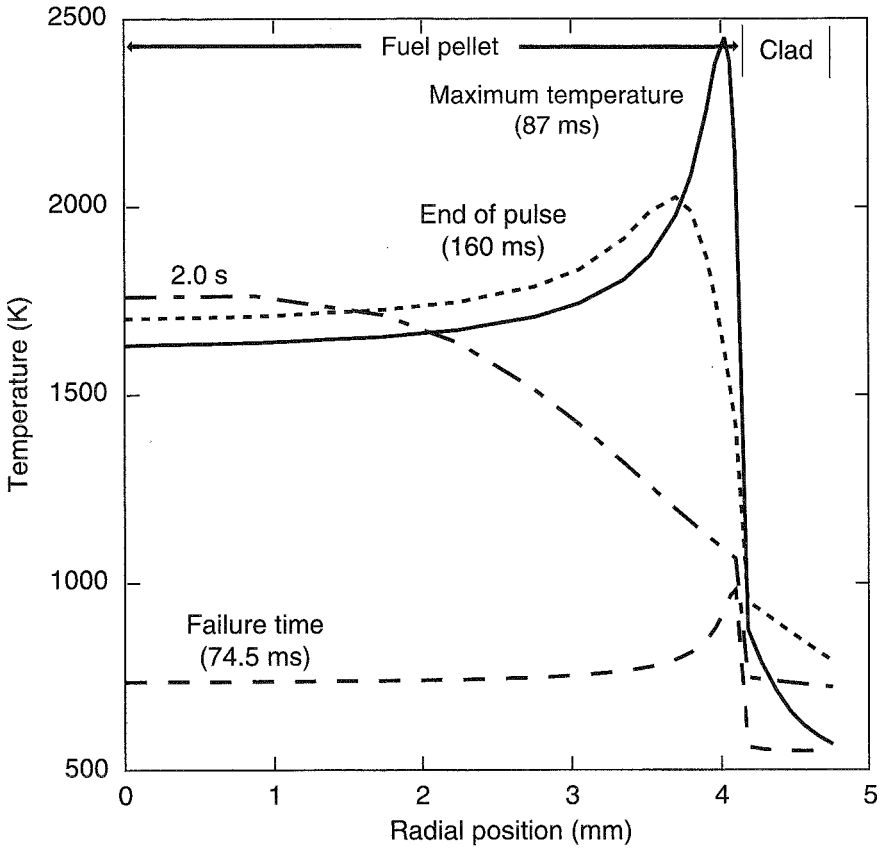

Fig. 2 Calculated radial temperature profile during the CABRI REP-Na1 transient.

once heat flow to the cladding and coolant begins to dominate.

A delay in clad heating is observed for the narrow-pulse RIA simulation tests because of the nearly adiabatic fuel-pellet heatup. For an illustration of the clad thermal response, the calculated cladding temperature profiles during the NSRR HBO-1 transient are shown in Fig. 3. At the time of failure, which corresponds to approximately 80% of the power pulse, very little heating of the cladding outer region has occurred, and, as a consequence, the temperature is still near the initial coolant temperature (~303 K). At this time in the power pulse, however, the cladding stresses produced by PCMI have reached a maximum. The lower temperature in the outer cladding region affects the local cladding ductility. The temperature effect on ductility is stronger in HBO-1 because of the presence of a hydride rim near the outer surface. The combination of the low cladding temperature and the local hydride concentration limits the amount of local ductility and thus causes the outer region to crack at or near the peak stress and propagate inward. These analytical results have identified a synergistic effect among the cladding temperature, the pulse width, the zirconium hydride content and distribution, and the peak stresses that can initiate brittle fracture when combined unfavorably; however, heat conduction during wider power pulses and higher initial cladding temperature would offset these effects for an in-reactor RIA event.

The analysis of the SPERT-CDC test rods indicates that the failure mechanism for the high-burnup test rods was very similar to that observed in NSRR HBO-1. The presence of a hydride blister on the outer cladding surface of test rod 859 is strong evidence that hydride accumulation and localization occurred during the base irradiation.[7] The analytical results show that the narrow power pulse and cold initial coolant temperature used in SPERT-CDC produced conditions similar to those experienced by NSRR HBO-1.

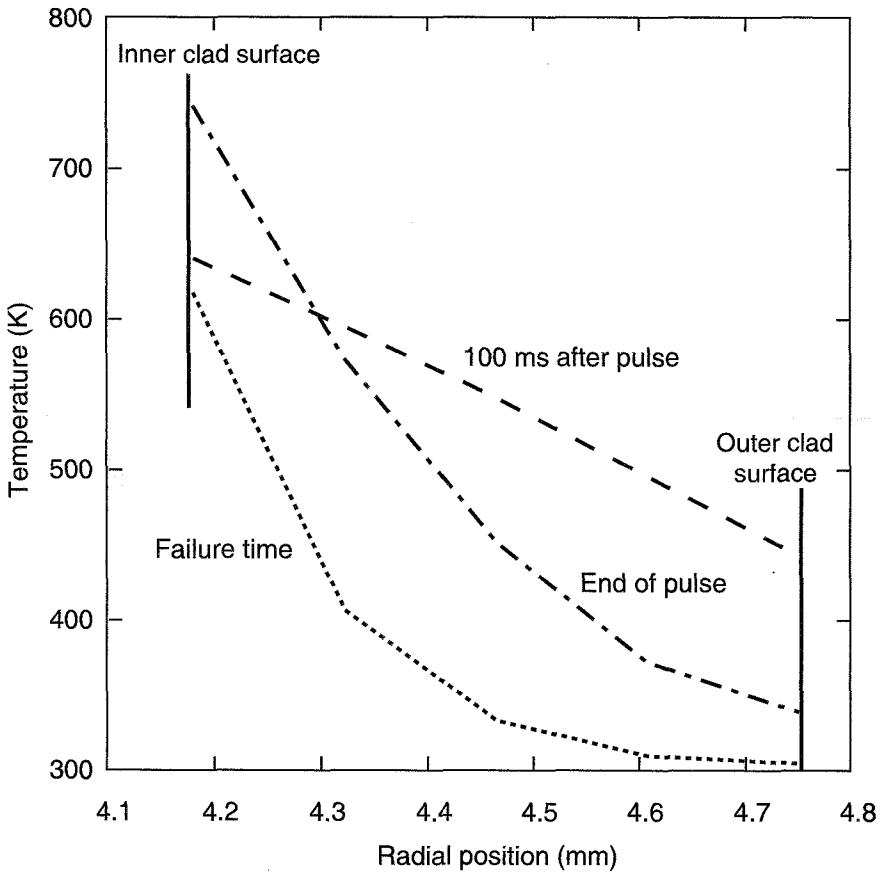

Fig. 3 Calculated cladding temperature profile during the NSRR HBO-1 transient.

Sensitivity Analyses

So that the impact of the test conditions on test rod behavior could be evaluated, sensitivity analyses were performed by modifying the coolant and power pulse conditions for NSRR HBO-1. Two sensitivity analyses were performed: (a) the coolant temperature was increased to PWR hot-zero power (HZP) standby conditions [260 °C, 15.51 mPa (500 °F, 2250 psia) and full reactor coolant pump flow] while maintaining the rapid power pulse, and (b) a pulse width of 80 ms was used with the same deposited energy at both HZP and BWR cold-zero power (CZP) coolant conditions.

The results of the sensitivity analyses are shown in Table 2. Increasing the initial coolant temperature or widening the power pulse decreases both the maximum cladding hoop stresses and the SED. On the basis of these results, the fuel–cladding mechanical interaction reaches a maximum for narrow power pulses with ambient coolant conditions. Widening the power pulse allows heat conduction to occur, which causes an increase in the outer cladding temperature. The higher cladding temperature produced by the heat conduction causes a low yield stress and an increase in the ductility. Also, higher initial temperatures during HZP conditions produce an increase in the cladding compliance and a decrease in the yield stress, which

Table 2 Sensitivity Analyses for NSRR HBO-1

	Maximum hoop stress, MPa	SED[a] at end of pulse, MJ/m^3
Test capsule (25 °C, 4.5 ms)	1174	10.6
PWR coolant (285 °C, 4.5 ms)	800	9.5
BWR cold-zero power conditions (25 °C, 80 ms)	850	9.0
PWR coolant and pulse conditions (285 °C, 80 ms)	490	6.8

[a]SED, strain energy density.

results in less duty on the cladding. The sensitivity analyses results have demonstrated that the test conditions (pulse shape and coolant conditions) for RIA-simulation experiments greatly influence the response of the test rods.

Pellet Rim Thermomechanical Analysis

A special-effects analysis was performed to evaluate the thermomechanical behavior of the fuel-pellet outer rim region during an RIA-simulation test. The analysis of fuel behavior indicates that the adiabatic heating of the fuel pellet results in pellet periphery temperatures that can exceed 2000 K, well above normal operating temperatures for this region. Because the pellet outer periphery contains a large density of fission products, of which a majority are in a gaseous state, some investigators have postulated that at high temperatures the pellet periphery can become unstable and thus produce gaseous swelling that enhances PCMI.[18] This scenario has been proposed as a possible mechanism for the low-enthalpy clad failure for CABRI REP-Na1 and NSRR HBO-1.[2,9]

Because experimental data supporting these hypotheses are unavailable, a series of special-effects calculations were performed with the use of a local effects model to assess the potential for unstable pellet rim behavior leading to enhanced PCMI. The results of these calculations provide a figure of merit regarding the potential effects of high-temperature rim behavior.

A pellet at high burnup contains a narrow rim approximately 100 to 200 μm thick near the outer periphery, which has accumulated a burnup that approaches twice the pellet average burnup and a power density that can be two to three times as great as the pellet average.[12] Recent investigators have found that the high concentration of gaseous fission products produces a region of high porosity in the pellet periphery. Also, the fuel grains undergo grain subdivision, which results in grain sizes as small as 0.5 μm. The occurrence of these pellet changes has been termed the "rim effect," and the amount of fuel impacted resides in the outer 5% of the pellet radius.[19,20]

The higher fuel temperatures during energetic power pulses can increase the gas pressure in the intergranular bubbles. If the mechanical capacity of the fuel material to restrain expansion of the bubbles has been reduced by these microstructural changes, two events could occur: (1) the bubbles could begin an uncontrolled expansion and thus cause gaseous swelling, or (2) the fuel material around the bubbles could fracture and thus liberate the high-pressure gas directly to the cladding. Both of these events enhance PCMI and could produce cladding failure; however, data on the mechanical instability of the rim region have not been developed to show degradation of the fuel tensile strength coincident with the high-burnup fuel restructuring into small grains. In fact, Spino et al.[21] have reported that, while preparing samples for ceramographic examinations, the rim material exhibited higher fracture resistance than unirradiated UO_2.

Analysis Approach. So that the high-temperature behavior of the pellet rim could be assessed, a thermal and mechanical analysis was performed with the use of the ABAQUS general-purpose structural analysis program.[22] The objective of the analysis was to evaluate the conditions that produce significant bubble expansion in the pellet rim, which was accomplished with the use of a two-dimensional (2-D) finite-element model of a segment of the outer pellet rim. The model contained an idealized matrix of bubbles representing the rim porosity. The pressure in the bubbles was increased to simulate the temperature effects during an RIA event. The parameter of interest was the amount of volumetric expansion (outer edge displacement) that was produced as a function of the bubble pressure.

A 2-D (r-θ) finite-element model representing a 20 μm × 20 μm portion of the porous rim was constructed which contained a 10 × 10 matrix of pores surrounded by 100% dense UO_2 material. Symmetry allowed the use of a 5 × 5 matrix of holes. The model is shown in Fig. 4. The holes representing the fission gas porosity were assumed to initially contain xenon gas at 60 MPa. The fission gas inventory in the pellet rim and the gas bubble density were used to estimate this initial gas pressure. Two different boundary conditions were employed at the nonsymmetric boundaries of the model: (1) unconfined (no outer edge confinement) and (2) 50-MPa confinement pressure to mechanically simulate the presence of the cladding.

A pore radius of 0.25 μm and edge-to-edge bubble spacing of 0.5 μm were used to perform the initial calculations. These dimensions produce an area porosity of 19.6% and a volume porosity of 6.54%. The pore radius was increased in the model to 0.375 μm, and by decreasing the bubble spacing to 0.25 μm, an area porosity of 44% and a volume porosity of 22% were achieved. On the basis of experimental observations, these two geometric models represent the lower and upper range of the estimated porosity in the rim region.[21] A majority of the rim porosity estimates are

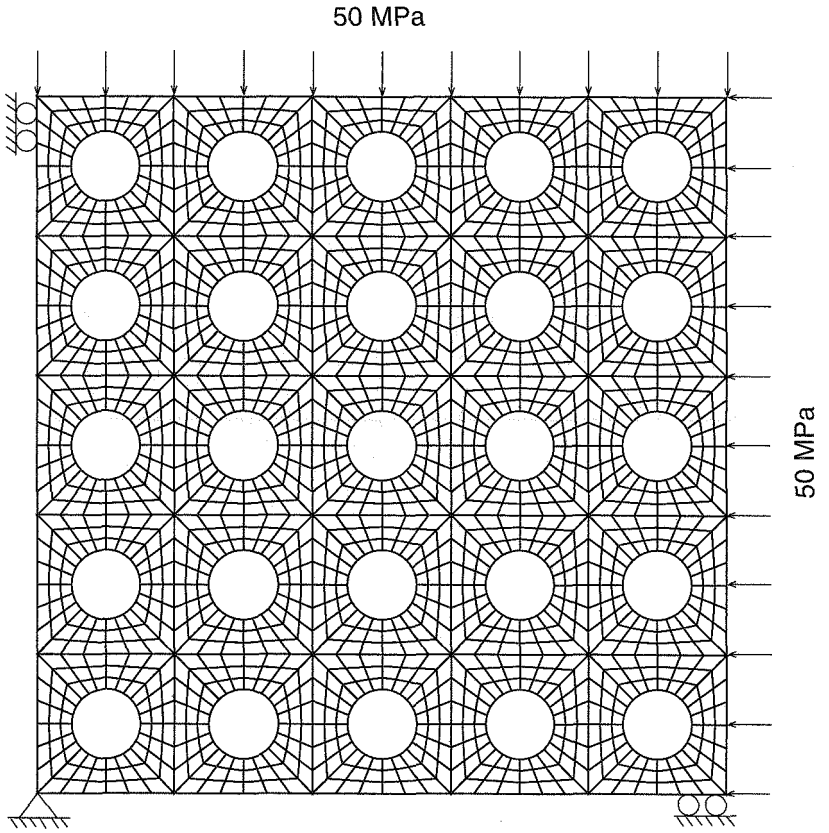

Fig. 4 Two-dimensional finite-element model of pellet rim with a 5 × 5 bubble matrix.

based on photomicrographs of the rim, and what is visibly apparent is the area porosity; the volumetric porosity must be estimated with the use of a variety of different interpolation techniques.[23]

The analysis approach described does not explicitly include the thermal expansion from the interior part of the fuel pellet. This produces a positive strain component in the pellet rim region; however, the temperature distribution during the earlier part of an RIA is peaked in the pellet periphery. Combined with the cladding confinement, the pellet thermal expansion places the pellet periphery into a state of hydrostatic compression with confinement stresses exceeding those used in the bubble expansion analysis. The following results represent a lower-bound limiting case for the amount of confinement pressure experienced by the pellet rim.

Bubble Expansion Analyses. Two different sets of analyses were performed to establish the response at the rim. First, an analysis was conducted in which the internal pressure in the bubbles was increased by a factor of 2 (simulating a twofold increase in temperature) with an unconfined outer boundary. In this calculation the fuel material yield stress was assumed to remain independent of temperature and was set to the unirradiated value. Second, a series of calculations was performed in which the yield stress of the solid fuel material was calculated with the use of the temperature-dependent relationship from FREY-01, and the pressure in each bubble was calculated as a function of temperature with the use of the ideal gas law. On the basis of the mechanical properties measurements performed by Spino et al.,[21] when unirradiated properties are used for the UO_2 yield stress, the strength of the rim region is underestimated by a factor of 2 or more. As a consequence, these calculations represent a conservative analysis of the rim mechanical stability. The second set of calculations was performed with two different boundary conditions: no outer edge confinement (unconfined) and an outer edge confinement of 50-MPa pressure to simulate the presence of the cladding (confined). A confinement pressure of 50 MPa was selected to represent embrittled cladding that

would have a low yield (or fracture) stress. This value represents a lower bound of the anticipated confinement pressure. In both sets of calculations, the displacement of the model outer edge was monitored to indicate the amount of volumetric growth produced by the expansion of the bubbles.

The results from the first set of analyses show that negligible volumetric expansion is produced by increasing the bubble pressure from 60 to 120 MPa. For tests in the CABRI facility, this pressure change represents an increase in the outer rim temperature from 280 to 830 °C. The fuel behavior analysis for CABRI REP-Na1 shows that the pellet rim temperature at the time of cladding failure was approximately 740 °C. On the basis of the pellet rim analysis, gaseous swelling from the pellet did not contribute to the cladding failure because the confinement provided by the fuel material is sufficient to withstand the internal gas pressure. The following discussion will show that these calculations overestimate the effects from the bubble pressure, even though the displacements were small, because the compressive hydrostatic stress provided by the cladding is ignored.

The second set of calculations was performed to evaluate the thermomechanical behavior of the rim at high temperature. The temperature of the fuel material was ramped linearly starting at 1000 °C and ending at 2150 °C. It was anticipated that, under high-temperature conditions, the confinement from the fuel and cladding may not be sufficient to withstand the gas pressure in the bubble porosity.

The results from the coupled thermomechanical analyses indicated that, at a certain temperature, the volume of the rim region begins to expand rapidly because of a combination of high bubble pressure and low fuel yield stress. This limit temperature represents a mechanical instability at which the rim cannot withstand the pressure in the bubbles and expands in an uncontrolled manner, thereby loading the cladding directly with the internal pressure. These results show that the instability temperature (T_{ins}) is a function of the cladding confinement pressure, the amount of porosity, and the initial bubble pressure.

Figure 5 shows T_{ins} as a function of both the confinement pressure and the amount of bubble porosity. As shown in Fig. 5, T_{ins} decreases with increasing

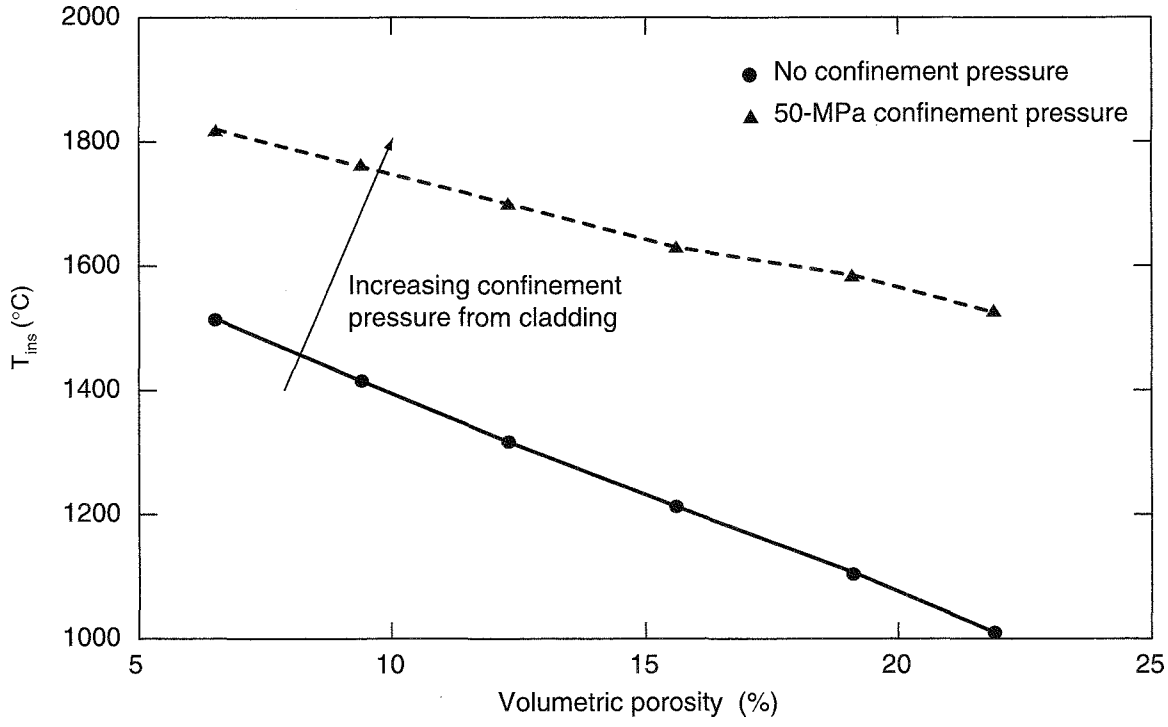

Fig. 5 Pellet rim instability temperature vs. volumetric porosity. (T_{ins} is the instability temperature at which the fuel material in the rim cannot withstand the pressure in the bubbles.)

volumetric porosity and increases with higher confinement pressure. The decrease as a function of porosity is caused by the increase in void-to-fuel material ratio (that is, less fuel material to provide confinement). The results from the unconfined case represent a condition in which the cladding provides no resistance to fuel expansion (that is, cladding failure). This would have been the situation in CABRI REP-Na1, which failed in the early part of the power pulse by other means, yet the fuel continued to be heated by the transient. In the range of 8 to 12% porosity, the calculated T_{ins} agrees closely with the maximum sodium temperature of approximately 1400 °C registered by thermocouples located in the flow channel of CABRI REP-Na1, which may have measured the passage of hot fuel and/or gas particles.

The results of these analyses demonstrate that during an RIA event the thermomechanically driven expansion of the high-burnup and high-porosity outer rim region could only occur at local temperatures above 1300 °C for unconfined fuel material and above 1700 °C for confined fuel material. Note that the mechanical confinement used in this analysis is only a fraction of that expected for high-integrity cladding. On the basis of the fuel behavior analysis, the hydrostatic stress state in the fuel produced by PCMI is considerably higher than that used in the pellet rim analysis because of the increased confinement provided by the cladding. Therefore the instability temperature could be much higher than that shown in Fig. 5.

Fission Gas Release During RIA Experiments

The thermomechanical response of the pellet rim during the power pulse has been shown to provide mechanical confinement to the fission gas resident in the rim porosity. The unique mechanical state caused by the fuel and cladding interaction results in a hydrostatic state of compression in the pellet rim during the power pulse. This response contains any fuel swelling or fission gas release from the pellet rim; however, cooling of the pellet rim region occurs by heat conduction to the cladding after the power pulse. This cooling effect produces thermal contraction of the fuel material away from the cladding, which relieves the hydrostatic compression and causes extensive pellet cracking in the rim region. Results from the fuel behavior analysis indicate that pellet cracking occurs in the outer 650-μm region near the periphery. The extent of this cracking depends on the amount of local temperature peaking in the pellet rim region produced by the power pulse. Temperature peaking refers to the ratio of the maximum pellet rim temperature and the centerline temperature and is a measure of the hydrostatic compression stress in the rim material. The amount of temperature peaking is a function of the fuel pellet burnup and the power pulse width.

The fission gas inventory across the radius of a PWR 17 × 17 fuel pellet is shown in Fig. 6 at an average burnup of 50 MWd/kgU. As shown in the figure, approximately 20% of the total fission gas inventory resides in the outer 8% of the fuel pellet. It is possible that cracking and fragmentation of the pellet rim region could release a significant amount of the fission gas, provided the fission gas resides on or near grain boundaries, crack faces, etc. The pellet rim restructuring observed in high-burnup fuel produces a fuel matrix microstructure in which a large fraction of the fission gas inventory has been swept from the intragranular locations into microporosity and grain boundaries.[19,21] The redistribution of fission gases in the pellet periphery, combined with extensive pellet cracking and fragmentation during cooling, could have produced the transient fission gas release observed in the HBO and CABRI REP-Na tests. The transient gas release would have occurred after the maximum PCMI forces were experienced and would thus limit the mechanical deformations produced by the gas release. A preliminary transient fission gas release model that considers the amount of temperature peaking in the pellet rim and the hydrostatic state of compression has shown good agreement with the observed transient gas release values reported for the HBO and CABRI REP-Na tests.

DISCUSSION OF RESULTS

Dimensional measurements have been obtained from the test rods that did not fail, which can be compared with the calculated values from the transient fuel behavior analysis. The residual cladding hoop strains and peak and residual cladding axial displacements provide data to validate the analysis methodology. Figure 7 shows the predicted vs. measured residual cladding hoop strains from the CABRI REP-Na test series. Figure 8 shows the predicted vs. measured cladding axial displacements for test rods from NSRR, CABRI REP-Na, and SPERT-CDC. The larger values are associated with the CABRI REP-Na tests, and the values below 1.0 mm are for the NSRR and SPERT-CDC test rods. The good agreement shown in these results validates the FREY-01 analysis capability used

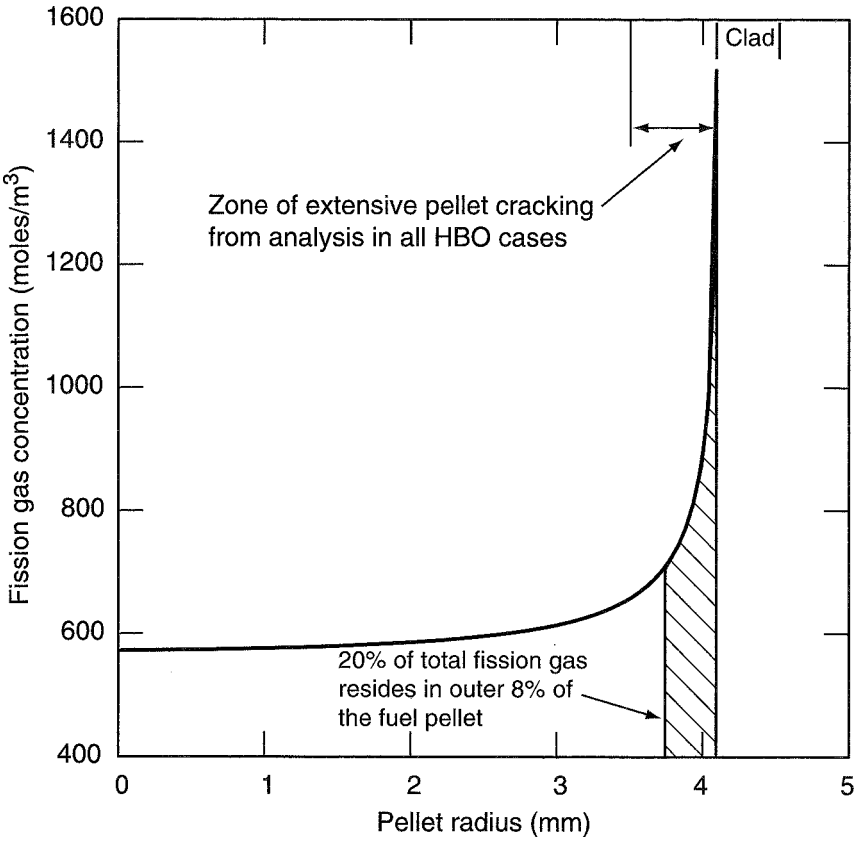

Fig. 6 Radial distribution of generated fission gas for a 17 × 17 fuel pellet at 50 MWd/kgU burnup.

to model RIA fuel behavior. Furthermore, these results indicate that the mechanical response of the fuel and cladding is dominated by the fuel-pellet thermal expansion produced by the energy deposition. The enhancement of PCMI forces by high burnup, other than through gap closure during the base irradiation, is not evident in these results.

The calculated SED at the end of the power pulse is shown in Fig. 9 as a function of the reported average hydrogen content in the cladding for the CABRI REP-Na test rods. These results (displayed as points) were obtained with the use of the model shown in Eq. 4. Also shown in Fig. 9 is the critical SED curve calculated with the use of Eq. 2. The tests CABRI REP-Na2, -Na3, and -Na5 reside well below the critical SED curve, which indicates that the potential for failure was low. The SED for CABRI REP-Na4 is very close to the critical SED curve. Because CABRI REP-Na4 performed successfully, this result suggests that the critical SED curve is somewhat conservative.

Unlike the other cases, the calculated SED for CABRI REP-Na1 at the time of failure, as determined by in-pile instrumentation, is shown in Fig. 9. The calculated value is well below the critical SED curve, even though the data used to develop this curve contained cladding samples from fuel rods with nonuniform hydride distributions and oxide spallation as extensive as that for CABRI REP-Na1.

Several investigators have attempted to explain the low-failure SED of CABRI REP-Na1 by invoking gaseous swelling in the pellet rim region.[2,9] As shown in the local pellet rim analysis, the combination of the low temperature and the compressive stress state suppresses the expansion of the pellet rim because of the increasing gas pressure in the gas bubble porosity. As a consequence, pellet rim instability could not have caused cladding failure in CABRI REP-Na1. These conclusions are supported by the good agreement in the residual cladding strains shown in Fig. 7 for the high-burnup test rods CABRI REP-Na3, -Na4,

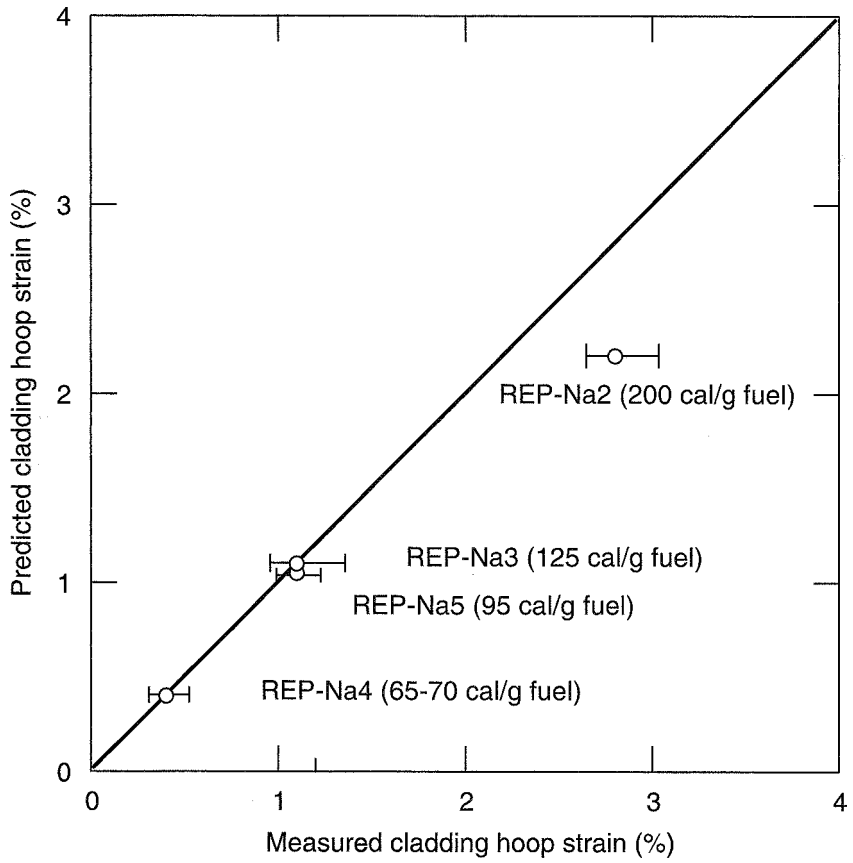

Fig. 7 Predicted vs. measured residual cladding hoop strains for CABRI REP-Na tests with the use of FREY-01.

and -Na5, which experienced enthalpy pulses higher than or equivalent to CABRI REP-Na1.

Uncertainties in the initial state of the test rod cladding may have significantly contributed to the premature failure observed in CABRI REP-Na1. As mentioned, pretest eddy-current measurements and posttest metallography indicate the existence of external, and possibly internal, incipient cladding defects. The external-defect indications were attributed to localized hydride accumulations similar to those observed previously in some high-burnup cladding that operated with an unusual amount of oxide spallation.[24] It is possible that cracking of these localized hydrides could have occurred by handling at room temperature during the refabrication process. These hydrided regions have no ductility and limited elastic capacity at room temperature. The activities associated with moving, cutting, and welding the test rod could have caused incipient cracking in the localized hydrides. Occurrence of preexisting incipient cladding cracks, which are not modeled in the present analysis, would account for the discrepancies observed in Fig. 9 for CABRI REP-Na1.

Finally, the review of the RIA tests on preirradiated test rods found that the failures are not a statistical representation of either the rod population in the RIA tests or LWR reactor fuel. The failures were not caused by operationally induced, statistically representative variations in material properties important to failure characterization such as yield strength, ductility, or fracture toughness. For each failed case, there are circumstances that make it unrepresentative to the remaining population of RIA test rods as well as in-reactor rods.

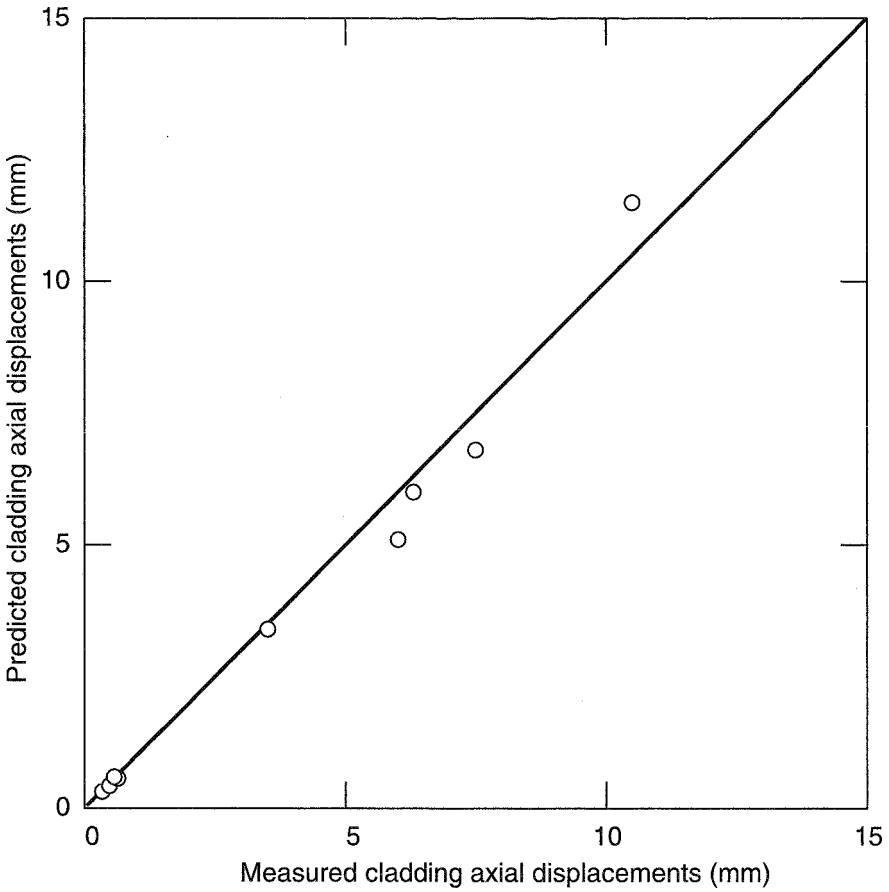

Fig. 8 Predicted vs. measured cladding axial elongation (peak and residual values) for test rods from NSRR, CABRI REP-Na, and SPERT-CDC. (The larger values are associated with the CABRI REP-Na tests; the values below 1.0 mm are for the NSRR and SPERT-CDC test rods.)

SUMMARY

The review and analysis of selected preirradiated RIA-simulation test rods have provided the following observations and conclusions:

1. A majority of the test rods that failed had either unusual hydride distributions or the hydride distribution coincided with the low-temperature cladding region that experienced high stresses. Sensitivity analyses have shown that the failure mechanisms in these tests would be absent under realistic conditions. The remaining failures occurred in fuel irradiated to an average burnup less than 5 MWd/kgU and were tested near the existing RIA limit.

2. The analysis results indicate that no unusual phenomena associated with high-burnup fuel behavior are causing test rods to fail during RIA-simulation experiments. A comparison of the calculated residual cladding deformations with posttest examination results indicates that transient gaseous swelling is not a driving force during the initial (or critical) phase of the RIA-simulation tests. Rather, the PCMI induced by pellet thermal expansion during the energy deposition is the major driving force for cladding deformations. Therefore the survivability of a fuel rod that experiences PCMI conditions during an RIA-simulation test depends on the residual capacity of the cladding under the test conditions.

ACKNOWLEDGMENTS

This work was sponsored by the Electric Power Research Institute with cofunding from nuclear fuel vendors and several foreign utility groups. This

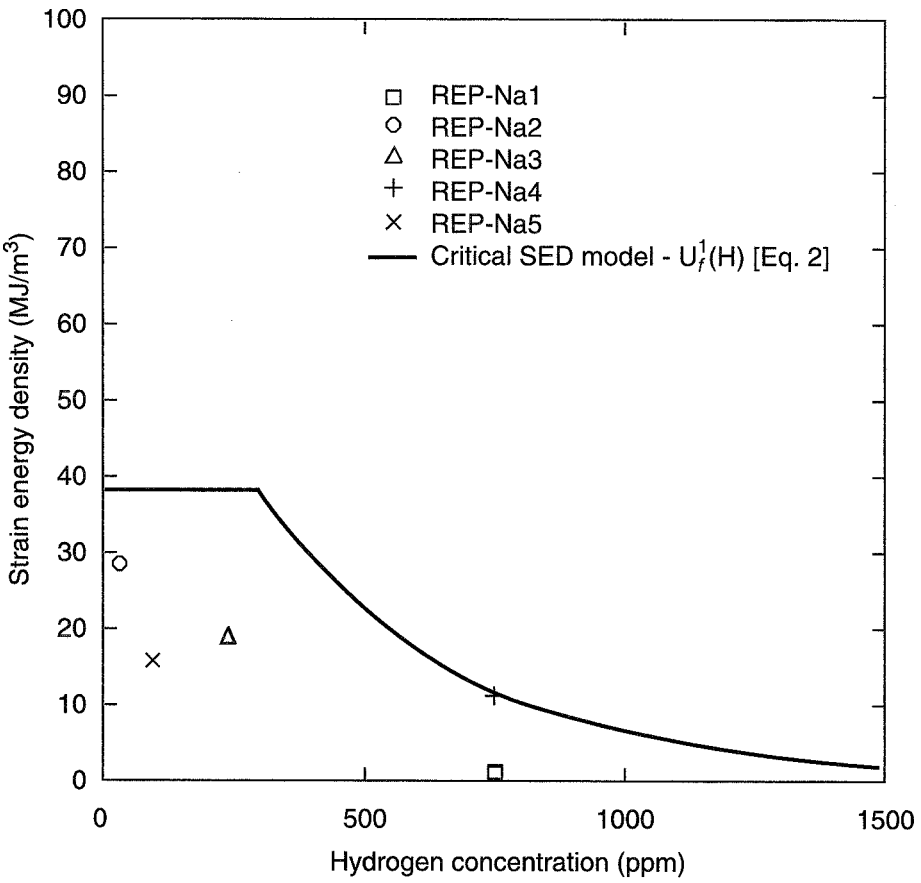

Fig. 9 Comparison of calculated strain energy density (SED) for CABRI REP-Na test rods and critical SED model at a fast fluence of 12×10^{25} neutrons/m^2.

industry-wide effort was directed by a Technical Steering Committee with representatives from electric utilities and fuel vendors. The guidance of the Technical Steering Committee under the direction of Steve Schultz of Yankee Atomic is gratefully acknowledged.

REFERENCES

1. P. E. MacDonald, S. L. Seiffert, Z. R. Martinson, R. K. McCardell, D. E. Owen, and S. K. Fukuda, Assessment of Light-Water-Reactor Fuel Damage During a Reactivity-Initiated Accident, *Nucl. Saf.,* 21(5): 582-602 (September–October 1980).
2. F. Schmitz and P. Permezel, Investigation of the Behavior of High Burnup PWR Fuel Under RIA Conditions in the CABRI Test Reactor, in *Transactions of the Twenty-Second Water Reactor Safety Information Meeting,* Bethesda, Maryland, Oct. 24–26, 1994, Report NUREG/CP-0139, pp. 107-108, October 1994.
3. T. Fujishiro and K. Ishijima, NSRR Experiments to Study the Effects of Burnup on the Fuel Behavior Under Reactivity Initiated Accident Conditions, in *Transactions of the Twenty-Second Water Reactor Safety Information Meeting,* Bethesda, Maryland, October 24–26, 1994, Report NUREG/CP-0139, pp. 109-110, October 1994.
4. U.S. Nuclear Regulatory Commission, *Supplement 1: Reactivity Insertion Transient and Accident Limits for High Burnup Fuel,* NRC IN 94-64, April 6, 1995.
5. R. O. Montgomery and Y. R. Rashid, *Evaluation of Irradiated Fuel During RIA Simulation Tests, Final Report,* Report EPRI-TR-106387, Electric Power Research Institute, August 1996.
6. R. W. Miller, *Effects of Burnup on Fuel Failure: II. Power Burst Tests on Fuel Rods with 13,000 and 32,000 MWd/tU Burnup,* Report IN-ITR-118, April 1971.
7. R. K. McCardell, Reassessment of the Basis for NRC Fuel Damage Criteria for Reactivity Transients, in *Transactions of the Twenty-Second Water Reactor Safety Information Meeting,* Bethesda, Maryland, October 24–26, 1994, Report NUREG/CP-0139, pp. 113-114, October 1994.

8. T. C. Rowland (Comp.), *Demonstration of Fuel Resistant to Pellet–Cladding Interaction: Phase 2 Final Report*, Report GEAP-25163-10, November 1984.
9. T. Fuketa, Y. Mori, H. Sasajima, K. Ishijima, and T. Fujishiro, Behavior of High Burnup PWR Fuel Under a Simulated RIA Condition in the NSRR, in *Proceedings of the CSNI Specialist Meeting on Transient Behavior of High Burnup Fuel,* Cadarache, France, September 12–14, 1995, Report NEA/CSNI/R(95) 22, pp. 59-85, 1996.
10. Y. R. Rashid, R. O. Montgomery, and A. J. Zangari, *FREY-01: Fuel Rod Evaluation System*, Report EPRI NP-3277, Vols. 1–4, Rev. 3, August 1994.
11. I. Fiero et al., *ESCORE—The EPRI Steady-State Core Reload Evaluator Code: General Description, Final Report*, Report EPRI NP-5100, April 1991.
12. K. Lassmann et al., The Radial Distribution of Plutonium in High Burnup UO_2 Fuels, *J. Nucl. Mater.*, 208(3): 223-231 (February 1994).
13. E. Kolstad and C. Vitanza, Fuel Rod and Core Materials Investigations Related to LWR Extended Burnup Operation, *J. Nucl. Mater.*, 188: 104-112 (June 1992).
14. G. Deletti and M. Charles, Thermal Conductivity of Fully Dense Unirradiated UO_2: A New Formulation from Experimental Results Between 100°C and 2500°C and Associated Fundamental Properties, in *Proceedings of the IAEA Technical Committee Meeting on Water Reactor Fuel Element Modeling at High Burnup and Its Experimental Support,* Windermere United Kingdom, September 1994, pp. 19-23.
15. S. L. Hayes and K. L. Peddicord, Radiative Heat Transfer in Porous Uranium Dioxide, *J. Nucl. Mater.*, 202(1-2): 87-97 (June 1993).
16. S. Timoshenko and J. N. Goodier, *Theory of Elasticity*, McGraw-Hill, New York, 1951.
17. G. P. Smith et al., *Hot Cell Examination of Extended Burnup Fuel from Calvert Cliffs-1*, Report EPRI TR-103302, July 1994.
18. F. Lemoine and F. Schmitz, Impact of Fission Gas on Irradiated PWR Fuel Behavior at Extended Burnup Under RIA Conditions, in *Proceedings of the CSNI Specialist Meeting on Transient Fuel Behavior of High Burnup Fuel,* Cadarache, France, September 12–14, 1995, Report NEA/CSNI/R(95)22, 1996.
19. M. E. Cunningham, M. D. Freshley, and D. D. Lanning, Development and Characteristics of the Rim Region in High Burnup UO_2 Fuel Pellets, *J. Nucl. Mater.*, 188:19-27 (1992).
20. C. T. Walker, T. Kameyama, S. Kitajima, and M. Kinoshita, Concerning the Microstructure Changes That Occur at the Surface of UO_2 Pellets on Irradiation to High Burnup, *J. Nucl. Mater.*, 188: 73-79 (June 1992).
21. J. Spino, K. Vennix, and M. Coquerelle, Detailed Characterisation of the Rim Microstructure in PWR Fuels in the Burn-up Range 40–67 GWd/tU, *J. Nucl. Mater.*, 231(3): 179-190 (August 1996).
22. Hibbitt, Karlsson, and Sorensen, Inc., *ABAQUS Theory and User's Manual*, Version 4–8, 1989.
23. S. R. Pati, A. M. Garde, and L. J. Clink, Contribution of Pellet Rim Porosity to Low-Temperature Fission Gas Release at Extended Burnup, in *ANS Topical Meeting on Light Water Reactor Fuel Performance,* Williamsburg, Virginia, April 17–20, 1988, p. 204.
24. P. Guedeney, M. Trotabas, M. Boschiero, C. Forat, and P. Blanpain, FRAGEMA Fuel Rod Behavior Characterization at High Burnup, in *ANS Topical Meeting on Light Water Reactor Fuel Performance,* Avignon, France, April 21–24, 1991, p. 639.

Operating Experiences

Edited by R. J. Belles

Reactor Shutdown Experience

Compiled by J. W. Cletcher[a]

This section presents a regular report of summary statistics relating to recent reactor shutdown experience. The information includes both numbers of events and rates of occurrence. It was compiled from data about operating events entered into the SCSS data system by the Nuclear Operations Analysis Center at the Oak Ridge National Laboratory and covers the six-month period of July 1–December 31, 1996. Cumulative information, starting from January 1, 1984, is also shown. Updates on shutdown events included in earlier reports are excluded.

Table 1 lists information on shutdowns as a function of reactor power at the time of the shutdown for both boiling-water reactors (BWRs) and pressurized-water reactors (PWRs). Only reactors in commercial operation at the start of the reporting period (July 1, 1996) are included. The second column for each reactor type shows the annualized shutdown rate for the reporting period. The third and fourth columns list cumulative data (numbers and rates) starting as of January 1, 1984.

Table 1 Reactor Shutdowns by Reactor Type and Percent Power at Shutdown[a] (Period Covered is the Second Half of 1996)

	BWRs (37)				PWRs (73)			
Reactor power (P), %	Number	Shutdown rate (annualized for the period)	Cumulative number	Cumulative shutdown rate per reactor year[b]	Number	Shutdown rate (annualized for the period)	Cumulative number	Cumulative shutdown rate per reactor year[c]
0	6	0.32	716	1.59	7	0.19	507	0.58
0 < P ≤ 10	4	0.21	149	0.33	0	0.00	175	0.20
10 < P ≤ 40	3	0.16	182	0.40	7	0.19	345	0.39
40 < P ≤ 70	2	0.11	166	0.37	5	0.14	198	0.22
70 < P ≤ 99	5	0.27	398	0.88	5	0.14	536	0.61
99 < P ≤ 100	13	0.70	549	1.22	25	0.68	1308	1.48
Total	33	1.77	2160	4.79	49	1.34	3069	3.48

[a]Data include shutdowns for all reactors of the designated type while in commercial service during all or part of the period covered. The cumulative data are based on the experience while in commercial service since the starting date of Jan. 1, 1984, through the end of the reporting period; it includes the commercial service of reactors now permanently or indefinitely shut down.

[b]Based on cumulative BWR operating experience of 450.48 reactor years.

[c]Based on cumulative PWR operating experience of 881.03 reactor years.

[a]Oak Ridge National Laboratory.

Table 2 shows data on shutdowns by shutdown type: *Shutdowns required by Technical Specifications* are automatic scrams under circumstances where such a shutdown was required; *Intentional or required manual reactor protection system actuations* are manual shutdowns in which the operators, for reasons that appeared valid to them, took manual actions to actuate features of the reactor protection system; *Required automatic reactor protection system actuations* are actuations that the human operators did not initiate but were needed; *Unintentional or unrequired manual reactor protection system actuations* are essentially operator errors in which the human operators took action not really called for; and *Unintentional or unrequired automatic reactor protection system actuations* are instrumentation and control failures in which uncalled-for protective actuations occurred. Only reactors in commercial operation are included. The second column for each type of reactor shows the annualized rate of shutdowns for the reporting period. Cumulative information is shown in the third and fourth columns for each reactor type.

Table 3 lists information about shutdowns by reactor age category, both total numbers and rates in that category; it also shows cumulative results. Note that the age groups are not cohorts; rather reactors move into and out of the specified age groups as they age. The reactor age as used in this table is the number of full years between the start of commercial operation and the beginning of the reporting period (July 1, 1996, for this issue). The first line of this table gives the information for reactors licensed for full power but not yet in commercial operation on that date.

Table 2 Reactor Shutdowns by Reactor Type and Shutdown Type[a] (Period Covered is the Second Half of 1996)

	BWRs (37)				PWRs (73)			
Shutdown (SD) type	Number	Shutdown rate (annualized for the period)	Cumulative number	Cumulative shutdown rate per reactor year[b]	Number	Shutdown rate (annualized for the period)	Cumulative number	Cumulative shutdown rate per reactor year[c]
SDs required by Technical Specifications	7	0.38	286	0.63	8	0.22	445	0.51
Intentional or required manual reactor protection system actuations	11	0.59	239	0.53	13	0.35	453	0.51
Required automatic reactor protection system actuations	13	0.70	1004	2.23	25	0.68	1708	1.94
Unintentional or unrequired manual reactor protection system actuations	0	0.00	10	0.02	0	0.00	22	0.02
Unintentional or unrequired automatic reactor protection system actuations	2	0.11	621	1.38	3	0.08	441	0.50
Total	33	1.77	2160	4.79	49	1.33	3069	3.48

[a]Data include shutdowns for all reactors of the designated type while in commercial service during all or part of the period covered. The cumulative data are based on the experience while in commercial service since the starting date of Jan. 1, 1984, through the end of the reporting period; it includes the commercial service of reactors now permanently or indefinitely shut down.

[b]Based on cumulative BWR operating experience of 450.48 reactor years.

[c]Based on cumulative PWR operating experience of 881.03 reactor years.

Table 3 Reactor Shutdowns by Reactor Type and Reactor Age[a] (Period Covered is the Second Half of 1996)

Years in commercial operation (C.O.)	BWRs (37)						PWRs (73)					
	Exposure during the period (in reactor years)	Number		Shutdown rate (annualized for the period)	Cumulative number	Cumulative shutdown rate per reactor year	Exposure during the period (in reactor years)	Number		Shutdown rate (annualized for the period)	Cumulative number	Cumulative shutdown rate per reactor year
		Reactors	Shutdowns					Reactors	Shutdowns			
Not in C.O.[b]	0.000	0	0	0.00	330	28.61	0.000	0	0	0.00	341	34.58
First year of C.O.	0.000	0	0	0.00	121	9.00	0.500	1	0	0.00	281	9.76
Second through fourth year of C.O.	0.000	0	0	0.00	264	6.29	0.500	1	2	3.97	533	5.51
Fifth through seventh year of C.O.	0.500	1	2	3.97	190	4.22	1.010	2	1	0.99	341	3.10
Eighth through tenth year of C.O.	2.490	5	6	2.41	246	4.54	5.390	12	9	1.67	428	3.28
Eleventh through thirteenth year of C.O.	3.560	8	4	1.12	307	5.05	6.910	16	10	1.45	539	3.79
Fourteenth through sixteenth year of C.O.	0.500	1	1	1.99	402	6.12	3.770	8	6	1.59	397	3.14
Seventeenth through nineteenth year of C.O.	0.500	1	0	0.00	288	4.38	2.480	6	2	0.81	287	2.59
Twentieth through twenty-second year of C.O.	4.100	10	7	1.71	196	3.43	6.680	17	5	0.75	158	1.86
Twenty-third through twenty-fifth year of C.O.	3.830	9	6	1.57	82	2.71	7.500	19	10	1.33	71	1.88
Twenty-sixth through twenty-eighth year of C.O.	2.640	6	5	1.89	20	1.96	1.510	4	3	1.98	24	2.56
Twenty-ninth through thirty-first year of C.O.	0.000	0	0	0.00	9	3.00	0.500	1	1	1.99	6	1.64
Thirty-second through ninety-ninth year of C.O.	0.500	1	2	3.97	8	2.90	0.000	0	0	0.00	0	0.00
Total	18.640		33	1.77	2463	5.33	36.770		49	1.33	3406	3.82

[a]Age is defined to be the time (in years) from the start of commercial operation to the time of the shutdown event, except for the first line, which lists reactors not yet in commercial service (see b below).
[b]This category includes reactors licensed for full-power operation but not yet in commercial operation. During this reporting period there were no reactors in this category.

Recent Developments

Edited by M. D. Muhlheim

Reports, Standards, and Safety Guides

By D. S. Queener

This article contains four lists of various documents relevant to nuclear safety as compiled by the editor. These lists are: (1) reactor operations-related reports of U.S. origin, (2) other books and reports, (3) regulatory guides, and (4) nuclear standards. Each list contains the documents in its category which were published (or became available) during the July 1996 through September 1996 reporting period, represented by this issue of *Nuclear Safety*. The availability and cost of the documents are noted in most instances.

OPERATIONS REPORTS

This category is listed separately because of the increasing interest in the safety implications of information obtainable from both normal and off-normal operating experience with licensed power reactors. The reports fall into several categories shown, with information about the availability of the reports given where possible. The NRC reports are available from the Nuclear Regulatory Commission (NRC) Public Document Room (PDR), 2120 L Street, NW, Washington, DC 20555.

NRC Office of Nuclear Reactor Regulation

The NRC Office of Nuclear Reactor Regulation (NRR) issues reports regarding operating experience at licensed reactors. These reports, previously published by the NRC Office of Inspection and Enforcement (IE), fall into two categories of urgency: (1) NRC Bulletins and Generic Letters, which require remedial actions and/or responses from affected licensees, and (2) NRC Information Notices and Administrative Letters, which are for general information and do not require any response from the licensee. The Administrative Letters, which contain information of an administrative or informational nature, were previously distributed under the generic letter category. No specific action is required in response to these Administrative Letters. The Bulletins and Information Notices are included in this issue.

NRC Bulletins

NRC B 96-04 *Chemical, Galvanic or Other Reactions in Spent Fuel Storage and Transportation Casks,* July 5, 1996, 9 pages plus one-page attachment.

NRC Information Notices

NRC IN 92-68, Suppl. 1 *Potentially Substandard Slip-on Welding Neck and Blind Flanges,* September 16, 1996, 9 pages plus one-page attachment.

NRC IN 96-09, Suppl. 1 *Damage in Foreign SG Internals,* July 7, 1996, 9 pages plus one-page attachment.

NRC IN 96-39 *Estimates of Decay Heat Using ANS 5.1 Decay Heat Standard May Vary Significantly,* July 5, 1996, 3 pages plus 3 pages of attachments.

NRC IN 96-40 *Deficiencies in Material Dedication and Procurement Practices and in Audits of Vendors,* July 25, 1996, 3 pages plus 2 pages of attachments.

NRC IN 96-41 *Effects of a Decrease in Feedwater Temperature on Nuclear Instrumentation,* July 26, 1996, 3 pages plus one-page attachment.

NRC IN 96-42 *Unexpected Opening of Multiple Safety Relief Valves,* August 5, 1996, 3 pages plus one-page attachment.

NRC IN 96-43 *Failures of General Electric Magne-Blast Circuit Breakers,* August 2, 1996, 4 pages plus one-page attachment.

NRC IN 96-44 *Failure of Reactor Trip Breaker From Cracking of Phenolic Material in Secondary Contact Assembly,* August 5, 1996, 3 pages plus one-page attachment.

NRC IN 96-45 *Potential Common-Mode Post-Accident Failure of Containment Coolers,* August 12, 1996, 3 pages plus 4 pages of attachments.

NRC IN 96-46 *Zinc Plating of Hardened Metal Parts and Removal of Protective Coatings in Refurbished Circuit Breakers,* August 12, 1996, 3 pages plus one-page attachment.

NRC IN 96-47 *Recordkeeping, Decommissioning Notifications for Disposals of Radioactive Waste by Land Burial Authorized Under Former 10CFR20.304, 20.302, and Current 20.2002,* August 19, 1996, 6 pages plus one-page attachment.

NRC IN 96-48 *Motor-Operated Valve Performance Issues,* August 21,1996, 8 pages plus one-page attachment.

NRC IN 96-49 *Thermally Induced Pressurization of Nuclear Power Facility Piping,* August 20, 1996, 3 pages plus one-page attachment.

NRC IN 96-50 *Problems with Levering-in Devices in Westinghouse Circuit Breakers,* September 4, 1996, 3 pages plus 10 pages of attachments.

NRC IN 96-51 *Residual Contamination Remaining in Krypton-85 Handling System After Venting,* September 11, 1996, 2 pages plus 2 pages of attachments.

NRC IN 96-52 *Cracked Insertion Rods on Troxler Model 3400 Series Portable Moisture Density Gauges,* September 26, 1996, 6 pages plus 2 pages of attachments.

Other Operations Reports

These are other reports issued by various organizations in the United States dealing with power-reactor operations activities. Most of the NRC publications (NUREG series documents) can be ordered from the Superintendent of Documents, U.S. Government Printing Office (GPO), P.O. Box 37082, Washington, DC 20013. NRC draft copies of reports are available free of charge by writing the NRC Office of Administration (ADM), Distribution and Mail Services Section, Washington, DC 20555. A number of these reports can also be obtained from the NRC Public Document Room (PDR). Specify the report number when ordering. Telephone orders can be made by contacting the PDR at (202) 634-3273.

Many other reports prepared by U.S. Government laboratories and contractor organizations are available from the U.S. Department of Commerce, Technology Administration, National Technical Information Service (NTIS), Springfield, VA 22161, and/or DOE Office of Scientific and Technical Information (OSTI), P.O. Box 62, Oak Ridge, TN 37831. Reports available through one or more of these organizations are designated with the appropriate information (i.e., GPO, PDR, NTIS, and OSTI) in parentheses at the end of the listing, followed by the price, when available.

NUREG/CR-5758, Vol. 6 *Fitness for Duty in the Nuclear Power Industry. Annual Summary of Program Performance Reports, CY 1995,* M. Silbernagel et al., Pacific Northwest Labs., WA, July 1996, 85 pages (GPO).

DOE- and NRC-Related Items

NUREG-1125, Vol. 17 *A Compilation of Reports of the Advisory Committee on Reactor Safeguards, 1995 Annual Report,* April 1996, 130 pages (GPO).

NUREG-1272, Vol. 9, No. 3 *Office for Analysis and Evaluation of Operational Data Annual Report, FY95, Technical Training,* September 1996, 35 pages (GPO).

NUREG-1307, Rev. 6 *Report on Waste Burial Charges. Escalation of Decommissioning Waste Disposal Costs at Low-Level Waste Burial Facilities,* September 1996, 55 pages (GPO).

NUREG-1437, Vols. 1&2 *Generic Environmental Impact Statement for License Renewal of Nuclear Plants, Main Report and Appendices, Final Report,* May 1996, 1150 pages (GPO).

NUREG-1440 *Regulatory Analysis for Amendments to Regulations for the Environmental Review for Renewal of Nuclear Power Plant Operating Licenses, Final Report,* May 1996, 30 pages (GPO).

NUREG-1509 *Radiation Effects on Reactor Pressure Vessel Supports,* R. E. Johnson and R. E. Lipinski, May 1996, 180 pages (GPO).

NUREG-1524 *A Reassessment of the Potential for an Alpha-Mode Containment Failure and a Review of the Current Understanding of Broader Fuel–Coolant Interaction Issues. Second Steam Explosion Review Group Workshop,* S. Basu and T. Ginsberg, August 1996, 200 pages (GPO).

NUREG-1529, Vols. 1&2 *Public Comments on the Proposed 10 CFR Part 51 Rule for Renewal of Nuclear Power Plant Operating Licenses and Supporting Documents: Review of Concerns and NRC Staff Response, Executive Summary and Appendices,* May 1996, 660 pages (GPO).

NUREG-1547 *Methodology for Developing and Implementing Alternative Temperature–Time Curves for Testing the Fire Resistance of Barriers for Nuclear Power*

Plant Applications, L. Y. Cooper and K. D. Steckler, August 1996, 115 pages (GPO).

NUREG/CR-6210 *Computer Codes for Evaluation of Control Room Habitability,* S. A. Stage, Pacific Northwest Labs., WA, June 1996, 160 pages (GPO).

NUREG/CR-6227 *Performance Demonstration Tests for Eddy Current Inspection of Steam Generator Tubing,* R. J. Kurtz et al., Pacific Northwest Labs., WA, May 1996, 45 pages (GPO).

NUREG/CR-6270 *Estimating Boiling Water Reactor Decommissioning Costs. A User's Manual for the BWR Cost Estimating Computer Program (CECP) Software, Final Report,* M. C. Bierschbach, Pacific Northwest Labs., WA, June 1996, 188 pages (GPO).

NUREG/CR-6384, Vols. 1&2 *Literature Review of Environmental Qualification of Safety-Related Electric Cables,* M. Subudhi, Brookhaven National Lab., NY, April 1996, 430 pages (GPO).

NUREG/CR-6392 *The Effects of Aging on Compressive Strength of Low-Level Radioactive Waste Form Samples,* J. W. McConnell, Jr., and R. M. Neilson, Jr., Idaho National Engineering Lab., ID, June 1996, 33 pages (GPO).

NUREG/CR-6455 *Data Analysis for Steam Generator Tubing Samples,* C. V. Dodd, Oak Ridge National Lab., TN, July 1996, 55 pages (GPO).

NUREG/CR-6463 *Review Guidelines on Software Languages for Use in Nuclear Power Plant Safety Systems, Final Report,* H. Hecht et al., SoHar Inc., CA, June 1996, 300 pages (GPO).

NUREG/CR-6465 *Development of Tools for Safety Analysis of Control Software in Advanced Reactors,* S. Guarro et al., ASCA Inc., CA, April 1996, 145 pages (GPO).

OTHER REPORTS

STI/PUB/1017 *IAEA Yearbook 1966,* International Atomic Energy Agency (IAEA), September 1996, 292 pages (available from UNIPUB, 4611-F Assembly Drive, Lanham, MD 20706-4391).

STI/PUB/1018 *Nuclear Power, Nuclear Fuel Cycle and Waste Management: Status and Trends,* IAEA, September 1996, 118 pages (available from UNIPUB).

STI/PUB/1019 *Nuclear Safety Review 1996,* IAEA, September 1996, 64 pages (available from UNIPUB).

U. S. Nuclear Plant Statistics, 1995, Utility Data Inst. (UDI), Washington, DC, June 1996 (available from UDI, 1200 G St. NW, Suite 250, Washington, DC 20005).

REGULATORY GUIDES

To expedite the role and function of the NRC, its Office of Nuclear Regulatory Research prepares and maintains a file of Regulatory Guides that define much of the basis for the licensing of nuclear facilities. These Regulatory Guides are divided into 10 divisions as shown in Table 1.

Table 1 Regulatory Guides

Division 1	Power Reactor Guides
Division 2	Research and Test Reactor Guides
Division 3	Fuels and Materials Facilities Guides
Division 4	Environmental and Siting Guides
Division 5	Materials and Plant Protection Guides
Division 6	Product Guides
Division 7	Transportation Guides
Division 8	Occupational Health Guides
Division 9	Antitrust and Financial Review Guides
Division 10	General Guides

Single copies of the draft guides may be obtained from NRC Distribution Section, Division of Information Support Services, Washington, DC 20555. Draft guides are issued free (for comment) and licensees receive both draft and final copies free; others can purchase single copies of active guides by contacting the U.S. Government Printing Office (GPO), Superintendent of Documents, P.O. Box 37082, Washington, DC 20013. Costs vary according to length of the guide. Of course, draft and active copies will be available from the NRC Public Document Room, 1717 H Street, NW, Washington, DC, for inspection and copying for a fee.

Revisions in these rates will be announced as appropriate. Subscription requests should be sent to the National Technical Information Service, Subscription Department, Springfield, VA 22161. Any questions or comments about the sale of regulatory guides should be directed to the Chief, Document Management Branch, Division of Technical Information and Document Control, Nuclear Regulatory Commission, Washington, DC 20555.

Actions pertaining to specific guides (such as issuance of new guides, issuance for comment, or withdrawal), which occurred during the reporting period, are listed below.

Division 1 Power Reactor Guides

1.160 (Proposed Rev. 2) *Monitoring Effectiveness of Maintenance at Nuclear Power Plants,* August 1996.

Draft Guide DG-1047 *Standard Format and Content for Application to Renew Nuclear Power Plant Operating Licenses,* August 1996.

Draft Guide DG-1055 *Configuration Management Plans for Digital Computer Software Used in Safety Systems of Nuclear Power Plants,* August 1996.

Draft Guide DG-1056 *Software Test Documentation for Digital Computer Software Used in Safety Systems of Nuclear Power Plants,* August 1996.

Draft Guide DG-1057 *Software Unit Testing for Digital Computer Software Used in Safety Systems of Nuclear Plants,* August 1996.

Division 3 Fuels and Materials Facilities Guides

3.69 *Topical Guidelines for Licensing Support Systems,* September 1996.

Division 10 General Guides

Draft Guide DG-0010 *Preparation of Petitions for Rulemaking Under 10CFR2.802 and Preparation and Submission of Proposals for Regulatory Guidance Documents, Guidelines for Reporting Reliability and Availability Information for Risk Significant Systems and Equipment in Nuclear Power Plants,* August 1996.

NUCLEAR STANDARDS

Standards pertaining to nuclear materials and facilities are prepared by many technical societies and organizations in the United States, including the Department of Energy (DOE) (NE Standards). When standards prepared by a technical society are submitted to the American National Standards Institute (ANSI) for consideration as an American National Standard, they are assigned ANSI standard numbers, although they may also contain the identification of the originating organization and be sold by that organization as well as by ANSI. We have undertaken to list here the most significant nuclear standards actions taken by organizations from July 1996 through September 1996. Actions listed include issuance for comments, approval by the ANSI Board of Standards Review (ANSI-BSR), and publication of the approved standard. Persons interested in obtaining copies of the standards should write to the issuing organizations.

American National Standards Institute

ANSI does not prepare standards; it is devoted to approving and disseminating standards prepared by technical organizations. It does publish standards, however, and such standards can be ordered from ANSI, Attention: Sales Department, 1430 Broadway, New York, NY 10018. Frequently, ANSI is an alternate source for standards also available from the preparing organization.

ANSI N14.1-1995 (Published) *Nuclear Materials—Uranium Hexafluoride—Packaging for Transport.*

American Society for Testing and Materials

Standards and other publications prepared by ASTM can be obtained from the Customer Services Department at 610/832-9585 (Fax 610/832-9555).

ASTM C1009-89 (Revised) *Guide for Establishing a Quality Assurance Program for Analytical Chemistry Laboratories Within the Nuclear Industry.*

ASTM C1133-89 (Revised) *Test Method for Nondestructive Assay of Special Nuclear Material in Low Density Scrap and Waste by Segmented Passive Gamma-Ray Scanning.*

ASTM C1316-95 (Published) *Test Method for Non-Destructive Assay of Nuclear Material in Scrap and Waste by Passive–Active Neutron Counting Using a 252CF Shuffler.*

ASTM D4227-95 (Revised) *Practice for Qualification of Journeyman Painters for Application of Coatings to Concrete Surface of Safety-Related Areas in Nuclear Power Facilities.*

ASTM E636-95 (New standard, for comment) *Guide for Conducting Supplemental Surveillance Tests for Nuclear Power Reactor Vessels.*

Institute of Electrical and Electronics Engineers

Standards prepared by IEEE can be obtained from IEEE, Attention: M. Lynch, 345 East 47th Street, New York, NY 10017.

IEEE 1290 (New standard, for comment) *Guide for MOV (Motor-Operated Valve) Motor Application, Protection, Control, and Testing in Nuclear Power Generating Stations.*

International Standards

This section includes publications for any of the three types of international standards:

–IEC standards (International Electrotechnical Commission)

–ISO standards (International Standards Organization)

–KTA standards [Kerntechnischer Ausschuss (Nuclear Technology Commission)].

Standards originating from the IEC and ISO can be obtained from the American National Standards Institute (ANSI), International Sales Department, 1430 Broadway, New York, NY 10018.

The KTA standards are developed and approved by the Nuclear Safety Standards Commission (KTA). The KTA, formerly a component of the Gesellschaft für

Reaktorsicherheit (GRS), is now integrated in the Federal Office for Radiation Protection (Bundesamt für Strahlenschutz BfS) in Salzgitter, Germany. Copies of these standards can be ordered from Dr. T. Kalinowski, KTA-Geschäftsstelle, Postfach 10 01 49, 3320 Salzgitter 1, Germany. These standards are in German and, unless otherwise noted, an English translation is available from the KTA. The IEC standards are included in this issue.

IEC

IEC 1344:1996 (Published) *Radiation Protection Instrumentation—Monitoring Equipment—Personal Warning Devices for X and Gamma Radiations.*

IEC 1559:1996 (Published) *Radiation in Nuclear Facilities—Centralized System for Continuous Monitoring of Radiation and/or Levels of Radioactivity.*

Proposed Rule Changes as of Dec. 31, 1996[a,b]

(Changes Since the Previous Issue of *Nuclear Safety* Are Indicated by Shaded Areas)

Number of part to be changed	Date published for comment	Date comment period expired	Date published; date effective	Topic or proposed effect	Current action and/or comment, *Federal Register* volumes and page numbers
10 CFR 2	8-23-94; 9-27-94; 11-28-94	10-24-94; 12-28-94		Reexamination of the NRC enforcement policy	Published for comment in 59:162 (43298); correction in 59:171 (46004); expanded scope in 59:186 (49215); revised in 59:227 (60697)
10 CFR 2, 13			10-11-96; 11-12-96	Adjustment of civil monetary penalties for inflation	Final rule in 61:199 Part III (53554); final rule correction in 61:214 (56623)
10 CFR 2, 50, 51			7-29-96; 8-28-96	Decommissioning of nuclear power reactors	Published for comment in 60:139 (37374); final rule in 61:146 (39278)
10 CFR 2, 51			8-22-96; 10-21-96	Deletion of outdated references and minor change	Direct final rule in 61:164 Part III (43406)
10 CFR 2, 51	8-22-96	9-23-96		Deletion of outdated references and minor change	Published for comment in 61:164 Part III (43409)
10 CFR 20	12-13-95	3-12-96		Constraint level for air emissions of radionuclides	Published for comment in 60:239 (63984)
10 CFR 20	1-31-96; 2-28-96	3-1-96; 3-31-96		Reporting requirements for unauthorized use of licensed radioactive material	Published for comment in 61:021 (3334); comment period extended in 61:040 (7431)
10 CFR 20			12-10-96; 1-9-97	Resolution of dual regulation of airborne effluents of radioactive materials: clean air act	Final rule in 61:238 Part III (65120)
10 CFR 20, 30, 40, 50, 51, 70, 72	8-22-94	12-20-94; 1-20-95		Radiological criteria for decommissioning	Published for comment in 59:161 Part III (43200); comment period extended in 59:236 (63733); schedule extension in 60:151 (40117)
10 CFR 20, 32, 35, 36, 39	10-7-96	12-23-96		Minor corrections, clarifying changes, and a minor policy change to the standards for protection against radiation	Published for comment in 61:195 (52388)
10 CFR 20, 35	6-15-94	8-29-94		Criteria for the release of patients administered radioactive material	Published for comment in 59:114 (30724)
10 CFR 21, 50, 52, 54, 100			12-11-96; 1-10-97	Reactor site criteria including seismic and earthquake engineering criteria for nuclear power plants	Final rule in 61:239 (65157)
10 CFR 25, 95	8-5-96	10-4-96		Access to and protection of classified information	Published for comment in 61:151 (40555)

Proposed Rule Changes as of Dec. 31, 1996 (Continued)

Number of part to be changed	Date published for comment	Date comment period expired	Date published; date effective	Topic or proposed effect	Current action and/or comment, *Federal Register* volumes and page numbers
10 CFR 26	5-11-94	9-9-94		Consideration of changes to fitness-for-duty (FFD) requirements	Published for comment in 59:090 (24373)
10 CFR 26	5-9-96	8-7-96		Modifications to fitness-for-duty program requirements	Published for comment in 61:091 (21105)
10 CFR 30, 32, 40, 50, 52, 60, 61, 70, 71, 72, 110, 150	10-4-96	12-18-96		Deliberate misconduct by unlicensed persons	Published for comment in 61:194 (51835)
10 CFR 33	11-14-96	2-12-97		Specific domestic licenses of broad scope for byproduct material	Advance notice published for comment in 61:221 (58346)
10 CFR 35	11-3-94	3-3-95		Request for comments regarding potential modifications of NRC's therapy regulations	Published for comment in 59:212 (55068)
10 CFR 50	9-19-94	12-5-94		Steam generator tube integrity for operating nuclear power plants	Published for comment in 59:180 (47817)
10 CFR 50	10-19-94; 10-25-94; 1-18-95	1-3-95; 2-3-95		Shutdown and low-power operations for nuclear power reactors	Published for comment in 59:201 (52707); correction in 59:205 (53613); comment period extended in 60:011 (3579)
10 CFR 50	2-12-96	6-11-96		Reporting reliability and availability information for risk-significant systems and equipment	Published for comment in 61:029 (5318)
10 CFR 50	4-8-96	6-24-96		Financial assurance requirements for decommissioning nuclear power reactors	Published for comment in 61:068 (15427)
10 CFR 50			8-8-96; 9-9-96	Codes and standards for nuclear power plants; subsection IWE and subsection IWL	Final rule in 61:154 (41303)
10 CFR 50	9-23-96; 12-11-96	12-9-96; 2-9-97		Draft policy statement on the restructuring and economic deregulation of the electric utility industry	Published for comment in 61:185 (49711); comment period extended in 61:239 (65190)

(Table continues on the next page.)

Proposed Rule Changes as of Dec. 31, 1996 (Continued)

Number of part to be changed	Date published for comment	Date comment period expired	Date published; date effective	Topic or proposed effect	Current action and/or comment, *Federal Register* volumes and page numbers
10 CFR 50, 52, 100	10-20-92	2-17-93; 3-24-93; 6-1-93; 2-14-95; 5-12-95		Reactor site criteria, including seismic and earthquake engineering criteria for nuclear power plants and proposed denial of petition for rulemaking from Free Environment, Inc., et al.	Published for comment in 57:203 (47802); comment period extended in 58:002 (271); extended again in 58:057 (16377); extended again in 59:199 (52255); extended again in 60:026 (7467); extension deadline set 60:039 (10810)
10 CFR 51			12-30-96; 1-17-97	Environmental review for renewal of operating licenses	Published for comment in 56:180 (47016); comment period extended in 56:228 (59898); supplemental proposed rulemaking in 59:141 (37724); final rule in 61:109 (28467); effective date delayed and comment period extended in 61:139 (37351); final rule correction in 61:147 (39555); final rule in 61:244 (66537); final rule correction in 61:251 (68543)
10 CFR 52	4-7-95; 4-24-96; 5-30-96	8-7-95; 5-24-96; 7-23-96		Standard design certification for the U.S. Advanced Boiling Water Reactor design	Published for comment in 60:067 (17902); SECY 96-077 published for comment in 61:080 (18099); comment period extended in 61:105 (27027)
10 CFR 52	4-7-95; 4-24-96; 5-30-96	8-7-95; 5-24-96; 7-23-96		Standard design certification for the System 80+ design	Published for comment in 60:067 (17924); SECY 96-077 published for comment in 61:080 (18099); comment period extended in 61:105 (27027)
10 CFR 53			7-9-96; 8-8-96	Removal of 10 CFR Part 53 - criteria and procedures for determining the adequacy of available spent nuclear fuel storage capacity	Final rule in 61:132 (35935)
10 CFR 60			12-4-96; 1-3-97	Disposal of high-level radioactive wastes in geologic repositories; design basis events	Published for comment in 60:055 (15180); final rule in 61:234 (64257)
10 CFR 60, 72, 73, 75	8-15-95	11-13-95		Safeguards for spent nuclear fuel or high-level radioactive waste	Published for comment in 60:157 (42079)

Proposed Rule Changes as of Dec. 31, 1996 (Continued)

Number of part to be changed	Date published for comment	Date comment period expired	Date published; date effective	Topic or proposed effect	Current action and/or comment, *Federal Register* volumes and page numbers
10 CFR 61	7-18-95	10-3-94; 12-2-94		Land ownership requirements for low-level waste sites	Published for comment in 59:148 (39485); comment period extended in 59:202 (52941); withdrawal of advanced notice of proposed rulemaking in 60:137 (36744)
10 CFR 110			7-8-96; 8-7-96	Export of nuclear equipment and materials	Final rule in 61:131 (35600)
10 CFR 150, 170	6-18-96	9-3-96		Recognition of agreement state licenses in areas under exclusive federal jurisdiction within an agreement state	Published for comment in 61:118 (30839)

[a]NRC petitions for rulemaking are not included here, but quarterly listings of such petitions can be obtained by writing to Division of Rules and Records, Office of Administration, U.S. Nuclear Regulatory Commission, Washington, DC 20555. Quarterly listings of the status of proposed rules are also available from the same address.

[b]Proposed rules for which the comment period expired more than 2 years prior to the start of the period currently covered without any subsequent action are dropped from this table. Effective rules are removed from this listing in the issue after their effective date is announced.

The Authors

A Regulatory Assessment of Test Data for Reactivity-Initiated Accidents

Ralph O. Meyer is a senior technical advisor at the Nuclear Regulatory Commission. He received the Ph.D. degree in physics from the University of North Carolina in 1966. He held research positions at the University of Arizona and Argonne National Laboratory prior to joining the Atomic Energy Commission (now Nuclear Regulatory Commission) in 1973. His background is in materials science, and his experience at the NRC, in both licensing and research, has been in the fields of reactor fuel behavior and severe accidents.

Current address: Office of Nuclear Regulatory Research, U.S. Nuclear Regulatory Commission, Washington, DC 20555.

Richard K. McCardell is a consulting scientist at Idaho National Engineering and Environmental Laboratory (INEEL). He received the M.S. degree in physics from Idaho State University in 1962. He has worked at INEEL since 1962 where he is involved with analytical and experimental programs on reactor safety. He participated in the original SPERT and PBF test reactor projects and more recently has applied that experience to understanding the behavior of high-burnup fuel.

Current address: DOE/NRC Support Programs, Idaho National Engineering and Environmental Laboratory, P. O. Box 1625, Idaho Falls, ID 83415.

Hee M. Chung is a staff metallurgist at Argonne National Laboratory (ANL). He received the Ph.D. degree in materials science and engineering from the University of Pennsylvania in 1972. He held research positions at Yale University before joining ANL in 1974. His background is in structural materials for fission and fusion reactors, and his field of expertise includes the use of zirconium-based alloys for light-water-reactor fuel rod cladding.

Current address: Energy Technology Division, Argonne National Laboratory, Argonne, IL 60439.

David J. Diamond is a nuclear engineer at Brookhaven National Laboratory (BNL). He received the Ph.D. degree in nuclear engineering from the Massachusetts Institute of Technology in 1968. He has worked at BNL since that time and has served as a consultant to the Atomic Energy Control Board of Canada and the International Atomic Energy Agency. His field of experience includes the interface of neutronics and reactor safety, and he has helped develop coupled neutronic and thermal–hydraulic computer codes for reactor safety analyses.

Current address: Department of Advanced Technology, Brookhaven National Laboratory, Upton, Long Island, NY 11973.

Harold H. Scott is a nuclear engineer at the Nuclear Regulatory Commission (NRC). He received the B.S. degree in chemical engineering from the University of Missouri at Rolla in 1968 and completed graduate courses in nuclear engineering at The Pennsylvania State University as part of the Atomic Energy Commission's (AEC's) intern program. He has worked for the AEC/NRC since then by managing research contracts in the area of fuel and core behavior and performing related assessments and analyses, including the FRAP-T calculations reported here.

Current address: Office of Nuclear Regulatory Research, U.S. Nuclear Regulatory Commission, Washington, DC 20555.

French Studies on High-Burnup Fuel Transient Behavior Under RIA Conditions

Jöelle Papin is head of the laboratory of physical studies on reactivity accidents at the Institute for Protection and Nuclear Safety. After a Ph.D. degree in thermal–hydraulics of two-phase flow, she has been involved in safety studies of fast breeder reactors (FBRs) dealing with code development and interpretation of experiments of core degradation (multiphase, multicomponents systems). From 1988 to 1990, she was also involved in severe core damage analysis for light-water reactors (LWRs). Since 1990 she has been in charge of the study of fuel behavior under reactivity accidents for both LWRs and FBRs.

Current address: DRS/SEMAR, Centre d'Etudes de Cadarache Bât, 702-13108 St. Paul Lez Durance CEDEX (FRANCE).

Marcel Balourdet is a research and development (R&D) engineer at the Institute for Protection and Nuclear Safety (IPSN). After an education in material science (Ph.D. degree in 1976), he specialized in condensed matter physics doing research work at CE-Grenoble about thermomigration in liquid metals. At

CE-Cadarache, he was involved in R&D on liquid-metal-reactor (LMR) fuel elements based on irradiation experiments in the Rapsodie and Phénix reactors. At the IPSN since 1984, he became involved in LMR and light-water-reactor safety, participating in the interpretation of CABRI and Scarabée experiments. His current focus is on post test examination, and he is interested in out-of-pile clad testing.

Current address: DRS/SEMAR, Centre d'Etudes de Cadarache Bât, 702-13108 St. Paul Lez Durance CEDEX (FRANCE).

Francette Lemoine is a research and development engineer at the Institute for Protection and Nuclear Safety (IPSN). She is a graduate of the E.S. P.C.I school with a DEA degree in theoretical physics. After 5 years with GAAA-NOVATOME, a nuclear firm, she joined the Commissariat à l'Energie Atomique and IPSN in 1980. After thermohydraulics studies on liquid-metal-reactor fuel in accident conditions, she has been in charge of fission gas behavior studies since 1983. Since 1990 her work has also included PWR fuel and fuel evolution under operating conditions related to its influence on transient behavior.

Current address: DRS/SEMAR, Centre d'Etudes de Cadarache Bât, 702-13108 St. Paul Lez Durance CEDEX (FRANCE).

François Lamare is a research and development engineer at the Institute for Protection and Nuclear Safety. He is a graduate engineer of Ecole Centrale de Lyon in general fields of physics, numerics, and data processing. His work involves the development and maintenance of the SCANAIR computer code used for modeling reactivity-initiated accidents in high-burnup fuel, thermal dynamics, structural mechanics, and transient behavior of fission gases.

Current address: DRS/SEMAR, Centre d'Etudes de Cadarache Bât, 702-13108 St. Paul Lez Durance CEDEX (FRANCE).

Jean-Michel Frizonnet is group leader for physics of reactivity accidents at the Institute for Protection and Nuclear Safety. He trained in general physical science at Paris University, specialized in seismology (Ph.D. degree in 1972), and moved to Cadarache in 1976 in the field of nuclear safety of fast breeder reactors. He has been involved in safety code development, safety in-pile experiment analysis (CABRI), and extension of in-pile accident code to reactor code and then to reactor safety analysis. Since 1995 he has been in charge of the interpretation of reactivity accident experiments and reactor applications for liquid-metal fast breeder and light-water reactors.

Current address: DRS/SEMAR, Centre d'Etudes de Cadarache Bât, 702-13108 St. Paul Lez Durance CEDEX (FRANCE).

Franz K. Schmitz is the leader of the reactivity accident research program at the Institute for Protection and Nuclear Safety, Department of Safety Research (IPSN/DRS). He received the M.S. degree in physics from the University of Kiel (Germany) in 1961 and the Ph.D. degree in physics from the University of Braunschweig (Germany) in 1965. He has held research positions at Chalmers Techniska Högskola at Göteborg (Sweden), at the Institut für Kern-und Radiochemie (Braunschweig), and at the European Research Center Ispra (Italy) before joining Euratom and being detached to the Commissariat à l'Energie Atomique (Fontenay aux Roses). His background in material science results from research work in the fields of properties of nuclear fuel and the influence of fission product accumulation on fuel behavior. Since 1976 he has been in charge of the safety-related aspects of fuel behavior at the Nuclear Research Center Cadarache within the framework of the international programs CABRI and Scarabée.

Current address: DRS/SEMAR, Centre d'Etudes de Cadarache Bât, 702-13108 St. Paul Lez Durance CEDEX (FRANCE).

NSRR/RIA Experiments with High-Burnup PWR Fuels

Toyoshi Fuketa received the B.S. degree in 1982, the M.S. degree in 1984, and the Ph.D. degree in 1987 in mechanical engineering science from the Tokyo Institute of Technology, Japan. He is a senior engineer in the Reactivity Accident Research Laboratory at Japan Atomic Energy Research Institute (JAERI). He has been involved in the Nuclear Safety Research Reactor project to study modes and consequences of failure of light-water-reactor (LWR) and research reactor fuels. His research interests include fuel–coolant interactions, fuel failure mechanisms, and transient fission gas behavior. He was engaged in small-scale steam explosion experiments at Sandia National Laboratories, Albuquerque, N. Mex., from 1988 to 1990.

Current address: Department of Reactor Safety Research, Japan Atomic Energy Research Institute, Tokai, Ibaraki 319–11 Japan.

Fumihisa Nagase received the B.S. degree in 1984, the M.S. degree in 1986, and the Ph.D. degree in 1997 in nuclear engineering at Tohoku University. He is a research engineer in the Fuel Reliability Research Laboratory at Japan Atomic Energy Research Institute. Since 1987, he has been engaged in research on light-water-reactor (LWR) core materials interaction during a severe accident. His current research interests include mechanical properties of high-burnup LWR fuel cladding under accident conditions.

Current address: Department of Reactor Safety Research, Japan Atomic Energy Research Institute, Tokai, Ibaraki 319–11 Japan.

Kiyomi Ishijima received the B.S. degree in 1971 and the M.S. degree in 1973 in nuclear engineering from Osaka University, Japan. He is head of the Reactivity Accident Research Laboratory at Japan Atomic Energy Research Institute (JAERI) and is in charge of the Nuclear Safety Research Reactor program devoted to nuclear fuel behavior in off-normal and accident conditions. In addition to his experience in the field of fuel behavior and reactor control studies at JAERI, he was assigned to Idaho National Engineering Laboratory from 1980 to 1982 as a visiting scientist and served in the Science and Technology Agency of Japan from 1985 to 1987 as a regulatory staff member.

Current address: Department of Reactor Safety Research, Japan Atomic Energy Research Institute, Tokai, Ibaraki 319–11 Japan.

Toshio Fujishiro received the B.S. degree in 1965 and the M.S. degree in 1967 in mechanical engineering and the Ph.D. degree in 1984 in nuclear engineering from The University of Tokyo. He began basic research in the field of heat transfer and thermal hydraulics at Japan Atomic Energy Research Institute (JAERI) in 1967. He has been engaged in the Nuclear Safety Research Reactor project from the beginning and supervised the project as a head and a department director. He has been Director General of Oarai Research Establishment of JAERI since 1997 and supervises such projects as the High-Temperature Test Reactor project and the Japan Materials Testing Reactor project.

Current address: Oarai Research Establishment, Japan Atomic Energy Research Institute, Oarai, Ibaraki 311–13 Japan.

The Russian RIA Research Program: Motivation, Definition, Execution, and Results

Vladimir Asmolov is Director of the Nuclear Safety Institute, Russian Research Centre "Kurchatov Institute" (RRC KI). He graduated in 1970 from the Moscow Power Engineering Institute. His work includes critical heat flux and DHB study for Russian VVER and RBMK reactors, study of the influence of noncondensable gas on heat transfer, Chernobyl accident mitigation and supervision of the sarcophagus design, and all kinds of severe accident research such as severe fuel damage and reactivity-initiated accidents. His institute is currently performing a number of severe accident studies, including an internationally sponsored test program on the interaction of molten core debris with the lower head of a reactor vessel.

Current address: Nuclear Safety Institute, Russian Research Center "Kurchatov Institute," Kurchatov Square, Moscow 123182, Russia.

Larissa Yegorova is a laboratory head and program manager for the Nuclear Safety Institute, Russian Research Centre "Kurchatov Institute" (RRC KI). She received a candidate of science (Ph.D.) degree in 1972 from Moscow Bauman State Technical University and worked in the nuclear space technology program at the Semipalatinsk Research Centre before joining the Kurchatov Institute in 1982. At the Kurchatov Institute, she has had responsibility for conducting the Russian reactivity-initiated accident research program and other severe fuel damage projects, and she led the study of VVER fuel bundle behavior at the CORA facility.

Current address: Nuclear Safety Institute, Russian Research Centre "Kurchatov Institute," Kurchatov Square, Moscow 123182, Russia.

Assessment of RIA-Simulation Experiments on Intermediate- and High-Burnup Test Rods

Robert Montgomery received the B.S. degree in 1984 and the M.S. degree in 1987, both in nuclear engineering, from Texas A&M University. He is the manager of Nuclear Technologies at ANATECH Corp. where he has been the project manager for several research and development projects related to modeling and analysis of nuclear fuel rod behavior during

normal operation and off-normal transient conditions. He has performed root cause evaluations of fuel reliability issues and has assessed the effects of high-burnup and irradiation conditions on transient fuel behavior. As project manager of the boiling-water reactor failed-fuel program, he was responsible for the development of a methodology to analyze the degradation behavior of defective fuel during operation. Prior to joining ANATECH Corp., he was a research associate for the Advanced Nuclear Fuels Laboratory at Texas A&M University and also a research engineer at Belgonucleaire in Brussels.

Current address: ANATECH Corp., 5435 Oberlin Drive, San Diego, CA 92121.

Y. R. Rashid received the B.S., M.S., and Ph.D. degrees in civil engineering from the University of California, Berkeley, in 1960, 1962, and 1965, respectively. He is the founder and technical leader of ANATECH Corp. He has extensive experience in the areas of structural mechanics, finite element modeling and solution techniques, computational fracture mechanics, and material constitutive modeling. He has developed analysis methods for reactor fuel elements, large-scale nuclear structures, and failure analysis of reactor vessel and containment structures. In the area of nuclear fuel rod behavior, he has developed failure models for stress corrosion cracking and material rupture during normal operation and high-temperature transient ballooning rupture during loss-of-coolant accidents. Following the Three Mile Island accident, he served as chairman of the Structural Mechanics Peer Review Group for the Vessel Investigation Project conducted jointly by the Nuclear Regulatory Commission and Office of Environmental Compliance and Documentation. Prior to ANATECH, he held the position of Manager, Fuel and Structural Mechanics, at General Electric and Manager, Analytical Research and Development, at General Atomic.

Current address: ANATECH Corp., 5435 Oberlin Drive, San Diego, CA 92121.

Odelli Ozer received the B.S., M.S., and D.E. Sc. degrees, all in nuclear engineering, from Columbia University. He is manager of light-water-reactor (LWR) fuel reliability in the Nuclear Power Group at the Electric Power Research Institute (EPRI) and has directed and managed numerous R&D projects that produced data on the performance of LWR fuel at high burnups. He has also supported the development of analytic capabilities needed for predicting the performance of sound fuel at high burnups as well as for predicting the operating conditions under which failed fuel will become subject to rapid degradation. His earlier responsibilities included development of core physics methods and pressure-vessel fluence analysis tools that utilized state-of-the-art nuclear cross section data and libraries (ENDF/B-V). Prior to joining EPRI, he worked at the National Nuclear Data Center, Brookhaven National Laboratory, where he was responsible for the assembly testing and release of an earlier version of the National Standard Cross Section Library (ENDF/B-IV).

Current address: Electric Power Research Institute, P. O. Box 10412, Palo Alto, CA 94303.

Rosa Lu Yang received her B.S. degree in nuclear engineering from National Tsing Hua University, Taiwan, in 1971. Her M.S. and Ph.D. degrees are from the University of California, Berkeley, in 1973 and 1980, respectively. She is the manager of fuel reliability, storage, and disposal in the Nuclear Power Division at the Electric Power Research Institute (EPRI) in Palo Alto, California. Before joining EPRI in 1987, she was with the nuclear fuel engineering department at the General Electric Company. She developed a mechanistic fuel rod thermal and mechanical performance code and managed and provided technical analysis for several internationally sponsored fuel programs. Her current responsibilities include managing issues related to the entire fuel cycle from manufacturing to in-core performance to on-site storage and final disposal.

Current address: Electric Power Research Institute, P.O. Box 10412, Palo Alto, CA 94303.

DISCLAIMER

(Continues from page ii)

France in the CABRI facility and one in Japan in the NSRR facility) with highly irradiated fuel producing cladding failures of 30 and 60 cal/g, respectively. These values were so far below the values for the cladding failure criteria established by the various regulatory bodies, the U.S. NRC included, that it led to expanded efforts by a number of countries. Additional experimental and analytical programs were directed toward gaining a more complete understanding of highly irradiated fuel behavior under accident conditions, including an assessment of the safety significance of the results obtained so far. The ultimate goal of these activities is the development of new regulatory criteria for high-burnup fuel under DBA conditions (initially for RIAs, but eventually including LOCAs as well).

The five papers in this issue of *Nuclear Safety* collectively address the various issues associated with the behavior of high-burnup fuels, especially under RIA conditions, and explain in detail the relevant mechanisms and parameters that have an effect on this behavior taking into account the tests that have been performed recently and insights from relevant analysis. These papers, which are contributed from four different countries (United States, France, Japan, and Russia), in addition to describing the specific national efforts, provide different perspectives on these issues and their significance. The general technical issues underpinning these perspectives, however, are the same in all papers. It is gratifying to see these important safety issues explored at such depths to ensure that the defense-in-depth concept, which is the basis for the design and licensing of most of the world's reactors, is not just a theoretical premise but an ongoing and living concept. These papers also highlight the international character of safety research in the 1990s and the deep international cooperation that has developed after the Three Mile Island accident and especially after the Chernobyl accident.

Dr. Themis P. Speis, *Deputy Director, Research*
U.S. Nuclear Regulatory Commission